ALMA MATER STUDIORUM
UNIVERSITÀ DI BOLOGNA

FACOLTÀ DI SCIENZE MATEMATICHE, FISICHE E NATURALI
Dipartimento di Astronomia

LOOKING FOR THE BUILDING BLOCKS OF THE GALACTIC HALO: VARIABLE STARS IN FORNAX AND BOOTES DWARFS AND IN NGC 2419

TESI DI DOTTORATO
DI
CLAUDIA GRECO

RELATORE : **PROF. B. MARANO**
CO-RELATORE : **DR. G. CLEMENTINI**
COORDINATORE : **PROF. L. MOSCARDINI**

SCUOLA DI DOTTORATO IN SCIENZE MATEMATICHE, FISICHE E ASTRONOMICHE

DOTTORATO DI RICERCA IN ASTRONOMIA, XIX CICLO (2003–2006)

SETTORE SCIENTIFICO DISCIPLINARE: AREA 02 - SCIENZE FISICHE
FIS/05 ASTRONOMIA E ASTROFISICA

Contents

Introduction

In Λ-cold-dark-matter hierarchical models of galaxy formation, the halo of the Milky Way (MW) has been assembled, at least in part, through the accretion of protogalactic fragments partially resembling the present-day dwarf spheroidal (dSph) satellites of the MW. A number of Galactic halo fragments, as well as a fraction of the halo globular clusters (GCs), may thus originate from dSph's that were accreted by the MW. Investigation of the stellar populations of the MW dSph companions can thus provide excellent tests to infer the dominant Galaxy formation scenario, whether merger/accretion or cloud collapse. Pulsating variable stars offer a very powerful tool in this context, since variables of different types allow to trace the different stellar generations in a galaxy and to reconstruct the galaxy star formation history and assembling back to the first epochs of galaxy formation. In particular, the RR Lyrae stars, belonging to the old population ($t >$ 10 Gyr), eyewitnessed the epoch of the halo formation, and thus hold a crucial role to identify the MW satellites that may have contributed to building the Galactic halo. In the MW, most of the GCs with an RR Lyrae population sharply divide into two distinct groups (Oosterhoff types I and II) based on the mean periods and the relative proportion of the fundamental mode (RRab) and first overtone (RRc) RR Lyrae stars (Oosterhoff, 1939). Among the Galactic GCs, a clear gap separates the two Oosterhoff types, with virtually no cluster intermediate between the two groups.

My Ph-D project has been focused on the identification of the possible "building blocks" of the Galactic halo, by investigating the Oosterhoff properties of a number of different stellar systems starting from relatively undisturbed dwarf galaxies (the Fornax dSph), through distorted and tidally disrupting ones (the Bootes dSph), to possible final relics of the disruption process (the Galactic globular cluster NGC 2419). We are addressing the question of whether the properties of the RR Lyrae stars in these systems conform to the Oosterhoff dichotomy characterizing the MW variables. If they do not, the Galaxy's halo cannot have been assembled by dSph-like protogalactic fragments resembling the present-day dSph companions of the MW.

The answer to this question is not only affecting the process and time scale of the Galactic halo formation, but the universality of the relation between HB luminosity and metallicity, too. The universality of the M_V(HB) - [Fe/H] relation, and hence the entire Population II distance scale, hinges on an answer to this

question. Because the periods of the RR Lyrae stars, which define the Oo type, simply reflect RR Lyrae luminousities, only after Oo types have been identified for globular clusters in other galaxies can we confidently assume that the HB luminosity level will be the same for the Galactic RR Lyrae stars used in calibrating this relation and for the extragalactic RR Lyrae used to actually infer the distance.

Our first target has been the Fornax dSph galaxy, one of the very few dwarf spheroidals, along with the Sagittarius and the Canis Maior dSph's, found to possess globular clusters. In order to make a comprehensive and deep ($V \leq 26$ mag) study of the variable star population in the Fornax dSph and in its globular clusters, we have carried out a wide-area ($\sim$ 1 deg^2) time-series photometric survey of the galaxy field with the wide field imager of the 2.2m ESO/MPI telescope in La Silla, and the 8 CCD's mosaic of the CTIO 4m Blanco telescope. High spatial resolution photometry of the Fornax GCs was obtained instead with the 6.5m Magellan/Clay telescope, and complemented by Hubble Space Telescope WFPC2 data. We have applied Image Subtraction Techniques to detect the variable stars, using the package ISIS2.1 (Alard, 2000) on the ESO data, and the SuperMacho pipeline for the CTIO data (Rest et al., 2005). Then we have used custom software optimized to the period search of periodic variable stars (Graphic Analyzer of TIme Series, see e.g.Di Fabrizio 1999; Clementini et al. 2000) to fit light curves and finally get the star pulsation parameters (period, amplitude and mean luminosity). In Fornax we have mapped the galaxy instability strip from the Dwarf Cepheids (DCs, V $\sim$24-25 mag) to the Anomalous Cepheids (ACs, V $\sim$19 mag). We are producing the largest catalog of variables ever obtained for a dSph galaxy. Thanks to the high performance of the Image Subtraction Technique we managed to identify the largest ($\sim$ 90 stars) sample of Dwarf Cepheids (DCs) ever detected in an extragalactic system, and established their period-luminosity relation. The vast majority of the variables detected in Fornax are of RR Lyrae type (including an extraordinary large number of double-mode pulsators), in agreement with the galaxy predominantly old stellar population. However, several ACs tracing the galaxy intermediate-age stars were also detected. According to the pulsation properties of the RR Lyrae stars the Fornax GCs have been found to belong to an Oosterhoff-intermediate class and fill the Oosterhoff-gap defined by Galactic GCs. The Fornax field RR Lyrae stars as well have an Oosterhoff-intermediate classification.

Our findings allow us to exclude that the MW halo can have been assembled by stripping of Fornax dSph-like protogalactic fragments, and demonstrate that the Fornax dSph conforms instead to the other already known dSph satellites of the MW, which are found to show noteworthy differences from most Galactic halo stars, both in chemistry of their old stars and in the properties of their variable star populations (see e.g. Venn et al., 2004, and reference therein).

In the last couple of years 10 new dSph companions of the MW have been discovered by the Sloan Digital Sky Survey (SDSS; York et al. 2000). The new systems all are found to hold rather unusual properties intermediate between those of GCs and dwarf spheroidals. They also appear less regular in shape as if they were in the process of being disrupted by tidal interactions. All these systems appear to be rather metal poor and show the presence of an ancient stellar component. We have

identified RR Lyrae stars in one of these newly discovered galaxies, the Bootes dSph (Dall'Ora et al., 2006). We have found that the Bootes RR Lyrae stars belong to an Oosterhoff II class. Only Ursa Minor of the previously known dSph companion of the MW, also belongs to the Oosterhoff II class. Our results for Bootes suggest that the newly discovered MW satellite might indeed be the "building blocks" of the Galactic halo. However, further observations to study the variables in the other galaxies of the sample are needed to confirm these preliminary findings.

The Galactic globular cluster NGC 2419, one of the brightest and most distant cluster in the MW halo, is a metal poor Oosterhoff type II system suspected to be the relic of an extragalactic system accreted by the MW (see e.g. Mackey & van den Bergh, 2005, and reference therein). We have obtained time-series photometry of NGC 2419 with the 3.5m TNG telescope and complemented it with archival data from the SUBARU 8m telescope and the WFPC2@HST. We have discovered many new variable stars with the Image Subtraction Technique, increasing by a factor two the total number of RR Lyrae stars known in the cluster. The newly discovered RR Lyrae stars mainly reside in the cluster most internal regions and are mainly first overtone pulsators (RRc). Some of the newly discovered variables appear to be of Oosterhoff-intermediate type, however, an Oosterhoff II behavior is fully confirmed for the cluster.

The Oosterhoff behaviour of different stellar systems, including the main targets of this thesis, was investigated to look for the key quantity defining Oosterhoff status. The minimum period of the *ab*-type RR Lyrae stars appears to be the key quantity defining whether a cluster has Oosterhoff I, II or Intermediate type.

In Chapter 1 we present a brief overview on the Galaxy formation mechanisms and discuss different types of "building blocks", inside and outside the Milky Way. In Chapter 2 we present our use of the variable stars as tools to investigate the halo formation epochs and describe our strategy. Chapter 3 is devoted to the Fornax dSph and to the variables we discovered in the field of this galaxy. We present the largest sample of Dwarf Cepheids ever detected in an extragalactic system. Results for variable stars in the Fornax globular clusters For 2, 3 and 5 are discussed in Chapter 4. In Chapter 5 we present the first study of variability ever performed in For 4, the more centrally located globular cluster in Fornax dSph. Results for variable stars in the newly discovered Bootes dwarf are presented in Chapter 6. In Chapter 7 we discuss the peculiar Galactic globular cluster NGC 2419, and present the catalog of new variables we have discovered within the cluster. In Chapter 8 we briefly analyze the Oosterhoff intermediate globular clusters as a class of objects by itself, comparing results from the most recent literature. Conclusions and future aspects of this work are summarized in Chapter 9.

Chapter 1

Galaxy Formation Mechanisms: Monolithic Collapse versus Hierarchical Merging

In recent years, the detailed study of individual stars in the Milky Way (MW) and of the resolved stellar populations in nearby galaxies, have turned out to be powerful tools for understanding the mechanisms which may have lead to the formation of the Galactic halo, making it possible to perform near-field cosmology using the Local Group (LG) as a true laboratory. Indeed, the chemistry, kinematics and spatial distribution of stars have unveiled precious informations about the early epochs of the MW formation.

Eggen, Lynden-Bell and Sandage (Eggen et al., 1962, hereafter ELS) studying the motion of Galactic high velocity stars, noted that as the star's metallicity decreases, the orbital energy and eccentricity increase, while the angular momentum decreases. They inferred the metal poor stars to reside in a halo formed in the fast collapse of protoclouds, in the very early stages of the Galaxy formation. This is the so-called *monolithic collapse scenario*, a halo formed in a rapid free-fall collapse. Some years later, Searle & Zinn (1978, hereafter SZ) found that the Galactic Globular clusters show a wide range in metal abundance which does not correlate with the distance from the Galactic center. This seems to support rather a *hierarchical* model: a halo built over an extended period of time from independent fragments. The fragments of these accretions are what we refer to as the "building blocks" of the Galactic halo.

The currently favored Λ-cold-dark-matter (Λ-CDM) cosmological model (see e.g. Spergel et al., 2006) predicts a hierarchical clustering scenario for the formation of structures. In this framework the dark matter halos of galaxies like the Milky Way were formed by the continual accretion of lower-mass systems. Some fractions of the accreted dark halos are expected to survive as sub-halos, if most of the extended dark halo is built up from merging systems that are tidally destroyed (Zentner & Bullock 2003). Similarly, if the accreted systems contain dissipation-less stars, e.g. in the form of dwarf galaxies, then this process naturally leads to the formation of

extended stellar halos. In a Λ-CDM scenario the expected accretion history is well-known theoretically, at least for the dark matter. Although dynamical friction and galactic tidal forces continuously act as to disrupt sub-halos once they fall within the potential of the massive system, the dense central cores of the merging satellites can survive as distinct entities for at least several orbital time-scales (Hayashi et al., 2003). Presently, the idea is that the main body of the Milky Way ($R_{\rm gc} < 10$ kpc) formed in a monolithic collapse, while the outer parts ($R_{\rm gc} > 15$) were assembled by capture of protogalactic fragments or at least experienced a number of merging events (van den Bergh & Mackey, 2004).

Signatures of the Galaxy assembling should be seen in the properties of its halo stellar populations, at least in the outer regions of the halo, where the dynamical mixing time-scales are long. It is therefore expected that the stellar halos of galaxies should posses spatial and metallicity substructures in the form of disrupted satellites. To recognize and study the local relics of such processes, in the Galaxy as well as in the Local Group, provide detailed constraints for models of galaxy formation. Many observational evidences of merging events have been found. Several sub-structures in the Galactic halo are being discovered thanks to new large surveys such as the Sloan Digital Sky Survey (SDSS; York et al., 2000) and the 2MASS (see Skrutskie et al., 2006, and reference therein). We are currently observing the Sagittarius dwarf galaxy , (hereafter the Sgr dSph Ibata et al., 1994a, 1997) during its disruption into a giant stream. This galaxy has left a debris stream fully encircling the MW (e.g. Ibata et al., 2001; Newberg et al., 2002, 2003); and is currently contributing to the assembly of the Galactic halo with both stars and globular clusters, whose properties are similar to those of Zinn's "young halo" ensemble (Da Costa & Armandroff, 1995; Ibata et al., 2001, 2002; Newberg et al., 2002; Majewski et al., 2003; Bellazzini et al., 2003a,b, and references therein). Like the Sgr dSph, also the Canis Major dSph (Martin et al., 2004, hereafter CMa dSph) is interacting with the Milky Way and there is a number of Galactic globular clusters possibly associated with this galaxy. The "Monoceros Ring" identified by Newberg et al. (2002) and Yanny et al. (2003) (sometimes known as the Galactic anti-center stellar structure – GASS) is probably the tidal debris of a destroyed dwarf galaxy whose nucleus lies towards the CMa dSph.

Furthermore, it is possible that each galaxy experienced its own series of merging events, in a very unique way, making it possible to see differences in the properties of the galactic stellar halos, even between systems of similar morphological type. It is interesting to test whether the halos of other disk galaxies also exhibit substructures and to investigate how the nature of these substructures varies with the properties of the host galaxy. Halo substructures as giant tidal streams could be a generic property of large spiral galaxies, testifying that the formation of galaxies continues at a moderate pace up to the present day.

The closest giant spiral galaxy, the Andromeda nebula (M31), is placed at about $\sim 780\ kpc$ from the MW. There are many similarities between the global properties of our Galaxy and M31, but the stellar halo of M31 has longly been known to differ from the Milky Way halo. Many studies indicate that the M31 halo is denser, larger and an order of magnitude more metal-rich than the Milky Way halo (e.g. Morris et al., 1994; Rich et al., 1996; Holland et al., 1996; Durrell

et al., 2001; Reitzel & Guhathakurta, 2002). A different, maybe more active accretion/merger history within M31 could be responsible for these differences. A giant stellar stream, overdensities and loops of stars (Ibata et al., 2001; Ferguson et al., 2002; McConnachie et al., 2003; Ferguson, 2006) have been revealed in the outskirts of M31. The source of these substructures could be the interaction with two dwarf companions of M31, namely M32 and NGC 205, that both may have lost a significant number of stars in the process of tidal interaction. Also two very luminous globular clusters, G1 and B-237, could be involved in such a scenario, being suggested to be relics of stripped dwarf galaxies cannibalized by M31 (Meylan & Heggie, 1997; Meylan et al., 2001).

Such currently disrupting galaxies do bring observational evidence for a hierarchical model, but tracing the past interactions is not straightforward. How did look like the "building blocks" of which the Galaxy accreted? And how can we recognize now such relics, inside and outside the Milky Way?

1.1 Globular Clusters as Tracers of the Galactic Halo Formation

To identify the relics of past accretions we shall look for among objects that are old, massive and spread all over the Galaxy. The ~ 150 Galactic globular clusters offer a fundamental tool for both tracing the properties of our Galaxy in the present epoch, and for piecing together its formation history, since they are old and generally bright, hence can be observed both to large Galactocentric distance ($\simeq 100$ kpc) and through regions of high extinction.

Consideration of the many parameters relevant to Galactic globular clusters reveals them to be a very intriguing and varied group. Some characteristics are influenced by evolution – e.g. the horizontal branch (HB) morphology, galactocentric distance, absolute V magnitude, and obviously age – while others, as the metal abundance and the half-light radius ($R_{\rm h}$) are stable and can provide important information on the physical conditions during the epoch of the cluster's formation. Even if they do generally show uniform characteristics, suggesting a common formation mechanism – e.g. the density distributions of most of them are well fitted by empirical models (King, 1962) – other properties allow to split the full sample into various different sub-systems.

Zinn (1993a) proposed one of the most successful and widely used classification scheme of the Galactic globular clusters. According to the HB morphology and metallicity, he found that in the bulge and in the disk of the Galaxy reside the most metal rich globular clusters while the most metal poor ones do occupy the Galactic halo. However, among the halo clusters there is a dispersion in HB morphology with metallicity, the so-called "second parameter effect". That's because metallicity is not the only parameter influencing the HB morphology. Showing the halo clusters two different trends in the HB-metallicity relation, and thus having different colors at given metallicity, Zinn divided them into two sub-groups: the "old halo" clusters (OH GCs) having bluer HBs, and the "young halo" clusters (YH GCs) that have redder HBs. Zinn (1993a) found that the 87 clusters in his sample split quite cleanly into these three different groups, and also found that clusters in the three sub-groups are quite distinct in terms of typical

ages, spatial distributions and mean dynamical characteristics. He argued that the observed trends suggest that the bulge/disk clusters and the majority of the old halo objects were formed during a dissipative collapse, as hypotized by ELS, while the young halo clusters were formed in external dwarf galaxies, and later accreted when the parent galaxies merged and were destroyed by the MW, in the hierarchical manner suggested by SZ. van den Bergh (1993b) reached a similar conclusion via an equivalent classification scheme. Also results by Zinn (1996), which are based on a slightly modified classification scheme, support this conclusion.

For a better agreement with the hierarchical scenario, the "young halo" clusters should bear at least some resemblance to the globular clusters which are now observed in the dwarf galaxies associated with the Milky Way.

1.2 Extragalactic Globular Clusters

Only five out of the 20 dwarf companions of the Milky Way (see Belokurov et al. 2007, and references therein) - the four most massive ones: the LMC, SMC, Fornax, Sagittarius, and, possibly the CMa dSph - are found to possess globular clusters. The LMC is the largest of these galaxies, at a distance of ~ 50 kpc, followed by the SMC at ~ 60 kpc. Both these galaxies contain systems of massive clusters, with ages ranging from a few Myr to essentially coeval to the oldest Galactic globulars. The LMC cluster system exhibits an age gap between $\sim 4 - 13$ Gyr (where the upper edge is set by the assumed age of globular clusters coeval with the Galactic globulars) with only one cluster – ESO121-SC03, with an age of ~ 9 Gyr – falling in the gap. The ensemble of very old clusters in this galaxy adds to 15 (Mackey & Gilmore 2004), with the most recent additions being NGC 1928 and NGC 1939. In the SMC only one cluster, NGC 121, is coeval to the majority of the Galactic halo objects (see Glatt et al. 2007) but the galaxy does possess a number of massive clusters with ages in the range from ~ 6 to 9 Gyr (thus matching some of the youngest globular clusters observed in the MW).

Fornax and Sagittarius are the nearest dwarf spheroidal galaxies with globular clusters and can be easily resolved into individual stars. The Fornax dSph contains five globular clusters (Shapley, 1938; Hodge, 1961, 1965, 1969) and contrary to the Sagittarius dSph which is obscured by dust and confused by the merging with the MW, the Fornax dSph is high above the Galactic plane, therefore easy to observe.

It is more difficult to define the cluster system of the almost disrupted Sagittarius dSph, since it is likely to have already lost some of its clusters into the Galactic halo. The four well established members in the main body of this galaxy are M54, Terzan 7, Terzan 8, and Arp 2 (Da Costa & Armandroff, 1995), although numerous additional previous members have been candidated (NGC 4147, NGC 5634, Palomar 12 and Whiting 1, Martínez-Delgado et al. 2002a; Palma et al. 2002; Bellazzini et al. 2003a; Martínez Delgado et al. 2004; Carraro et al. 2007). The CMa dSph also possesses some globular clusters, namely NGC 1851, NGC 2808, NGC 5286, and maybe NGC 1904, NGC 2298, plus a number of old open clusters (Martin et al., 2004; Bellazzini et al., 2003b; Frinchaboy et al., 2004).

We need some proper tools to compare and distinguish globular clusters likely accreted by the MW from genuine in-Galaxy-born ones, and some general

properties to significantly compare the Galactic and extragalactic globular clusters.

1.3 The $\log R_{\rm h}$ vs. M_V Plane

Hints on peculiar behaviors of some globular clusters can be derived by comparing the cluster's compactnesses and luminousities.

As a globular cluster evolves dynamically its core contracts and its envelope expands. However, N-body calculations (Aarseth & Heggie, 1998, and reference therein) show that the half-light radius $R_{\rm h}$ - the radius that contains half of the cluster stars in projection - generally changes very little over periods as long as ten relaxation times. This suggests that $R_{\rm h}$, like [Fe/H], may provide valuable informations on the physical conditions at the era of the globular clusters formation.

Figure 1.1 shows the plot of $\log R_{\rm h}$ vs. M_V for Galactic globular clusters. We note the very sharp edge of the upper left distribution of the MW globulars. The vast majority of the Galactic clusters lie below the line described by the empirical relation

$$\log R_{\rm h} = 0.25 M_V + 2.95 \tag{1.1}$$

defined by Mackey & van den Bergh (2005)

Only three clusters in the MW lie above this line: ω Centauri, M54 and NGC 2419. ω Centauri shows evidence for age/metallicity substructures in its color-magnitude diagram (Ideta & Makino, 2004; Bekki & Freeman, 2003; Pancino et al., 2003, and references therein). The presence of multiple stellar populations suggests that the cluster could be the stripped core of a former dwarf spheroidal or dwarf elliptical galaxy. Furthermore, Ibata et al. (1994b, 1995) have shown that M54 is associated with the central region of the Sagittarius dwarf galaxy, and some authors (see e.g. Layden & Sarajedini, 2000a) suggest that the cluster is indeed the core of this galaxy. Finally, van den Bergh & Mackey (2004) suggested that NGC 2419 might also be the remaining core of a defunct dwarf spheroidal-type galaxy.

It may not be just by chance that these three clusters, all previously and independently suggested to be cores of cannibalized dwarf galaxies, form such a distinct group of objects in the $\log R_{\rm h}$ vs. M_V plane. Also G1 and B-327 in M31 are found to lie in the region above the line described by Eq. 1.1. Both these clusters are more luminous than any Galactic globular cluster. In G1, as in ω Centauri and M54, convincing evidence has been gathered for a real abundance dispersion (van den Bergh, 1968; Barmby et al., 2002). No published colour magnitude diagram exists of B-327, a very red cluster quite hard to resolve into stars (Ma et al., 2006a). In analogy to their MW counterparts both these M31 clusters are thought to be possible remnants of dwarf galaxies which have been interacting with M31 (Meylan & Heggie, 1997; Meylan et al., 2001; Ma et al., 2006a, 2007).

1.4 The Oosterhoff Dichotomy Inside and Outside the Milky Way

Pulsating stars such as the RR Lyrae variables, the Dwarf Cepheids, and the Anomalous Cepheids offer a powerful and independent tool for deriving

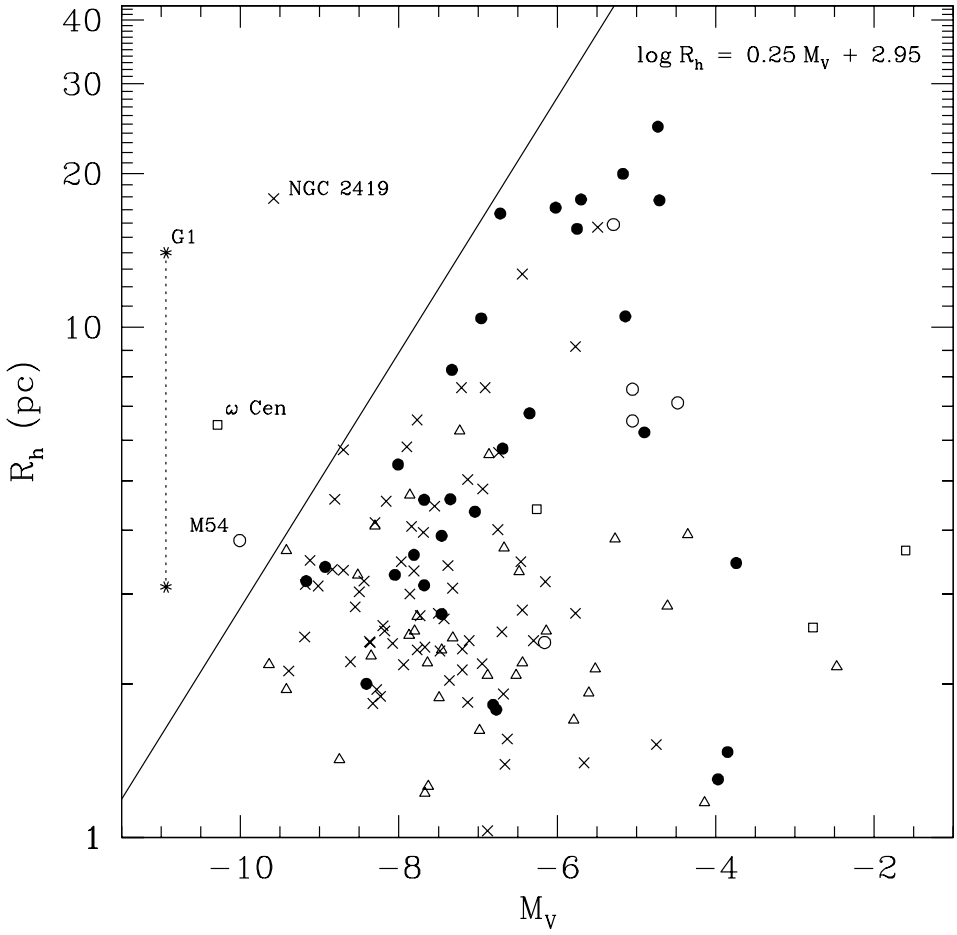

Figure 1.1 $\log R_{\rm h}$ vs. M_V plot for the Galactic globular clusters. Also shown is the giant M31 globular cluster G1 (the two linked stars) which is plotted according to the two discrepant $R_{\rm h}$ values existing for the cluster (Mackey & van den Bergh, 2005). Different symbols are: Galactic bulge clusters (open triangles); Old Halo Galactic clusters (crosses); Young Halo Galactic clusters (filled circles); Sgr dSph clusters (open circles); unclassified Galactic clusters (open squares).

informations on the stellar system to which they belong. They are easily identified, even in high crowding conditions, thanks to the light variation, and their periods are independent from reddening and distance. Different variable types are valuable tracers of the different stellar generations in a galaxy: the RR Lyrae stars trace the oldest populations ($t > 10$ Gyr), and the Anomalous Cepheids the intermediate age stars, allowing one to identify different star formation episodes that have occurred in the host stellar systems.

RR Lyrae stars have been found in all the Local Group dsph's where observations were deep enough to reach the HB level. Belonging to the oldest population, these stars were eyewitnesses to the first epochs of star formation and thus hold a crucial role for identifying the "building blocks" of the galactic halo and for understanding which galaxy formation scenario (merger/accretion or cloud collapse) is dominant. Almost all globular clusters (GCs) of the MW which contain significant numbers of RR Lyrae stars sharply divide into two very distinct classes, the Oosterhoff types (Oosterhoff, 1939), according to the mean pulsation periods of their RR Lyrae stars and the relative proportions of fundamental and first overtone-mode pulsators: Oosterhoff type I ("OoI") clusters have $\langle P_{\rm ab} \rangle \simeq 0.56$ d, and Oosterhoff type II ("OoII") globulars have $\langle P_{\rm ab} \rangle \simeq 0.66$ d (Clement et al., 2001). This phenomenon is called the Oosterhoff dichotomy. There is evidence (van den Bergh, 1993a; Yoon & Lee, 2002) that the OoII clusters of the MW have different kinematic and spatial distributions from OoI ones, thus possibly originating in different accretion/formation events in the halo. This is supported also by a difference in mean chemical abundance (OoII clusters being on average more metal-poor than OoI clusters) and possibly by a difference in age (metal-poor clusters being on average slightly older than the intermediate-metallicity clusters, as suggested by van den Bergh (1993a) and De Angeli et al. (2005). Whatever the mechanism, it is clear that the Oosterhoff dichotomy reflects conditions within the MW halo at the time of globular cluster formation. In the MW there are *virtually* no clusters with periods intermediate between the two types. The $\langle P_{\rm ab} \rangle$ vs. [Fe/H] distribution of Galactic clusters having at least 5 RRab stars is shown in Figure 1.2 using metallicities from Harris et al. (1996). Forty-six globulars are shown in the figure, covering the $\langle P_{\rm ab} \rangle$ range from 0.525 (NGC 4147) to 0.708 d (NGC 4833). The 0.04 d wide shaded region from 0.58 to 0.62 d is the so-called "Oosterhoff gap". This gap represents $\simeq 22$ % of the full distribution. In addition, if we consider the cluster's classification into Zinn's subsystems, it is very clear that both "young" and "old" halo clusters present the Oosterhoff dichotomy.

Eight out of the 46 Galactic globulars shown in the figure fall close to the edges of this gap. They are IC 4499, Arp 2, NGC 362, M 75, NGC 6284, M 54, NGC 5285 and Rup 106. Among them M 54 and Arp 2 are associated with the Sgr dSph, NGC 5286 belongs to the CMa dSph and a further one - Rup 106 - is suggested to be connected with the stream of the Sgr dSph (Bellazzini et al., 2003a). Thus, only 4 out of 46 clusters, hence less than $\simeq 9$ % of the full distribution, are in the gap.

In the MW's immediate vicinity, the situation is quite different, with important implications for the formation of the Galactic halo (Catelan et al., 2007). In the satellite galaxies of the Milky Way, the field stars as well as their respective globular clusters, fall *preferentially* in the "Oosterhoff gap" region. In particular, globular

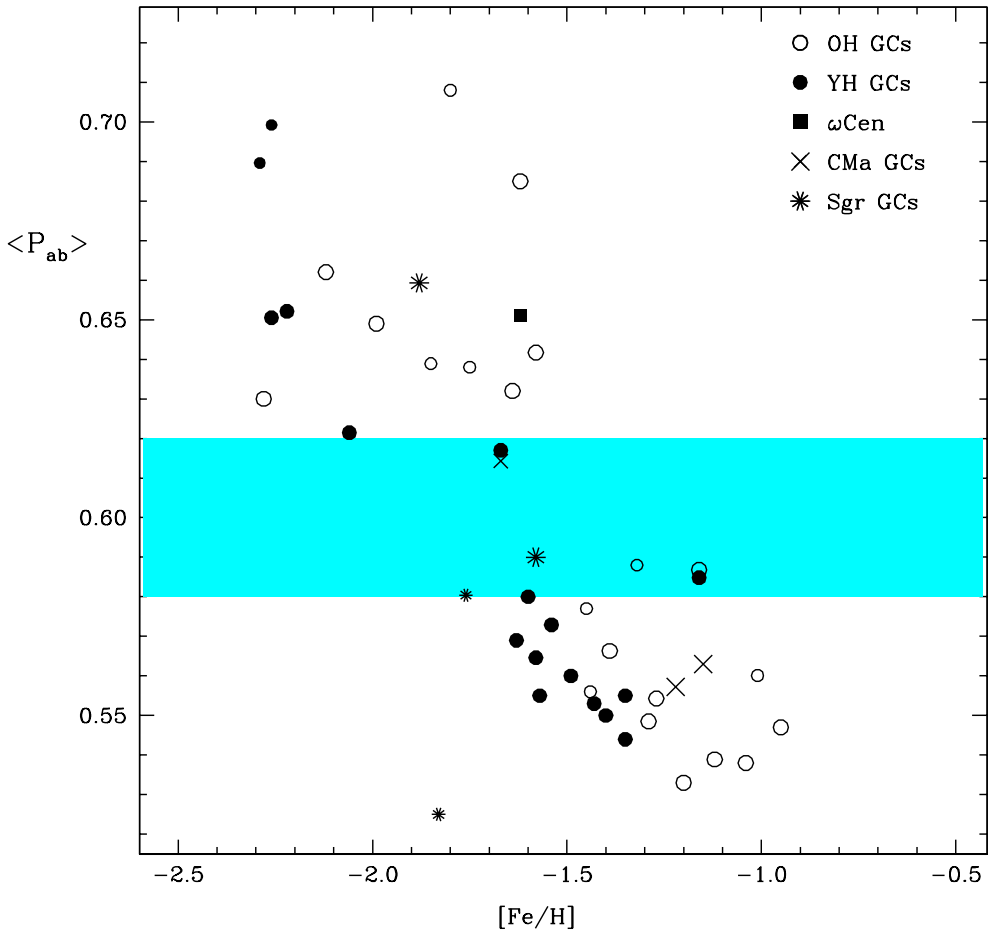

Figure 1.2 Oosterhoff dichotomy among the MW, the CMa and the Sgr globular clusters. Clusters belonging to the "young halo" (YH GCs), in the Mackey & van den Bergh (2005) classification scheme, are shown by filled circles; "old halo" clusters (OH GCs) by open circles. Smaller symbols are used for clusters having less than 10 RRab stars with measured periods.

clusters of the Large Magellanic Cloud, as well as in other LG dwarf galaxies among which the Fornax dSph (see Chapter 4), fall between the two main groups and are classified as "Oosterhoff-intermediate", in spite of their having similar ages to the MW clusters. This is shown in Figure 1.2, where the satellite galaxies of the Milky Way and their respective globular cluster systems have been added to the previous plot. This plot dramatically illustrates the contrast between Oosterhoff behavior of the MW clusters and that of systems associated with the Milky Way satellites.

Do the clusters in the MW satellites indicate a continuous trend in RR Lyrae properties rather than an Oosterhoff dichotomy? And can we infer the frequency of merging events that has contributed in creating the Galactic halo?

On the other hand, if the Oosterhoff types of the present-day companions of the MW do not conform to the Oosterhoff dichotomy shown by the Galactic globular clusters then these galaxies cannot be representatives of the protogalactic fragments from which the Galaxy's halo has been assembled.

Figure 1.4 (right panel) compares the global $\langle P_{\rm ab} \rangle$ distributions of Galactic and nearby extragalactic globular cluster systems. Simple eye inspection clearly reveals that the two distributions are remarkably different, in spite of them having almost the same average values. The MW cluster distribution is bimodal with two well defined peaks (the Oosterhoff types) at $\langle P_{\rm ab} \rangle \simeq 0.56$ d and $\langle P_{\rm ab} \rangle \simeq 0.66$ d, respectively. The extragalactic system's distribution is strongly peaking at an intermediate value $\langle P_{\rm ab} \rangle \simeq 0.60$ d.

In this thesis, we have investigated the Oosterhoff types of three of different stellar systems: the Fornax dSph, the Bootes dSph, the Galactic globular cluster NGC 2419. We are addressing the crucial question of whether the RR Lyrae pulsation properties in these systems conform to the Oosterhoff dichotomy characterizing the MW variables. If they do not, the Galaxy's halo cannot have been assembled by protogalactic fragments resembling these present-day companions of the MW. The answer to this question is not only affecting the process and time scale of the Galactic halo formation, but the universality of the relation between HB luminosity and metallicity, too. The universality of the M_V(HB) - [Fe/H] relation and hence the entire Population II distance scale, hinges on an answer to this question. Because the periods of the RR Lyrae stars, which define the Oo type, simply reflect RR Lyrae luminousities, only after Oo types have been identified for globular clusters in other galaxies can we confidently assume that the HB luminosity level will be the same for the Galactic RR Lyrae stars used in *calibrating this relation* and for the extragalactic RR Lyrae used to actually *infer the distance*.

1.5 Dwarf Galaxies as Possible "Building Blocks"

The vast majority of the Local Group galaxies are dwarf spheroidals, the least massive and least luminous type of the known galaxies, often satellites of giant galaxies, like the Milky Way or M31, and lying within less than 300 kpc (see e.g. Grebel et al., 2003; van den Bergh, 1999). They are less luminous than $M_V \sim -11.0$ and can be found all over the Local Group, where they represent the dominant population, by number.

Studies of nearby galaxy clusters (see e.g. Phillipps et al., 1998, and reference

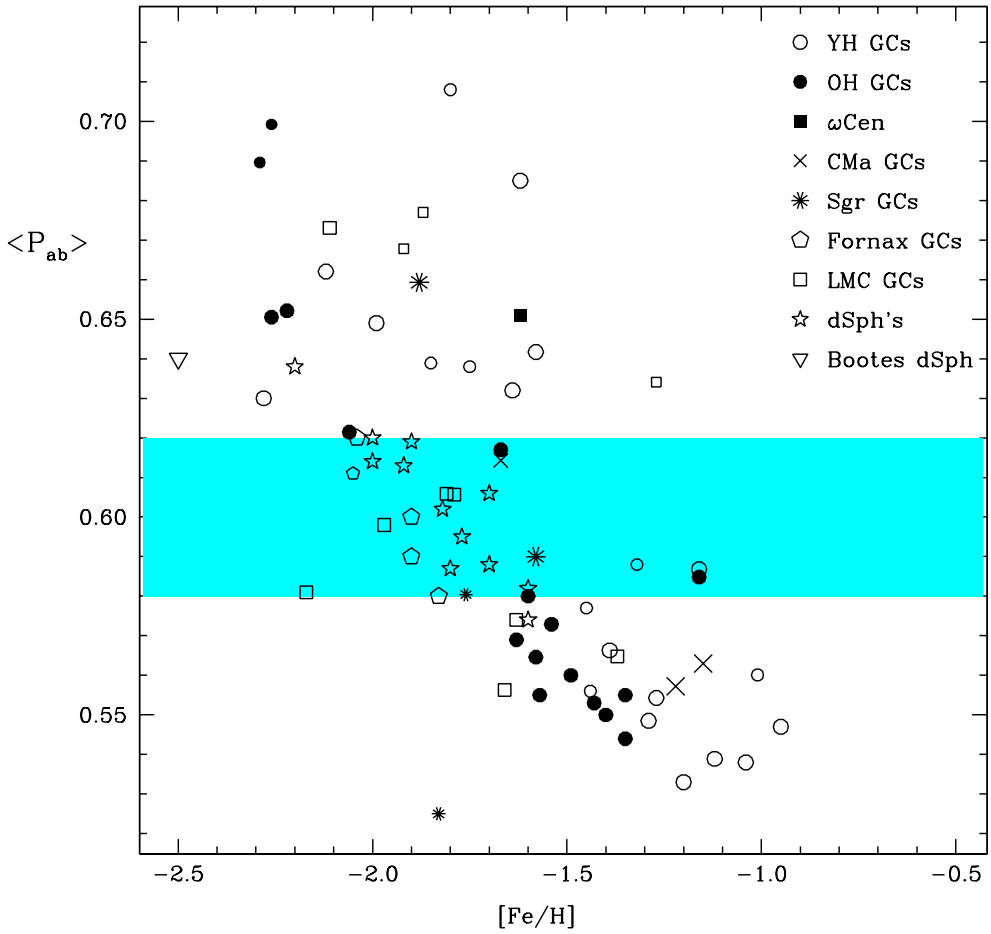

Figure 1.3 Same as in Fig. 1.2, but now including dwarf satellites of the Milky Way, the Magellanic Clouds, and their associated globular clusters. The galaxies orbiting the Milky Way and their associated globular clusters preferentially *occupy* the Oosterhoff gap region, in stark contrast with the Galactic globular clusters.

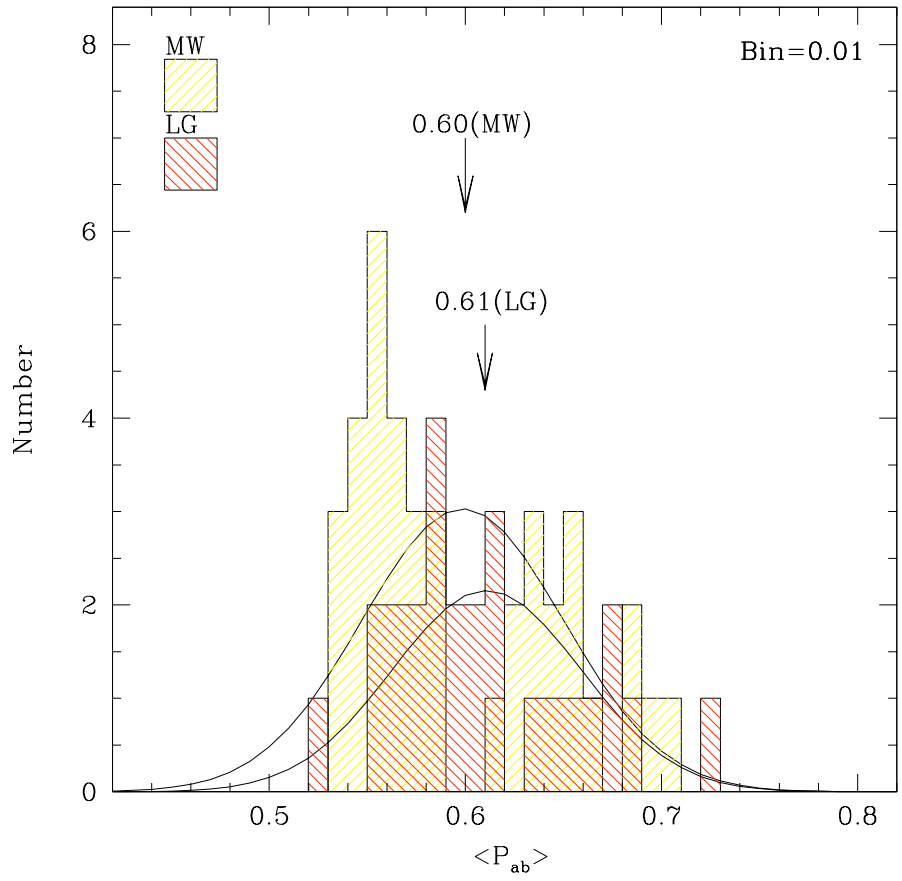

Figure 1.4 $\langle P_{\rm ab} \rangle$ distributions of Galactic and nearby extragalactic globular cluster systems.

therein) suggest that the summed optical luminosity of all dwarfs may rival that of the giant, high-surface brightness galaxies in these environments (Mateo et al., 1998, and reference therein). Dwarf galaxies are the darkest object we know in the Universe, with mass-to-light ratios ranging from $M/L \sim 5$ to $M/L \sim 100$ for systems such as Draco and Ursa Minor (Mateo et al., 1998; Kleyna et al., 2003; Wilkinson et al., 2004), respectively. dSph's exhibit complex, varied and peculiar star-formation and chemical enrichment histories (see e.g. Gallagher & Wyse, 1994; Mateo et al., 1998; Odenkirchen et al., 2001; Kleyna et al., 2001; Klessen et al., 2003; Wilkinson et al., 2004, 2006). If low-luminosity galaxies are dominated by dark matter they could account for a large fraction of the mass of galaxy clusters, and perhaps of the entire Universe. This makes it particularly important to understand their evolution and interaction histories and their role in the formation of the Milky Way. Formation and evolution of galaxy satellites has been a puzzling problem. According to the hierarchical scenario, small dark matter halos should collapse earlier than larger ones. Dark matter overdensities collapsed and formed halos, with the smallest and least massive halos being the densest. Thus, it is likely that the satellites of the MW galaxy were formed before the main body of the MW was assembled. Some of the satellites may have survived the very early process of the MW formation, whereas others may have been accreted by the MW at later stages.

Prior to the Sloan Digital Sky Survey (SDSS; York et al., 2000), there were 9 widely-accepted Milky Way dwarf spheroidal companions, namely Draco, Ursa Minor, Fornax, Carina, Sculptor, Leo I, Leo II, Sextans and the Sagittarius dSph (Mateo et al., 1998). Due to the intrinsically low surface brightnesses of these gas-deficient galaxies, the dSph census in the Local Group has longly been incomplete. The simulations of Moore et al. (1999) predicted hundreds of small Galactic satellite halos, a number at least two order of magnitudes larger than the then known satellites of the Galaxy. If each small dark matter halo indeed is the seed of a small galaxy, then there was a dramatic conflict between predictions and observations, a puzzle known as the " *missing satellite problem*" (Mateo et al., 1998; Klypin et al., 1999). It was unclear whether theory or observations were responsible for this discrepancy. On the theoretical hand, some people have been trying to reconcile the discrepancy by developing models that suppress gas accretion (see e.g. Efstathiou, 1992) or star formation, at least in low mass halos. These models produce a large population of entirely dark satellites (see e.g. Bullock et al., 2000; Kravtsov et al., 2004), together with a much smaller number of dSph's, roughly in agreement with the datum of nine dSph's. Others, like Kauffmann et al. (1993), proposed models with very high efficiency of dynamical friction, but then making it difficult to explain system as massive as the LMC to survive. An interesting comparison between observations and simulations, before the discovery of SDSS dwarfs is presented in Klypin et al. (1999).

Thirteen new Local Group dSph candidates have been discovered in the Sloan Digital Sky Survey (SDSS) photometric catalogue in the last couple of years. Ten of them are new MW companions, namely Ursa Major I, Canes Venatici I, Bootes, Ursa Major II, Coma Berenices, Willman I, Canes Venatici II, Leo IV, Leo T and Hercules, thus increasing the number of known MW dSph satellites to 20, including

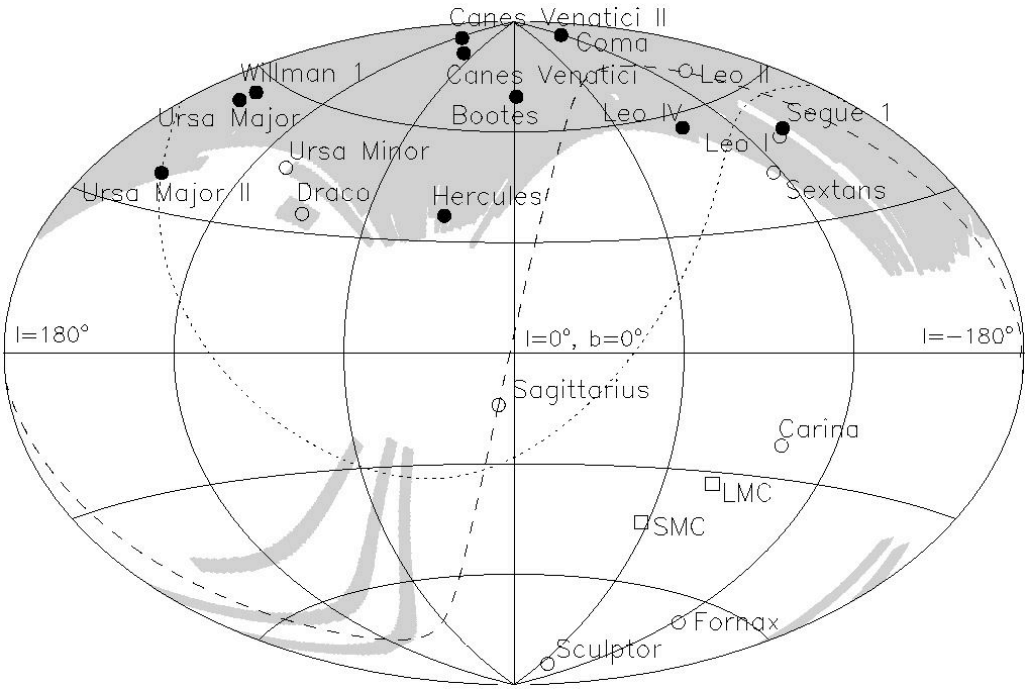

Figure 1.5 Locations of the Milky Way satellites in the Galactic plane. Filled circles are the new MW satellites recently discovered by the SDSS, open circles are previously known MW dSph companions. Shown in light grey is the area of sky covered by the SDSS survey and its extensions to date. The dashed and dotted lines show the orbital planes of the Sagittarius and Orphan Streams, respectively, taken from Fellhauer et al. (2006) and Fellhauer & Lin (2007).

accreted companions, such as the Sgr and CMa dSph's (see Belokurov et al. 2007). The location on the Galactic plane of the presently known MW satellites is shown in Figure 1.5. More than 75% of them are found within 150 kpc from the Milky Way; only three additional dSph's believed to be Galactic satellites are found at larger distances (Koch et al., 2007).

It had long been suspected that there might be some missing dSph's at low Galactic latitude in the Zone of Avoidance (see e.g. Mateo et al., 1998). However, the SDSS objects all lie at high Galactic latitude, as the survey is concentrated around the North Galactic Pole. The abundance of discoveries in the SSDS strongly suggests that there might be much more low surface brightness MW satellites waiting to be discovered, at least 50 according to Belokurov et al. (2007), thus directly bearing upon "the missing satellite problem". None of these newly discovered galaxies clearly shows up as a galaxy on the SDSS images, all have been recognized as overdensities of resolved stellar objects. They haven't been discovered previously because they all are much fainter than the previously known Local Group dSph's with effective surface brightnesses $\mu_v \gtrsim 28$ mag arcsec^{-2}, while previously known MW and M31 dSph's all lie above the line marking $\mu_v = 27$ mag arcsec^{-2} (Belokurov et al 2006b, astro-ph/0608448). Colour-magnitude diagrams (CMDs) reaching the HB have been published for all these new galaxies and all show the presence of an ancient stellar component, in agreement with the predictions of a hierarchical scenario (Zucker et al., 2004, 2006b,a,c; Willman et al., 2005a; Belokurov et al., 2006a, 2007; Martin et al., 2006a). They appear also less regular in shape, and there seems to be a correlation between irregularity and distance, as the closest ones (namely Bootes, UMaII and Coma) appear to be the more distorted as if they were in the process of being disrupted by tidal interactions. All the new systems appear to be rather metal-poor, with morphological features of the CMD resembling those of metal-poor GCs like M92. However, they are larger and somewhat less luminous than typical MW GCs. They all are found to hold properties intermediate between those of globular clusters and dwarf spheroidals. The Galactic halo contains a significant fraction of stars more metal-poor than [Fe/H] ~ -2.0 (see e.g., Christlieb et al., 2004; Beers et al., 2005) with no counterpart in the previously known dSph companions of the MW, which all contain very few metal-poor stars (see e.g., Tolstoy et al., 2004; Koch & Grebel, 2006). The new SDSS discoveries could indeed be the shreds from the violent building phase of the MW, and the representatives of the population that built the old, metal-poor component of the Milky Way halo.

Spectroscopic studies are required to infer the dark matter content of these newly discovered galaxy. Currently we have kinematic data only for two of them. Kleyna et al. (2005) measured velocities for seven stars in Ursa Major I (UMa I) and obtained a velocity dispersion of ~ 9 km/s and a mass-to-light ratio of ~ 500. Munoz et al. (2006) measured the radial velocities of seven stars in the Bootes dSph and found a velocity dispersion ~ 7 km/s and a mass-to-light ratio between 130 and 680. Based on these results, UMa I and Bootes would be the two most dark matter dominated objects known in the Universe. The implication is that the SDSS discoveries may belong to the class of low stellar mass, dark matter dominated galaxies predicted by Λ-CDM.

Figure 1.6 shows the location of different classes of objects in the plane of absolute magnitude vs. half-light radius. The MW globular clusters and dSph companions (including the 10 new SDSS discoveries) are plotted along with the M31 dSph satellites (including the 3 discoveries by Martin et al. 2006b), the three unusually extended globular clusters found in M31 by Huxor et al. (2005), the ultra-compact dwarf galaxies (UCDs) in the Fornax and Virgo clusters (Mieske et al., 2002; De Propris et al., 2005a; Hasegan, 2005) and globular clusters from the nearby giant elliptical NGC 5128 (Gómez et al., 2006; Harris et al., 2002). The plot shows the great variety of structures among which we can look for the counterparts of the "building blocks" who have contributed to the formation of the Galactic halo: globular clusters, dwarf spheroidals, ultra compact dwarf and more exotic groups, like the extended, luminous star clusters found by Huxor et al. (2005) in M31. For instance, it is quite clear that, this latter class of objects is likely missing in the MW, since, if present they should have been found already in the SDSS data.

A sparsely populated vertical band corresponding to half-light radii between ~ 40 pc to ~ 100 pc separates globular clusters from dwarf galaxies. The gap is significant: all objects to the left of the gap show no evidence of dynamically significant dark matter, hitherto. All the objects to the right with measured kinematics are consistent with substantial amounts of dark matter.

1.6 Constraints on Merging Episodes

If the Galaxy formed by continual accretion of small dwarf galaxies, then it should be possible to trace this assembling as well as to identify the "building blocks" that build up the halo, by recognizing a variety of abundance ratios in stars of different ages and dwarf galaxy origin. Therefore, "chemical-tagging" (Freeman & Bland-Hawthorn, 2002; Pritzl et al., 2005a) of stellar populations in the Galaxy should be possible.

Several studies have also demonstrated that the merger scenario is not inconsistent with the observed properties of the Galactic halo field stars, but a number of constraints are requested. For example, Unavane et al. (1996) examined the fraction of stars in the halo which have colours consistent with a metal-poor, intermediate-age population matching those typically observed in Local Group dwarf spheroidal galaxies. They conclude that the star counts imply an upper limit of ~ 60 mergers with low luminosity dwarf spheroidals like, for instance, the Carina dSph, or ≤ 6 mergers with more luminous objects like, for instance, the Fornax dSph, within the last ~ 10 Gyr.

On the other hand, Shetrone et al. (2001) find that there is strong consistency in the abundance patterns of the low luminosity dSph's Draco, Sextans, and Ursa Minor, but the measured $[\alpha/\mathrm{Fe}]$ ratios are ~ 0.2 dex lower than those of the Galactic halo field stars in the same metallicity range. These observations, along with several additional mismatches in elemental abundance ratios led these authors to conclude that the Galactic halo cannot have been assembled entirely through the accretion of low luminosity dwarfs similar to Draco, Sextans, and Ursa Minor; however, they place no constraints on the accretion of more luminous and complex dwarf galaxies such as the Fornax and Sagittarius dSph's .

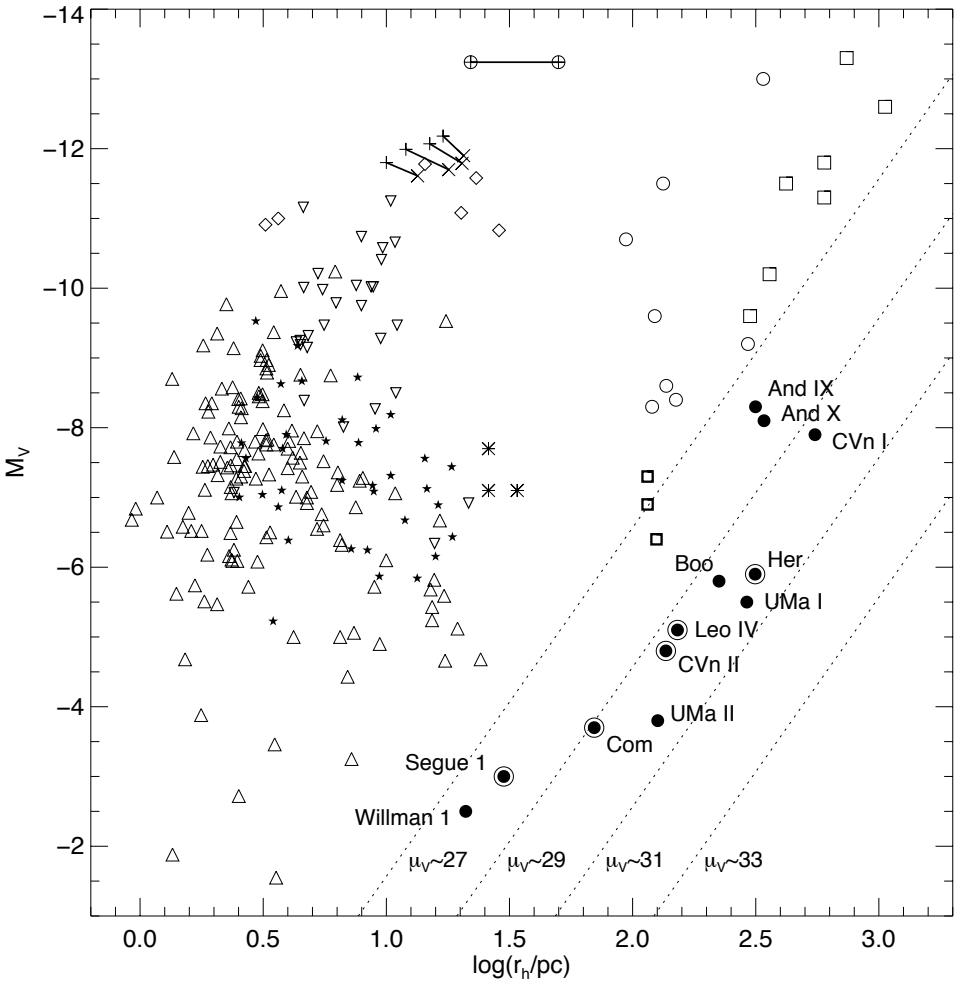

Figure 1.6 Location of different classes of object in the plane of absolute magnitude vs. half-light radius. Lines of constant surface brightness are marked. Filled circles are the SDSS discoveries including the 10 new Milky Way satellites (Willman et al., 2005b, 2006; Zucker et al., 2006b,c; Belokurov et al., 2006b), as well as And IX and X (Zucker et al., 2004, 2006a). Open circles are the eight previously known Milky Way dSph's with Sgr omitted (Irwin & Hatzidimitriou, 1995a; Mateo et al., 1998), squares are the M31 dSph's (McConnachie & Irwin, 2006), bold squares are three new M31 dSph's recently discovered by Martin et al. (2006b), triangles are the Galactic globular clusters (Harris, 1996). A variety of other extragalactic objects are also plotted: asterisks are the extended M31 globular clusters discovered by Huxor et al. (2005), pluses and crosses are UCDs in the Fornax cluster from Mieske et al. (2002) and De Propris et al. (2005a) respectively, diamonds are the so-called Virgo dwarf-globular transition objects (Hasegan, 2005), while filled stars and inverted triangles are globular clusters from the nearby giant elliptical NGC 5128 from Harris et al. (2002) and Gómez et al. (2006) respectively. Different measurements of the same object are connected by straight lines. The straight line connecting the circled plus symbols refer to measurements by Mieske et al. (2002) and Drinkwater et al. (2003) of UCD3 in Fornax.

More recently, Venn et al. (2004) have extended this idea, compiling a large amount of data concerning the chemistries of stars in several different regions of the Galaxy and on a number of nearby low mass dSph's. Like Shetrone et al. (2001), these authors find that the chemical signatures of most of the dSph stars are distinct from those of the MW stars. This implies that no Galactic component can have been formed *primarily* via accretion of low mass dSph systems at late epochs, although the authors do not rule out very early mergers with such objects, before a significant chemical enrichment can have occurred, nor mergers with larger systems like the Sagittarius dSph or the LMC.

Finally, Pritzl et al. (2005a) compared the chemistry of Galactic field stars, dSph field stars, and Galactic globular clusters, trying to identify globulars that show the signature of an extragalactic origin from the abundance ratios. They find some hints in favor of an extragalactic origin for Rup106 and Palomar 12, two clusters already associated to the Sagittarius Stream by Brown et al. (1997a); Dinescu et al. (1999); Bellazzini et al. (2003a).

Chapter 2

Variable Stars as a Tool: Properties and Strategy

All stars show variations in brightness and colors during the different stages of their evolution. However, a star is usually called "variable" when its brightness and colour vary on time-scales that can be observed and measured, at least in part. Variations in the stellar light output may be periodic, semi-periodic or irregular, with time scales ranging from fractions of seconds to over a century. In order to classify variable stars and to place them into the appropriate class both photometric and spectroscopic observations are needed. From photometric studies we can deduce the typical time scale, the amplitude of the brightness variation and the shape of the light curve; from the spectra we can infer the spectral type, the luminosity class, the chemical composition and the star's radial velocity curve. Traditionally, variable stars are classified into two main families: *intrinsic* and *extrinsic*. The former are stars that vary due to physical processes occurring in the stars themselves and include the pulsating stars, the eruptive and explosive variables; the latter are stars that vary due to external processes and include eclipsing variable, rotational variables, pulsars and stars that have interaction with the interstellar and circumstellar medium. The *light curve* of a variable shows how the star magnitude varies with time. If the variation is regular, it is possible to define the period and amplitude of the light variation. During a period, also density, spectral type, radius, effective temperature and radial velocity of the star envelope vary.

Among the intrinsic variables, the pulsating stars show periodic expansions and contractions of their surface layers. Pulsations may be radial or non-radial, depending on whether the stellar form does or does not periodically deviate from the spherical shape. Pulsating variable stars are usually classified according to a number of pulsation parameters that include: the period, amplitude, evolutionary phase and the stellar population to which they belong.

In this thesis variable stars are used as a *tool* for a better understanding on how the Milky Way halo formed. Thus we concentrate on the pulsating variable stars and, according to the time sampling of our observations, we will mainly refer to

short period variables with periods $P \leq 3$ d.

2.1 Pulsating Variable Stars

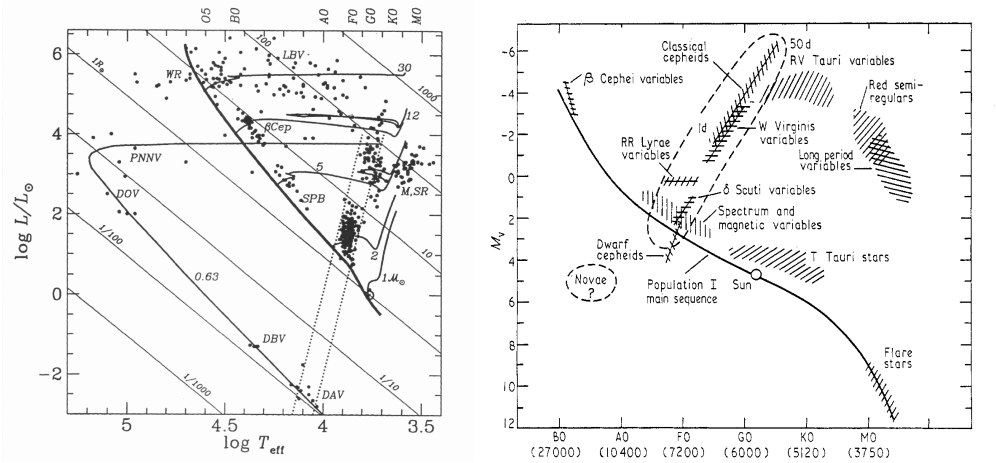

Figure 2.1 Left panel: position of the different types of intrinsic variable stars in the $\log L/L_{\odot} - logT_{eff}$ plane. Right panel: zoom of the effective temperature region from 3.4 to 4.4 in $\log T_{eff}$. Evolutionary tracks for different mass values and lines of constant radii are also shown (see left panel of the figure). Dotted lines and an oval-shaped region mark the *Classical Instability Strip* (from Gautschy & Saio 1995; Cox 1974, respectively). Labels indicate the different types of variables in the left panel of the figure. WR: Wolf-Rayet stars; LBV: Luminous Blue Variables; SPB: Slowly Pulsating B Stars; M: Mira variables; SR: Semiregular variables; PNNV: Variable Planetary Nebulae Nuclei; DIV, DDB, DAV: White Dwarf Variables of DO, DB and DA types.

Pulsating variable stars generally occupy a well defined region in the theoretical Hertzsprung-Russell (H-R) diagram, as well as in its observational counterpart, the Color-Magnitude diagram (CMD). This *locus* is called the *Classical Instability Strip*. The position of different types of intrinsic variables in the H-R and CM diagrams are shown in Figures 2.1 and 2.2, respectively. Two dotted lines and an oval-shaped region mark the *Classical Instability Strip* in the two panels of Figures 2.1. When the evolutionary track of a star, no matter the mass, crosses this region, the stellar envelope becomes unstable and the star starts the pulsation. Different types of pulsating variable stars are found across the *Classical Instability Strip*. In order of decreasing luminosity, we find: the Classical Cepheids (δ Cephei), the Population II Cepheids (W Virginis and BL Herculis stars), the Anomalous Cepheids, the RR Lyrae stars, and the δ Scuti and SX Phoenicis variables. Main characteristics of the variable stars in the *Classical Instability Strip* are summarized in Tab. 2.1.

The main characteristic of a pulsating star is the period of the light/radial velocity variations, an important observable, that can be estimated at great precision and is unaffected by distance and reddening. The light variation makes a variable easy to recognize among other stars even in very crowded regions, as the center of globular clusters, or in distant compact galaxies dominated by young stars. Indeed,

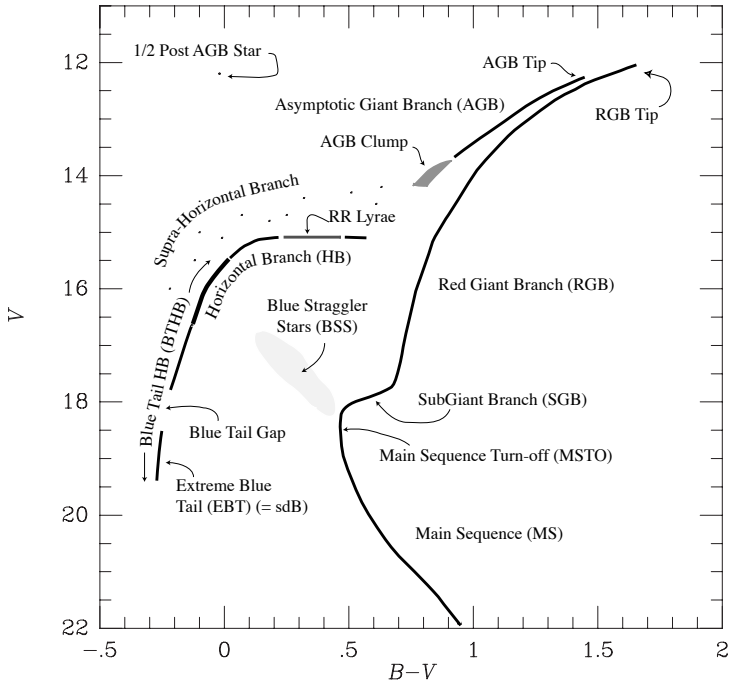

Figure 2.2 Schematic V-$B-V$ CMD displaying different evolutionary phases for stars in a globular clusters (from Rood et al. 1998).

Table 2.1 Classification and main characteristics of the pulsating stars in the *Classical Instability Strip*.

Type	Period (day)	$< M_V >$ (mag)	A_V (mag)	Spectral Type	Pop.	Evol. Phase
δ Scuti	≤ 0.02	$2 \div 3$	≤ 0.5	A-F	I	MS
SX Phoenicis	≤ 0.1	$2 \div 3$	<1.5	A-F	II	MS
RR Lyrae ab-type	$0.45 \div 1$	$0.0 \div 1.0$	$\geq 0.6 \div 1$	A2-F2	II	HB
RR Lyrae c-type	< 0.4	$0.0 \div 1.0$	$0.4 \div 0.6$	A2-F2	II	HB
Anomalous Ceph.s	$0.3 \div 2$	$-2 \div 0$	<1.5	A-F	?	HB?
W Virginis	$10 \div 50$	$-3 \div -1$	<1.5	F2-G6 (?)	II	post-HB
BL Herculis	$2 \div 10$	$-1 \div 0$	≤ 1.5	F2-G6(?)	II	post-HB
Classical Ceph.s	$1 \div 100$	$-7 \div -2$	≤ 1.5	F6-K2	I	blue loop

variable stars are now being detected and studied all over the Local Group.

Since different types of variables in the *Classical Instability Strip* are in different evolutionary phases and belong to different stellar populations, they can be used as tracers of the different components in a stellar system. Their role can become decisive when the stellar population is not simple as in a galaxy, and stars with different ages and metallicities share the same region of the CMD. RR Lyrae and SX Phoenicis stars trace the oldest populations (t $\geq$ 10 Gyr) in a galaxy, the Anomalous Cepheids the intermediate-age stars, and the Classical Cepheids and the δ Scuti stars the young population.

Pulsating variable stars such as the RR Lyrae stars and the Cepheids are also

standard candles to measure the distance of the host systems. The period-luminosity relation of Classical Cepheids and the luminosity-metallicity relation for RR Lyrae stars are powerful methods for determining the astronomical distance scale.

In the following subsections we present a description of the main characteristics of the types of variables that we have detected and studied in this thesis.

2.1.1 δ Scuti and SX Phoenicis Stars

Stars with masses in the range $1.5 < M/M_{\odot} < 2.5$ enter the lower part of the *Classical Instability Strip* either in their core-hydrogen burning phase or when they move towards the sub-giant branch during their shell-hydrogen burning phase. Their oscillation periods are in the range $0.02 < P < 0.25$ d (i.e. from 1 to 6 hours), and typically < 0.20 d with amplitudes typically of the order of a few tenth of a magnitude in the V band. These variable are called δ Scuti (δ Sct) stars if they are rich in metals ($Z > 0.01$, or SX Phoenicis (SX Phe) stars if they are metal poor ($Z < 6 \times 10^{-3}$, [Fe/H] < -0.5 dex). In the Milky Way there is a physical distinction between δ Sct and SX Phe stars: the δ Scuti are Population I (Pop. I) stars, while the SX Phoenicis trace the metal poor Population II (Pop. II) stars. Amplitudes of the Pop. I stars can vary from a few 0.001 mag to several 0.1 mag. Even if high–amplitude δ Sct (HADS) stars are generally radial pulsators, several of these variables also exhibit non-radial modes (Poretti, 2003). In similar way, SX Phe stars show a mixture of modes, especially those found in globular clusters. Therefore, the separation between HADS and SX Phe stars is not an easy task if no details about the metal abundance are known. Since the light curves of both HADS and SX Phe stars are asymmetrical and resemble those of the Classical Cepheids, and since these variables too do obey to a Period - Luminosity relation, it is quite common to group both HADS and SX Phe stars under the common term "Dwarf Cepheids". ($P - L$) relation. This term, however, has unclear meaning in the astrophysical context, since it groups stars belonging to different populations. Therefore, while it is appropriate to use the SX Phe term to identify the short–period variables found in Pop. II simple systems like the globular clusters, it is more appropriate to retain the distinction between HADS and SX Phe stars when considering mixed population environments such as the Milky Way and the other galaxies, where stars of different ages and metallicities are both present. An excellent review of the properties of these stars can be found in Breger (2000).

Since these variables obey a $P - L$ relation they can be utilized as standard candles to find distances. Their use as distance indicators has made some progress in the last years, particularly in the case of globular clusters Pych et al. (see e.g. 2001); Mazur et al. (see e.g. 2003). On the other hand, given their intrinsic faintness and the short time scale of their variations, the known samples of δ Scuti stars almost exclusively belong to the Milky Way where they are found in the field and in both globular and open clusters (Nemec et al., 1994; Rodríguez & López-González, 2000; Rodríguez et al., 2000) Since their detection requires time-consuming observations reaching about 2-3 magnitudes below the horizontal branch (HB) of the old population, after the pioneering studies in Carina by Mateo et al. (1998) and Poretti (1999) who reanalyzed the Carina dwarf Cepheids (δ Scuti stars)

discovered by Mateo et al., so far only few further of these variables have been identified in systems external to the Milky Way. Namely, about 30 δ Scuti stars have been discovered in the LMC (Clementini et al., 2003; Di Fabrizio et al., 2005; Kaluzny & Rucinski, 2003; Soszynski et al., 2003; Kaluzny et al., 2006) and used by McNamara et al. (2007) to define the $P - L$ relation of the Large Magellanic Cloud (LMC) and to calculate the distance to the LMC.

Finally, about 90 SX Phoenicis variables have been found in the Fornax dSph galaxy in the course of this thesis (see Section 3). They represent the largest sample of SX Phe stars ever detected in an extragalactic system.

2.1.2 RR Lyrae Stars

RR Lyrae stars are radial pulsators with period in the range $0.2 < P < 1.0$ d. They are helium burning stars that entered the Zero Age Main Sequence (ZAMS) with masses around 1 $M_{\odot}$. During the horizontal branch of their evolution, they cross the *Instability Strip* and their envelopes become unstable. The position that an RR Lyrae star occupies inside the strip depends on the amount of mass the star has lost in the previous red giant branch evolutionary phase, the higher being the mass loss the bluer being the star's color.

Being stars of little mass, it has taken them almost an Hubble time ($t > 8$ Gyr) to reach the HB. Thus, the RR Lyrae stars represent the ancient component of the systems to which they belong, and are optimal tracers of populations older than 10 Gyr both in the Milky Way and in the external galaxies. They are quite luminous A-F giants, and have been found in all the LG systems where they have been searched for, including the field (Brown et al., 2004a) and the globular clusters (Clementini et al., 2001) of the Andromeda galaxy. Indeed, they are the most common and numerous type of variables in the LG, and are the typical variables found in globular clusters. The presence of RR Lyrae stars in almost all the LG galaxies does testify that star formation begun about $8 - 10$ Gyr ago in all the Local Universe. Being so old, they eye-witnessed the epochs of the Galactic halo formation and thus can bear crucial informations on how the Galaxy built up (see Section 1.4).

Based on the shape of the light curves, Bailey (1899, 1900) divided the RR Lyrae stars into two main groups: the *ab*- type (RRab), fundamental mode pulsators with relatively high amplitude ($0.4 < A_V < 1.5$ mag), asymmetric light curves and periods in the range from $\sim$ 0.45 to 1 d; and the *c*- type (RRc), first overtone pulsators, with smaller amplitudes ($0.2 < A_V < 0.6$ mag), sinusoidal light curves and periods in the range from $\sim$ 0.2 to 0.4 d. Some RR Lyrae stars show simultaneous excitation of two pulsation modes: they are called double-mode RR Lyrae stars or *d*- type (RRd). For RRd stars the ratio between first overtone (P_1) and fundamental mode (P_0) periods appears to be a function of both star mass and luminosity: $P_0/P_1 = f(M, L)$. This period ratio can be used to get an estimate of the star pulsation mass by comparing P_1/P_0 and P_0 with the predictions of theoretical pulsation models at different metallicities (the Petersen diagram, Petersen 1972). Finally, about 20-30% of the *ab*-type RR Lyrae stars show long term modulations of the amplitude and shape of their light curves (with typical periodicities of $10 - 500$ d). This phenomenon is known as Blazhko Effect (Blazhko, 1907) and its causes are still not understood.

The location of the RR Lyrae on the HB makes them to have approximately the same $langleV\rangle$ luminosity. So they have been extensively used to determine distances of Galactic globular clusters where other standard candles like the Classical Cepheids are missing, or other distance indicators like the tip of the Red Giant branch are scarcely populated, as well as of galaxies prevalently hosting an old stellar population.

The V absolute magnitude of the RR Lyrae stars is known to be a function of metallicity (Sandage, 1981a,b) through a relation generally assumed to be of linear form:

$$M_V(\mathrm{RR}) = \alpha \times [\mathrm{Fe/H}] + \beta \tag{2.1}$$

Sandage (1981a,b) derived empirically a rather high value of 0.35 mag/dex for the slope α of this relation. Subsequent estimates based on the Baade-Wesselink method (Fernley et al., 1998) and on synthetic Horizontal Branch models (Lee et al., 1990, 1994) found "shallower" values , around $0.17 \simeq 0.20$ mag/dex. Most recent values of α were derived by Clementini et al. (2003) and Gratton et al. (2004) using more than a hundred RR Lyrae stars in the LMC: α=0.214 mag/dex ± 0.047; and by Rich et al. (2005): α=0.20 mag/dex ± 0.09, from the HB luminosity of 20 globular clusters in M31.

It should be noted that, regardless the assumed input physics, all evolutionary models (Dorman, 1992; Caloi et al., 1997; Cassisi et al., 1999; Ferraro et al., 1999; Demarque et al., 2000a; VandenBerg et al., 2000) as well as the pulsation (Caputo et al., 2000) suggest that the RR Lyrae $M_V - \mathrm{Fe/H}$ relation may be not unique and not strictly linear. Furthermore, the evolutionary tracks show that RR Lyrae stars evolve with different luminousities depending on whether their originate from the blue or the red side of the instability strip. At fixed metallicities, RR Lyrae stars should be more luminous in clusters with blue horizontal branch morphologies than in red horizontal branch clusters. Finally the evolution of RR Lyrae stars inside the instability strip causes an intrinsic spread in the horizontal branch luminosity varying from $\simeq 0.1$ to 0.5 mag as a function of the metallicity (Sandage, 1990). However, since a fit over the metallicity range $-2.2 < [\mathrm{Fe/H}] < 0.0$ dex) leads to maximum deviations of only 0.04 mag in $M_V(\mathrm{RR})$ of a simple linear fit from the relationships derived directly from the models, it's justified to assume a linear relation between $M_V(\mathrm{RR})$ and $[\mathrm{Fe/H}]$ for distance determinations (Chaboyer, 1999).

In the remaining of this thesis we shall adopt the "shallow slope" $\alpha = 0.214 \pm 0.047$ mag/dex, in agreement with Clementini et al. (2003) and Gratton et al. (2004)

Many estimates of the zero point β or, alternatively, of $< M_V(\mathrm{RR}) >$ at fixed metal abundance, can be found in the literature. We will assume $< M_V(\mathrm{RR}) >= 0.59 \pm 0.03$ mag that was derived by Cacciari & Clementini (2003) from the weighted average of several independent $M_V(\mathrm{RR})$ determinations based on different methods, both theoretical (e.g. pulsation and evolutionary models) and observational (e.g. statistical and trigonometric parallaxes).

2.1.3 Anomalous Cepheids

Anomalous Cepheids are helium burning, $M \leq 2.5 M_{\odot}$ stars older than ~ 1 Gyr, from about 0.5 to 2 mag brighter than the RR Lyrae stars, with typical periods in the range from 0.3 to 2 d. From an evolutionary point of view, they are doing the hooks of intermediate-age He-burning stars that reach the instability strip only for metal abundances as low as $[\mathrm{Fe/H}] \sim 10^{-4}$ (Norris & Zinn, 1975). First observed in the Draco dwarf spheroidal galaxy by Baade & Swope (1961), they occur in all the known dwarf spheroidal galaxies of the Local Group (see Pritzl et al., 2002, and reference therein). They have been found also in some dwarf Irregular galaxies (the Magellanic Clouds, Graham 1975; Smith et al. 1992; Di Fabrizio et al. 2005), but only very few are known in the Milky Way: an Anomalous Cepheid has been found in NGC 5466 by Nemec et al. (1994), and a couple in ω Centauri by Kaluzny et al. (1997). Zinn & Searle (1976) named them Anomalous Cepheids because they do not follow the period-luminosity relation of Classical and Population II Cepheids but obey their own $P - L$.

2.2 Strategy

In this thesis we have identified and studied the variable star populations in a number of different LG stellar systems (the Fornax and Bootes dSph's, and the MW globular cluster NGC 2419) using a homogeneous and consistent approach based on most suited and up-to-date observing strategies and data analysis techniques. Important assets of our study have been (1) the collection of time-series photometric data with wide field imagers (WFIs) and large aperture telescopes (e.g. the WFIs of the ESO/MPI 2.2-m and CTIO 4-m Blanco telescopes, the 2.3-m WIRO, the 3.5-m TNG, the 6.5-m LCO/Magellan and the 8-m SUBARU telescopes) covering large areas ($\sim$ 1 deg^2) of the target systems, and the implementation of the proprietary data with Hubble Space Telescope WFPC2 archive data; (2) the use of best-performing point-spread-function (PSF) reduction packages (DAOPHOT/ALLSTAR/ALLFRAME, Stetson 1994, 1996) to perform the photometric reductions, of both ground-based and HST datasets; (3) the detection of the variable stars with the Image Subtraction Technique (see Section 2.2), namely the package ISIS2.1 (Alard, 2000) and the SuperMacho pipeline (Rest et al., 2005); (4) the use of custom software specifically developed to study periodic variables (Graphic Analyzer of TIme Series, Di Fabrizio 1999; Clementini et al. 2000) to fit the light curves and finally get the star pulsation parameters (period, amplitude and mean luminosity).

The studies in this thesis are part of a large international collaboration involving researchers from the Pontificia Università de Chile (PUC) and the Michigan State University, as well as from the Padova, Napoli and Milano-Merate Observatories.

2.2.1 Identification of the variable stars

Variable stars in the stellar systems analyzed in this thesis were generally identified using packages based on the Image Subtraction Technique (ISIS2.1, Alard 2000, and the SuperMacho pipeline, Rest et al. 2005). Here we briefly describe the

standard procedure that was applied to the data, as performed within the package ISIS2.1 (Alard, 2000); application of the technique to specific objects is then described more in detail in the following chapters of this thesis.

First applied in the large scale surveys of the LMC by the MACHO (Alcock et al., 2000) and OGLE (Alard, 1999; Pigulski et al., 2003) collaborations, the Image Subtraction Technique is a very powerful method which allows to detect variable sources in very crowded regions, (e.g. the inner region of an extragalactic globular cluster observed with ground-based telescopes), from differential flux measurements of the sources.

The flux of a star in each frame of a temporal sequence is described by a constant part plus a portion varying from frame to frame along the time series:

$$F_{i,tot} = F_0 + \Delta F_i \tag{2.2}$$

Non variable stars have $\Delta F_i = 0$

ISIS2.1 was run on each photometric band of our datasets independently. For each photometric band ISIS2.1 creates a reference image by stacking a selection of the frames taken in best seeing conditions. This image is called "ref.fits". Each individual frame of the time-series was then subtracted from the reference image after having been convolved with a suitable kernel to match seeing variations and geometrical distortions of the individual images.

$$F_{i,image} = F_{i,ref} - F_{i,image} \tag{2.3}$$

The output of ISIS2.1 is a median image of all difference frames (called "var.fits"), in which non-variable objects disappear and candidate variable ($\Delta F_i \neq 0$) sources stand out as positive (bright) or negative (dark) peaks. ISIS2.1 automatically masks pixels with flux higher than a threshold defined by the parameter "saturation". However, only the very central pixels of the saturated stars are actually masked, while pixels around the saturated stellar cores may still appear on the "var.fits" and produce many false detections. Selection of true candidate variables on the "var.fits" frames is done "by eye", excluding false detections due to CCD bad columns and hot pixels, passage of satellites, and saturated objects. Since defects of each image of the time-series are reflected in the "var.fits", only about 10% of the detections generally turns out to be *bona fide* candidate variable stars.

Candidate variables identified by ISIS are then counter-identified against the photometric catalogues produced by the DAOPHOT/ALLSTAR/ALLFRAME photometric reductions of the time-series data, and then studied to define the periods and produce the multiband light curves. ISIS2.1 produces also differential flux light curves that were used to derive periods and infer the type of variability for variables in the very internal regions of the Fornax dSph globular clusters where we lack reliable PSF photometry.

Chapter 3

Variable Stars in the Field of the Fornax dSph

The Fornax dSph, one of the 9 traditional dwarf spheroidal satellites of the Milky Way, was first detected by Shapley (1939) on Harvard blue photographic plates. It looked like a diffuse system which could be separated into individual stars only by the most powerful telescopes of the time. The galaxy is located at $138\pm$ 8 kpc from the Milky Way (Mateo et al., 1998) and covers a large area on the sky. Its tidal radius is $71' \pm 14$ (Irwin & Hatzidimitriou, 1995b), corresponding to 2.85 ± 0.16 pc.

It is the most massive and luminous among the undisrupted dSph's (Mateo et al., 1998). Its mass calculated from a best-fit King profile, is $6.8 \times 10^7\ M_\odot$ and the absolute magnitude in the V band is $M_V = -13.2$ mag. Only the Sagittarius dSph is more luminous and massive. Like the Sgr and the CMa dSph's Fornax has a system of globular clusters. The galaxy main characteristics are summarized in Tab. 3.1

The Fornax dSph is an interesting object both in terms of star formation history and chemical enrichment. It shows a wide range in metal abundance ($-2.0 \leq$ [Fe/H] ≤ -0.4) with mean value -0.9 dex (see e.g. Pont et al., 2004), a characteristic shared only by the Sgr among the Milky Way dSph satellites. Saviane et al. (2000) find that stars in Fornax can be divided into three main classes: (i) an old population (t$>$ 10 Gyr) identified by the old horizontal branch, the old red giant branch (RGB) and the RR Lyrae stars; (ii) an intermediate-age population, represented by the upper asymptotic giant branch (AGB), part of the RGB, and the red clump, and; (iii) a population of young main sequence stars (t $\leq$ 2 Gyr) that may include stars as young as 200 Myr. In conclusion, the star formation in Fornax appears to have started approximately 12 Gyr ago and have been continuing almost to the present day (Tolstoy et al., 2003). Maybe such a continuous star formation history could have been triggered by tidal interaction with the Milky Way.

Pont et al. (2004) find that the galaxy metal abundance rose to [Fe/H] ~ -1.0 within the first few Gyrs, and that the system has also experienced a significant increase in chemical enrichment in the last $\sim$4 Gyr. The chemical enrichment

Table 3.1 Fornax dSph characteristics (Mateo et al., 1998).

α_{2000}	02:39:59	
δ_{2000}	$-34:27.0$	
l	237.1	
b	-65.7	
R_c	13.8±0.8	arcmin
R_t	71±4	arcmin
e	0.31±0.03	
M_V	-13.2	mag
M_B	-12.6	mag
$(B-V)_T$	0.63±0.05	mag
V_T	7.6±0.3	mag
$(m-M)_0$	20.70±0.12	mag
E(B-V)	0.03±0.01	mag
M_{TOT}	68 $\times 10^6$	$M_\odot$
M_{HI}/M	0.001	
$(M/L)_{0,V}$	4.4[a]	$(M/L)_0$
$< [Fe/H] >$	-1.3 ± 0.2	[b]
σ_*	10.5±1.5	km s^{-1}
$V_\odot$	53±3	km s^{-1}

[a] Mass to light ratio in the V band: M_{tot}/L_V; [b] average metal abundance ($< [Fe/H] >$) of the old and intermediate age populations.

history of Fornax makes the galaxy more similar to the LMC or the Galactic disk rather than to the other Milky Way dwarf satellites. Fornax dSph has also been able to retain substantial amounts of metals during its evolution, as hinted by the width of its RGB (Saviane et al., 2000). Thus the metal content of a galaxy seems better related to the system ability to retain the produced metals, which may have to do with effects of SNe explosions on the interstellar medium, and the depth of the galaxy potential well (Ferrara & Tolstoy, 2000, and reference therein) rather than to the star formation history itself.

The various stellar populations show different spatial distributions throughout Fornax. The old and intermediate stars have the most extended distribution, while the young main sequence stars are more centrally concentrated, and appear to define a bar with position angle of the major axis offset by approximately 30° from that of the galaxy (Coleman et al., 2005). It is also possible that the young stars are concentrated towards both ends of this bar, suggesting a "bilateral rather than a rotationally symmetric structure" (Stetson et al., 1998). Thus, the recent star formation appears to have occurred irregularly throughout Fornax (Coleman et al., 2005). Given its recent star formation, one might expect to detect H I in Fornax. However, Young (1999) did not find H I in the galaxy center at a column density detection limit of 4.6×10^{18} cm^{-2}, nor at a limit of 7.9×10^{18} cm^{-2} within one core radius (i.e., $M_{HI} < 0.7 \times 10^6$ M$_\odot$). They concluded that the bursts of star formation ionized the gas or possibly ejected it beyond their search area. But other mechanisms such as ram-pressure stripping may also explain how the galaxy got rid of its gas.

Lynden-Bell (1976, 1982), Kunkel & Demers (1976) and Kunkel (1979) pointed out that the Galaxy's dSph companions, as well as a number of globular clusters, seem to collect along distinct planar alignments and suggested that these alignments reflect distinct *orbital* planes. One of these orbital planes is the Magellanic plane which consists of the Magellanic Clouds, the H I gas trailing the Magellanic clouds (also known as the Magellanic Stream), and the Ursa Minor, Draco, and Carina dSph's. A second plane includes Fornax, Leo I, Leo II and Sculptor. Majewski (1994) re-investigates this issue and adds Sextans and perhaps Phoenix to the Fornax-Leo-Sculptor alignment, which is now known as the FL^{2}S^2 plane. To explain the alignments, a common origin via the disruption of larger satellites orbiting in these planes is usually invoked, with the smaller dSphs forming as tidal condensations or broken-off fragments during the dynamical interaction between the Milky Way and a massive satellite (Kroupa, 1997), much like the tidal dwarfs seen in extragalactic contexts (see e.g. Knierman et al., 2003). As parent satellites have been proposed the LMC for the Magellanic plane, and the Fornax dSph for the FL^{2}S^2 plane (Lynden-Bell, 1982). To ascertain these spatial alignments one should test whether the member objects share a common angular momentum. This requires determining the dSph's absolute proper motions.

Studies of the kinematic properties of the Fornax field stars indicated a central mass-to-light ratio $M/L \gtrsim 5(M/L_{\rm V})_\odot$, possibly as high as 26 (e.g. Mateo et al., 1998), and a global $M/L_{\rm V} \sim$ 10-40, hence larger than the $M/L_{\rm V}$ of the luminous component (Walker et al., 2006). The approximately spherical shape of Fornax is incompatible with tidal models used to explain the high internal stellar velocity

dispersions observed in many dwarf spheroidal galaxies. Therefore, dark matter dominance is suggested.

Coleman et al. (2004, 2005) examined the overdensity of stars situated approximately $17'$ from the center of the Fornax dSph. This overdensity seems not correlated to any previously reported asymmetry in the distribution of the Fornax stars. They have determined the surface brightness and dimensions of this feature by using accurate photometry down to the red clump at $V = 21$. They found that the overdensity is dominated by a relatively young main sequence stellar population and argue that the clump of stars may be the first detection of a shell structure in a dwarf galaxy. The origin of the shell could be a tidal interaction between Fornax and the Milky Way similar to that occurring between the Galaxy and the Ursa Minor dSph (UMi; Martínez-Delgado et al. 2001; Bellazzini et al. 2002; Palma et al. 2003 and Kleyna et al. 2003). However, the Fornax dSph is more massive and far away and the MW tidal forces less strong than for UMi. Moreover, the stellar population in the shell differs from the bulk of the Fornax stars. A tidal explanation for the shell shall foresee the same stellar populations as seen in the rest of the galaxy.

They propose then that the Fornax dSph experienced a merging event with a relatively gas-rich low mass dwarf galaxy approximately 2 Gyr ago. The gas accreted from the companion triggered a new burst of star formation and what we currently see in the shell are both the new population and the ancient stars once belonging to the accreted dwarf (see also Olszewski et al., 2006). A recent accretion event, is also suggested by Battaglia et al. (2006) that based on spectroscopic studies, find that the ancient stellar population in the center of Fornax does not exhibit equilibrium kinematics. They interpret this evidence as the signature of a relatively recent accretion of external material.

3.1 The Fornax Project

The study of the Fornax dSph described in this thesis is part of the Fornax Project (Clementini et al., 2003), an international collaboration set up to make a comprehensive and deep study of the short period variable stars in the field and in the globular clusters (GCs) of this dSph galaxy. Previous studies of variable stars in Fornax include a survey of the 0.5 deg^2 central region of the galaxy by Bersier & Wood (2002), and the detection of candidate variable stars in Fornax dSph clusters 1, 2, 3 and 5, based on HST archive data by Mackey & Gilmore (2003b). Both these studies were lacking in several respects, since they were either too shallow, or spanned a too short time baseline to reliably determine the pulsation characteristics and to detect variables as faint as the Dwarf Cepheids (DCs) in Fornax. Our survey supersedes these previous works in spatial coverage, time resolution, depth and photometric accuracy. Data collection and variable star identification strategies of the Fornax Project were optimized to cover the *Classical Instability Strip* of the Fornax dSph field and globular clusters from $V \sim 24 - 25$ mag to $V \sim 19$ mag. This magnitude range encompasses the galaxy RR Lyrae stars, DCs, Anomalous Cepheids (ACs) and Population II Cepheids (P2Cs). For all these types of variables we have been obtaining well sampled, deep and accurate light curves allowing independent estimates of the star's periods and pulsation properties.

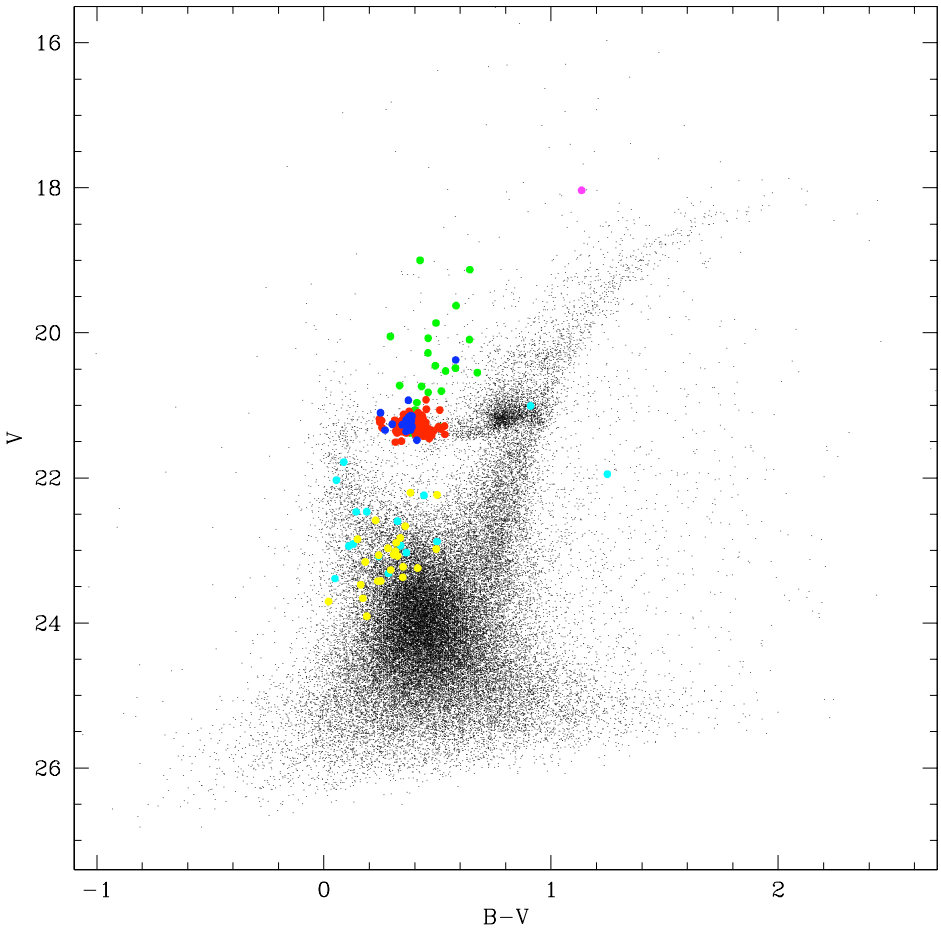

Figure 3.1 Color-Magnitude of a 0.04 deg^2 of the Fornax dSph field. Variable stars populating the *Classical Instability Strip* are shown by solid circles of different colours. Candidate Semiregular variable: magenta; Cepheids: green; *ab*- and *c*- type RR Lyrae stars: red; *double mode* RR Lyrae stars: blue; eclipsing binaries: cyan; Dwarf Cepheids: yellow.

3.2 Observations and Data Reductions

Our dataset on the Fornax dSph field consists of deep ($V \sim$ 24-26 mag), high accuracy, well-sampled B, V time-series data covering about 1 deg^2 of the galaxy, obtained with the WFI of the 2.2m ESO-MPI and the 8-CCD's mosaic of the 4-m Blanco CTIO telescopes, through two adjacent pointings at each telescope, respectively: Field_1 and Field_2 at the 2.2-m ESO, and CTIO_1 and CTIO_2 at the 4-m Blanco telescope.

High spatial resolution photometry of 4 of the Fornax globular clusters was also obtained with the 6.5 m LCO Magellan/Clay telescope and complemented with with WFPC2@HST archive data. The cluster's dataset will be discussed in Chapter 4. Observations were optimized to allow a good sampling of the DCs light curves (typical periods $P \leq$0.2 d) and to detect brighter variables with periods $P \lesssim$ 2 d (e.g. ACs). They extended over a time interval of 2 years from 2002 November to 2004 October (see Table 3.2).

Table 3.2 Photometric data of the Fornax dSph field.

Target	α_{2000}	δ_{2000}	Dates	Telescope & Instrum.	FOV	N_V	N_B
Field_1(For 3)	$02^h39^m59^s$	$-34^\circ10'00''$	3 nights, Nov. 2002	2.2 m ESO WFI	$33' \times 34'$	17	61
Field_2(For 2,4)	$02^h39^m45^s$	$-34^\circ39'00''$	4 nights, Nov. 2004	2.2 m ESO WFI	$33' \times 34'$	16	59
Field_A(For 4,5)	$02^h41^m05^s$	$-34^\circ17'30''$	3 nights, Nov. 2003	4 m CTIO WFI	$36' \times 36'$	145	64
Field_B(For 2,3,4)	$02^h39^m24^s$	$-34^\circ33'16''$	2 nights, Oct. 2004	4 m CTIO WFI	$36' \times 36'$	16	8

Point-spread-function (PSF) photometry of the time series data was performed with DAOPHOT-ALLSTAR II (Stetson, 1996) and ALLFRAME (Stetson, 1994). Variable stars were identified with the Image-Subtraction Method as performed within the package ISIS2.1 (Alard 2000), for the 2.2 m ESO WFI data and the SuperMACHO pipeline (Rest et al. 2005), for the 4 m CTIO WFI data. Both packages are optimized to detect variable stars in crowded fields, and are much more effective than traditional techniques to identifying low-amplitude, faint variables such as the DCs. Data analysis is still in progress, and here we present partial results on the variable stars found in the four lower chips of the 2.2 m ESO WFI mosaic covering a $33' \times 34'$ portion of Fornax centered at $\alpha_{2000} = 02^h39^m59^s$, $\delta_{2000} = -34^\circ10'00''$ (hereafter Fornax Field_1).

3.3 Variable Stars in the Fornax dSph Field_1

The 4 lower CCDs of Fornax Field_1 cover an area of about 0.16 deg^2, that includes the cluster Fornax 3 on Chip 6 of the WFI mosaic. They are found to contain 706 candidate variable stars. We have already confirmed and classified 355 of them. Study of the remaining objects is in progress. This number gives a lower limit for the variable star density in Fornax twice as large as that derived by Bersier & Wood (2002), corresponding to more than 2000 variable stars in the total area of Fornax we have surveyed. The variables classified in types include: 247 RR Lyrae

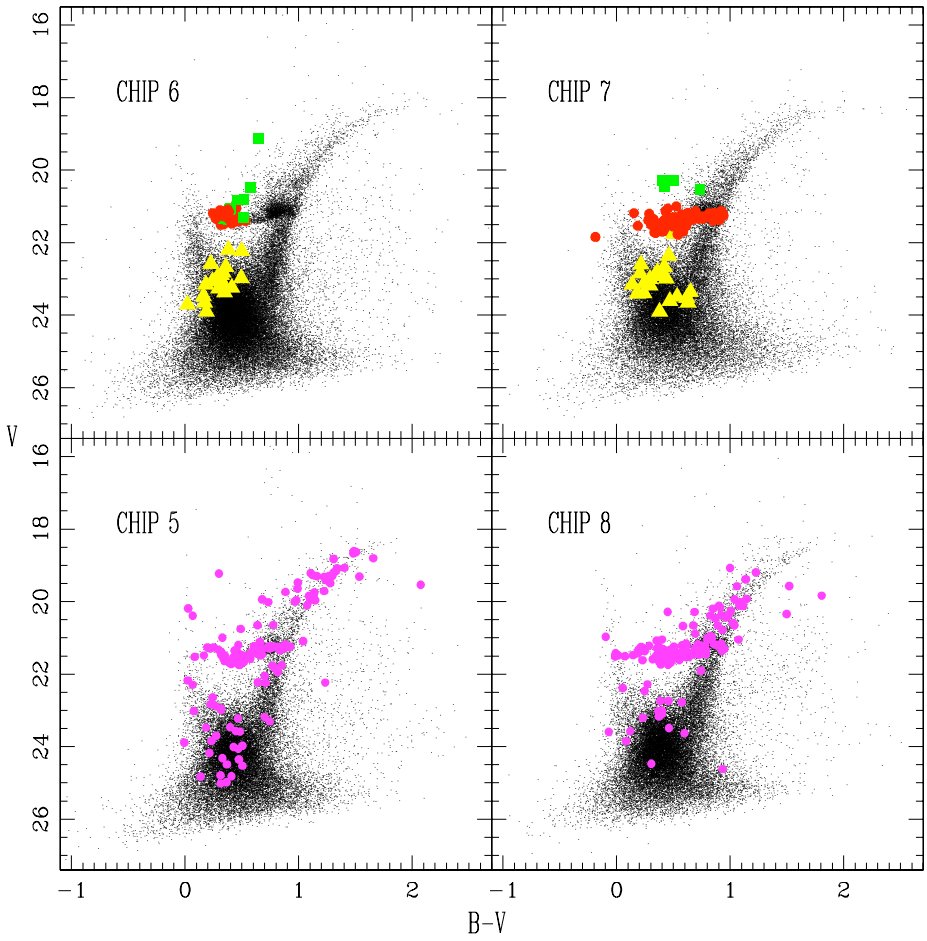

Figure 3.2 Color-magnitude diagrams of the lower 4 CCDs of Fornax Field_1. Different symbols in the two upper panels of the figure indicate: RR Lyrae stars (filled circles), ACs (filled squares), and DCs (triangles). Filled circles in the two lower panels are candidate variables not yet classified. According to the location on the horizontal branch many of them are likely RR Lyrae stars.

stars (among which are about 50 double-mode pulsators), 11 ACs, 90 DCs, and 30 binary systems. Further 23 DCs have been identified in the 4 upper CCDs of Fornax Field_1, making a total of 67 DCs in this 0.16 deg^2 Northern portion of the galaxy. The DCs sample in Fornax is by far the largest ever observed in an extragalactic stellar system to date and, being comprised of variable stars of same type and at same distance, is indeed quite unique in number and homogeneity. The number of variables identified in the lower half portion of Fornax Field_1 summarized in Table 3.3.

Fig. 3.2 shows the color-magnitude diagrams of the four lower CCDs of Fornax Field_1 with the variable stars marked by filled symbols.

Table 3.3 Candidate variables in the lower four CCDs of the Fornax dSph Field_1.

CCD	RR Lyrae stars	ACs	DCs	Binaries	Total
Chip 6[a]	110	11	23	15	159
Chip 7	137	–	23	15	175
Chip 5	–	–	7	–	209[b]
Chip 8	–	–	14	–	163[b]

[a] Numbers for Chip 6 include variables belonging to For 3(see Chapter 4. [b] The study of the light curves and the classification in types for the variables in Chip 5 and 8 is still in progress, only the DCs have been classified so far. Total numbers for these two chips may include spurious detections.

We have fully analyzed the variable stars in one of these four CCDs (namely Chip 6) and found for the RR Lyrae stars average periods of 0.595 d (r.m.s.= 0.039) for the *ab*-type, and 0.361 d (r.m.s.= 0.040) for the *c*-type variables, respectively. Thus, similarly to other Local Group dSphs, the field RR Lyrae stars in Fornax appear to have properties "intermediate" between the two Oosterhoff types (Oosterhoff, 1939) observed among the Milky Way cluster variables (see Section 1.4). The average V magnitude of the field RR Lyrae stars in Chip 6 is: $\langle \mathrm{V(RR)_{field}} \rangle = 21.28 \pm 0.01$ mag and leads to a distance modulus of: μ_{Fornax}=20.72$\pm$0.10 mag, (on the assumption of: $M_V(RR) = 0.50$ mag at $[\mathrm{Fe/H}] = -1.5$, ; $\Delta M_V(RR)/\,[\mathrm{Fe/H}] = 0.22$ mag/dex, from Gratton et al. 2004; $E(B-V) = 0.04 \pm 0.03$, and the standard extinction law; [Fe/H]=-1.77 ± 0.20 for the average metallicity of the field RR Lyrae stars in Fornax, from Greco 2003), in very good agreement with previous distance estimates by Buonanno et al. (1999), Saviane et al. (2000), Mackey & Gilmore (2003b).

3.4 A Large and Homogeneous Sample of High–Amplitude SX Phe stars

The feasibility of detecting SX Phe stars in extragalactic systems has been fully demonstrated by our observations of the Northern portion of the Fornax dSph galaxy with the WFI@2.2-mESO/MPI telescope. Since the expected periods were very short, we took three consecutive images in B–light (700 sec each), followed by a single exposure in V–light (1000 sec). This strategy ensured the dense B time series needed to perform a reliable frequency analysis and allowed us to obtain the mean brightness and amplitude values in a two–colour system.

The Fornax galaxy is known to host "a mix of old and intermediate–age stars with different metal abundances" (Held, 2005) and therefore we should distinguish between HADS and SX Phe stars (see Section 2.1.1) in our DCs sample. However, we are prone to consider the DC variable stars we discovered in Fornax SX Phe stars, i.e., stars belonging to the old and intermediate populations. This assumption is also corroborated by the very short periods we have derive in the period search

(see Section 3.5). The average [Fe/H] value for these populations is –1.3±0.2 (Mateo et al., 1998), rather typical for Galactic SX Phe stars, but not for Galactic HADS stars.

3.4.1 The SX Phe Sample in Field_1

The time-series of the candidate variables detected by ISIS in Field_1 were analyzed to search for periodicities. We emphasize that this process was not so obvious for the SX Phe variables. Indeed, while the variability of the RR Lyrae stars shows up rather clearcut just looking at the intra-night light curves: this is not the case for the SX Phe stars, since the shorter periods and the smaller amplitudes make the regular variability hardly discernible simply plotting the data-points. For these stars we thus performed a frequency analysis by using the least–squares iterative sine–wave method (Vanicek, 1971) and applied it both to the whole time-series and to measurements of the individual nights. This procedure allowed us to reject spurious candidates, i.e., stars for which the scatter in just one night (or in a part of it) could mimic an apparent variability. In turn, we accepted as *bona fide* SX Phe stars the variables whose power spectra showed the presence of a significant peak at same frequency value in all the three nights of observation (see Dell'Arciprete (2006) for details).

Fig. 3.3 shows the depth of our survey in the Fornax Field_1. The faintest SX Phe stars have $B \sim 24.0$ and amplitudes $A_B \sim 0.50$ mag. The detectable amplitudes became smaller with increasing the star brightness and a 0.25–mag variability could be detected in stars with $B \sim 23.0$.

At the end of this procedure we have a sample of 67 confirmed SX Phe stars in the lower half portion of the Fornax Field_1, their identifications and basic properties are provided in Tables 3.4 and 3.5. Not all these SX Phe stars belong to the field of the Fornax galaxy. In Chip #6 the globular cluster Fornax 3 is resolved into stars. The close vicinity of V40765 and V38403 to Fornax 3 suggests that they are likely cluster members (see Chapter 4). On the other hand, V22094 is 1.0 mag brighter than other SX Phe stars with same period. Assuming they also have same absolute magnitude, then the distance to V22094 is 0.6 times smaller, therefore, the star probably does not belong to the Fornax galaxy. The light curve parameters (amplitudes, mean magnitudes and colours) have been calculated by means of least–squares fits. The lower panel of Fig. 3.3 shows the distribution of the standard deviations, clearly indicating an average precision of 0.08 mag.

Further 23 SX Phe stars have been detected in the upper half portion of Field_1 (analysis of these additional variables is in progress), making a total of 90 *bona fide* SX Phe variables in this Northern portion of the Fornax dSph galaxy.

Being all the *bona fide* SX Phe variables in Fornax fainter than $B \sim 22.5$, we cannot confirm the presence of smaller amplitude (<0.10 mag) pulsators in the galaxy. On the other hand, we stress the fact that the Fornax dSph is unique in richness of high–amplitude, short–period pulsators. The globular clusters ω Cen (Olech et al., 2005) and M55 (Pych et al., 2001) are also rich in SX Phe stars, but most of them have an amplitude less than <0.10 mag and they seem to pulsate in nonradial modes. The Fornax sample is a genuine sample of high–amplitude, short–period radial pulsators.

Results from this study are presented in (Poretti et al., 2007).

3.4.2 $P - L$ Relation of the Fornax SX Phe Stars

Fig. 3.4 shows the colour–magnitude diagram of the lower half portion of Fornax Field_1. All the SX Phe stars are located in a narrow $B - V$ range, below the horizontal branch, from about 0.8 to 2.0 mag below the RR Lyrae stars. The SX Phe sample is very homogeneous, and the Fornax strip appears to be larger than that observed in the Milky Way (see Fig. 2 in McNamara 2000). The most direct use of the values listed in Tab. 3.4 is to calculate the slopes of the Period–Luminosity ($P - L$) relationships defined by the Fornax field SX Phe stars. Fig. 3.5 shows the periods plotted versus the apparent V–magnitudes for the 64–stars in the galaxy field we have fully analyzed so far. This figure has a rather large scatter. The difference in magnitude between two stars having same absolute magnitude and located at opposite sides of the Fornax galaxy is about 0.10 mag (considering the galaxy tidal radius). Therefore, the cause of the dispersion in Fig. 3.5 is not geometrical. By calculating the least–squares fits we obtain a slope of -3.10 ± 0.48 in V and -2.94 ± 0.44 in B. The large error-bars are not surprising, since we are considering a very small interval in $\log P$ (from -1.35 to -0.90). We also note that there are three outliers (open circles in Fig. 3.5), clearly brighter than the rest of the sample. By omitting these three stars (V816, V19268 and V1625) the B–slope becomes -3.02 ± 0.44 and in the V–light we obtain (61 points)

$$M_V = 19.60(\pm 0.51) \; - 3.02(\pm 0.44) \times \log P \tag{3.1}$$

The standard deviation of the least–squares linear fit is $\pm$0.31 mag. Our slope values confirm the most recent values obtained in Milky Way δ Sct stars (–2.90, McNamara et al. 2004), significantly less steeper than the previous values (–3.725, McNamara 1997). The large scatter deserves some comments. Firstly, we note that it is uniform around the least–squares line (Fig. 3.5). In the case of RR Lyrae stars we have no evidence of differential reddening and therefore the origin of the scatter it likely physical, and not due to variable absorption. The scatter around a $P - L$ line is often explained by excitation of overtone modes. However, in the case of Fornax, high–order radial modes cannot be invoked to account for the observed the scatter, since their $P - L$ lines should be obviously located only in the above part (dashed lines in Fig. 3.5). An *ad hoc* explanation could be the presence of an additional lower sequence, perhaps composed of sub-luminous stars belonging to the oldest Fornax population, but this attractive hypothesis seems rather speculative at the moment. The present discussion has been focused on the 64 SX Phe stars of the Fornax field that we have fully analyzed so far. This sample is incomplete at present, since further 23 SX Phe variables have been found in this Field_1 of Fornax and a large harvest might be present in Field_2, the galaxy field covering the central region of Fornax. It seems thus reasonable to postpone any further discussion on the scatter of the $P - L$ relation to when the complete sample of SX Phe stars is Fornax will be available.

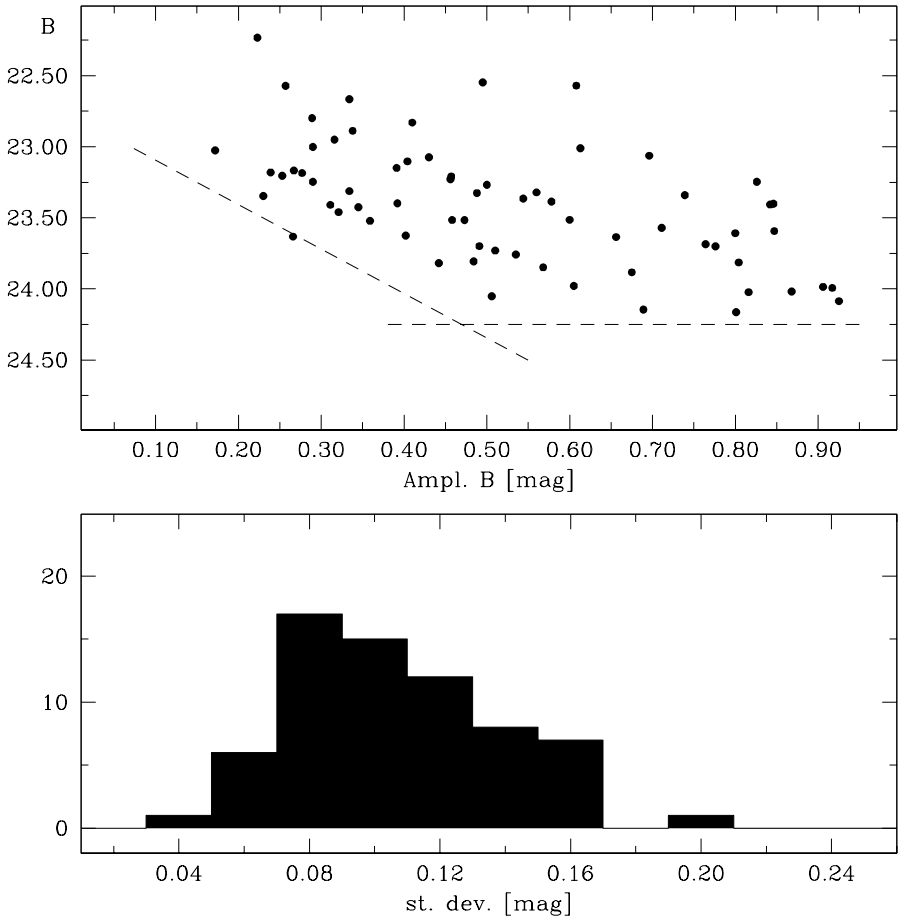

Figure 3.3 Precision and depth of our survey. Upper panel: amplitude of the detected light variability as a function of magnitude (B–light). Lower panel: distribution of the standard deviations showing the actual precision for variable stars in the $B = 22.5 - 24.0$ mag range.

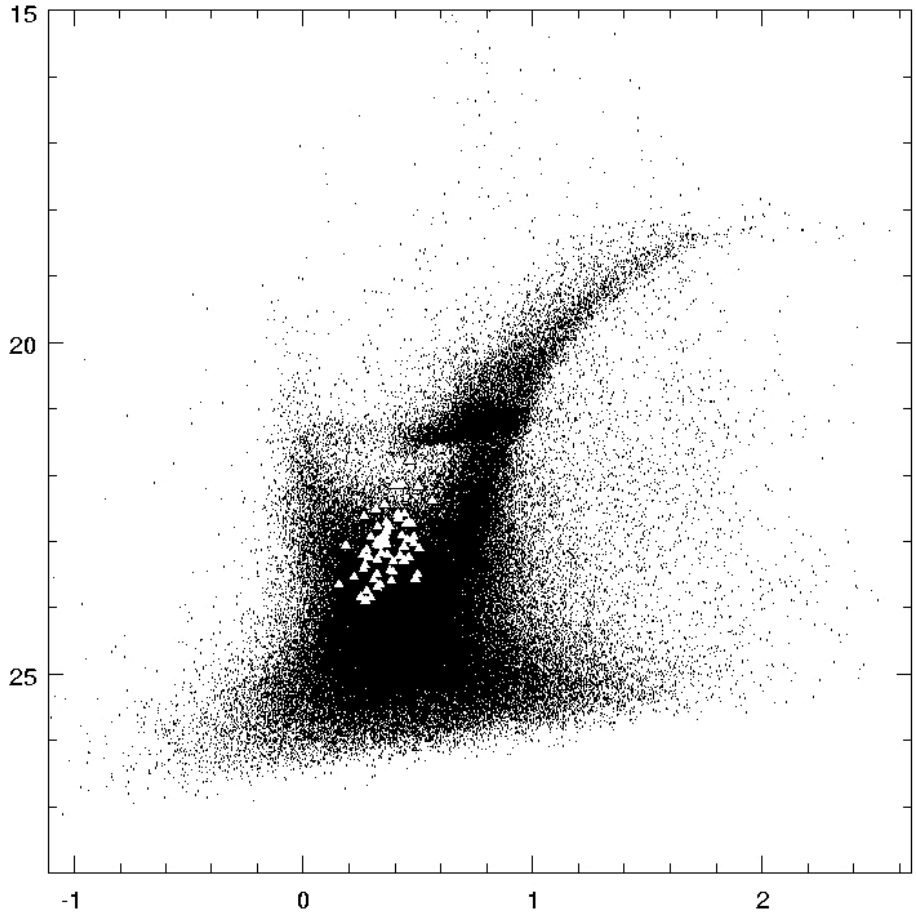

Figure 3.4 Colour–magnitude diagram of the lower half portion of Fornax Field$_1$; SX Phe stars are marked by big triangles.

3.4.3 Comparison with Other $P - L$ Relationships

We stress that the $\log P$ range covered by the Fornax SX Phe stars is half of that covered by their Milky Way counterparts. Therefore, the comparison between the two $P - L$ relationships can be made only on the short period interval covered by the Fornax variables. The $P - L$ relation of SX Phe and HADS stars in the Milky Way given by McNamara et al. (2004) is drawn in Fig. 3.5 as a dashed line. We have assumed an apparent distance modulus $(m - M)_V = 20.84$ for Fornax and [Fe/H]=–1.3 (Mateo et al., 1998) for the galaxy SX Phe stars. This modulus is consistent with that derived from the average luminosity of the RR Lyrae stars (see Section 3.3). The two lines are nearly coincident in the period range covered by the Fornax variables, strongly supporting the universal nature of the period–luminosity–metallicity relationship for SX Phe stars. We also note that Pych et al. (2001) obtained a value of –2.9 for the slope of the $P - L$ relationship in M55.

It should be noted the different period range spanned by the fundamental radial mode pulsators in different environments. In Fornax periods are in the range 0.05–0.10 d, with just a couple of stars at 0.12–0.13 d; in the Carina dSph galaxy they are even more grouped in the 0.045–0.075 d interval (Poretti, 1999); while in the LMC they are in the range 0.15–0.20 d , with just two double–mode pulsators at 0.28–0.29 d (McNamara et al., 2007). Since in the Milky Way we find pulsators spanning the full period range going from the Carina to the LMC variables, it looks like the width of the period range to be proportional to the metallicity spread observed in any given environment.

The general agreement between $P-L$ relationships of SX Phe stars in different environments allows us to infer the distance to the Fornax galaxy from its SX Phe stars. We use the $P - L$ of the Milky Way stars by (McNamara et al., 2004) and an average [Fe/H]=$-$1.3 for Fornax (Mateo et al., 1998). The average distance modulus of Fornax derived from the sample of 64 SX Phe stars is then 20.73, with standard deviation of 0.34 mag, or $m-M$=20.76, s.d. 0.30 mag if the 3 outliers stars are excluded. These values are in excellent agreement with the distance modulus value derived from the RR Lyrae stars and with the previous literature estimates (e.g. Buonanno et al., 1999; Saviane et al., 2000).

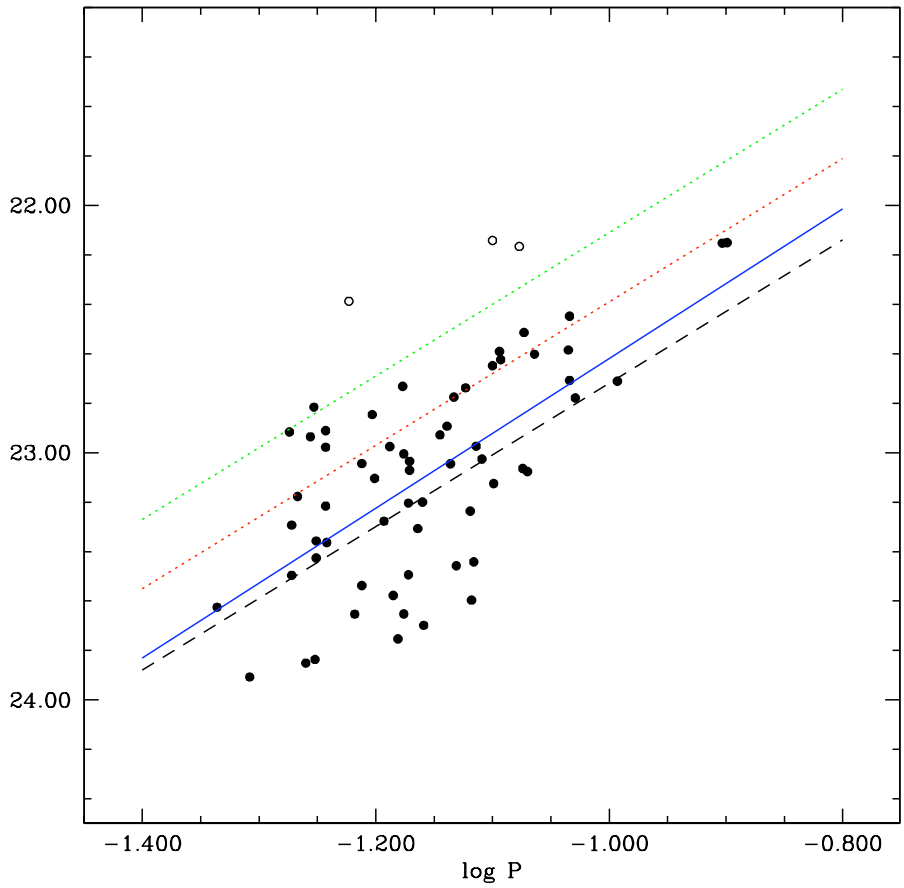

Figure 3.5 The solid line (least–squares fit) is the $P-L$ relation at V derived for the Fornax SX Phe variables discarding the three outliers marked by open circles. The dashed line is the $P-L$ relation of SX Phe and HADS stars in the Milky Way (McNamara et al., 2004) assuming $(m-M)_V$=20.84 for Fornax. The dotted lines are the $P-L$ relations of first and second overtone radial pulsators.

Table 3.4: *Bona fide* SX Phe stars in the Fornax dSph Field_1. Variable stars are listed in order of increasing period.

CCD n.	Star Id.	Period	E_{max}	$< B >$	A_B	$< B > - < V >$
8	V9899	0.04619	0.1282	24.052	0.506	0.488
7	V8618	0.04917	0.0716	24.163	0.801	0.271
5	V6170	0.05326	0.1293	23.346	0.230	0.428
5	V15474	0.05338	0.0777	23.730	0.510	0.438
5	V16343	0.05339	0.0959	23.993	0.917	0.497
7	V5215	0.05413	0.1004	23.516	0.473	0.339
6	V15390	0.05493	0.0645	24.145	0.689	0.294
7	V4659	0.05545	0.1478	23.229	0.456	0.293
7	V6056	0.05569	0.0636	23.181	0.239	0.363
7	V7347	0.05596	0.0770	24.086	0.925	0.250
7	V19493	0.05613	0.1215	23.625	0.402	0.268
6	V8812	0.05616	0.1535	23.685	0.764	0.261
7	V13345	0.05713	0.1136	23.312	0.334	0.334
7	V19309	0.05716	0.1518	23.268	0.500	0.357
6	V44543	0.05717	0.1586	23.635	0.656	0.421
7	V33186	0.05726	0.1490	23.632	0.266	0.269
8	V1625	0.05971	0.0990	22.950	0.316	0.562
6	V10371	0.06054	0.0693	23.806	0.484	0.154
6	V49021	0.06134	0.1062	23.364	0.544	0.320
8	V28121	0.06147	0.1321	23.758	0.535	0.221
6	V18889	0.06265	0.1409	23.209	0.457	0.362
5	V26561	0.06303	0.1405	23.608	0.800	0.504
6	V35797	0.06420	0.1450	23.593	0.847	0.322
6	V37637	0.06481	0.0816	23.321	0.560	0.346
6	V39151	0.06529	0.1109	23.883	0.675	0.306
5	V510	0.06596	0.1318	24.023	0.816	0.276
7	V2872	0.06661	0.0862	23.986	0.906	0.334
7	V34972	0.06662	0.1778	23.326	0.488	0.321
8	V4532	0.06668	0.1446	23.204	0.253	0.472
6	V22746	0.06722	0.1351	23.571	0.711	0.367
7	V15830	0.06729	0.1427	23.814	0.804	0.320
7	V18358	0.06739	0.1762	23.398	0.392	0.327
8	V9427	0.06741	0.1026	23.515	0.458	0.482
6	V44201	0.06849	0.1147	23.699	0.491	0.392
7	V6259	0.06921	0.2026	23.460	0.321	0.259
7	V16899	0.06945	0.1850	24.018	0.868	0.321
6	V5831	0.07168	0.0947	23.409	0.311	0.481
6	V3640	0.07256	0.0755	23.247	0.290	0.354
6	V38875	0.07316	0.1894	23.406	0.842	0.361
6	V37380	0.07362	0.0228	23.149	0.391	0.375
8	V10941	0.07373	0.1311	23.848	0.568	0.390
8	V18853	0.07531	0.1946	23.185	0.277	0.447
7	V35654	0.07598	0.2075	23.521	0.359	0.285
7	V9132	0.07623	0.2119	23.979	0.605	0.383
8	V22313	0.07669	0.1548	23.819	0.442	0.377
8	V9363	0.07694	0.2181	23.425	0.345	0.452
8	V7020	0.07776	0.1124	23.386	0.578	0.359
6	V816	0.07942	0.2044	22.572	0.257	0.431
5	V2834	0.07952	0.1944	23.063	0.696	0.415
6	V33971	0.07977	0.2224	23.401	0.846	0.275

Table 3.4: - *continued* -

CCD n.	Star Id.	Period	E_{max}	$< B >$	A_B	$< B > - < V >$
5	V2985	0.08045	0.0813	23.001	0.290	0.411
7	V25610	0.08064	0.0855	22.888	0.338	0.264
6	V19268	0.08365	0.1376	22.666	0.334	0.500
7	V1671	0.08427	0.1705	23.247	0.826	0.184
6	V14592	0.08458	0.2255	22.830	0.410	0.316
8	V20859	0.08515	0.1894	23.514	0.600	0.438
6	V10166	0.08639	0.2540	23.011	0.613	0.409
8	V10823	0.09221	0.2157	23.025	0.172	0.441
8	V30859	0.09245	0.1950	23.167	0.267	0.458
7	V19699	0.09254	0.2297	22.798	0.289	0.353
7	V21373	0.09345	0.2141	23.103	0.404	0.324
7	V32007	0.10151	0.1895	23.074	0.430	0.362
8	V33331	0.12508	0.2564	22.548	0.495	0.394
6	V19089	0.12619	0.2694	22.570	0.608	0.418
7	V22094	0.06717	0.1677	22.233	0.223	0.464

Table 3.5 SX Phe stars belonging to the globular cluster Fornax 3.

CCD n.	Star Id.	Period	E_{max}	$< B >$	A_B	$< B > - < V >$
6	V40765	0.06073	0.1412	23.701	0.776	0.460
6	V38403	0.07532	0.1658	23.341	0.739	0.357

Chapter 4

Variable stars in the Fornax dSph Globular Clusters: Fornax 2, 3 and 5

The Fornax globular cluster system contains 5 clusters, namely Fornax 1, 2, 3 ,4, and 5 (hereafter For 1, 2, 3, 4, 5; Hodge 1961, 1965, 1969), spread all over the galaxy, with Fornax 4 located near the galaxy center and For 5 and 1 in the galaxy outskirts, on the East and West sides. If we compare the number of globular clusters (GCs) in Fornax with the galaxy luminosity, we find the GCs specific frequency is $S_N \sim 20$, the highest S_N known for any galaxy.

It is likely that other dSph's besides Fornax also once had their own GCs. We can see GCs associated with the now disrupting Sgr and CMa dSph's. Maybe the "safety" distance between Fornax and the Milky Way prevented this dSph from losing its GCs. This could imply that large numbers of GCs were present in dSph galaxies at the early epochs of the Galaxy, thus supporting a hierarchical scenario for the formation of the Galactic halo.

The Fornax dSph globular clusters are all metal poor ($-2.0 \leq$ [Fe/H] ≤ -1.5) and have rather similar masses, while those of the Sgr span a large range in metallicity ($-2.0 \leq$ [Fe/H] ≤ -0.6) and mass (see e.g. Strader et al., 2003; Mackey & Gilmore, 2003a; Dinescu et al., 2004). Oh et al. (2000) claim that the Fornax GCs should have sunk to the center of the galaxy, being the expected time-scale for mass segregation in the Fornax galaxy potential ~ 1 Gyr. Thus, they infer that there must be some other mechanisms kinematically exciting the clusters into their present orbits and suggest that tidal effects from the Milky Way may torque the cluster's orbits. Though dynamical friction within Fornax should counteract the MW torque, the present-day wide spread location of the Fornax GCs seems to suggest that this galaxy may have been undergoing a significant mass loss (by at least 30% of its original total mass) and that a Hubble time ago the Fornax dSph was much more massive, thus possibly explaining its high GC specific frequency.

The globular cluster system of the Fornax dSph is complex, with no straightforward correlations existing between galactocentric distances, metallicities and ages. Buonanno et al. (1998, 1999) published color magnitude diagrams of the Fornax GCs based on HST observations. They find that HB morphology of

the Fornax GCs is affected by the second parameter effect, and that the clusters resemble the "Young Halo" Galactic GCs in having HBs quite redder than Galactic globular clusters of same metallicity. The surface brightness profiles reveal differences among the Fornax clusters: For 1 e 2 are well fitted by King profiles with tidal truncation, while For 5 seems a post-collapse cluster (Mackey & Gilmore, 2003a).

There is only one previous study of the variable stars in the Fornax dSph globular clusters. Based on HST archival data, Mackey & Gilmore (2003b) identified several candidate RR Lyrae stars in four of the Fornax GCs (namely, For 1, 2, 3, and 5). They determined periods by fitting template RR Lyrae light curves to the data, since the limited number and short baseline of the archive observations did not allow them to determine periods in independent way. They conclude that the Fornax clusters are unusual in that their RR Lyrae populations have mean characteristics intermediate between the Oosterhoff groups. No variability study has been performed instead of For 4, the cluster near the Fornax galaxy center.

We have identified and obtained well-sampled light curves for variable stars in four of the Fornax dSph globular clusters (namely, For 2, 3, 4 and 5), based on high quality B, V time-series photometry reaching below the cluster's Turn-Off obtained with the 6.5-m LCO Magellan and the 2.2-m ESO/MPI telescopes and complemented by HST archive data. Our observations span a large time baseline and both observing strategy and data-reductions have been optimized to allow the detection and study of variables as faint as the SX Phe stars in the Fornax GCs.

In this Chapter we present results for variables in For 2, 3 and 5. Results from the first variability study of For 4 will be presented in Chapter 5. These studies allow us to firmly place the Fornax dSph globular clusters in the Oosterhoff plane (see Chapter 8).

4.1 Observations and Data Reductions

4.1.1 Fornax 2 and 5

B, V time series photometry of For 2 and For 5 was obtained with the MagIC camera of the Magellan/Clay 6.5-m telescope over three nights in 2003 November. For each cluster we covered a total field of view of $2.4' \times 2.4'$, centered on the cluster at RA$= 2:38:44.2$, DEC$= -34:48:33.1$ (J2000) and RA$= 2:42:2.3$, DEC$= -34:06:05.2$ (J2000) for For 2 and 5, respectively. Nights were photometric with seeing conditions varying from $0.45''$ to $0.65\ ''$. We acquired total numbers of 18 V and 6 B images of For 2, and 52 V and 20 B images of For 5. Average exposure times were of 500 seconds for the V frames and 700s for the B ones. Observations of the standard fields TPhe and Ru149 (Landolt 1992) were obtained along the same nights, to calibrate the data to the standard Johnson-Cousins photometric system.

The Magellan data were complemented by WFPC2@HST archival observations. HST archival data (Program ID 5917) are available for both these clusters from the same dataset used by (Mackey & Gilmore, 2003b) to search for variable stars in these clusters. The WFPC2 dataset consists of 14 F555W (V) and

16 F814W (I) images for each cluster. Exposure times vary from 160s to 600s in the V band, and from 20s to 900s in the I band. The combined Magellan+HST datasets of both clusters make a total of three nights spread on seven years from 1996 to 2003. Logs of the observations and details of the instrumental set-ups are given in Table 4.1.

The Magellan frames were bias-subtracted and flatfield-corrected using the MagIC tool in IRAF*. Time series photometry for all the stars was produced with ALLFRAME (Stetson, 1994, 1996). The photometric precision at the HB level is 0.01 mag. The absolute photometric calibration of the Magellan data was derived using standard stars observed at the Magellan telescope on the night of 2003 November 13. A set of linear calibration relations was computed:

$$\begin{aligned} B &= b' + 0.051(B-V) + 26.87 \\ V &= v' - 0.049(B-V) + 26.81 \end{aligned}$$

where b' and v' are the instrumental magnitudes normalized to 1-s exposure and corrected for atmospheric extinction by adopting the mean extinction coefficients $k_B = 0.22$ and $k_V = 0.12$. The zero point uncertainties of the calibration relations are estimated of the order 0.05 mag in B and V, and 0.03 mag in $(B-V)$, from the night-to-night scatter of the standard stars. These relations were used to calibrate the instrumental magnitudes, and aperture corrections were applied based on photometry of relatively isolated stars.

4.1.2 Fornax 3

B, V time series photometry of the For 3 was obtained with the WFI camera of the ESO/MPI 2.2-m telescope on three nights in 2002 November. For 3 is imaged on Chip # 6 of the WFI image of Fornax Field_1. This field covers a $33' \times 34'$ Northern portion of the Fornax galaxy, and it is centered at RA=2:39:59.4, DEC=$-$34:11:53.4, (J2000). Nights were photometric with seeing conditions varying from $1.5''$ to $1.8''$. We acquired a total number of 16 V and 61 B images of this field. Exposures were in the range from 400 to 500s for the V frames and from 300 to 350s for the B ones. Observations of the standard fields TPhe, Ru152 and Ru149 (Landolt 1992) were obtained along the same nights, allowing us to calibrate the data to the standard Johnson-Cousins photometric system.

The WFI/ESO data have been complemented by WFPC2@HST archival data (Program ID 5917). The WFPC2 dataset consists of 22 F555W (V) and 16 F814W (I) images. Exposure times vary from 160s to 600s in the V band and from 20s to 900s in the I band. The time series data of For 3 cover in total six nights from 1999 to 2002. Logs of the observations and details on the instrumental set-ups are given in 4.1.

*IRAF is distributed by the National Optical Astronomical Observatories, which are operated by the Association of Universities for Research in Astronomy, Inc., under cooperative agreement with the National Science Foundation

The WFI/ESO sequences were bias-subtracted and flatfield-corrected using the MSCRED tool in IRAF (Valdes, 1997). Photometric reductions of the full dataset of For 3 were then performed with DAOPHOT-ALLSTAR-ALLFRAME (Stetson, 1994, 1996). The internal photometric precision at the HB level is 0.02 mag. The calibration of the WFI/ESO photometry was obtained using the Landolt's (1992) standard stars observed during the 2002 November run. A set of linear calibration relations was obtained:

$$\begin{aligned} B &= b' + 0.289(B-V) + 24.659 \\ V &= v' - 0.090(B-V) + 24.222 \end{aligned}$$

where b' and v' are the instrumental magnitudes normalized to 1-s exposure and corrected for atmospheric extinction by adopting the mean extinction coefficients $k_B = 0.23$ and $k_V = 0.16$. The zero point uncertainties of the calibration relations are estimated of the order 0.06 and 0.05 mag in B and V, respectively. These relations were used to calibrate the instrumental magnitudes, and aperture corrections were applied based on photometry of relatively isolated stars.

Our observations produced color-magnitude diagrams reaching $V \sim 24.5$, 25.5 and 26 mag for For 2, 3 and 5, respectively. These CMDs are shown in Figures 4.1, 4.2, and 4.3. No reliable photometry could be obtained for stars inside a radius of $7''$ from the cluster center of For 5 due to crowding. The CMD in Figures 4.3 is drawn by cutting off this central region.

4.2 Variable Star Identification and Study

Variable stars were identified by applying the Image Subtraction Technique (ISIS2.1, Alard 2000) to the cluster's V and B time series data, independently. The B,V catalogs of candidate variables were cross-identified in order to select objects displaying variability in both bands. This procedure produced catalogs of 150, 200 and 300 candidate variables in For 2, For 3 and For 5, respectively. The ISIS catalogs were then cross-identified against the DAOPHOT/ALLFRAME photometric catalogs obtaining light curves in magnitude scale and confirming the variability for 32 stars in For 2, 39 stars in For 3, and 18 stars in For 5. Further 10 variables were recovered in the central regions of For 5, where we lack reliable PSF photometry. For these stars we have analyzed the light curves in differential flux produced by ISIS. The time series B, V photometry of the confirmed variable stars with light curves in magnitude scale is provided in Table 4.2.

Study of the light curves (period search, classification of the variables in types and definition of the variable star's characteristics) was performed with GrATiS (Di Fabrizio, 1999; Clementini et al., 2000) a custom software developed at the Bologna Observatory. Results from the study of the light curve of the For 2, 3 and 5 variable stars are summarized in Table 4.3, where we provide the number and type of the variable stars with well sampled light curves identified in each cluster in Columns 2–4, and the total number of frames in each band in Column 5–7.

Table 4.1 Instrumental set-ups and logs of the observations of For 2, 3 and 5

Target	Dates	Telescope/Instrument	Detector (pixel)	Resolution (″/pixel)	FOV	N_B	N_V	N_I	Photometric accuracy (HB level) (mag)
For2, For5	Jun.4 − 6, 1996	HST/WFPC2/PC	800 × 800 SITe	0.0455	$36'' \times 36''$	–	14	16	0.03 − 0.05
For2, For5	Jun.4 − 6, 1996	HST/WFPC2/WF	3 × 800 × 800 SITe	0.0996	$80'' \times 80''$	–	14	16	0.03 − 0.05
For3	Jun.2 − 5, 1996	HST/WFPC2/PC	800 × 800 SITe	0.0455	$36'' \times 36''$	–	22	16	0.03 − 0.05
For3	Jun.2 − 5, 1996	HST/WFPC2/WF	3 × 800 × 800 SITe	0.0996	$80'' \times 80''$	–	22	16	0.03 − 0.05
For3	Nov.9 − 11, 2002	ESO/WFI	8 × 2048 × 4098 SITe	0.238	$34' \times 34'$	–		61	0.03 − 0.05
For2	Nov.15, 2003	Magellan/MagIC	2048 × 2048 SITe	0.069	$2.35' \times 2.35'$	6	18	–	0.01
For5	Nov.13 − 15, 2003	Magellan/MagIC	2048 × 2048 SITe	0.069	$2.35' \times 2.35'$	20	52	–	0.01

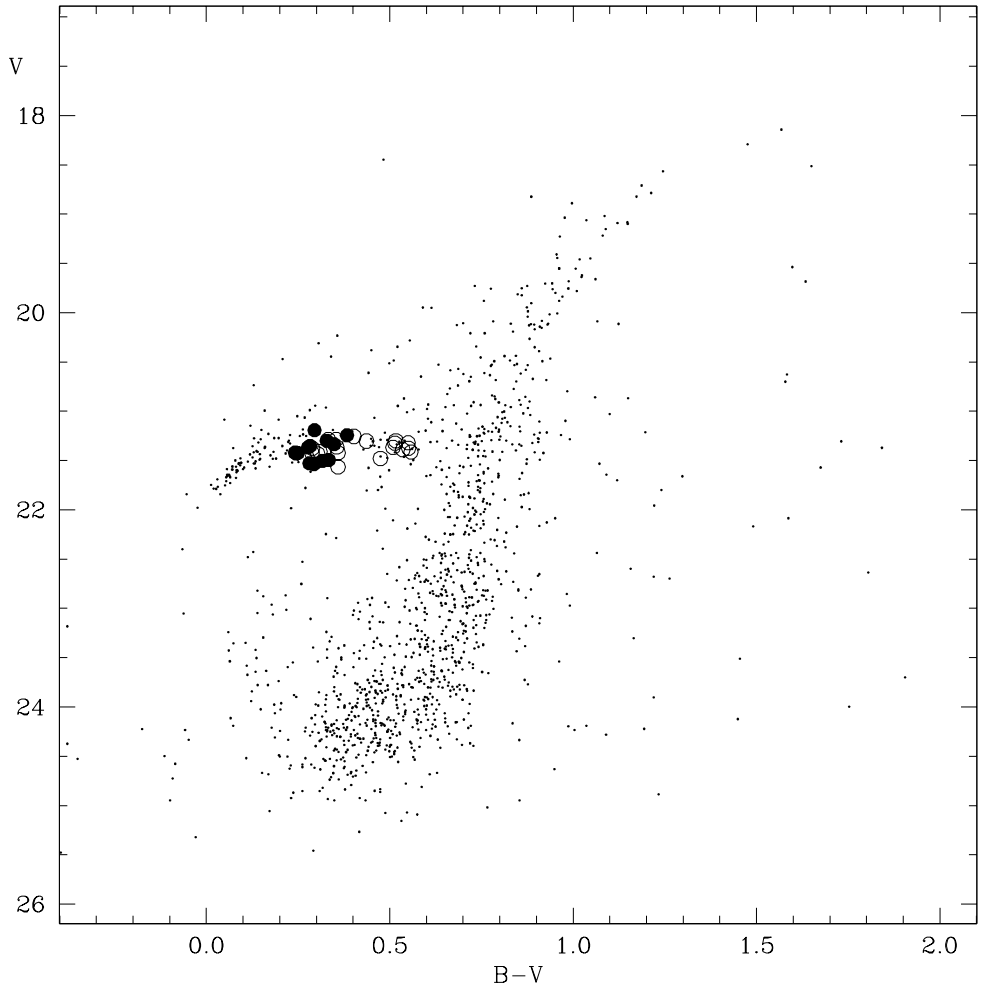

Figure 4.1 Color-magnitude diagram of For 2 from the Magellan dataset. Variable stars are displayed with different symbols. Open circles: *ab*-type RR Lyrae stars; filled circles: first overtone RR Lyrae stars (RR_c).

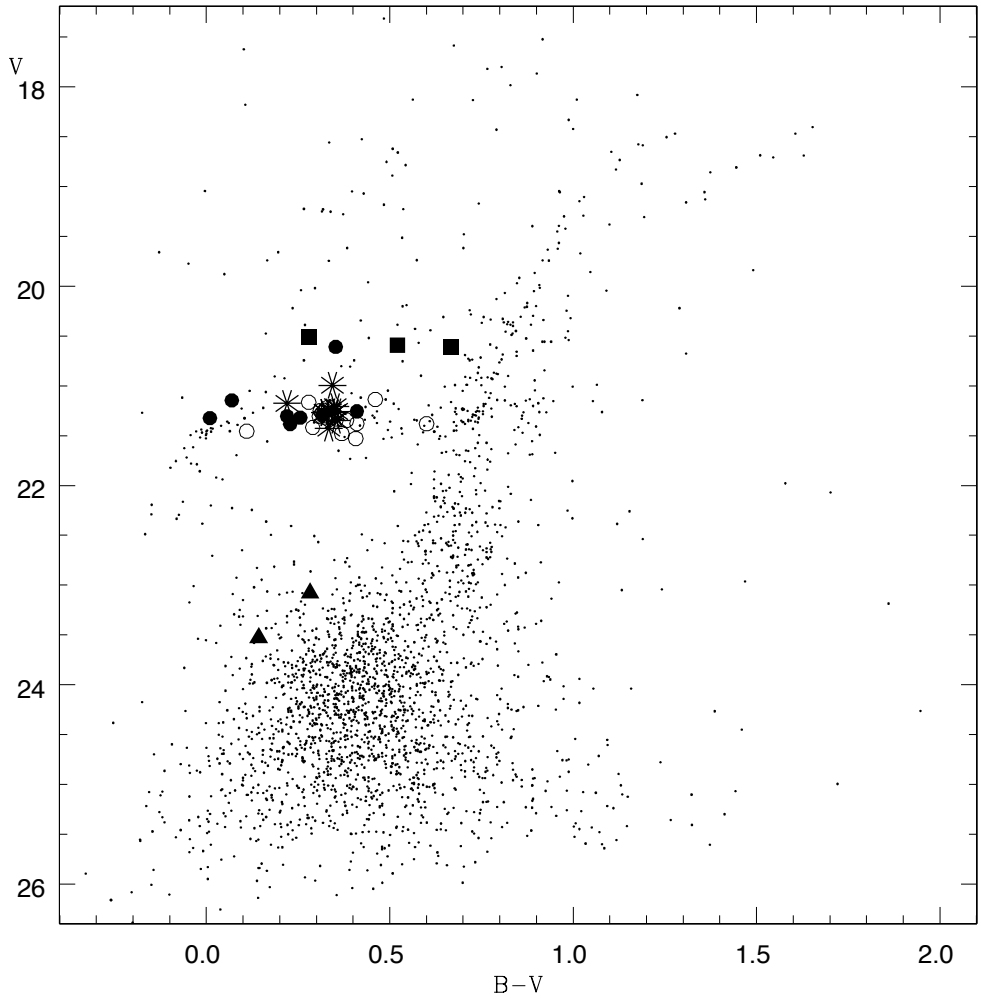

Figure 4.2 Color-magnitude diagram of For 3 from the WFI/ESO data. Variable stars are displayed with different symbols. Open circles: *ab*-type RR Lyrae stars; filled circles: first overtone RR Lyrae stars; asterisks: *double mode* RR Lyrae; filled squares: candidate Anomalous Cepheids; filled triangles: Dwarf Cepheids (SX Phe stars).

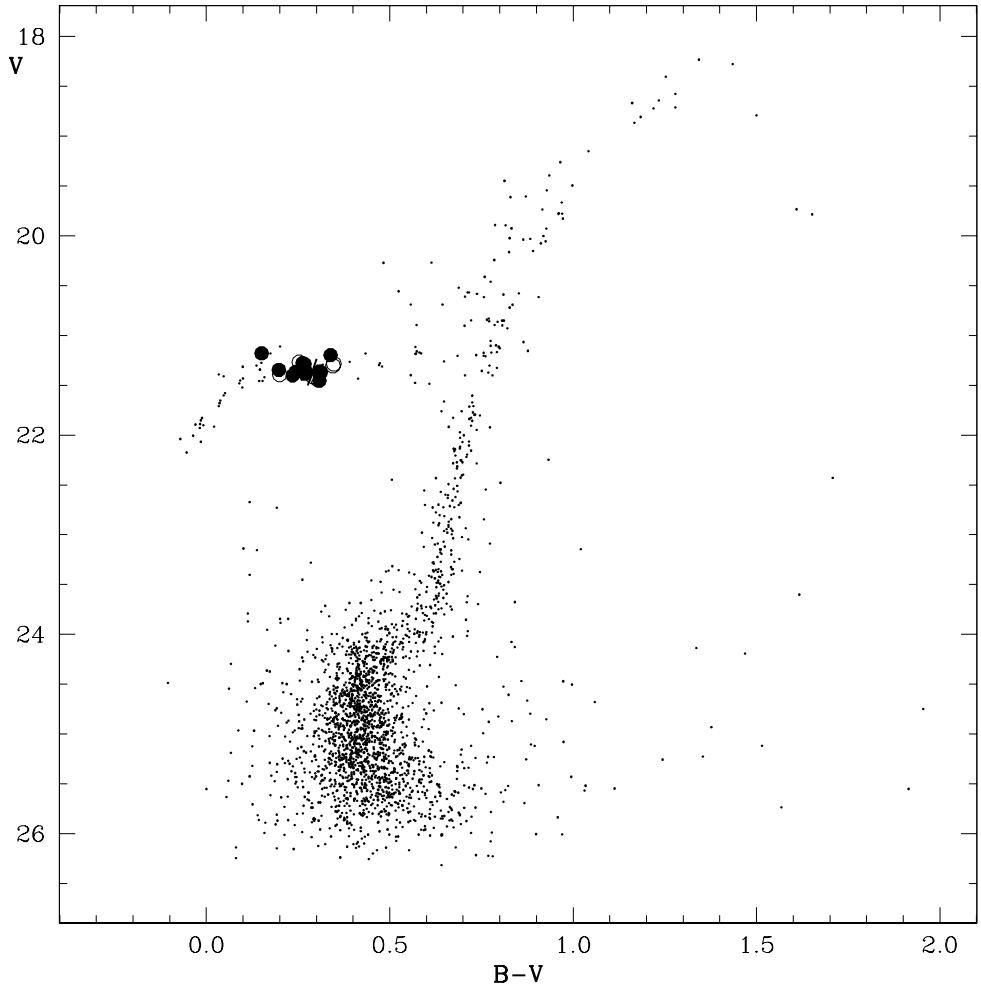

Figure 4.3 Color-magnitude diagram of For 5 from the Magellan data. Variable stars are displayed with different symbols. Open circles: *ab*-type RR Lyrae stars; filled circles: first overtone RR Lyrae stars; asterisk: *double mode* RR Lyrae star.

Table 4.2 V, B photometry of variable stars with light curves in magnitude scale.

For 5 - Star V22 - RRc			
HJD	V	HJD	B
(-2450238)		(-2452956)	
0.708973	21.37	0.0365	21.29
0.711751	21.34	0.1245	21.34
0.717307	21.36	0.2107	21.44
0.788839	21.45	0.2971	21.48
0.796246	21.43	0.3351	21.58
0.835948	21.50	0.3507	21.56
0.843587	21.50	0.3845	21.62
0.922873	21.19	0.4400	21.67
0.930281	21.15	0.4558	21.70
0.970677	21.23	0.4704	21.76

A portion of Table 4.2 is shown here for guidance regarding its form and content.

Table 4.3 Variable stars with well sampled light curves identified in For 2, 3 and 5.

Cluster	RR Lyrae stars	DCs	ACs	N_B	N_V	N_I
For 2	32 (19ab, 13c)	-	-	6	32	16
For 3	34 (16ab, 8c, 10d)	2	3	61	38	16
For 5	28 (13ab, 14c, 1d)	-	-	10	55	16

The pulsation properties of the RR Lyrae stars identified in For 2, 3 and 5 are summarized in Table 4.4 where we list the number of fundamental mode (RRab), first overtone (RRc) and double mode pulsators (RRd) in Columns 2–4; the average periods of the *ab*- and *c*-type RR Lyrae stars, in Columns 5 and 6, respectively; the ratio of number of RRc to number of RRc+RRab in Column 7; the shortest period RRab and the longest period RRc in Columns 8 and 9. Based on the average period of the fundamental mode RR Lyrae stars $\langle P_{\rm ab} \rangle$ the 3 clusters thus appear to have mean characteristics intermediate between the Oosterhoff groups, as previously suggested by Mackey & Gilmore (2003b).

Coordinates, period, type, time of maximum light, number of phase points (in the Magellan/ESO and HST datasets separately), intensity-averaged $\langle \rm V \rangle$ and $\langle \rm B \rangle$ magnitudes, and amplitudes of the light variation ($\rm A_V$ and $\rm A_B$) of the variable stars identified in For 2, 3 and 5, are provided in Tables 4.5, 4.6 and 4.7, respectively. Examples of light curves for variable stars in For 2 and 5 are shown in Figure 4.4. The complete atlas of light curves for all the three clusters is presented in the Appendix Sections A, B, and D.

Period-amplitude distributions for the For 2, 3 and 5 RR Lyrae stars with light curves in magnitude scale are shown in Figures 4.5, 4.6, and 4.7. Expanded symbols are used for the variable stars whose cluster's membership is more certain.

Table 4.4 Pulsation properties of the RR Lyrae stars identified in For 2, 3 and 5.

Cluster	N_{RRab}	N_{RRc}	N_{RRd}	$\langle P_{ab} \rangle$	$\langle P_c \rangle$	f_c (a)	$P_{ab,min}$	$P_{c,max}$
For 2	19	13	-	0.58	0.36	0.41(0.28)	0.51621	0.42500
For 3	16	8	10	0.62	0.37	0.33(0.31)	0.50648	0.40956
For 5	13	14	-	0.60	0.36	0.52(0.48)	0.53297	0.40606

[a] Values in brackets are considering only RR Lyrae stars more likely cluster members (see Section 4.4)

Table 4.5 Identification and properties of the For 2 variable stars.

Name (a)	Id	α (2000)	δ (2000)	Type	P (days)	Epoch (-2400000)	$\langle V \rangle$	N_V	$\langle B \rangle$	N_B	A_V	A_B	Notes
$V1$	51452	2 : 38 : 46.163	−34 : 48 : 19.81	RRab	0.54966	50239.979	21.30	11 + 18	21.82	6	0.49	···	
$V2$	2093	2 : 38 : 46.345	−34 : 48 : 22.37	RRab	0.71785	50235.136	21.29	14 + 15	21.62	6	0.55	···	
$V3$	1636	2 : 38 : 46.217	−34 : 48 : 17.01	RRc	0.34409	52958.838	21.37	11 + 18	21.64	6	0.60	0.47	
$V4$	200168	2 : 38 : 46.514	−34 : 48 : 18.82	RRab	0.57987	50240.194	21.42	14 + 17	21.78	5	0.65	···	
$V5$	1572	2 : 38 : 46.076	−34 : 48 : 16.16	RRc	0.33044	50239.58	21.34	14 + 18	21.68	6	0.53	0.80	
$V6$	200215	2 : 38 : 45.877	−34 : 48 : 21.49	RRab	0.59669	50239.98	21.32	14 + 18	21.84	6	1.09	···	
$V7$	2068	2 : 38 : 45.871	−34 : 48 : 22.03	RRab	0.52550	52958.856	21.32	14 + 18	21.87	6	1.38	···	
$V8$	2251	2 : 38 : 46.110	−34 : 48 : 24.45	RRab	0.64958	50238.093	21.39	12 + 18	21.93	6	0.87	0.41	
$V9$	200130	2 : 38 : 45.998	−34 : 48 : 16.13	RRab	0.57279	50239.287	21.37	14 + 18	21.93	6	0.47	···	
$V10$	51476	2 : 38 : 45.804	−34 : 48 : 20.46	RRab	0.56367	50239.651	21.36	14 + 18	21.72	6	0.79	0.97	
$V11$	2248	2 : 38 : 46.454	−34 : 48 : 24.46	RRab	0.64989	50243.445	21.41	14 + 18	21.72	6	0.65	0.73	
$V12$	1979	2 : 38 : 45.702	−34 : 48 : 21.08	RRab	0.59946	52958.715	21.42	14 + 18	21.71	6	1.13	1.43	
$V13$	1797	2 : 38 : 46.773	−34 : 48 : 19.10	RRab	0.53984	50233.894	21.56	14 + 18	21.92	6	0.74	0.73	
$V14$	200271	2 : 38 : 46.048	−34 : 48 : 26.59	RRc	0.42996	52958.862	21.19	14 + 14	21.49	6	0.58	0.27	
$V15$	1401	2 : 38 : 45.909	−34 : 48 : 14.05	RRab	0.58842	50240.675	21.41	13 + 18	21.97	6	1.14	···	
$V16$	2070	2 : 38 : 46.788	−34 : 48 : 22.23	RRc	0.40	52958.675	21.24	5 + 18	21.63	6	0.70	0.84	
$V17$	2329	2 : 38 : 46.641	−34 : 48 : 25.67	RRab	0.56217	50239.418	21.30	14 + 18	21.74	6	1.09	···	
$V18$	51817	2 : 38 : 46.710	−34 : 48 : 25.17	RRab	0.51982	50240.296	21.29	13 + 18	21.64	6	0.85	···	
$V19$	1514	2 : 38 : 46.813	−34 : 48 : 15.52	RRc	0.33655	50240.355	21.35	12 + 18	21.63	6	0.64	0.49	
$V20$	1200	2 : 38 : 46.152	−34 : 48 : 11.08	RRc	0.34184	50239.79	21.30	13 + 18	21.63	6	0.48	···	
$V21$	1345	2 : 38 : 45.703	−34 : 48 : 13.09	RRc	0.37031	50239.495	21.43	13 + 18	21.67	6	0.46	0.57	
$V22$	51597	2 : 38 : 45.395	−34 : 48 : 21.80	RRab	0.51621	50239.678	21.48	14 + 18	21.95	6	0.64	0.70	
$V23$	1075	2 : 38 : 46.440	−34 : 48 : 09.23	RRab	0.60145	50240.016	21.37	14 + 18	21.87	6	0.54	···	
$V24$	1408	2 : 38 : 45.275	−34 : 48 : 14.01	RRab	0.52318	50239.647	21.38	14 + 17	21.67	6	0.75	···	
$V25$	959	2 : 38 : 45.586	−34 : 48 : 07.08	RRab	0.55984	50239.775	21.26	14 + 18	21.66	6	0.81	0.64	
$V26$	1924	2 : 38 : 44.722	−34 : 48 : 20.37	RRc	0.37993	50239.701	21.49	13 + 18	21.83	6	0.46	···	
$V27$	2689	2 : 38 : 44.771	−34 : 48 : 31.07	RRc	0.33406	50240.005	21.51	14 + 18	21.82	6	0.37	0.31	
$V28$	783	2 : 38 : 47.453	−34 : 48 : 04.70	RRc	0.34682	50240.081	21.42	14 + 18	21.66	6	0.56	···	
$V29$	423	2 : 38 : 46.444	−34 : 47 : 57.78	RRc	0.39674	50239.110	21.43	14 + 18	21.67	6	0.55	0.39	
$V30$	2225	2 : 38 : 44.085	−34 : 48 : 23.83	RRc	0.37979	50239.777	21.53	14 + 18	21.81	6	0.52	0.60	
$V31$	592	2 : 38 : 48.202	−34 : 48 : 01.63	RRc	0.35178	50239.999	21.53	14 + 18	21.83	6	0.37	0.53	
$V32$	879	2 : 38 : 44.075	−34 : 48 : 05.72	RRab	0.58964	50239.505	21.43	5 + 18	21.74	6	0.34	0.53	

[a] Variable stars were assigned increasing numbers starting from the cluster center that was set at $\alpha = 02 : 38 : 44.2$, $\delta = -34 : 48 : 33.1$ (J2000). Stars from V1 to V25 are located within $35''$ from the For 2 center, hence are more likely cluster members (see Section 4.4).

Table 4.6 Identification and properties of the For 3 variable stars.

Name (a)	Id	α (2000)	δ (2000)	Type	P (days)	Epoch (-2400000)	$\langle V \rangle$	N_V	$\langle B \rangle$	N_B	A_V	A_B	Notes
$V1$	42721	2 : 39 : 48.202	−34 : 15 : 15.22	RRc	0.37927	2450238.500	21.15	0 + 20	21.22	61	0.57	0.45	
$V2$	42816	2 : 39 : 47.851	−34 : 15 : 13.42	AC	0.58720	2452223.750	20.59	6 + 7	21.11	34	0.55	0.64	
$V3$	42655	2 : 39 : 47.390	−34 : 15 : 17.17	RRab	0.69957	2450238.750	21.38	14 + 20	21.98	49	0.75	1.12	
$V4$	42385	2 : 39 : 47.104	−34 : 15 : 23.50	RRc	0.39761	2452224.750	21.32	0 + 20	21.33	50	0.45	0.47	
$V5$	42531	2 : 39 : 49.426	−34 : 15 : 19.12	RRab	0.59065	2452223.750	21.25	14 + 13	21.57	60	1.03	1.07	
$V6$	42695	2 : 39 : 47.161	−34 : 15 : 15.68	RRab	0.60991	2450238.750	21.38	13 + 14	21.79	60	1.12	1.16	
$V7$	43228	2 : 39 : 48.124	−34 : 15 : 05.38	RRd	0.40791	2450238.500	21.27	16 + 18	21.59	60	0.41	0.51	
$V8$	41774	2 : 39 : 46.887	−34 : 15 : 33.38	RRd	0.44100	2452223.750	21.00	8 + 5	21.34	33	0.30	0.24	
$V9$	41315	2 : 39 : 48.747	−34 : 15 : 42.15	RRc	0.35725	2450238.500	20.61	15 + 20	20.96	53	0.32	0.47	
$V10$	43284	2 : 39 : 48.642	−34 : 15 : 04.01	RRc	0.28945	2450239.500	21.38	16 + 12	21.61	59	0.48	0.58	
$V11$	41242	2 : 39 : 48.575	−34 : 15 : 43.75	RRd	0.43000	2452222.500	21.18	6 + 7	21.40	37	0.48	0.51	
$V12$	42473	2 : 39 : 49.887	−34 : 15 : 18.90	RRab	0.55776	2452223.500	21.53	14 + 9	21.94	35	1.31	1.55	
$V13$	41489	2 : 39 : 47.065	−34 : 15 : 38.85	RRab	0.71797	2452223.500	21.17	9 + 19	21.44	59	0.77	0.87	
$V14$	41160	2 : 39 : 47.558	−34 : 15 : 45.43	RRab	0.69229	2452223.500	21.21	15 + 20	21.54	61	0.73	0.85	
$V15$	43571	2 : 39 : 47.223	−34 : 14 : 58.21	RRab	0.57845	2452222.500	21.30	16 + 18	21.63	60	1.15	1.30	
$V16$	40891	2 : 39 : 47.450	−34 : 15 : 51.16	RRab	0.60090	2452221.750	21.27	9 + 7	21.59	37	0.95	1.06	
$V17$	40765	2 : 39 : 47.467	−34 : 15 : 53.35	DC	0.06080	2452222.000	23.52	6 + 7	24.67	36	0.88	0.77	
$V18$	44053	2 : 39 : 47.514	−34 : 14 : 48.16	RRab	0.58191	2452222.750	21.34	15 + 18	21.69	61	1.10	1.19	
$V19$	44052	2 : 39 : 49.167	−34 : 14 : 48.15	RRd	0.42200	2452224.750	21.21	8 + 6	21.56	36	0.56	0.68	
$V20$	44116	2 : 39 : 48.825	−34 : 14 : 46.49	RRd	0.41955	2452222.750	21.35	13 + 20	21.70	37	0.40	0.46	
$V21$	43915	2 : 39 : 46.436	−34 : 14 : 50.99	RRc	0.37820	2452221.750	21.32	14 + 14	21.58	59	0.56	0.66	
$V22$	41303	2 : 39 : 51.119	−34 : 15 : 42.35	RRab	0.57941	2452224.750	21.31	13 + 18	21.62	31	0.64	0.72	
$V23$	43434	2 : 39 : 51.000	−34 : 15 : 01.14	RRd	0.43290	2452224.500	21.26	8 + 7	21.60	38	0.53	0.51	
$V24$	44516	2 : 39 : 48.744	−34 : 14 : 37.66	RRd	0.39000	2452224.500	21.43	9 + 7	21.76	38	0.43	0.48	
$V25$	42983	2 : 39 : 51.886	−34 : 15 : 10.07	RRab	0.62852	2450238.250	21.48	15 + 18	21.85	60	0.65	0.76	
$V26$	42697	2 : 39 : 44.478	−34 : 15 : 15.63	AC	0.78530	2452221.500	20.51	0 + 18	20.79	58	1.68	1.27	
$V27$	44819	2 : 39 : 49.949	−34 : 14 : 30.85	RRc	0.40956	2450239.500	21.29	15 + 14	21.61	59	0.48	0.50	
$V28$	39786	2 : 39 : 50.692	−34 : 16 : 13.21	RRc	0.40337	2450238.750	21.26	14 + 19	21.67	60	0.52	0.54	
$V29$	41798	2 : 39 : 52.951	−34 : 15 : 33.03	RRd	0.42400	2452224.750	21.27	8 + 7	21.59	35	0.67	0.69	
$V30$	39970	2 : 39 : 51.540	−34 : 16 : 09.52	RRd	0.40481	2452223.500	21.27	14 + 20	21.62	37	0.49	0.56	
$V31$	45314	2 : 39 : 48.732	−34 : 14 : 19.74	AC	0.59473	2452223.500	20.61	9 + 7	21.28	39	0.39	0.54	
$V32$	39758	2 : 39 : 51.986	−34 : 16 : 13.81	RRab	0.59885	2452223.750	21.25	9 + 20	21.56	38	1.17	1.15	
$V33$	44591	2 : 39 : 43.828	−34 : 14 : 36.05	RRab	0.61400	2452223.500	21.35	16 + 15	21.73	60	0.72	0.86	
$V34$	44036	2 : 39 : 42.942	−34 : 14 : 48.46	RRd	0.41198	2452224.500	21.26	12 + 21	21.61	37	0.43	0.49	
$V35$	40262	2 : 39 : 42.754	−34 : 16 : 03.53	RRc	0.31140	2452221.750	21.30	9 + 7	21.52	39	0.58	0.73	
$V36$	38403	2 : 39 : 46.816	−34 : 16 : 40.73	DC	0.07530	2452222.000	23.08	8 + 7	23.37	60	0.52	0.71	
$V37$	45426	2 : 39 : 52.209	−34 : 14 : 17.11	RRab	0.65875	2452224.750	21.14	15 + 6	21.60	61	0.44	0.50	
$V38$	45123	2 : 39 : 43.529	−34 : 14 : 24.20	RRab	0.55271	2450238.500	21.42	16 + 11	21.71	61	0.97	1.20	
$V39$	44096	2 : 39 : 54.608	−34 : 14 : 46.90	RRab	0.50648	2452221.750	21.46	15 + 17	21.57	61	1.20	1.40	

[a] Variable stars were assigned increasing numbers starting from the cluster center that was set at $\alpha = 02 : 39 : 48.236, \delta = -34 : 15 : 23.36$ (J2000). Stars from V1 to V26 are located within $50''$ from the For 3 center, hence are more likely cluster members (see Section 4.4).

Table 4.7 Identification and properties of the For 5 variable stars.

Name (a)	Id	α (2000)	δ (2000)	Type	P (days)	Epoch (-2400000)	$\langle V \rangle$	N_V	$\langle B \rangle$	N_B	A_V	A_B	Notes
$V1$	LC117	2 : 42 : 21.246	−34 : 06 : 07.60	RRab	0.64444	52955.315	···	55	···	···	···	···	(*b*)
$V2$	LC77	2 : 42 : 21.014	−34 : 06 : 10.56	RRc	0.40450	52955.678	···	55	···	···	···	···	(*b*)
$V3$	LC103	2 : 42 : 21.400	−34 : 06 : 08.64	RRc	0.28401	52955.776	···	55	···	···	···	···	(*b*)
$V4$	LC166	2 : 42 : 21.340	−34 : 06 : 03.19	RRc	0.36333	52955.629	···	55	···	···	···	···	(*b*)
$V5$	LC172	2 : 42 : 21.195	−34 : 06 : 02.17	RRab	0.56330	52955.827	···	55	···	···	···	···	(*b*)
$V6$	LC175	2 : 42 : 21.021	−34 : 06 : 01.68	RRab	0.65210	···	···	55	···	···	···	···	(*b*)
$V7$	LC136	2 : 42 : 20.539	−34 : 06 : 05.83	RRab	0.58830	52955.753	···	55	···	···	···	···	(*b*)
$V8$	LC149	2 : 42 : 21.580	−34 : 06 : 05.01	RRab	0.56215	52955.940	···	55	···	···	···	···	(*b*)
$V9$	LC98	2 : 42 : 21.631	−34 : 06 : 08.83	RRab	0.63309	52956.629	···	55	···	···	···	···	(*b*)
$V10$	LC118	2 : 42 : 21.680	−34 : 06 : 07.49	RRab	0.60412	53955.404	···	55	···	···	···	···	(*b*)
$V11$	3583	2 : 42 : 20.511	−34 : 06 : 10.69	RRc	0.36552	52957.602	21.29	51 + 14	21.55	20	0.60	0.78	
$V12$	2577	2 : 42 : 21.670	−34 : 06 : 04.63	RRab	0.53356	50238.145	21.27	51 + 14	21.52	20	0.99	1.09	
$V13$	2537	2 : 42 : 21.720	−34 : 06 : 07.58	RRc	0.40606	50237.193	21.37	50 + 12	21.68	20	0.35	0.41	
$V14$	2482	2 : 42 : 21.793	−34 : 06 : 01.59	RRab	0.53297	50237.615	21.39	50 + 14	21.59	18	0.56	0.94	
$V15$	3845	2 : 42 : 20.209	−34 : 06 : 05.88	RRc	0.34403	50238.940	21.20	47 + 14	21.54	17	0.25	0.41	
$V16$	3631	2 : 42 : 20.466	−34 : 05 : 59.59	RRab	0.60595	50238.796	21.29	49 + 14	21.63	20	1.02	1.28	
$V17$	3274	2 : 42 : 20.868	−34 : 06 : 20.18	RRd	0.37023	50238.720	21.37	52 + 14	21.66	19	0.45	0.58	(*c*)
$V18$	2818	2 : 42 : 21.385	−34 : 05 : 52.21	RRc	0.37204	52957.782	21.36	52 + 14	21.67	20	0.43	0.60	
$V19$	3936	2 : 42 : 20.087	−34 : 06 : 18.66	RRab	0.74740	52957.668	21.44	50 + 14	21.75	18	0.64	0.81	
$V20$	2663	2 : 42 : 21.583	−34 : 05 : 50.29	RRc	0.30725	50237.875	21.40	52 + 14	21.64	18	0.65	0.88	
$V21$	4097	2 : 42 : 19.858	−34 : 05 : 56.09	RRc	0.33329	50237.850	21.37	47 + 14	21.61	20	0.61	0.70	
$V22$	1673	2 : 42 : 22.836	−34 : 06 : 11.51	RRc	0.31376	50237.685	21.35	51 + 14	21.54	17	0.37	0.50	
$V23$	4350	2 : 42 : 19.516	−34 : 05 : 48.13	RRc	0.36593	52957.715	21.38	50 + 14	21.65	18	0.49	0.67	
$V24$	5057	2 : 42 : 18.294	−34 : 06 : 13.03	RRc	0.38930	52955.858	21.28	50	21.54	19	0.48	0.73	
$V25$	970	2 : 42 : 24.042	−34 : 06 : 11.83	RRab	0.58806	50238.152	21.30	52 + 14	21.65	20	0.99	1.20	
$V26$	4853	2 : 42 : 18.686	−34 : 05 : 43.30	RRc	0.37602	52957.645	21.45	50	21.76	18	0.30	0.34	
$V27$	5472	2 : 42 : 17.459	−34 : 07 : 16.14	RRab	0.53780	52956.547	21.41	52	21.70	20	1.21	1.52	
$V28$	157	2 : 42 : 25.644	−34 : 05 : 07.30	RRc	0.39085	52956.691	21.18	50	21.33	19	0.51	0.78	

[a] Variable stars were assigned increasing numbers starting from the cluster center that was set at $\alpha = 02 : 42 : 21.067$, $\delta = -34 : 06 : 07.49$(J2000). Stars from V1 to V26 are located within $45''$ from the For 5 center, hence are more likely cluster members (see Section 4.4).

[b] Light curves available in differential flux only.

[c] Double-mode RR Lyrae star with fundamental mode period P_0= 0.49602 and period ratio of P_1/P_0=0.74604, in the table we list the star first overtone period.

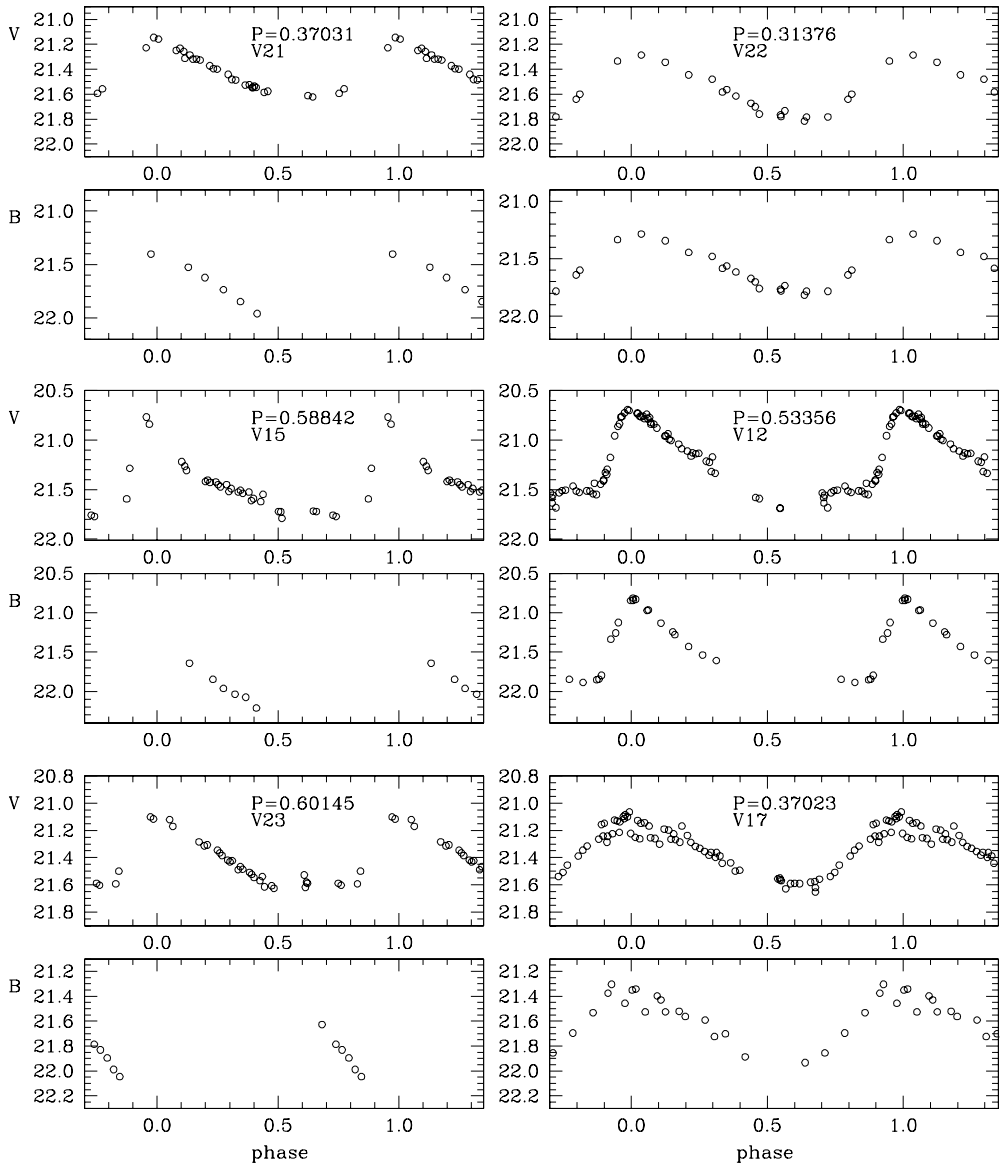

Figure 4.4 V, B light curves of variable stars in For 2 (left panel) and in For 5 (right panel)

4.3 Membership Probabilities

Contamination by field variable stars was checked for each of the clusters considered in this Chapter. Given the different stellar content of the globular clusters and the surrounding Fornax field populations, and the presence of a stellar population gradient in Fornax, estimating the expected number of cluster RR Lyrae variables from the surface density profile in our small observed fields is not straightforward. To illustrate the difference between the stellar populations of the cluster and the field, for each cluster we have selected stars in two regions, inner

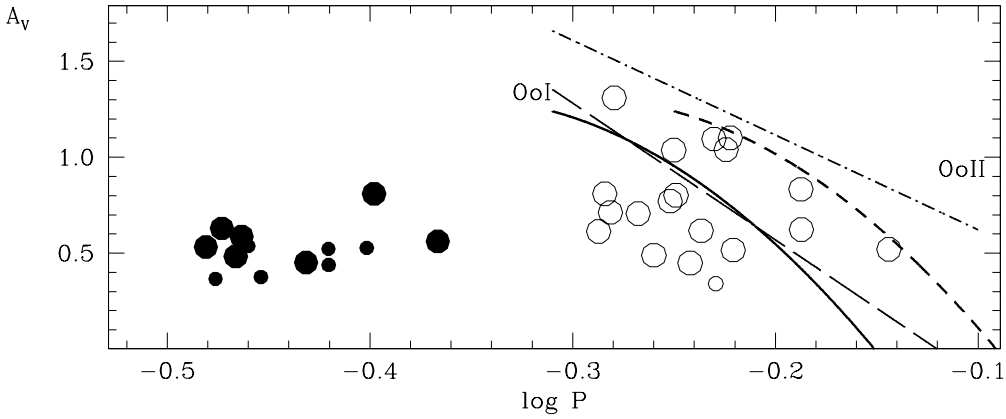

Figure 4.5 Period-amplitude diagram in the V band of the For 2 RR Lyrae stars. The straight lines are the positions of the OoI and OoII Galactic GCs according to Clement & Rowe (2000). Period-amplitude distributions of the *bona fide* regular (solid curves) and well-evolved (dashed curves) *ab* RR Lyrae stars in M3 from Cacciari et al. (2005) are also shown for comparison. Larger symbols are variable stars located within $35'$ from the For 2 center.

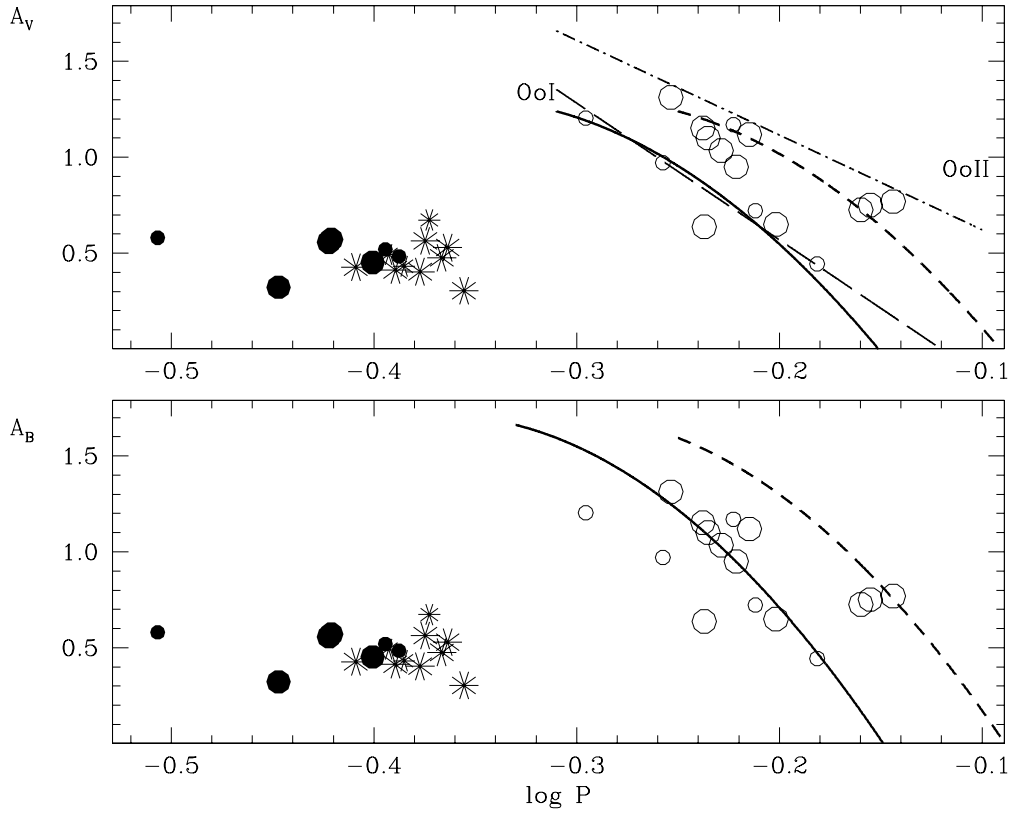

Figure 4.6 V, B period-amplitude diagrams of the For 3 RR Lyrae stars. The straight lines are the positions of the OoI and OoII Galactic GCs according to Clement & Rowe (2000). Period-amplitude distributions of the *bona fide* regular (solid curves) and well-evolved (dashed curves) *ab* RR Lyrae stars in M3 from Cacciari et al. (2005) are also shown for comparison. Larger symbols are variable stars located within 50′ from the For 3 center.

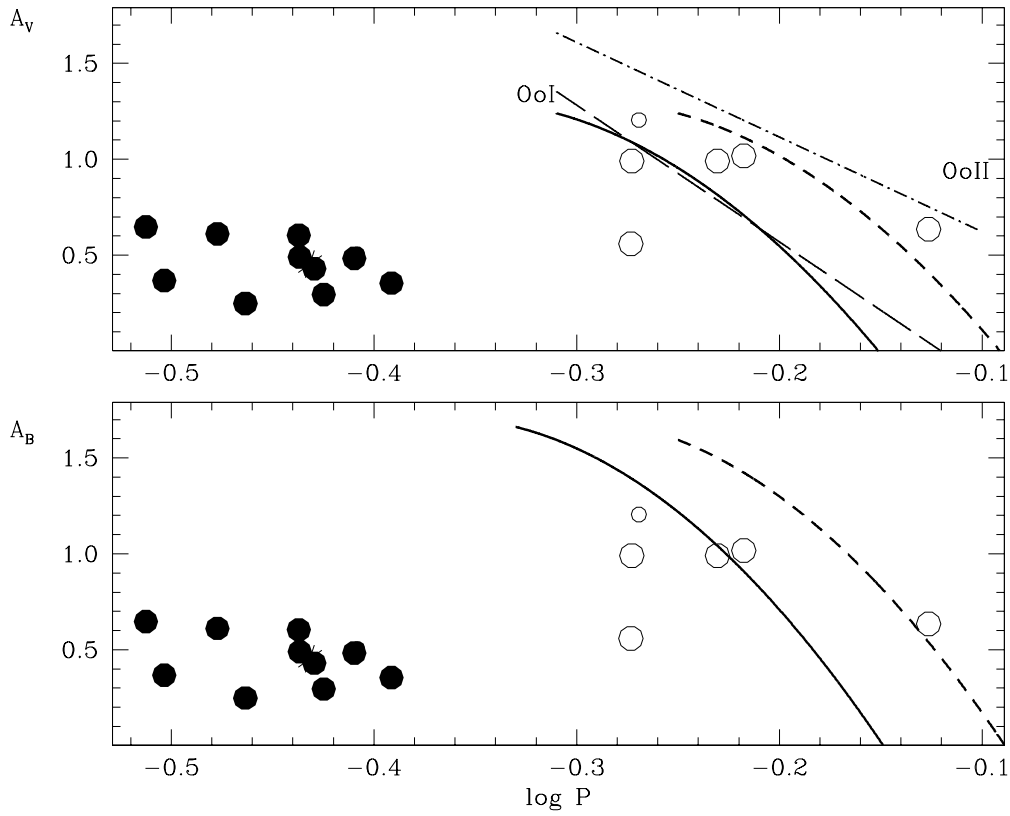

Figure 4.7 V, B period-amplitude diagrams of the For 5 RR Lyrae stars.The straight lines are the positions of the OoI and OoII Galactic GCs according to Clement & Rowe (2000). Period-amplitude distributions of the *bona fide* regular (solid curves) and well-evolved (dashed curves) *ab* RR Lyrae stars in M3 from Cacciari et al. (2005) are also shown for comparison. Larger symbols are variable stars located within 45″ from the For 5 center.

and outer. Then we have used the outermost variable stars in the field to empirically estimate the expected surface density of RR Lyrae stars in the Fornax galaxy.

In our Magellan data of For 2, 7 variable stars have been identified beyond $35''$, in an area of 1.6×10^4arcsec^2. On the basis of the overall surface density profile of the cluster, we assume that these variables are not associated with For 2. This provides an *upper limit* to the number density of field variable stars. Then we estimated a surface density of 4.4×10^{-4} RR Lyrae per arcsec^2 in the adjacent Fornax field. In the inner region, within a radius of $35''$ from the center, 1.7 field RR Lyrae stars are therefore expected.

The count excess produced by the stars in the globular cluster For 3 is very small beyond $R = 50''$. This is consistent with the density profile of For 3 obtained by Mackey & Gilmore (2003a). In our ESO-2.2m/WFI data, 13 variable stars, among which 10 are RR Lyrae stars, have been identified beyond $50''$, in an area of 1.3×10^4 arcsec^2. On the basis of the overall surface density profile of For 3, we assume that these variables are not associated with the cluster. This provides an *upper limit* to the number density of field variable stars. Then we estimate a surface density of 8.0×10^{-4} RRL per arcsec^2 in the adjacent Fornax field. Note that this result is nearly independent of the radius chosen for separating the inner/outer region. In the inner region, within a radius of 50 $''$ from the center of For 3, 6.3 field RR Lyrae stars are therefore expected.

The count excess produced by the stars in the globular cluster For 5 is very small beyond $R = 45''$. This is consistent with the density profile of For 5 obtained by Mackey & Gilmore (2003a). In our Magellan data, 2 variable stars have been identified beyond $45''$, in an area of 1.4×10^4 arcsec^2. On the basis of the overall surface density profile of For 5, we assume that these variables are not associated with the cluster. This provides an *upper limit* to the number density of field variable stars. Then we estimate a surface density of 1.5×10^-4 RR Lyrae per arcsec^2 in the adjacent Fornax field. In the inner region, within a radius of $45''$ from the center, 0.9 field RR Lyrae stars are therefore expected.

4.4 Cluster's Distances

In order to derive the distance to For 2, 3 and 5 from the average luminosity of their RR Lyrae stars we need estimates of the cluster's reddenings and metallicities, as well as values for the slope and zero point of the RR Lyrae luminosity-metallicity relation. We have assumed an absolute magnitude of M_V = 0.59$\pm$0.03 for RR Lyrae stars of [Fe/H] =$-$1.5 (Cacciari & Clementini, 2003), and $\Delta M_V/[\mathrm{Fe/H}]$=0.214$\pm$0.047 (Clementini et al., 2003; Gratton et al., 2004) for the slope of the luminosity-metallicity relation. We then adopt a standard extinction law (A_V=3.1$\times E(B-V)$) and reddening values of $E(B-V)$=0.05 $\pm$ 0.01; 0.04 $\pm$ 0.01; and 0.03 $\pm$ 0.01 for the three clusters, respectively, in agreement with (Mackey & Gilmore, 2003b). These values are also consistent with the color shifts required to match the blue edge of the RR Lyrae strip in M3 (assumed to have $E(B-V)$=0.01) to the colors of the bluest RR Lyrae stars in the three clusters.

We summarize in Table 4.8 a number of estimates for the metal abundances of the three clusters found in the literature. Metal abundances were also estimated from

the average period of the fundamental mode RR Lyrae stars ($\langle P_{ab} \rangle$) using Sandage (1993) formulas, they are given in Column 3 of Table 4.8. For For 2 and 3 we adopt the metal abundances from Buonanno et al. (1998) for consistency with the analysis of For 4 (see Chapter 5). These metallicities are in reasonably good agreement with values by both Strader et al. (2003) and Mackey & Gilmore (2003b), and are also consistent to the values inferred from the RR Lyrae stars (see Table 4.8). Buonanno et al. (1998) metal abundance for For 5 is instead significantly lower than found by Strader et al. (2003). For this cluster we will use both the metal abundance by Buonanno et al. (1998) and the metallicity by Strader et al. (2003).

Table 4.8 Comparison of metallicity estimates for the Fornax dSph clusters 2, 3 and 5.

Cluster	$\langle P_{ab} \rangle$	[Fe/H] $_a$	[Fe/H] $_b$	[Fe/H] $_c$	[Fe/H] $_d$
For 2	0.58	-1.66	-1.78 ± 0.20	-1.76 ± 0.41	-1.83 ± 0.07
For 3	0.62	-1.97	-1.96 ± 0.20	-1.84 ± 0.18	-2.04 ± 0.07
For 5	0.60	-1.82	-2.20 ± 0.20	-1.73 ± 0.13	-1.90 ± 0.06

^{a} metallicity from the $\langle P_{ab} \rangle$, this work; ^{b} metallicity from Buonanno et al. (1998); ^{c} metallicity from Strader et al. (2003); ^{d} metallicity from Mackey & Gilmore (2003b).

The V band average luminosity of the RR Lyrae stars that are more likely cluster members is: $\langle V(RR) \rangle$=21.35$\pm$0.02 mag (σ=0.08 mag, average on 25 stars), $\langle V(RR) \rangle$=21.30$\pm$0.03 mag (σ=0.12 mag, average on 22 stars), and $\langle V(RR) \rangle$=21.34$\pm$0.02 mag (σ=0.07 mag, average on 16 stars), in For 2, 3 and 5, respectively.

Clusters distance moduli then are: μ_0(For 2)=20.66$\pm$0.07 (D=135.1$\pm$4.3 kpc), μ_0(For 3)=20.68$\pm$0.07 (D=136.8$\pm$4.3 kpc), and μ_0(For 5)=20.81$\pm$0.07 (D=145.2$\pm$4.8 kpc) if we adopt for the cluster the metal abundance by Buonanno et al. (1998), or μ_0(For 5)=20.71$\pm$0.07 (D=138.7$\pm$4.5 kpc) if we adopt Strader et al. (2003) metallicity. Here, the errors are the sum in quadrature of uncertainties of 0.02, 0.03 and mag in $\langle V(RR) \rangle$ (dispersion of the average of For 2, 3 and 5, respectively), 0.05 mag in the zero point of the photometry, 0.01 mag in $E(B-V)$ (corresponding to 0.03 mag in A_V), and of 0.03 mag and 0.047 mag/dex, respectively, in the zero point and in the slope of the RR Lyrae luminosity-metallicity relation.

Derived distances compare very well with estimates for the 3 clusters by (Mackey & Gilmore, 2003b) particularly when the higher metallicity is adopted for For 5. Results from the study of the variable stars in For 2, 3 and 5 are presented in Greco et al. (2007a) and Greco et al. (2007b).

Chapter 5

Variable Stars in the Fornax dSph Globular Clusters: Fornax 4

Fornax 4 (For 4), is the most compact and centrally located of the Fornax GCs, for which it has been suggested that it might actually be the nucleus of the Fornax dSph galaxy (Hardy, 2002; Strader et al., 2003). Buonanno et al. (1998, 1999) published color magnitude diagrams of the Fornax GCs based on HST observations from which they estimated the clusters' relative ages and metallicities. They concluded that For 4 differs both in horizontal branch (HB) morphology and age from the other GCs in Fornax: it is a metal-poor cluster ([Fe/H]=-2.01 ± 0.20, on the Zinn & West 1984 metallicity scale,(Buonanno et al., 1999) with a red HB and seems to be 3-4 Gyrs younger than the other clusters. They also noted that the cluster CMD is virtually identical to that of the "outer halo" Galactic cluster Ruprecht 106 (Rup 106), an unusual cluster often considered to have once been a member of a dwarf galaxy tidally disrupted by the Milky Way (e.g. Brown et al., 1997a; Buonanno et al., 1999; Bellazzini et al., 2003a). More recently, Strader et al. (2003) used low-resolution, integrated Keck spectra to measure metallicities and infer ages for the five GCs in Fornax. The new ages and metallicities are different than found byBuonanno et al. (1998, 1999). According to Strader et al.. the metallicity of For 4 is [Fe/H]=-1.5 ± 0.12 (on the Zinn & West 1984 metallicity scale), and they estimate that the age of For 4 is the same as that of Fornax 1, 2 and 3, all older than Fornax 5 by 2-3 Gyr.

For 4 has never been surveyed for variability, in spite of clear indications, from its HB morphology (Buonanno et al., 1999), that it should contain RR Lyrae stars. In this Chapter we present results from an extensive study of the variable star population in this extragalactic GC that resulted in the discovery of 29 variable stars of which 27 are certainly RR Lyrae stars. The average luminosity of the RR Lyrae stars is used to measure the cluster distance. The periods, amplitudes, and period-amplitude distributions allow us to define the Oosterhoff type (Oo-type) of For 4 and to verify whether it conforms to the Oosterhoff dichotomy shown by the Galactic GCs.

5.1 Observations and Data Reductions

B, V time series photometry of For 4 and of its surrounding field was obtained with the MagIC camera of the Magellan/Clay 6.5-m telescope on two nights in November 2003 and on two nights in December 2004.

We covered a total field of view of $2.4' \times 2.4'$, centered on the cluster at RA=2:40:07.33, DEC=$-$34:32:17.4 (J2000). Nights were photometric with seeing conditions varying from 0.45″ to $0.65''$. We acquired a total number of 58 V and 19 B images. Average exposure times were 500 seconds for the V frames and 700s for the B ones. Observations of the standard fields TPhe and Ru149 (Landolt, 1992) were obtained on the same nights, to calibrate the data to the standard Johnson-Cousins photometric system.

The Magellan data were complemented by observations of the Fornax dSph field containing For 4 obtained with the wide field imager of the 4-m Blanco/CTIO telescope. Data were collected over three runs for a total of 5 nights spread on three years from 2003 to 2005. The images were taken on the Mosaic II imager, which has a $36' \times 36'$ field of view centered at RA=2:41:07.29 and DEC= $-$34:16:35.6 (J2000) with a plate-scale of 0.27 ″/pixel. The cluster was imaged on amplifier 1 of the 16 amplifier mosaic. The conditions during the three runs were photometric or nearly photometric. The seeing varied over the range of 0.8″ to 1.9″. The exposures times varied from 100s to 60s in V and 200s to 600s in B with 100s and 200s being typical, respectively. The CTIO dataset consists of 142 V and 61 B images. Logs of the observations and details of the instrumental set-up at the two telescopes are given in Table 5.1.

Table 5.1 Instrumental set-ups and logs of the observations.

Dates UT	Telescope	Instrument	Detector (pixel)	Resolution (″/pixel)	FOV	N_B	N_V	Photometric accuracy (HB level) (mag)
Nov., 13 − 15, 2003	Magellan/Clay	MagIC	2048 × 2048 SITe	0.069	$2.35' \times 2.35'$	10	39	0.01
Dec., 1 − 2, 2004	Magellan/Clay	MagIC	2048 × 2048 SITe	0.069	$2.35' \times 2.35'$	9	19	0.01
Nov., 14, 2003	Blanco/CTIO	MosaicII	2048 × 4096 SITe	0.27	$36' \times 36'$	8	16	0.03 − 0.05
Oct., 25 − 26, 2004	Blanco/CTIO	MosaicII	2048 × 4096 SITe	0.27	$36' \times 36'$	51	124	0.03 − 0.05
Sept., 9, 2005	Blanco/CTIO	MosaicII	2048 × 4096 SITe	0.27	$36' \times 36'$	2	2	0.03 − 0.05

The Magellan frames were bias-subtracted and flatfield-corrected using the MagIC tool in IRAF*. Then they were reduced with DAOPHOT-ALLSTAR. Time series photometry for all the stars was produced with ALLFRAME (Stetson, 1994, 1996). The photometric precision at the HB level is 0.01 mag. The photometric calibration was derived using the standard stars observed at the Magellan telescope on the night of Nov. 13, 2003 (UT).

A set of linear calibration relations was computed:

$$B = b' + 0.051(B - V) + 26.87$$

*IRAF is distributed by the National Optical Astronomical Observatories, which are operated by the Association of Universities for Research in Astronomy, Inc., under cooperative agreement with the National Science Foundation

$$V = v' - 0.049(B - V) + 26.81$$

where b' and v' are the instrumental magnitudes normalized to 1-s exposure and corrected for atmospheric extinction by adopting the mean extinction coefficients $k_B = 0.22$ and $k_V = 0.12$. The zero point uncertainties of the calibration relations are estimated of the order 0.05 mag in B and V, and 0.03 mag in $(B - V)$, from the night-to-night scatter of the standard stars. These relations were used to calibrate the instrumental magnitudes, and aperture corrections were applied based on photometry of relatively isolated stars.

The Magellan observations of For 4 produced a color-magnitude diagram (CMD) reaching $V \simeq 25$ mag. This CMD is shown in Figure 5.1. Although the cluster area observed with the Magellan telescope mainly contains stars within the For 4 tidal radius, the cluster CMD is contaminated by stars belonging to the Fornax field, since the cluster lies in the center of the Fornax dSph galaxy. On the other hand no reliable photometry could be obtained for stars inside a radius of $7''$ from the cluster center due to crowding. The CMD in Figure 5.1 was drawn cutting off this central region.

The images taken at the 4-m Blanco telescope were reduced using the SMSN pipeline (Rest et al., 2005) originally created for the SuperMACHO and ESSENCE projects. The images were cross-talk corrected, astrometrically calibrated, split into the 16 amplifiers, and standard reduced. Since the images are optically distorted due to the large field of view, they were then deprojected into a tangential plane using a customized version of Swarp (Bertin et al., 2002). DoPHOT (Schechter et al., 1993) was then used on the frames to get profile-fitted photometry of the stars (and other objects), with photometric precision of 0.03-0.05 mag for stars on the HB. Local standards were used to transform individual images to the standard system. Final photometric calibration was then obtained by adjusting to the zero points of the Magellan dataset.

5.2 Variable Star Identification

Variable stars in For 4 were identified by applying the Image Subtraction Technique, as performed by ISIS2.1 (Alard, 2000), to the 2003+2004 Magellan V dataset (58 frames in total), producing a catalog of about 400 candidate variable stars. The ISIS catalog was cross-identified against the DAOPHOT/ALLFRAME photometric catalog obtaining light curves in magnitude scale and confirming the variability for 20 stars. A further 9 variable stars were recovered in the cluster's central region where we lack reliable PSF photometry. For these stars we analyzed the differential flux light curves produced by ISIS.

Variable stars were independently identified from the CTIO dataset, using difference image analysis (Phillips & Davis, 1995; Alard & Lupton, 1998; Alard, 2000) We used the HOTPANTS package (Becker et al., 2004) to match the PSF of the image and template by applying a spatially varying kernel to the image with the better seeing before the template is subtracted. One of the main problems with the image differencing approach, is that there are more residuals, e.g. cosmic rays and bleeds, than genuinely variable objects in the difference image. Therefore a

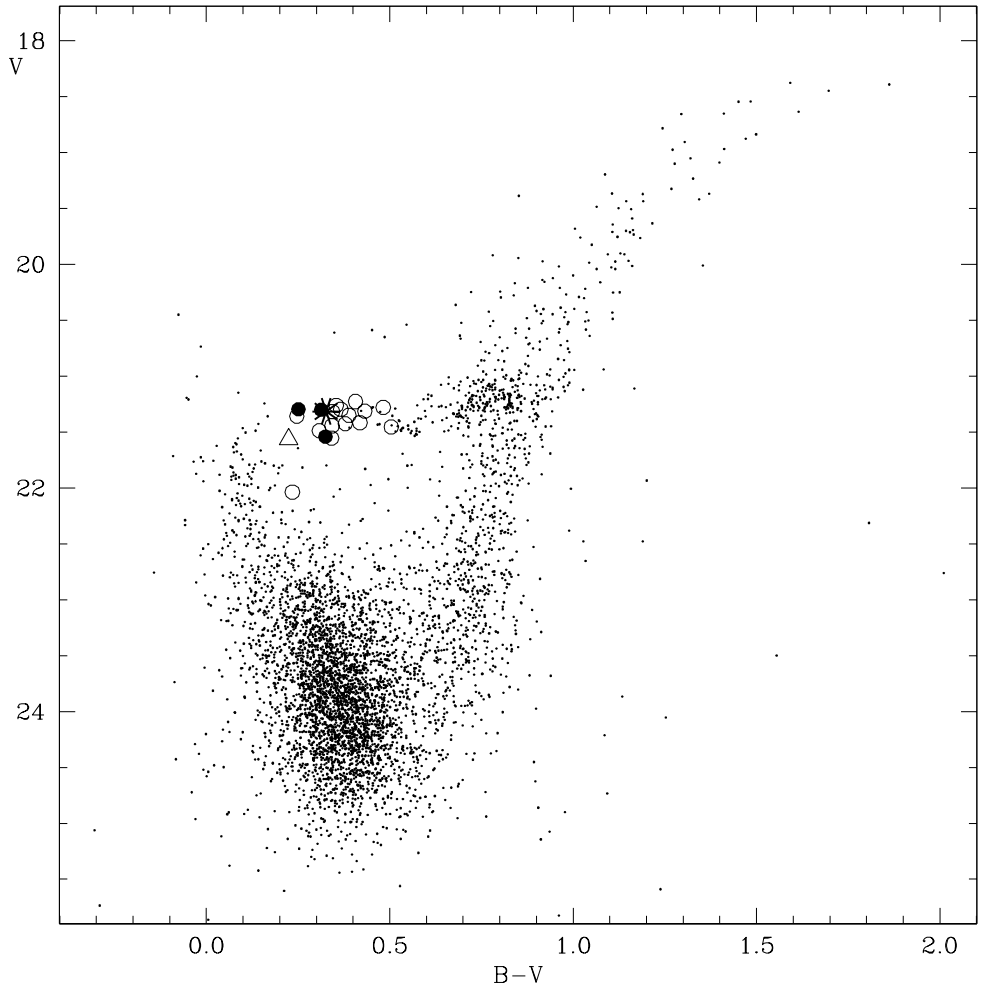

Figure 5.1 Color-magnitude diagram of For 4 from the Magellan data. Variable stars are displayed with different symbols. Open circles: *ab*-type RR Lyrae stars; filled circles: first overtone RR Lyrae stars; asterisk: double-mode pulsator (RRd). The open triangle marks a peculiar RR Lyrae star (V13).

standard profile-fitting software like DoPHOT has problems determining the proper PSF used to perform photometry in the difference image. The difference image was analyzed with our customized version of DoPHOT, where we forced the PSF to be the one determined for the original, flattened image. Applying this a priori knowledge of the PSF helped to guard against bright false positives, such as cosmic rays and noise peaks, which generally do not have a stellar PSF.

By matching the coordinates we were able to cross-identify 20 of the variable stars identified from the Magellan dataset. Fifteen of them had been independently recognized as variable stars from the CTIO data. Due to the high crowding no reliable match could be obtained for variable stars in the cluster central region. The time series B, V photometry of the 20 confirmed variable stars with light curves in magnitude scale is provided in Table 5.2.

Table 5.2 V, B photometry of the For 4 variable stars with light curves in magnitude scale

Star V18 - RRab			
HJD	V	HJD	B
(-2452956)		(-2452956)	
0.697471	21.86	0.749611	22.26
0.702402	21.79	1.563541	21.66
0.708871	21.76	1.604275	21.93
0.714947	21.79	1.631649	21.97
0.729866	21.77	1.665676	22.10
0.735942	21.83	1.690539	22.18
0.742018	21.83	1.717479	22.24
0.757122	21.84	1.744663	22.33
0.763198	21.84	1.772030	22.31
0.784262	21.84	2.554781	20.88

A portion of Table 5.2 2 is shown here for guidance regarding its form and content.

5.3 Period Search and Pulsation Properties of the Variable Stars

The time series of the 400 candidate variable stars were analyzed using two different codes. We used GrATiS (Graphical Analyzer of Time Series), a custom software developed at the Bologna Observatory by P. Montegriffo (see Di Fabrizio, 1999; Clementini et al., 2000) which uses both the Lomb periodogram (Lomb, 1976; Scargle, 1982) and the best fit of the data with a truncated Fourier series (Barning, 1963), as well as the iterative sine–wave least–squares method (Vanicek, 1971), combined with a Fourier series decomposition limited to significant terms only (Poretti, 2001). Visual inspection of the intranight light curves was also performed.

After having compared the results, only candidate variable stars confirmed by both methods have been accepted (29 stars in total). Both the Magellan and CTIO datasets were used, when available, to determine the pulsation characteristics of the variable stars from the study of their light curves. The possibility of

combining the two datasets allowed us to increase the time–on–targets, greatly improving the phase coverage. In such a way we could solve the alias ambiguities at $f \pm 1$ cycle/day, which were very severe when considering only one dataset. The merged datasets also returned a better estimate of the period, epoch of maximum light and amplitudes of the light variation of the confirmed variable stars. We were able to derive reliable periods and light curves for 20 variable stars observed with both the Magellan and CTIO telescopes and for 3 stars with differential fluxes from the Magellan dataset only. For the remaining six cases we can only provide a rough estimate of the period or simply an identification of variability. The spectral window of our data is dominated by strong aliases at n cycles per year (with $-3 \leq n \leq 3$). We used period values to the fifth digit to fold the light curves, since this allowed us to significantly reduce the r.m.s scatter of the light curve best fitting models. However, our period determinations are not free from the annual aliasing effect, and this can easily affect the fourth digit. In other words, the true frequency could be an alias at n cycle/year of that corresponding to the periods finally adopted for the variable stars (see Table 5.3). The standard deviations of the least–square fits of the Magellan light curves are in the range from 0.02 to 0.04 mag and from 0.01 to 0.07 mag in V and B respectively, quite acceptable and comparable with the expected precision of stars with $V \sim 21.5$ mag in a very crowded field.

Twenty seven of the variable stars detected in For 4 clearly appear to be RR Lyrae stars: 22 *ab*-, 3 *c*-type, and 2 double-mode pulsators. However, among the listed fundamental mode pulsators three have uncertain classifications, and a fourth one, star V13, has the typical period of a fundamental mode pulsator, but the light curve shape of a first overtone variable star. An RRab star with similar behavior was observed in NGC6441 by Pritzl et al. (2003). Coordinates for the variable stars are provided in Table 5.3, along with period, type, time of maximum light, number of phase points in the Magellan and CTIO data-sets separately, intensity-averaged $\langle \mathrm{V} \rangle$ and $\langle \mathrm{B} \rangle$ magnitudes, and amplitudes of the light variation (A_V and A_B). Examples of light curves are shown in Figure 5.2. The complete atlas of light curves is presented in the Appendix.

The folded light curves of V14 show a scatter larger than for the other variables, in the CTIO dataset in particular, therefore the star mean magnitudes and amplitudes are uncertain. However, the individual measurements seem to confirm the intrinsic faintness of V14, that appears to be about 0.6 mag fainter than the average level of the cluster HB. This faint magnitude would put V14 likely beyond the limits of Fornax if the star is a *bona-fide* RR Lyrae variable. Stars V10, V15 and V29 also are interesting given their small amplitudes for their periods. The Magellan light curves of V5 clearly show maxima at different height, suggesting a double-mode nature.

5.4 Membership Probability

Given the different stellar content of the globular cluster For 4 and the surrounding Fornax field populations, estimating the expected number of RR Lyrae variables belonging to cluster For 4 from the overall surface density profile is not straightforward. We have used both the outermost variable stars in the Magellan

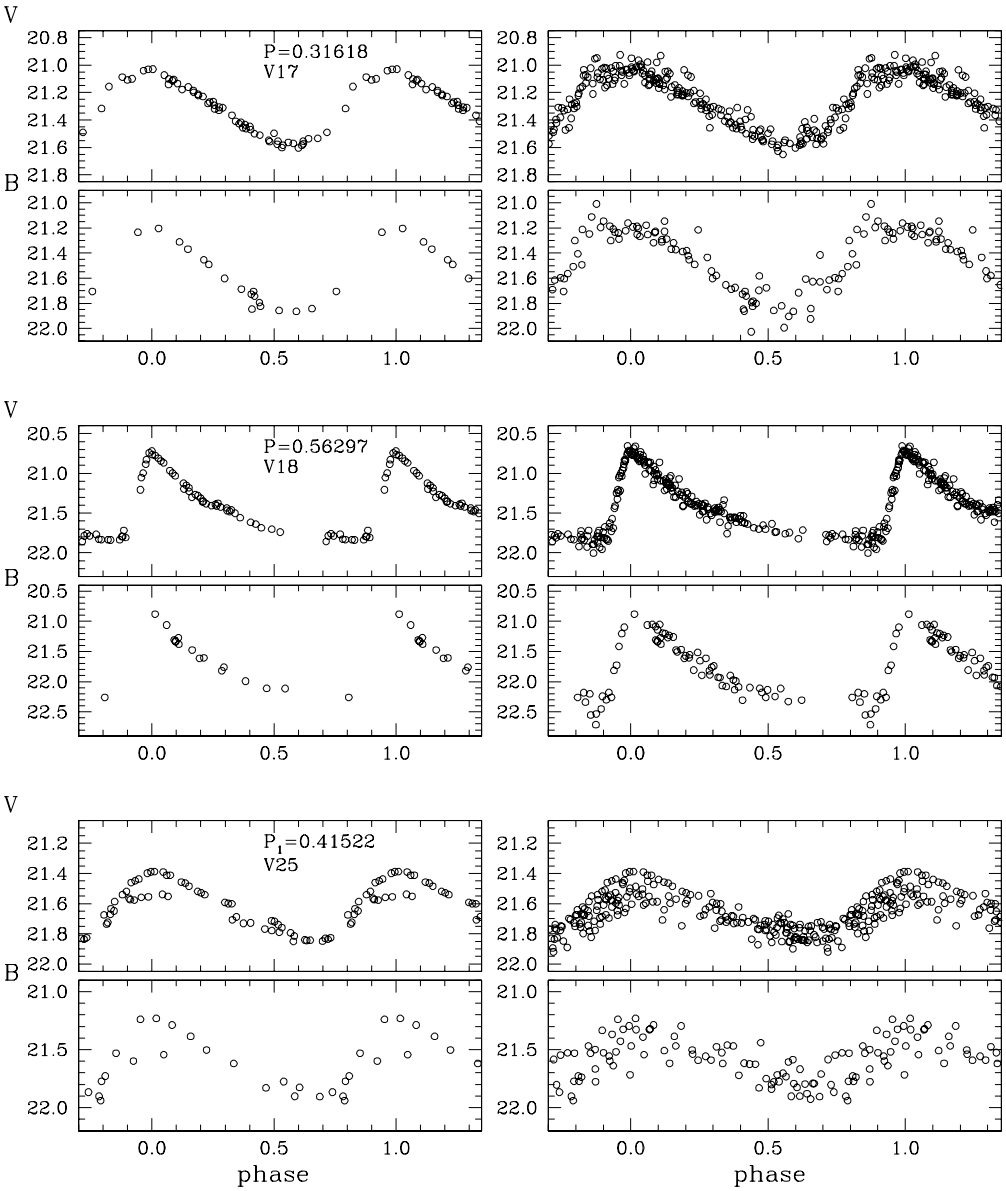

Figure 5.2 V, B light curves of RR Lyrae stars in For 4. Left panels, from top to bottom: an RRc, an RRab and an RRd star from the Magellan dataset only. Right panels: same as before but for the combined Magellan + CTIO dataset.

Table 5.3 Identification and properties of the For 4 variable stars

Name (a)	Id	α (2000)	δ (2000)	Type	P (days)	Epoch (-2450000)	$\langle V \rangle$	N_V	$\langle B \rangle$	N_B	A_V	A_B	Notes
V1	LC378	2 : 40 : 07.62	−34 : 32 : 09.4	RRab	0.54 ::	···	···	54	···	···	···	···	(b, c)
V2	LC360	2 : 40 : 07.70	−34 : 32 : 09.8	RRab	0.6261	2955.77	···	52	···	···	···	···	(b)
V3	LC330	2 : 40 : 07.47	−34 : 32 : 10.7	RRab	0.5968	3342.640	···	56	···	···	···	···	(b, c)
V4	LC386	2 : 40 : 07.75	−34 : 32 : 09.0	RRab	0.65 ::	···	···	53	···	···	···	···	(b, c)
V5	LC319	2 : 40 : 07.80	−34 : 32 : 11.0	RRd	0.46 ::	···	···	57	···	···	···	···	(b)
V6	LC381	2 : 40 : 07.33	−34 : 32 : 09.2	RRab	0.52936	2956.736	···	55	···	···	···	···	(b)
V7	LC178	2 : 40 : 07.49	−34 : 32 : 15.1	RRab	0.5 ::	···	···	55	···	···	···	···	(b, c)
V8	LC486	2 : 40 : 07.40	−34 : 32 : 05.1	RR?	0.83 ::	···	···	57	···	···	···	···	(b, c)
V9	LC291	2 : 40 : 07.99	−34 : 32 : 11.5	RR?	0.69 ::	···	···	57	···	···	···	···	(b, c)
V10	2658	2 : 40 : 07.34	−34 : 32 : 03.6	RRab	0.64450	2956.740	21.31	51	21.75	19	0.40	0.49	
V11	2051	2 : 40 : 08.39	−34 : 32 : 09.7	RRab	0.53085	3342.568	21.42	57 + 136	21.80	17 + 60	1.06	1.36	
V12	2272	2 : 40 : 07.99	−34 : 32 : 20.5	RRab	0.59506	3342.545	21.35	58 + 139	21.74	19 + 61	0.83	1.03	
V13	2949	2 : 40 : 06.81	−34 : 32 : 16.9	RRab	0.58767	2958.620	21.57	52	21.79	13	0.85	0.75 ::	(d)
V14	1956	2 : 40 : 08.55	−34 : 32 : 12.4	RRab	0.64520	3303.680	22.04	55 + 109	22.27	19 + 47	1.14	1.40	
V15	2076	2 : 40 : 08.33	−34 : 32 : 19.8	RRab	0.67000	2958.640	21.45	58 + 139	21.96	18 + 58	0.27	0.42	
V16	2651	2 : 40 : 07.35	−34 : 31 : 55.7	RRab	0.51910	3341.555	21.49	57	21.80	17	0.64	0.83	
V17	2664	2 : 40 : 07.33	−34 : 32 : 25.9	RRc	0.31618	2958.573	21.30	57 + 141	21.55	17 + 63	0.53	0.67	
V18	3177	2 : 40 : 06.38	−34 : 32 : 15.7	RRab	0.56297	2958.5475	21.44	58 + 124	21.79	19 + 39	1.15	1.54	
V19	3303	2 : 40 : 06.14	−34 : 32 : 08.8	RRab	0.52651	2958.600	21.55	58 + 136	21.90	19 + 52	1.20	1.50	
V20	1685	2 : 40 : 09.09	−34 : 32 : 17.2	RRc	0.36479	3342.544	21.54	52 + 141	21.87	18 + 51	0.40	0.43	
V21	2948	2 : 40 : 06.80	−34 : 32 : 33.9	RRc	0.39962	3341.663	21.30	56 + 131	21.62	19 + 50	0.36	0.42	
V22	3544	2 : 40 : 05.68	−34 : 32 : 20.4	RRab	0.65250	3341.540	21.42	57	21.83	19 + 49	0.57	0.71	
V23	1130	2 : 40 : 10.29	−34 : 32 : 12.4	RRab	0.55746	3342.595	21.28	56 + 136	21.76	19 + 56	0.54	0.69	
V24	4153	2 : 40 : 04.39	−34 : 32 : 40.9	RRab	0.61631	2958.695	21.30	58 + 140	21.66	19 + 59	0.69	0.90	
V25	2219	2 : 40 : 07.91	−34 : 33 : 07.2	RRd	0.41522	2958.570	21.31	56 + 137	21.64	19 + 61	0.31	0.56	(e)
V26	4779	2 : 40 : 03.13	−34 : 31 : 43.4	RRab	0.61610	2958.600	21.31	57	21.66	19	1.18	1.46	
V27	4989	2 : 40 : 02.63	−34 : 32 : 42.0	RRab	0.59643	3341.620	21.36	58 + 140	21.60	19 + 61	0.84	1.12	
V28	437	2 : 40 : 11.81	−34 : 31 : 13.6	RRab	0.55954	3303.880	21.26	55 + 119	21.62	17 + 51	0.97	1.24	
V29	5361	2 : 40 : 01.81	−34 : 32 : 54.7	RRab	0.69860	2958.587	21.23	58 + 134	21.64	19 + 61	0.40	0.65	

[a] Variable stars were assigned increasing numbers starting from the cluster center that was set at $\alpha = 02 : 40 : 07.6$, $\delta = -34 : 32 : 10.0$ (J2000). Stars from V1 to V22 are located within $30''$ from the For 4 center, hence are more likely cluster members.

[b] Light curves available in differential flux only.

[c] Stars with gaps in the folded light curve.

[d] Star with the typical period of a fundamental mode pulsator, but with the light curve of a first overtone pulsator.

[e] Double-mode RR Lyrae star with fundamental mode period P_0= 0.56284 and period ratio of P_1/P_0=0.7377, in the table we list the star first overtone period.

field and the variables found in the larger CTIO field to empirically estimate the expected surface density of RR Lyrae in the Fornax galaxy. In the Magellan data, 6 variable stars have been identified beyond $50''$, in an area of 1.23×10^4 arcsec^2. On the basis of the overall surface density profile of For 4, we can assume that these variables are not associated with the cluster. Then we estimate a surface density of 4.9×10^{-4} RRL per arcsec^2 in the Fornax field. As for the CTIO data, RR Lyrae stars have been counted in an annulus between $140''$ and $220''$ from the center of For 4, which is an optimal compromise between the statistical benefits of sampling a large area and the need to keep our measurement *local* in view of the spatially varying stellar populations of Fornax. A surface density of 7.2×10^{-4} RRL arcsec^{-2} is inferred from the CTIO dataset. In the inner region, within a radius of $30''$ from the center, 1.4 and 2.0 field RR Lyrae stars are therefore expected, respectively. In conclusion, among the RR Lyrae stars within about $30''$ from Fornax 4, about 2 stars are possibly belonging to the Fornax dSph field.

The same exercise for the innermost variables found with ISIS shows that they

are most likely to be all cluster members.

5.5 Oosterhoff Type

The pulsation properties of the For 4 RR Lyrae stars are summarized in Table 5.4 where we list the number of fundamental mode (RR_{ab}), first overtone (RR_c) and double mode pulsators (RR_d) in the first three Columns, respectively; the ratio of number of RR_c to total number of RR Lyrae stars (RR_{tot}), in Column 4; the average periods of the *ab*- and *c*-type RR Lyrae stars, in Columns 5 and 6; and the shortest and longest RR_{ab} periods, in Columns 7 and 8. The average period of the *c*-type RR Lyrae stars is: $\langle P_c \rangle$=0.36 d (σ=0.04 d, average on 3 stars), or 0.37 d (σ=0.04 d, average on 4 stars), if the RRd star is included. The *ab*-type RR Lyrae stars have $\langle P_{ab} \rangle$=0.59 d (σ=0.05 d, average on 19 stars). V13 and V14 were not considered. Average and σ do not change if V13 is included, but $\langle P_{ab} \rangle$=0.60 d if V14 is added. The shortest period RRab is star V16 with $P_{ab,min}$=0.5191 d, and the longest period RRab is star V29 with $P_{ab,max}$=0.6986 d.

Table 5.4 Average quantities of the For 4 RR Lyrae stars

N_{RRab} (a)	N_{RRc} (a)	N_{RRd} (a)	$N_{RRc}/N(RR_{tot})$ (a,b)	$\langle P_{ab} \rangle$ (c)	$\langle P_c \rangle$ (d)	$P_{ab,min}$	$P_{ab,max}$
22(16)	3(3)	2(1)	0.12(0.16)	0.59	0.36	0.5191	0.6986
			0.19(0.20)	0.60	0.37		

[a] Values in brackets are considering only RR Lyrae stars within $30''$ from the cluster center.

[b] Ratio of RRc to total number of RR Lyrae stars with (lower value) and without (upper values) the RRd stars.

[c] Fundamental mode average period with (lower value) and without (upper value) stars V13 and V14.

[d] First overtone average period with (lower value) and without (upper value) the double mode star V25.

The period distribution of the RRab stars seems to show two separate peaks at $\langle P_{ab} \rangle$=0.55 d and $\langle P_{ab} \rangle$=0.64 d, respectively —thus resembling the case of NGC 1835 in the Large Magellanic Cloud (Soszynski et al., 2003). However, a KMM test (Ashman et al., 1994a) performed on our data shows that they are consistent with a unimodal distribution in P_{ab}. According to the RR Lyrae star average periods For 4 appears to be an Oosterhoff-intermediate (Oo-Int) cluster, an Oo-type that has no counterpart among the Milky Way GCs. Even if we only consider stars in the inner region of the cluster ($R \leq 30''$) and if we also take into account that one or two of them could not belong to the cluster (see Section 4.1), we have $\langle P_{ab} \rangle$=0.59, thus confirming a true Oosterhoff-intermediate behavior for this cluster, similarly to what found for the other 4 GCs in Fornax by our study (see Chapter 4) and by Mackey & Gilmore (2003b).

Period-amplitude distributions for the For 4 RR Lyrae stars with light curves in magnitude scale are shown in Figure 5.3.

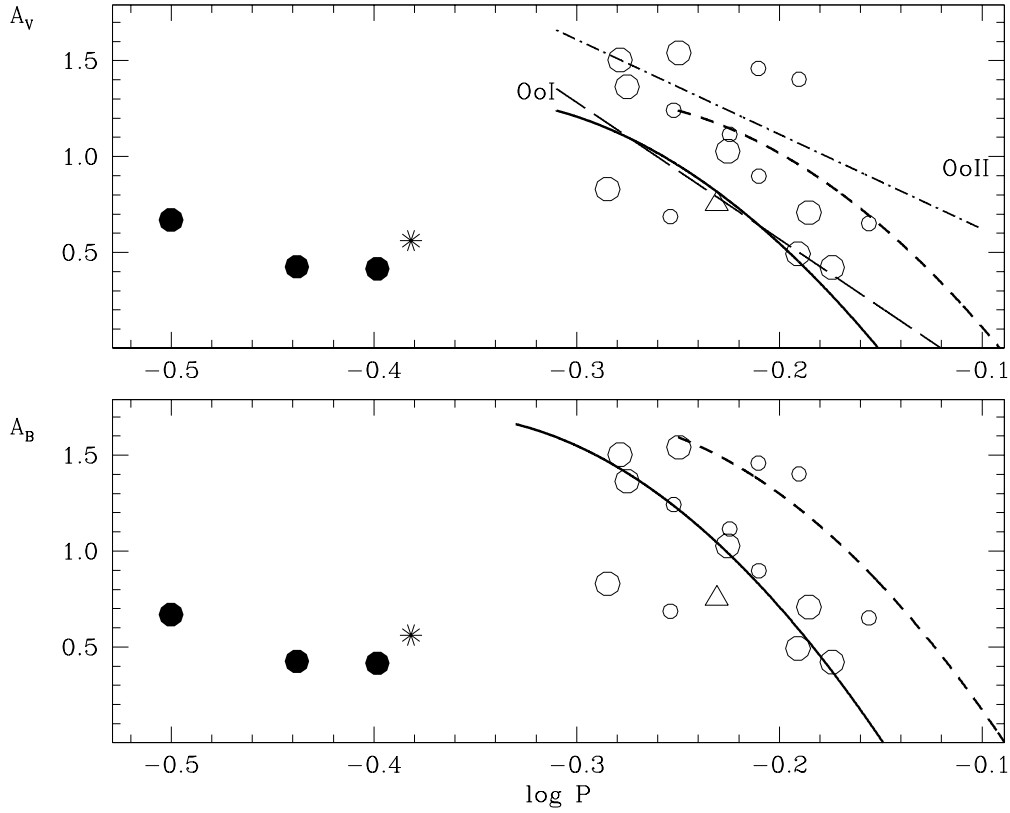

Figure 5.3 V, B period-amplitude diagrams of For 4 RR Lyrae stars. Symbols are as in Figure 1, but those indicating variable stars located at distances less than 30′ from the cluster center are expanded. The straight lines are the positions of the OoI and OoII Galactic GCs according to Clement & Rowe (2000). Period-amplitude distributions of the *bona fide* regular (solid curves) and well-evolved (dashed curves) *ab* RR Lyrae stars in M3 from Cacciari et al. (2005) are also shown for comparison.

Expanded symbols are used for stars located at distances less than $30''$ from the cluster center. Figure 5.3 shows that the majority of the *ab*-type RR Lyrae stars in For 4 appears to be on the OoI line. It is also noteworthy that the ratio of RRc to the total number of RR Lyrae stars is more like OoI (RRc/RRtot = 0.12 without the RRd stars and 0.19 with them, or 0.16 and 0.20, respectively, depending upon whether we consider all the RR Lyrae stars in For 4, or just those within $30''$ from the cluster center). In Figure 5.3 there are, however, a number of RRab's that pile up near the OoII location. However, the two stars closer to the OoII line are located outside R=30″, thus their membership is less certain.

The metal abundance of For 4 is somewhat uncertain being [Fe/H]=−2.0 in Buonanno et al. (1999) study, and [Fe/H]=−1.5 in Strader et al. (2003). There are some metallicity estimates that can be made using the pulsation properties of the RR Lyrae stars. Applying the Alcock et al. (2000) relation, which is based on the period and V-band amplitude of RRab stars, we found a mean metallicity of -1.68 for the cluster (or -1.66 for the 10 RRab stars within $30''$ from the cluster center). This is intermediate between Buonanno et al. and Strader et al. values. Using relations from Sandage (2006), we find [Fe/H] values of -1.96 from the mean period of the fundamental mode RR Lyrae stars; -2.25 from the shortest period RRab: V16, a star located within $30''$ from the cluster center, hence very likely belonging to For 4; and -1.38 from the longest period RRab: star V29, the most external of the variables in our sample, hence probably belonging to the Fornax dSph field. Finally, from Sandage (1993), we find [Fe/H]=−1.90 from the mean period of the three cluster RRc stars, which all are located within $30''$ from the For 4 center.

Thus, the cluster RR Lyrae stars seem to suggest a low metal abundance for For 4, closer to the Buonanno et al. (1999) estimate.

We note, however, that none of the conclusions on the Oosterhoff-intermediate status of For 4 are affected in any way by a change in the cluster metal abundance from -2.0 to -1.5 dex. Indeed, for both values of metallicity For 4 is found to fall in the Oo-Int region in the $\langle P_{ab}\rangle - [\mathrm{Fe/H}]$ diagram (Pritzl et al. 2002; Catelan 2007). In particular, adopting a metallicity of [Fe/H] = -1.5 according to Strader et al. (2003), would place For 4 right in the middle of the Oosterhoff- intermediate band in the [Fe/H]-HB type diagram (see Fig. 8 in Catelan 2006), whereas adopting [Fe/H]=−2.0 actually places the cluster slightly to the left of this band. In fact, and as discussed in Chapter 8, the key quantities defining Oosterhoff status appear to be the average and minimum periods of the *ab*-type RR Lyrae stars. In terms of both these quantities, For 4 appears entirely consistent with an Oosterhoff-intermediate classification. This is also what is generally expected on the basis of the position of the cluster in the HB type-metallicity plane (see Fig. 8 in Catelan 2006). Note, in this sense, that our photometry and preliminary number counts suggest a revised Lee-Zinn HB type of $(B-R)/(B+V+R) \approx -0.75$ for the cluster—where B, R, and V represent the numbers of blue, red, and variable stars on the HB, respectively. The Oo-Int behavior of For 4 further supports the cluster similarity with the unusual "young halo" Galactic cluster Rup 106, and strengthen the claim for an extragalactic origin of this MW cluster. Indeed, with $\langle P_{ab}\rangle$=0.61 (Clement et al., 2001) and [Fe/H]=−1.67 (Catelan, 2006), Rup 106 is one of the few Galactic GCs falling in the Oosterhoff-intermediate band in the [Fe/H]-HB type diagram (see Fig. 8 in

Catelan 2006).

5.6 Cluster Distance

The average luminosity of the RR Lyrae stars within $30''$ from For 4 center (hence more likely cluster members), and excluding star V14 which may be a background object, is $\langle V(RR)\rangle$=21.43±0.03 mag (σ=0.10 mag, average on 12 stars) and $\langle B(RR)\rangle$=21.76±0.04 mag (σ=0.13 mag, average on 12 stars). Average values become instead $\langle V(RR)\rangle$=21.38±0.02 mag (σ=0.10 mag, average on 19 stars) and $\langle B(RR)\rangle$=21.74±0.03 mag (σ=0.11 mag, average on 19 stars) if we consider "all" the variables in the field of For 4 but V14. Both these values, and the latter in particular, are consistent with the value of $\langle V(HB)\rangle$=21.37 ± 0.04 mag, for the mean level of the red old-HB stars in the Fornax field derived by Saviane et al. (2000). On the other hand, our values are respectively 0.09 and 0.14 mag brighter than V_{HB}=21.52 ± 0.05 found by Buonanno et al. (1999) using HB stars within a distance of $18''$ from the For 4 center. The 0.09 mag difference remains even if we consider only the 8 RR Lyrae stars with reliable photometry, located within $18''$ from the cluster center. Unfortunately, we lack reliable photometry for a further 9, more internal, RR Lyrae stars which are within $8''$ from the cluster center. However, we note that a $\sim$ 0.1 difference between our $\langle V(RR)\rangle$ and Buonanno et al. (1999) V_{HB} could easily be accounted for if the For 4 RR Lyrae stars were more evolved than their HB non-variable counterparts, as it is observed in a number of the metal poor GCs in the MW.

In order to derive the distance to For 4 from the average luminosity of its RR Lyrae stars we need an estimate of the cluster reddening and metallicity, as well as values for the slope and zero point of the RR Lyrae luminosity-metallicity relation. We have assumed an absolute magnitude of M_V = 0.59±0.03 for RR Lyrae stars of [Fe/H] =$-$1.5 (Cacciari & Clementini, 2003), and $\Delta M_V/[\mathrm{Fe/H}]$=0.214±0.047 (Clementini et al., 2003; Gratton et al., 2004) for the slope of the luminosity-metallicity relation. We then adopt a standard extinction law (A_V=3.1×$E(B-V)$) and a reddening value of $E(B-V)$=0.10 ± 0.02 for the cluster, which is the weighted average of Buonanno et al. (1999) $E(V-I)$=0.15 ± 0.06 (transformed to $E(B-V)$ using Cardelli et al. 1989 relation $E(B-V)$=1.31×$E(V-I)$), Mackey & Gilmore (2003b) $E(B-V)$=0.12 ± 0.05, and $E(B-V)$=0.08 ± 0.03, which is the color shift required to match the blue edge of the RR Lyrae strip in M3 (assumed to have $E(B-V)$=0.01) to the colors of the bluest RR Lyrae stars in For 4.

For [Fe/H]=-2.0 (Buonanno et al., 1999), the cluster distance modulus is then 20.64± 0.09 mag (D=134±6 kpc), while it becomes 20.53± 0.09 (D=128±6 kpc), if Strader et al. (2003) metallicity is adopted. Here, errors are the sum in quadrature of uncertainties of 0.03 mag in $\langle V(RR)\rangle$ (dispersion of the average), 0.05 mag in the zero point of the photometry, 0.02 mag in $E(B-V)$ (corresponding to 0.06 mag in A_V), and of 0.03 mag and 0.047 mag/dex, respectively, in the zero point and in the slope of the RR Lyrae luminosity-metallicity relation.

Previous distance estimates for the Fornax dSph field range from μ_0=20.59± 0.22 mag (Buonanno et al., 1985) to 20.76 (Demers et al. 1990; Buonanno et al. (1999, for an assumed metal abundance of the Fornax field stars of -1.4). Saviane

et al. (2000) infer μ_0=20.70$\pm$ 0.12 mag from the tip of the field stars RGB and μ_0=20.76$\pm$ 0.04 mag from the mean magnitude of Fornax old horizontal branch stars which are assumed to have [Fe/H]~ -1.8 and $E(B-V)$=0.03 mag. Buonanno et al. (1999) derive an average modulus of μ_0=20.62$\pm$ 0.08 mag for the Fornax clusters #1,2,3 and 5 and, more recently, Mackey & Gilmore (2003b) find for the same clusters distance moduli in the range from 20.58$\pm$0.05 to 20.74$\pm$0.05 mag, with average value of μ_0=20.66$\pm$ 0.03 (random) $\pm$ 0.15 (systematic). Finally, we have derived distance moduli in the range from 20.64$\pm$0.09 to 20.71$\pm$0.07 (or 20.81$\pm$0.07 depending on the metal abundance adopted for For 5) for the Fornax clusters #2,3,4 and 5. For ease of comparison we have summarize in Table 5.6 the various distance determinations and the different assumptions about reddening, metallicity and RR Lyrae luminosity-metallicity relation they are based on.

Table 5.5 Distance determinations based on the HB luminosity of the Fornax dSph field and globular clusters

V_{HB} (mag)	$E(B-V)$ (mag)	[Fe/H]	M_V *vs*[Fe/H]	μ_0	Reference
21.60$\pm$0.04 (field)	0.03 ± 0.3	-		20.59$\pm$0.22	Buonanno et al.(1985)
21.37$\pm$0.04 (field)	0.03	-1.8	0.17$\times$([Fe/H]+1.5)+0.57	20.76$\pm$0.04	Saviane et al. (2000)
21.36$\pm$0.14 (field)	0.05	-2.30 ± 0.30		20.76$\pm$x.xx	Demers et al.(1990)
21.28$\pm$0.06 (field)	0.05	-	0.17$\times$([Fe/H]+1.5)+0.57	20.68$\pm$0.08	from Buonanno et al.(1999)
21.28$\pm$0.01 (field)	0.04$\pm$0.03	-1.77 ± 0.20	0.22$\times$([Fe/H]+1.5)+0.50	20.72$\pm$0.10	Greco et al. (2007)
21.20$\pm$0.05 (For 1)	0.04$\pm$0.05	-2.20 ± 0.20	0.17$\times$([Fe/H]+1.5)+0.57	20.62$\pm$0.08	Buonanno et al.(1999)
21.35$\pm$0.05 (For 2)	0.07$\pm$0.05	-1.78 ± 0.20			Buonanno et al.(1999)
21.20$\pm$0.05 (For 3)	0.04$\pm$0.05	-1.96 ± 0.20			Buonanno et al.(1999)
21.20$\pm$0.05 (For 5)	0.06$\pm$0.05	-2.20 ± 0.20			Buonanno et al.(1999)
21.27$\pm$0.01 (For 1)	0.07$\pm$0.01	-2.05 ± 0.10	0.23$\times$([Fe/H]+1.6)+0.56	20.58$\pm$0.05	Mackey & Gilmore (2003)
21.34$\pm$0.01 (For 2)	0.05$\pm$0.01	-1.83 ± 0.07		20.67$\pm$0.05	Mackey & Gilmore (2003)
21.24$\pm$0.01 (For 3)	0.04$\pm$0.01	-2.04 ± 0.07		20.66$\pm$0.05	Mackey & Gilmore (2003)
21.33$\pm$0.01 (For 5)	0.03$\pm$0.01	-1.90 ± 0.06		20.74$\pm$0.05	Mackey & Gilmore (2003)
21.21$\pm$0.02 (For 3)	0.04$\pm$0.03	-1.91 ± 0.20	0.22$\times$([Fe/H]+1.5)+0.50	20.68$\pm$0.11	Greco (2003)
21.35$\pm$0.02 (For 2)	0.05$\pm$0.01	-1.78 ± 0.20	0.214$\times$([Fe/H]+1.5)+0.59	20.66 ± 0.07	see Chapter 3
21.30$\pm$0.03 (For 3)	0.04$\pm$0.01	-1.96 ± 0.20	0.214$\times$([Fe/H]+1.5)+0.59	20.68 ± 0.07	see Chapter 3
21.43$\pm$0.03 (For 4)	0.10$\pm$0.02	-2.01 ± 0.20	0.214$\times$([Fe/H]+1.5)+0.59	20.64 ± 0.09	see Chapter 4
		-1.52 ± 0.12		20.53 ± 0.09	
21.34$\pm$0.02 (For 5)	0.05$\pm$0.01	-2.20 ± 0.20	0.214$\times$([Fe/H]+1.5)+0.59	20.81 ± 0.07	see Chapter 3
		-1.73 ± 0.13		20.71 ± 0.07	

Our "long" distance modulus of 20.64$\pm$ 0.09 mag, based on [Fe/H]=$-$2.0 and $E(B-V)$=0.10 mag for For 4, agrees well with both the Saviane et al. (2000) and the Mackey & Gilmore (2003b) estimates, once differences in the adopted reddening, cluster metallicity, and RR Lyrae luminosity-metallicity relation are properly accounted for. It is however 0.09 mag shorter than one would infer by assuming Buonanno et al. (1999) V_{HB}=21.52 $\pm$ 0.05 for the cluster. On the other hand, the "short" distance modulus of 20.53$\pm$ 0.09 mag, based on [Fe/H]=$-$1.5 for For 4, is significantly shorter than any previous distance determination for the Fornax system.

Mackey & Gilmore (2003) find that the distance moduli of the Fornax clusters # 1,2,3 and 5 are consistent with a line of sight depth of $\sim 8-10$ kpc for this

galaxy. The distance moduli of For 4 and results from the study of the RR Lyrae stars in For 2, 3 and 5 presented in Chapter 4, show that For 4 is at the center of the Fornax GCs distance moduli distribution, and confirm Mackey & Gilmore (2003) finding of a line of sight depth in Fornax, although reducing its extent to about 8 kpc. Further insight on the line of sight depth of the Fornax dSph will be gained from our study of the galaxy's field variables.

Chapter 6

Variable Stars in the Bootes dSph Galaxy

The Bootes dSph galaxy (Belokurov et al., 2006a) is one of the ten new satellite companions of the Milky Way recently discovered in the SDSS. (Belokurov et al., 2006a) named the galaxy the Bootes dSph after the constellation of Bootes, in which the structure was detected. Munoz et al. (2006) obtained spectroscopy of red and asymptotic giant branch stars in the Bootes dSph galaxy from which they measured a very low metal abundance of [Fe/H]~ -2.5 dex, confirming the results obtained by (Belokurov et al., 2006a) based on the galaxy color magnitude diagram. This low metallicity makes Bootes the most metal-poor Local Group dSph known so far. Galaxies like the Bootes dSph are among the best candidates for the "building blocks" that may have contributed to the formation of the Galactic halo, and studying their stellar content can provide fundamental insights to reconstruct the star formation history and the merging episodes that led to the Galactic halo early assembling.

The Bootes galaxy $i, g-i$ CMDs published by Belokurov et al. (2006a) and Munoz et al. (2006) clearly show a horizontal branch that extends to the blue enough to cross the *classical instability strip*, thus suggesting that RR Lyrae stars should be present in the Bootes We have identified and obtained V, I light curves for 11 RR Lyrae stars (5 RRc, 5 RRab and 1 RRd) and one long period variable in the Bootes dSph and have investigated the Oosterhoff classification of this newly discovered dwarf galaxy with the RR Lyrae stars. We find that the RR Lyrae parameters support an Oosterhoff II class for the Bootes dSph and that the galaxy *ab*-type RR Lyrae stars might be slightly evolved objects.

6.1 Observations and Data Reductions

Time series V, I photometry of the Bootes dSph galaxy has been collected between 2006 April and June with the Bologna Faint Object Spectrograph and Camera at the 1.52 m telescope of the Bologna Observatory in Loiano*, and with the Device

*http://www.bo.astro.it/loiano/index.htm

Optimized for the LOw RESolution (DOLORES) at the 3.5 m Telescopio Nazionale Galileo (TNG) telescope[†], whereas B, V, I observations have been gathered at the 2.3 m Wyoming Infrared Observatory (WIRO) telescope, using the WIRO-Prime CCD prime focus camera [‡]. Table 6.1 summarizes the main characteristics of the three instruments and describes the distribution of the phase points among them. Due to the different field of view of the three instrumental set-ups, the number of phase points ranges from a minimum of 17 and four to a maximum of 52 and 17 in the V and I bands, respectively. Typical internal errors of our V-band photometry for single phase points at the level of the HB are in the range from 0.01 to 0.03 mag.

Table 6.1 Instrumental set-ups and number of observations per instrument.

Instrument	CCD	Resolution arcsec/pixel	FOV arcmin^2	N V,I	Photometric error mag
PrimeFocus@WIRO	2048 × 2048 Marconi	0.55	20 × 20	13,4	< 0.01
DOLORES@TNG	2048 × 2048 Loral	0.275	9.6 × 9.6	12,9	$0.01 \div 0.03$
BFOSC@Loiano	1340 × 1300 EEV	0.58	13 × 13	27,4	$<0.01 \div 0.02$

Images were prereduced following standard techniques (bias subtraction and flat-field correction) with IRAF[§], and I-band images were corrected for fringing by adopting, for each instrument, a well-suited fringing map. We measured the star magnitudes by aperture photometry, since the field is not crowded and the image quality of a number of frames was not sufficient for a satisfactory point-spread function (PSF) evaluation. After a preliminary PSF reduction performed with the DaophotII/Allstar packages (Stetson, 1987, 1992), aperture photometry was carried out with a radius of 1.5 FWHM for each individual image. The absolute photometric calibration was obtained during the night of May 8 2006 through the observation at the TNG of standard stars in Landolt field PG1633 (Landolt, 1992) as extended by P.B. Stetson[¶]. For the atmospheric extinction coefficient, we adopted the average value for La Palma[‖]. A total number of 67 standard stars covering approximately the color interval 0.6 mag $< V-I <$ 2.7 mag were used to derive the calibration equations which have $\sigma = \pm 0.016$ and ± 0.019 mag scatter, in V and I, respectively. The derived color terms are in good agreement with those found on the DOLORES@TNG web page and in the literature. Since the aperture photometry of the standard stars was performed with an aperture radius of 5.5 arcsec, we derived a correction for the (smaller) aperture used in the two reference scientific frames. This correction is 0.06 and 0.07 ± 0.03 mag in V and I, respectively. The total uncertainty of our photometry is σ_V=0.035 mag and σ_I=0.04 mag, in V and I, respectively.

[†] http://www.tng.iac.es/instruments/lrs/

[‡] http://physics.uwyo.edu/ãmonson/wiro/prime.html

[§] IRAF is distributed by the National Optical Astronomical Observatories, which are operated by the Association of Universities for Research in Astronomy, Inc., under cooperative agreement with the National Science Foundation

[¶] http://cadcwww.dao.nrc.ca/standards/

[‖] see http://www.ast.cam.ac.uk/dwe/SRF/camc_extinction.html

6.2 The Galaxy CMD

The $I, V-I$ CMD of the Bootes dSph is shown in Figure 6.1. The two lines are the mean ridge lines of the globular clusters M15 (solid line) and M3 (dashed line), drawn from the cluster's CMDs available at Padua University WEB site**, and shifted in magnitude and color to fit the galaxy HB.

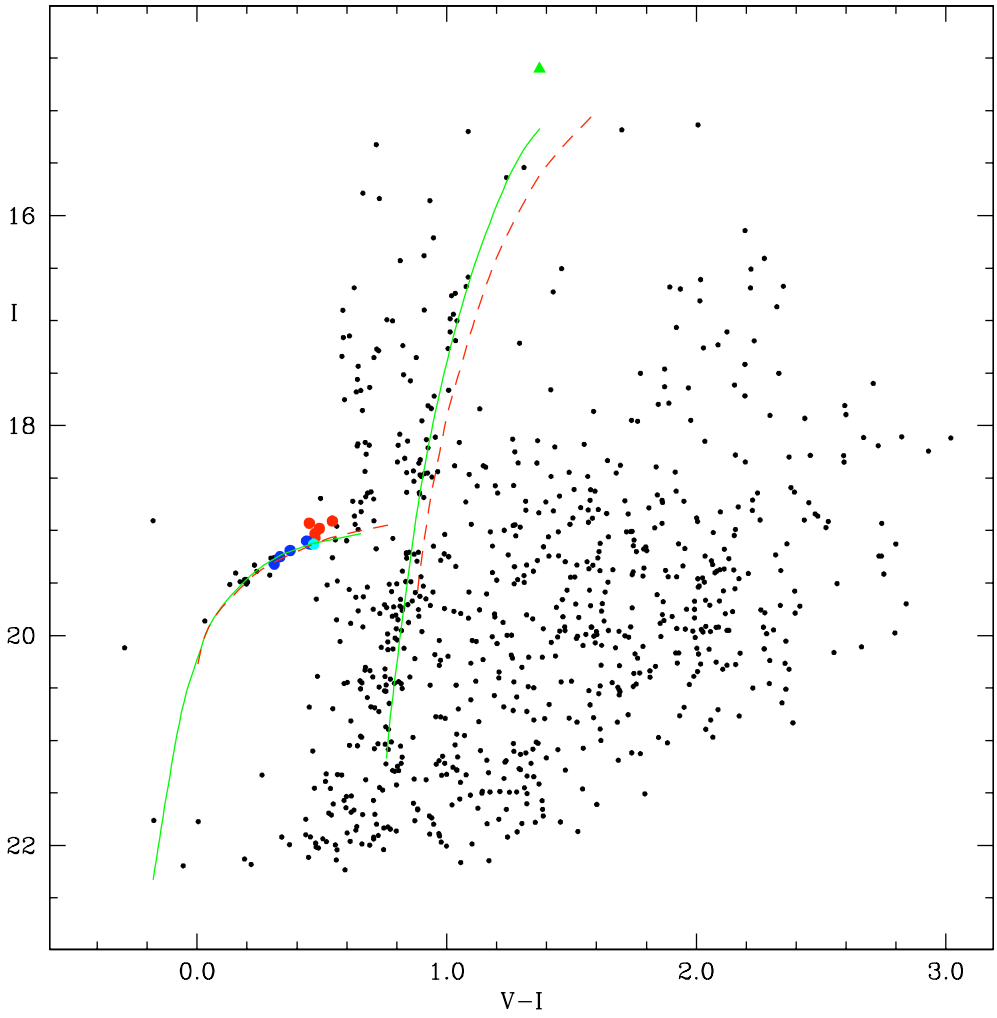

Figure 6.1 I, $V-I$ CMD of the Bootes dSph galaxy with the variable stars plotted in different colors. Red circles are *ab*-type RR Lyrae stars (RRab's) and the variable ~ 0.2 mag above the galaxy HB; blue and cyan circles are first overtone (RRc) and double-mode (RRd) pulsators, respectively; the green triangle is a long period variable (LPV). Solid and dashed lines show the mean ridge lines of M15 and M3, shifted in magnitude and adjusted in reddening to fit the galaxy HB.

The Bootes red giant branch (RGB) is very well fitted by a metal-poor cluster

**http://dipastro.astro.unipd.it/globulars, note that the Padua photometry is calibrated to the Landolt standard system.

like M15 ([Fe/H]~ -2.3), thus supporting the low metal abundance derived for the galaxy by Munoz et al. (2006). A low metal abundance in the range from ~ -2.0, to -2.5 dex is also suggested by the location in the Petersen diagram of a double mode pulsator we have identified in the galaxy (see Section 6.4). If we adopt for the galaxy the distance modulus we infer from the average luminosity of the RR Lyrae stars (see Section 6.4) and adopt the Bellazzini et al. (2004) calibration of the tip I luminosity, we estimate that the galaxy RGB tip is at I=15.40 mag for [Fe/H]=-2.5. Bootes's brightest star in our CMD is V16 at V=15.97 and I=14.60, hence about 0.8 mag above the galaxy tip.

6.3 Identification of the Variable Stars

Variable stars were identified from the V band time series where we have a larger number of phase points and then counter-identified in I. First we calculated the Fourier transform (in the Schwarzenberg-Czerny 1996 formulation) for each star in the photometric catalog with at least 12 epochs, then we averaged this transform to estimate the noise and calculated the signal-to-noise ratios. We then checked all the stars with high S/N, which for the RR Lyrae stars typically went from 25 to 160. Coordinates for the variable stars were obtained cross correlating our catalog with the catalog MAST/casg[††] The r.m.s of the cross correlation is 0.07 arcsec for both coordinates.

All the RR Lyrae stars in our sample are also in the S06 database, while S06's V1, V7, V11 and V13 are outside our field of view. We were able as well to assess the variability of the bright star located close to the tip of the Bootes RGB (see Fig. 6.1 for which S06 does not provide a light curve.

Periods were derived using GRaTiS (Graphical Analyzer of Time Series) a custom software developed at the Bologna Observatory (see Di Fabrizio 1999; Clementini et al. 2000). We were able to derive reliable periods for 11 of the 12 stars we identified in the Bootes dSph. Given the about 100 days window of our observations these periods are accurate to the fourth digit. Along with the star's average luminosity, the light variation amplitude and CMD position allowed us to classify the variable star type. Our sample includes 5 RRc's, 5 RRab's, 1 RRd and 1 long period variable (LPV). The properties of the variable stars are summarized in Table 6.2.

Examples of the light curves are shown in Figure 6.2, where data for the RR Lyrae stars are folded using the periods and epochs of maximum light provided in Table 6.2. V16 turned out to be a LPV.

In the 100 days spanned by our observations we only observed a portion of the star's light curve, thus only a rough estimate of the period could be obtained. In Figure 6.2 we show for V16 the sequence of observations in HJD.

Our periods agree with S06's periods rounded to the second digit for 9 out of the 11 variables we have in common. However, the S06 periods, although similar to ours, do not provide the best fit to our data. Furthermore, there are two remarkable differences with respect to S06 classification, namely stars: V5 and V12. These stars have been classified by S06 respectively RRc and RRab. The S06 period for

[††] Available at http://www-gsss.stsci.edu.

Table 6.2 Identification and properties of the variable stars in the Bootes dSph galaxy

Name (a)	α (2000)	δ (2000)	Type	P (days)	Epoch (-2450000)	$\langle V \rangle$ (b)	N_V	$\langle I \rangle$ (b)	N_I	A_V	A_I	Notes
V2	13 : 59 : 51.34	14 : 39 : 06.0	RRc	0.3119 :	3852.729 :	19.63	14	19.32	3	0.34 :	> 0.13	
V3	14 : 00 : 26.86	14 : 35 : 33.1	RRc	0.3232	3852.808 :	19.58	19	19.25	3	0.57	> 0.15	
V4	14 : 00 : 08.90	14 : 34 : 24.1	RRc	0.3860	3847.4073	19.57	42	19.19	7	0.59	0.20	
V5	14 : 00 : 21.56	14 : 37 : 28.8	RRab :	0.6506 :	3886.8486	19.38	15	18.93	4	0.33	-	(c)
V6	13 : 59 : 45.95	14 : 31 : 40.7	RRc	0.3919	3852.778	19.58	50	19.13	15	0.53	0.22	
V8	13 : 59 : 59.69	14 : 27 : 34.0	RRc	0.4179	3852.891	19.54	49	19.10	17	0.40	0.26	
V9	13 : 59 : 47.28	14 : 27 : 56.3	RRab	0.5755	3881.4475	19.55	52	19.07	14	1.00	> 0.41	
V10	14 : 00 : 25.75	14 : 33 : 08.4	RRab	0.6280	3860.418	19.47	27	18.98	4	1.09	> 0.24	
V12	13 : 59 : 56.00	14 : 34 : 55.0	RRd	0.3948	3852.891	19.59	41	19.13	8	0.53	> 0.20	(d)
V14	13 : 59 : 25.75	14 : 23 : 45.3	RRab	0.7186	3846.994 :	19.50	13	19.03	2	0.44 :	-	
V15	14 : 00 : 11.09	14 : 24 : 19.7	RRab	0.8456	3851.856	19.45	41	18.91	14	0.48	0.28 :	
V16	13 : 59 : 48.74	14 : 34 : 48.2	LPV	~ 85	-	15.97	33	14.60	1	> 0.43	-	

[a] Variable stars from V2 to V15 coincide with stars in S06.

[b] $\langle V \rangle$ and $\langle I \rangle$ values are intensity-averaged mean magnitudes.

[c] Variable star about 0.2 mag brighter than the galaxy HB.

[d] Double mode RR Lyrae star with fundamental mode period P_0=0.5296 d, and period ratio P_1/P_0=0.7455.

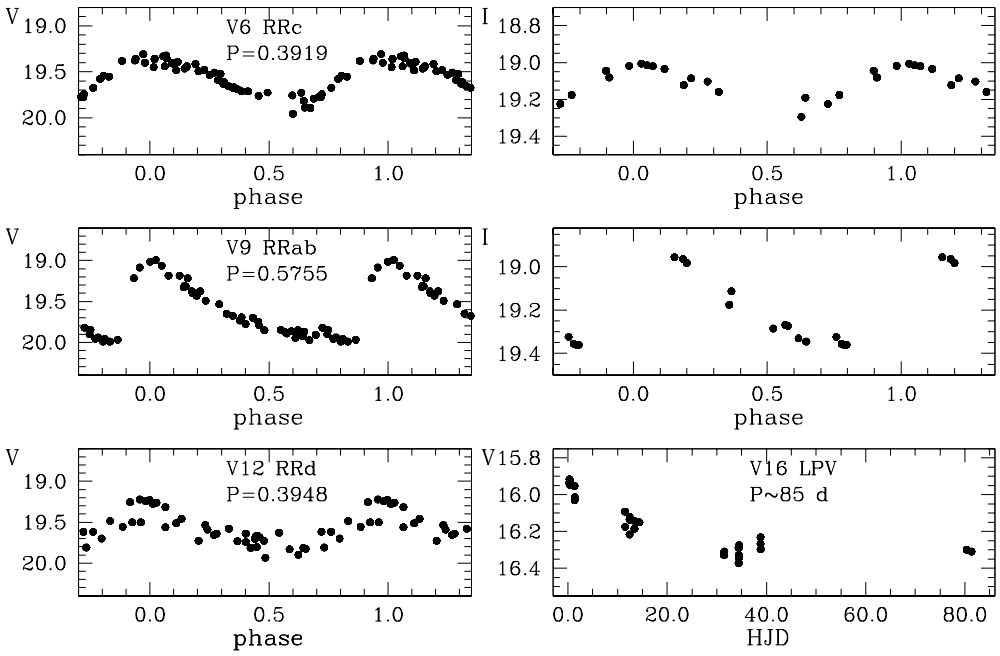

Figure 6.2 V and I light curves of variable stars in the Bootes dSph galaxy. Top panels: *c*- and *ab*-type RR Lyrae stars. Bottom left: V light curve of the RRd star; bottom right: light curve in Heliocentric Julian Day (HJD) of the LPV.

V5 (0.3863158 d) does not phase our data. Our best fit period for the star is 0.6506 d. A shorter period of about 0.3943 d could possibly phase our data, although with a larger scatter and it is thus considered less likely. We also find that the star has very

small amplitude, on average about 0.2 smaller than other *c*-type RR Lyrae stars, and is about 0.2 mag brighter than the galaxy HB. Both the reduced amplitude and the over-luminosity might be caused by V5 being blended with a companion star. However, additional and better resolution data would be needed to assess the star actual nature. Given its peculiarities and the less certain classification in type, in the following discussion this star will always be considered separately. The most striking difference with S06 is star V12 that we find to be a double mode RR Lyrae star, with periods of P_1=0.3948 and P_0=0.5296 d, and period ratio of 0.7455 d. The double mode behavior of V12 is clearly seen in Figure 6.2, and the star's position near the transition between *c*- and *ab*- type RR Lyrae stars seem to support our finding.

6.4 The Oosterhoff type of the Bootes dSph

The average periods of the RR Lyrae stars are: $\langle Pc \rangle$=0.37 d (σ=0.04, average on 5 stars; average and σ do not change whether we include or not the double mode star) and $\langle Pab \rangle$=0.69 d (σ=0.12, average on 4 stars) or 0.68 (σ=0.10, average on 5 stars) if the variable star brighter than the HB is considered. These average values and the high frequency of *c*-type stars are consistent with the Bootes dSph being an Oosterhoff type II system (Oosterhoff 1939), and along with the low metal abundance make of the galaxy an analog of the Ursa Minor dSph galaxy. The V period-amplitude relation of the Bootes RR Lyrae stars is shown in Figure 6.3 and compared with the distributions of the M3 RRab stars.

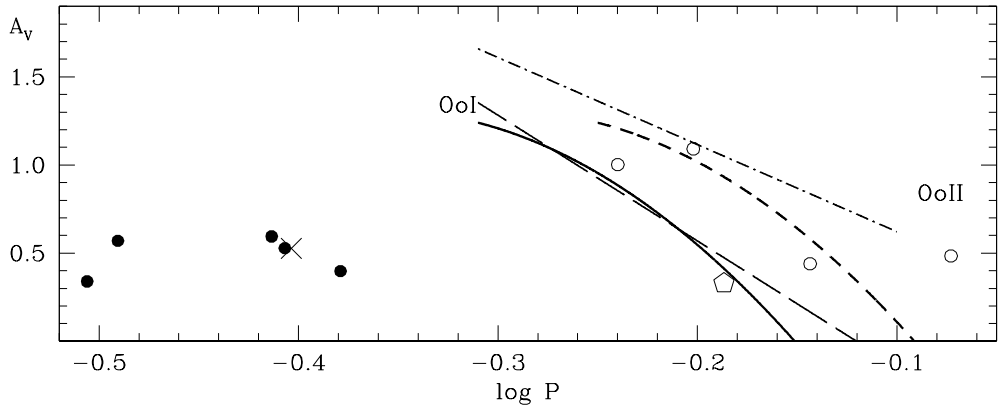

Figure 6.3 Period-Amplitude diagram in the V band for the Boo RR Lyrae stars. Filled and open circles are *c*- and *a*b-type RR Lyrae stars, respectively. The X sign is the double mode star. The large pentagon is V5 the variable about 0.2 mag above the HB having rather small amplitude. The straight lines are the positions of the Oosterhoff type I (OoI) and II (OoII) Galactic GCs according to Clement & Rowe (2000). Period-amplitude distributions of the *bona fide* regular (solid curve) and well-evolved (dashed curve) *ab*-type RR Lyrae stars in M3 from Cacciari et al. (2005) are also shown for comparison.

The 4 Bootes *ab*-type RR Lyrae stars with certain classification (open circles

in Figure 6.3) are found to lie close to the region occupied by the well-evolved M3 RRab stars (dashed curve in Figure 6.3, taken from Cacciari et al. 2005) and the Oosterhoff type II locus. According to Table 6.2 these stars appear also to be slightly brighter than the average level of the Bootes HB and in Figure 6.1 lie slightly above the HB ridge lines of M15 and M3, thus confirming they could be evolved objects. In conclusion, all the evidence agrees that the Bootes dSph is an old, metal-poor object of Oosterhoff II class.

6.5 The Distance to the Bootes dSph

The average luminosity of the Bootes RR Lyrae stars is $\langle \mathrm{V} \rangle$=19.546 ± 0.018 (σ=0.057, average on 10 stars) and $\langle \mathrm{V} \rangle$=19.531 ± 0.022 (σ=0.073, average on 11 stars) if the over-luminous star is included. Assuming for the absolute luminosity of the RR Lyrae stars at [Fe/H]=-1.5 M_V=0.59$\pm$0.03 (Cacciari & Clementini 2003), $\Delta M_V/[Fe/H]$=0.214 ($\pm$ 0.047) mag/dex (Clementini et al. 2003, Gratton et al. 2004) for the slope of the luminosity metallicity relation, $E(B-V)$=0.02 (according to Belokurov et al. 2006a and in agreement with the small color shift required to match M15 and the Bootes horizontal and red giant branches), and [Fe/H]=-2.5 (Munoz et al. 2006), the galaxy distance modulus is: 19.11 $\pm$ 0.08 or 19.09 $\pm$ 0.08 if the overluminous variable is included, where errors include the standard deviation of the average, and the uncertainties in the photometry, reddening, and RR Lyrae absolute magnitude.

The presence of a double-mode RR Lyrae star in Bootes allows us to estimate its mass, hence derive the galaxy distance, by comparing observed and predicted period ratios in the Petersen diagram (Petersen, 1972) for double mode RR Lyrae stars. Clementini et al. (2004) published an updated version of this diagram and compared it with the pulsation models of Bono et al. (1996) and Bragaglia et al. (2001). The position of V12 in the Petersen diagram is shown in Figure 6.4 which is an update of Clementini et al. (2004) figure 14. The star location in the diagram seems consistent with RRd stars in OoII clusters, and we find the star's mass is close to 0.80 $M\odot$, in agreement with the evolutionary predictions for HB stars populating the instability strip at Z=0.0001 (see e.g. Pietrinferni et al. 2004). This mass, combined with the luminosity provided by the Petersen diagram and the observed fundamental period of V12, allows us to evaluate the star's $\log T_e$ from the pulsation equation. We used Equation 1 in Di Criscienzo et al. (2004). Once the mass, luminosity, and effective temperature are known, the star's absolute visual magnitude was calculated using the model atmospheres by Molaro et al. (1997a,b). We find M_V(V12)=0.52, with a conservative error of $\sim$ 0.13 mag. The corresponding distance modulus for the Bootes dSph is then $\mu_0 = V_0 - M_V = 19.01 \pm 0.15$ mag.

We estimated the distance to the Bootes system with two further independent methods: i) the comparison of theoretical and empirical RR Lyrae first overtone blue edges (FOBE) and fundamental red edges (FRE) in the M_V versus $\log P$ plane (see Caputo 1997, Caputo et al. 1999, Di Criscienzo et al. 2004) and, ii) the theoretical Wesenheit function (see Di Criscienzo et al. 2004). From the first technique we find that the Di Criscienzo et al. (2004) theoretical boundaries of the instability strip

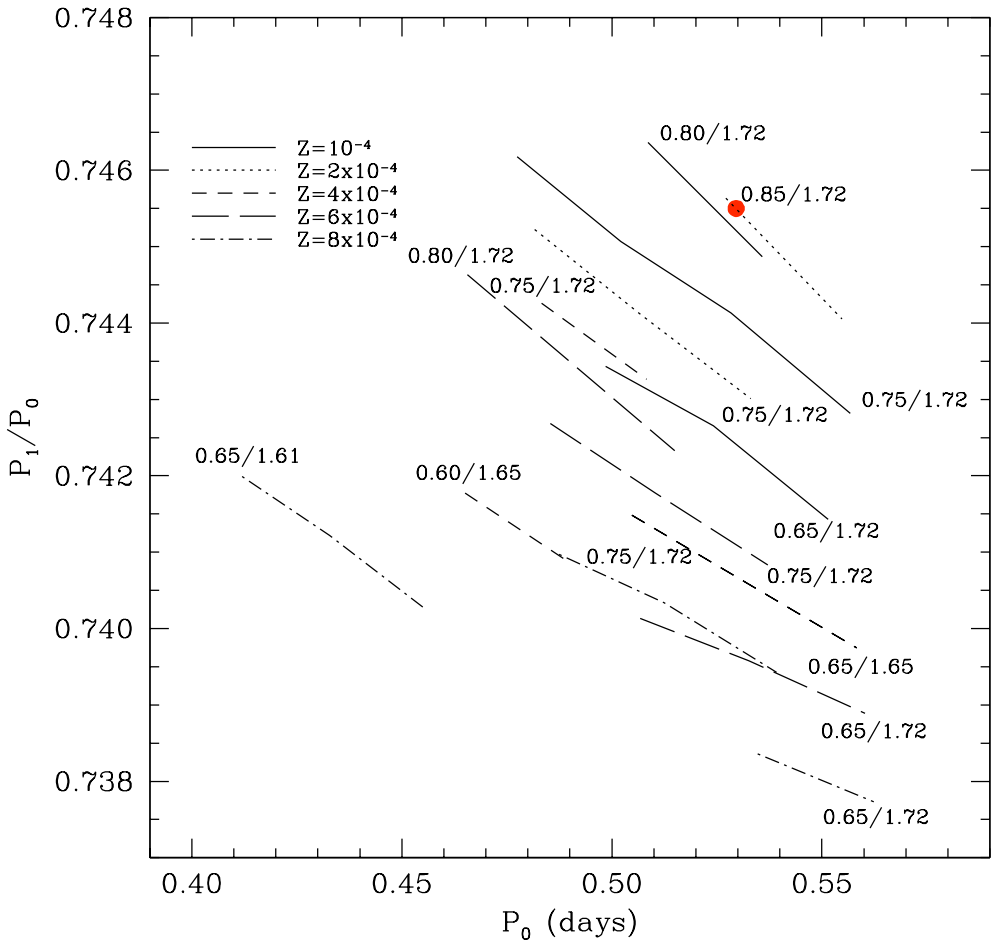

Figure 6.4 Comparison between the observed location of the RRd star V12 (filled circle) in the Petersen diagram, and the theoretical predictions of Bono et al. (1996) and Bragaglia et al. (2001) pulsation models. Numbers near each line indicate the model mass and luminosity.

(FOBE and FRE) for metal poor pulsators with mean mass of 0.80 $M_{\odot}$ match the observed RR Lyrae stars in Bootes for a distance modulus of 19.21±0.10 mag. A distance modulus of 19.17 ± 0.12 mag is obtained instead by adopting the theoretical Wesenheit relation for the same value of the mass and discarding V5. All these independent distance determinations based on the RR Lyrae stars are well consistent to each other within their quoted uncertainties. In summary, from the average luminosity of the RR Lyrae stars the Bootes galaxy distance modulus is μ_0=19.11 ± 0.08 mag (D=66 ± 3 kpc). Three further RR Lyrae-based independent methods confirm this distance within the observational errors, leading to a weighted mean modulus of μ_0=19.14 ± 0.07 mag (D=67 ± 2 kpc). Results from this study have

already been published (Dall'Ora et al., 2006).

Chapter 7

Variable Stars in the Remote Galactic Globular Cluster NGC 2419

NGC 2419 is an outer halo Galactic globular cluster and one of the most metal poor and luminous clusters in the Milky Way. Being one of the most remote Galactic clusters, it is located at $R_{\rm gc} \sim 90$ kpc, it has been used to quantify the mass enclosed within the Galaxy (Bellazzini, 2004a). Although both the distance and the dynamical parameters (core radius: $\rm r_c \sim 9$ pc, and half-light radius $\rm r_h \sim 19$ pc) put NGC 2419 among the outer halo Galactic globulars, the cluster has several exceptional properties with respect to other outer halo clusters, that make it one of the most intriguing Galactic clusters. According to the metal abundance ($[\rm Fe/H] \simeq -2.12$; Harris 1996) and the horizontal branch morphology, well populated from the red to the blue, NGC 2419 belongs to the most metal-poor group of known Galactic clusters. Comparison of the NGC 2419 color-magnitude diagram to that of the similarly metal-poor 'standard' cluster M92 shows that they have virtually the same age within 1 Gyr (Harris et al., 1997). Comparison of the low-metallicity globular clusters all throughout the Milky Way halo also shows that they share a same age to within ~ 1 Gyr, leading to the conclusion that the globular cluster formation has begun at same time in the Galactic halo over a region now extending almost 200 kpc in diameter. Indeed, for the most metal-poor clusters in the Milky Way halo there is no detectable age gradient with Galactocentric distance.

Outer halo clusters deserve particular attention when attempting to trace the formation of the Galaxy halo. Many papers have been devoted both to their global properties and to properties of individual clusters in the group. Out of the about 150 Galactic clusters in the Harris Catalogue (Harris, 1996), we can consider in this group 34 clusters having $R_{\rm gc} > 15$Kpc plus NGC 2808, which is at $R_{\rm gc} = 11.1$ kpc, but it has been associated with the CMa dSph. It has been known for some time that globular clusters in the Milky Way outer halo are, on average, fainter than those in the inner halo (see Figure 7.1). Evidence becomes even more straightforward if we compare the Galactic clusters at $R_{\rm gc} \geq 50$ with those at smaller Galactocentric radii. In this most distant sample only NGC 2419 breaks the rule, with an absolute visual magnitude $\rm M_V = -9.6$ mag (Harris, 1996). However, this does not seem to be a

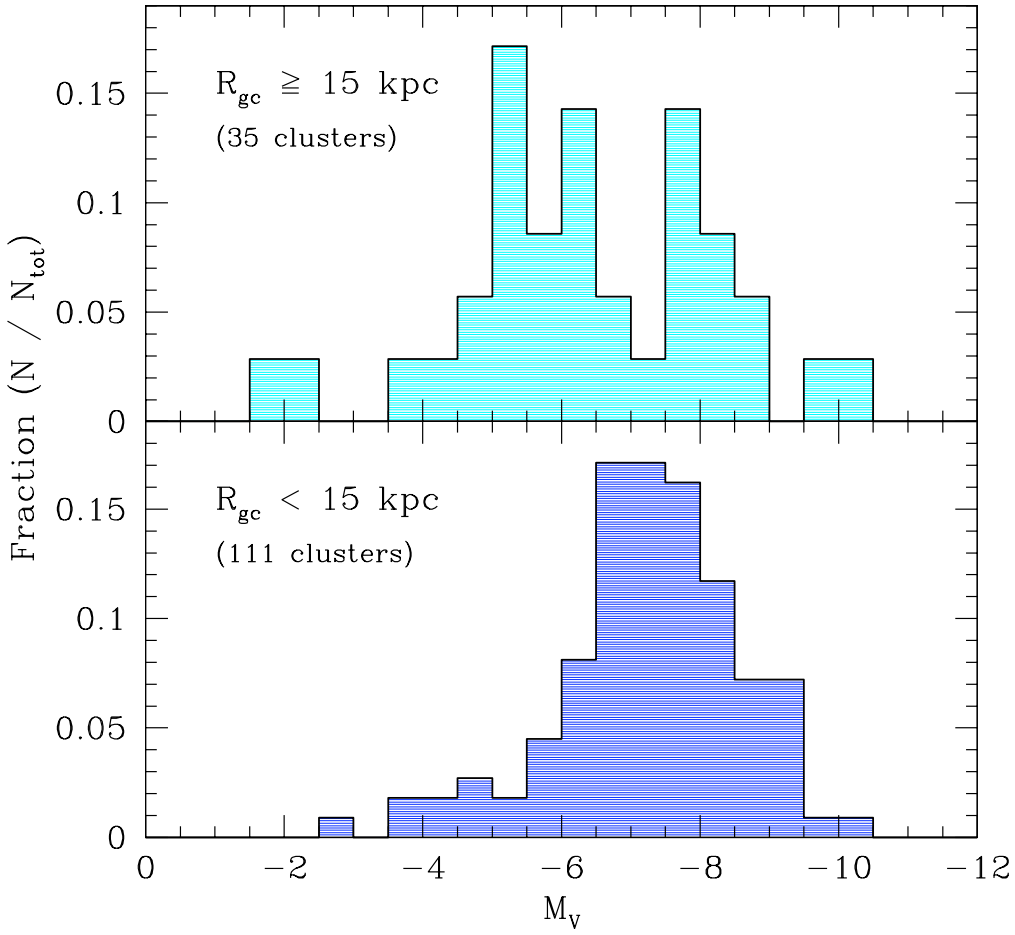

Figure 7.1 Luminosity distributions of Galactic inner halo ($R_{\rm gc} < 15$ kpc, lower panel) and of the outer halo ($R_{\rm gc} \geq 15$ kpc, upper panel) globular clusters.

general property of giant galaxy's halos, since several globular clusters as luminous as NGC 2419 are found instead in the outer halo of the giant elliptical NGC 5128 (see Fig. 1.6 of Chapter 1). NGC 2419 shows a peculiar behaviour in the half-light radius R_h versus V absolute magnitude plane too (see Chapter 1). There are only two other Galactic clusters with similar properties in this plane: ω Cen and M54. The former is known to host multiple stellar populations Norris (see e.g. 2004); Rey et al. (see e.g. 2004); Sollima et al. (see e.g. 2005); Villanova et al. (see e.g. 2007) and its properties appear to be consistent with the cluster being the stripped core of a now defunct dSph or dwarf elliptical galaxy. Similarly, M54 is thought to be the core of the Sagittarius dSph which is currently in the process of being merged with the Galaxy (see e.g. Layden & Sarajedini, 2000b). All these peculiarities and the similarity to ω Cen and M 54 suggest that also NGC2419 might be the relic of a disrupted dwarf spheroidal galaxy. However, substructures in the color magnitude diagram due to age/metallicity spreads of a possible composite population like that observed in ω Cen might not be observable in NGC 2419. Indeed, the cluster low metal abundance ([Fe/H]=-2.12 dex compared to [Fe/H]=-1.62 of ω Cen) would make any metallicity spreads rather small, and difficult to detect because NGC 2419 is significantly more distant than ω Cen. Moreover, the thin red giant branch of NGC 2419 (see the Figures 7.3, 7.4) clearly claims against any significant metallicity spread in the cluster. Finally, Newberg et al. (2003) find that NGC 2419 appears to be within an overdensity of A-type stars which is in nearly the same plane as previously discovered tidal tails of the Sgr dSph and conclude that the cluster might have once been associated to the Sagittarius galaxy.

In order to investigate the true nature of NGC 2419 it can be useful to check the cluster location in the plane defined by the V-band absolute magnitude (M_V) and the central velocity dispersion (σ_0; Djorgovski et al. 1997, McLaughlin 2000 , and references therein), a sort of "fundamental plane" for globular clusters. The "fundamental planes" of globular clusters and elliptical galaxies (Faber-Jackson relationship, Faber & Jackson 1976) are compared in Figure 7.2. Milky Way and M31 globular clusters are found to follow in this plane the $L_V - \sigma_0$ empirical relationship:

$$\frac{L_V}{L_\odot} \propto \sigma_0^{1.57\pm0.10}(\mathrm{km\ s^{-1}}) \tag{7.1}$$

by de Grijs et al. 2005, which is represented by the long-dashed line in Figure 7.2. In this plane, object with elliptical-galaxy nature should lie on the Faber-Jackson relationship (dotted line in Figure 7.2). Thus, we would expect a cluster to be either located close to the Faber-Jackson relation if it were the stripped core of a galaxy, or to the fundamental plane correlation for Galactic GCs if it were a genuine GC (see e.g. Dubath & Grillmair, 1997; McLaughlin, 2000). Indeed, peculiar clusters like ω Centauri and G1 in M31 lie close to the intersection between the two lines. NGC 2419 locates instead far away from any of the two relationships. Therefore, this kind of analysis does not seem to support the hypothesis that NGC 2419 is the stripped core of a dSph galaxy (de Grijs et al., 2005).

An alternative tool for investigating the true nature of NGC 2419 is to study the cluster's variable stars and compare them to variables in other Galactic

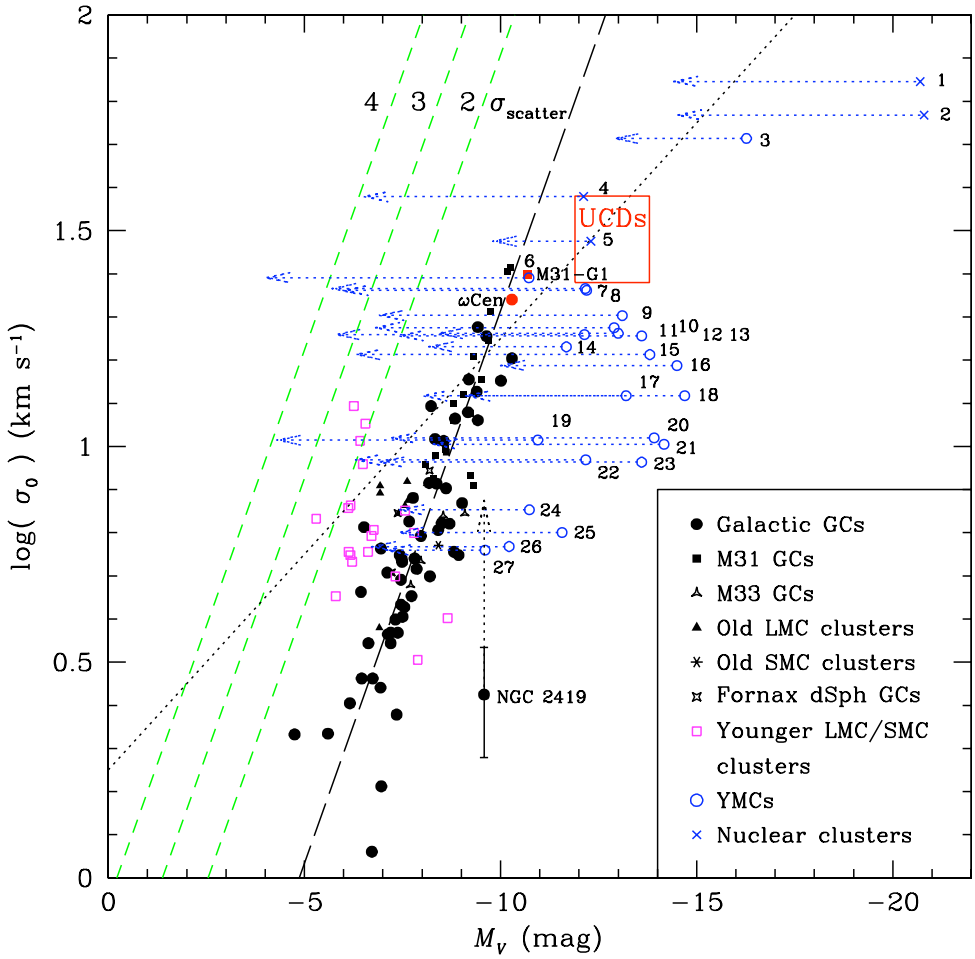

Figure 7.2 “Fundamental planes” of globular clusters and elliptical galaxies (from de Grijs et al. 2005). The filled symbols correspond to the old GCs in the Local Group, as indicated in the legend; the best-fitting relation for these old clusters is shown by the long-dashed line. The short-dashed (green) lines are displaced from this best-fitting relationship by, respectively, 2, 3, and 4 times the scatter in the data points around the best-fitting line, $\sigma_{\rm scatter}$, adopting a Gaussian distribution of the scatter for simplicity. The dotted line corresponds to the Faber-Jackson relationship for elliptical galaxies.

and extragalactic globular clusters. Study of the variable star population in NGC 2419 dates back to the work by Pinto & Rosino (1978) who collected photographic plates and detected 41 variables, among which 32 RR Lyrae stars (25 fundamental mode and 7 first-overtone pulsators), 1 Population II Cepheid, and 4 red irregular/semiregular variables, mainly confined in the cluster external regions. Based on the average period of the fundamental mode RR Lyrae stars ($\langle P_{ab} \rangle = 0.654\ d$) Pinto & Rosino (1978) classified NGC 2419 as an Oosterhoff type II cluster (OoII, Oosterhoff 1939).

We have undertaken a new, large-area (50×43 arcmin^2), deep ($V \sim 26$ mag) CCD photometric survey of NGC 2419 aimed at unveiling the census of the cluster variable star population, as well as at obtaining CMDs at different radii from the cluster center and look for possible substructures around NGC 2419.

7.1 Observations and Data Reduction

Time series B, V photometry of NGC 2419 was collected between 2003 September and 2004 February with DOLORES at the 3.5 m TNG telescope*. Center field coordinates were RA=07:38:24.0, DEC=38:54:00 (J2000). The observing strategy was devised in order to optimize the detection and coverage of the light curves for variable stars of RR Lyrae type. We have complemented these observations with the following archival data: i) images of two fields (Field_A and Field_B, respectively) of NGC 2419 with the Wide Field Planetary Camera 2 (WFPC2) on board of the HST† obtained across several cycles spread over 7 years from 1994 May to 2000 March. Data for Field_A were collected between 1994 May and 2000 March (Programs ID 5481, 7628) for a total of $10\ I$ and $18\ V$ frames. Data for Field_B were collected in 1997 November (Program ID 7630) for a total of $39\ I$ an $7\ V$ frames; ii) $165\ V$ and $16\ I$ images obtained with the Supreme-Cam of the SUBARU 8.2m telescope‡ along eight nights in 2002 December.

The SUBARU data cover a total field of view of 50×43 arcmin^2 which includes both the TNG and the HST fields. The total number of phase points of the combined dataset reaches 20, 205 and 48 in the B, V and I bands, respectively. However, we note that the I data have rather poor time sampling. Typical internal errors of the V band photometry for single phase points at the level of the HB are in the range from 0.01 to 0.02 mag.

Images were pre-reduced following standard techniques (bias subtraction and flat-field correction) with IRAF§. We measured the star magnitudes by PSF photometry running the DAOPHOTII/ALLSTAR/ALLFRAME packages (Stetson, 1987, 1992) on the TNG, HST and SUBARU datasets, separately. We checked for consistency the photometry by randomly extracting several pairs of images and computing the differences of the magnitudes of the stars in common to each pair, which showed a scatter compatible with the intrinsic photometric error, with no trend with magnitude and position of the stars along the frames.

*http://www.tng.iac.es/instruments/lrs/

†http://www.stsci.edu/hst/wfpc2

‡http://www.subarutelescope.org/Observing/Instruments/SCam/index.html

§IRAF is distributed by the National Optical Astronomical Observatories, which are operated by the Association of Universities for Research in Astronomy, Inc., under cooperative agreement with the National Science Foundation

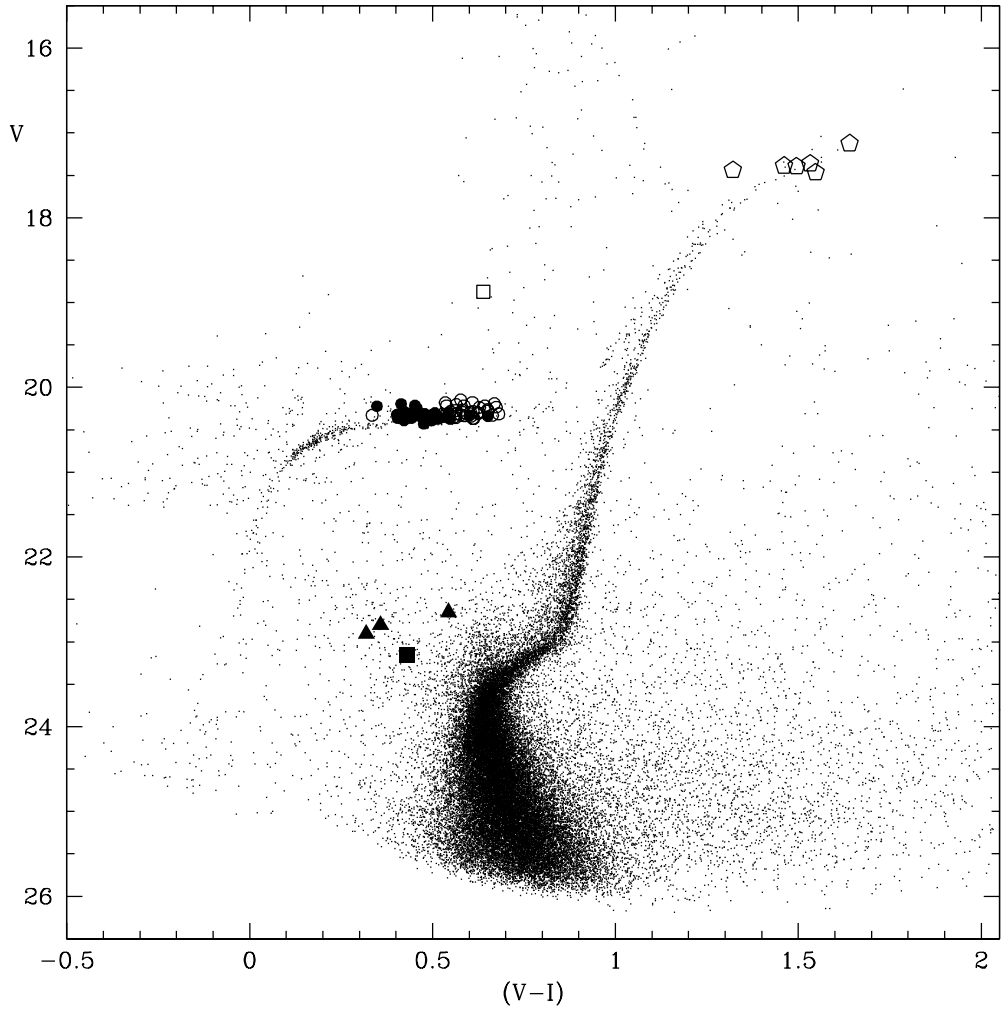

Figure 7.3 V, $V-I$ color magnitude diagram of NGC 2419 based on the SUBARU data. Variable stars are plotted according to their intensity-averaged magnitudes and colours using different symbols for the various types. Open circles: ab-type RR Lyrae; filled circles: c-type RR Lyrae; asterisks: double mode RR Lyrae stars; filled triangles: SX Phoenicis stars; filled square: eclipsing binary; open square: Cepheid: open pentagons: red irregular/semiregular (RIV) and Tip variables.

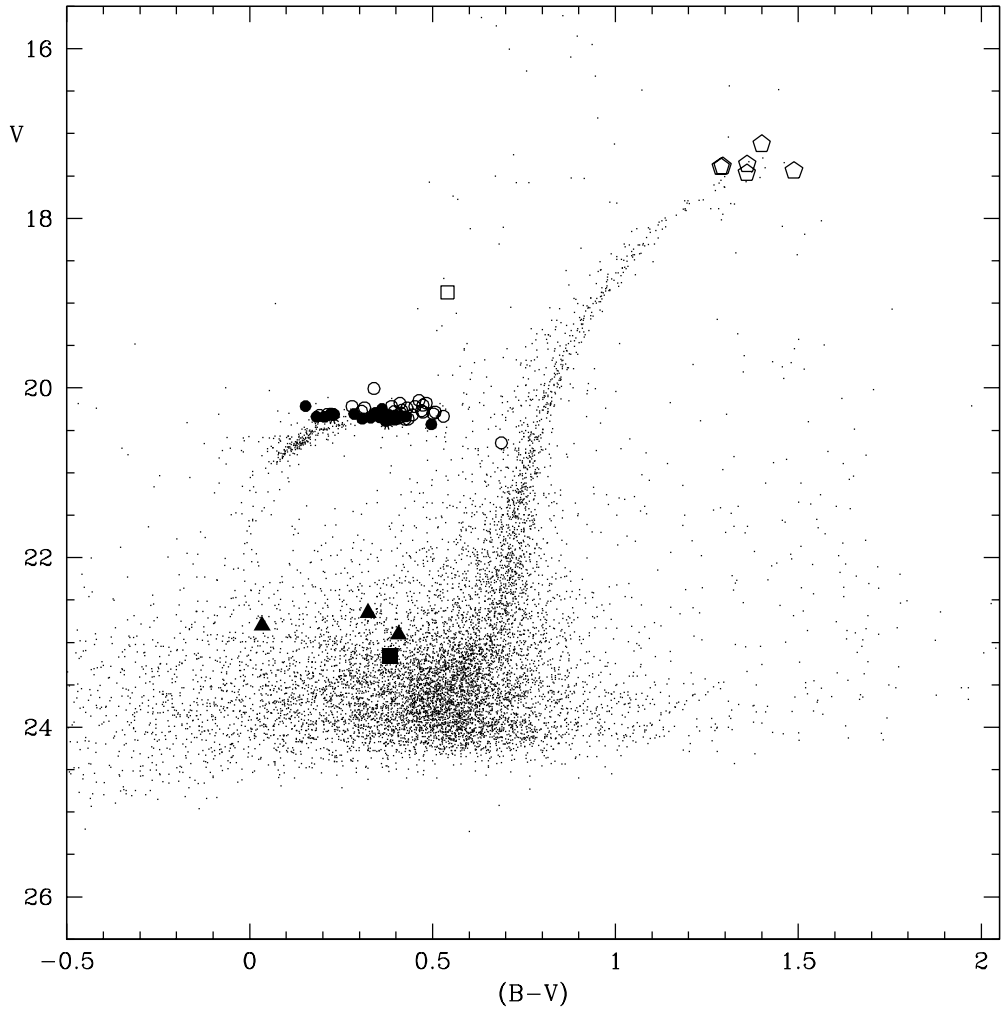

Figure 7.4 V, $B-V$ color magnitude diagram of NGC 2419 based on TNG observations. Variable stars are plotted according to their intensity-averaged magnitudes and colours using the same symbols as in Figure 7.3

The absolute photometric calibration was obtained by using local standards in NGC 2419 from P.B. Stetson's list[¶]. A total number of about 400 standard stars covering approximately the color intervals $-0.2 < (B-V) < 1.8$ and $-0.2 < (V-I) < 2.0$ were used to derive a set of linear calibration equations:

$$
\begin{aligned}
B &= b_{TNG} + (0.017 \pm 0.003) \times (b_{TNG} - v_{SUBARU}) + (7.709 \pm 0.0003) \quad \sigma = 0.022 \\
V &= v_{SUBARU} + (6.123 \pm 0.014) \quad \sigma = 0.014 \\
I &= i_{SUBARU} + (0.039 \pm 0.002) \times (v_{SUBARU} - i_{SUBARU}) + (5.811 \pm 0.002) \quad \sigma = 0.014
\end{aligned}
$$

The zero point uncertainties of the calibration equations are estimated of the order of 0.022, 0.014 and 0.014 mag in B, V and I, respectively.

7.2 Identification of the Variable Stars

Variable stars were identified on the V frames of NGC 2419 obtained at the TNG using the Image Subtraction technique as performed within the package ISIS 2.1 (Alard, 2000). We identified 283 candidate variables all over the TNG field of view, including the cluster inner regions. To extend our study deeper inside the cluster center, and to obtain a better definition of periods and light curves, the TNG time series were complemented by F555W(V), F814W(I) WFPC2@HST and SUBARU V, I data, by counter-identifying the candidate variable stars among the three photometric catalogs.

Additional variable stars were also identified in the cluster outer regions, where only the wide-field SUBARU observations are available. Identification of these further variables from the SUBARU data was done primarily in the V band, where the number of phase points is larger. The following procedure was adopted: i) we calculated the Fourier transform (in the Schwarzenberg-Czerny 1996 formulation) for each star in the photometric catalogue for which we have at least 90 epochs; ii) we averaged this transform to estimate the noise; 3) we calculated the signal-to-noise ratio by dividing the peak with the maximum amplitude in the transform by the noise estimated as in the previous point. We then analyzed all the stars with high S/N, that for the RR Lyrae stars typically goes from 20 to 110.

Periods for the candidate variables were derived using GRaTiS (Graphical Analyzer of Time Series) a private software developed at the Bologna Observatory (see e.g. Di Fabrizio, 1999; Clementini et al., 2000), which uses both the Lomb periodogram (Lomb, 1976; Scargle, 1982) and the best fit of the data with a truncate Fourier series (Barning, 1963). Whenever possible, study of the light curves was done by combining data from the three different catalogs (TNG, HST, SUBARU). The large time baseline (nine years) covered by the combined dataset, allowed us to solve alias ambiguities which were rather severe when considering only the individual datasets. The merged datasets also returned a better estimate of the period, epoch of maximum light and amplitudes of the light variation of the confirmed variable stars. Periods accurate to 6 decimal places are obtained

[¶] Available at http://cadcwww.dao.nrc.ca/standards/

when all three datasets are available. We confirmed the variability and were able to derive reliable periods for 82 stars from our candidate variable list, thus "doubling" the sample of 41 known variables in NGC 2419 from Pinto & Rosino (1978) study. Our variable star sample includes 71 RR Lyrae stars (38 *ab*-, 30 *c*-, and 3 *double mode* pulsators), 3 SX Phoenicis stars, 1 eclipsing binary, 1 Cepheid and 5 luminous variables located close to the cluster red giant branch tip. Identification and coordinates of the variable stars are provided in Table 7.11, along with period, type, time of maximum light, number of phase points in the SUBARU, TNG and HST data-sets separately, intensity-averaged $\langle \mathrm{V} \rangle$, $\langle \mathrm{B} \rangle$ and $\langle \mathrm{I} \rangle$ magnitudes, and amplitudes of the light variation (A_V, A_B and A_I). Variables from V1 to V41 were already known from Pinto & Rosino (1978) study, stars from V42 to V82 are new variables identified in the present study, they have been given increasing numbers with increasing the distance from the cluster center. Examples of light curves are shown in Figure 7.5.

7.3 Comparison with Previous Studies

Pinto & Rosino (1978) detected 41 variables in NGC 2419 in their study based on photographic plates: 32 RR Lyrae stars (25 fundamental mode and 7 first overtone pulsators), 1 Cepheid, 4 red irregular/semiregular variables, and further 5 variables for which they were not able to provide period and classification. Clement (1990) later found that V39 in Pinto & Rosino (1978) list is a *double-mode* RR Lyrae star. Most of the Pinto & Rosino (1978) variables are in the cluster external regions. In our study, we recovered and were able to derive reliable periods for all the previously known variable stars in NGC 2419, as well as detected 41 new variables that are mainly RR Lyrae stars (35 objects) and are generally located in the cluster inner region. The new variables include: 11 *ab*-, 23 *c*-, 1 *d*-type RR Lyrae stars, 3 SX Phe variables, 1 short period binary system and 2 bright variables close to the cluster red giant tip. We also found that one of the variable stars in Pinto & Rosino (1978) sample (V27) shows in fact a *double-mode* behaviour, thus bringing to 3 the total number of RRd pulsators known in the cluster. The number of new RRc variable we discovered in the cluster is remarkably high. Most of these stars were missed by Pinto & Rosino (1978) because their small amplitudes and the location in the central region of the cluster makes them rather difficult to detect with tradition techniques. Since NGC 2419 is an Oosterhoff type II cluster, it was expected to contain a larger number of first overtone pulsators than found by Pinto & Rosino (1978). Indeed, the new discoveries bring the ratio of number of RRc to number of RRc+RRab (f_c) from 0.19 to 0.44, a value in much better in agreement with expectations for an Oo II cluster. Similarly, the newly discovered RRab stars extend the period range of the fundamental mode pulsators to longer periods. Longer period RR Lyrae stars tend to have smaller amplitudes: that's why Pinto & Rosino (1978) missed them. The period distributions of already known and newly discovered RR Lyrae stars in NGC 2419 are compared in Figure 7.6, for *ab*- and *c*-type variables separately. It appears clearly that Pinto & Rosino (1978) missed the smaller amplitude variables. The period distribution of the total sample of RR Lyrae stars in NGC 2419 is shown in Figure 7.7.

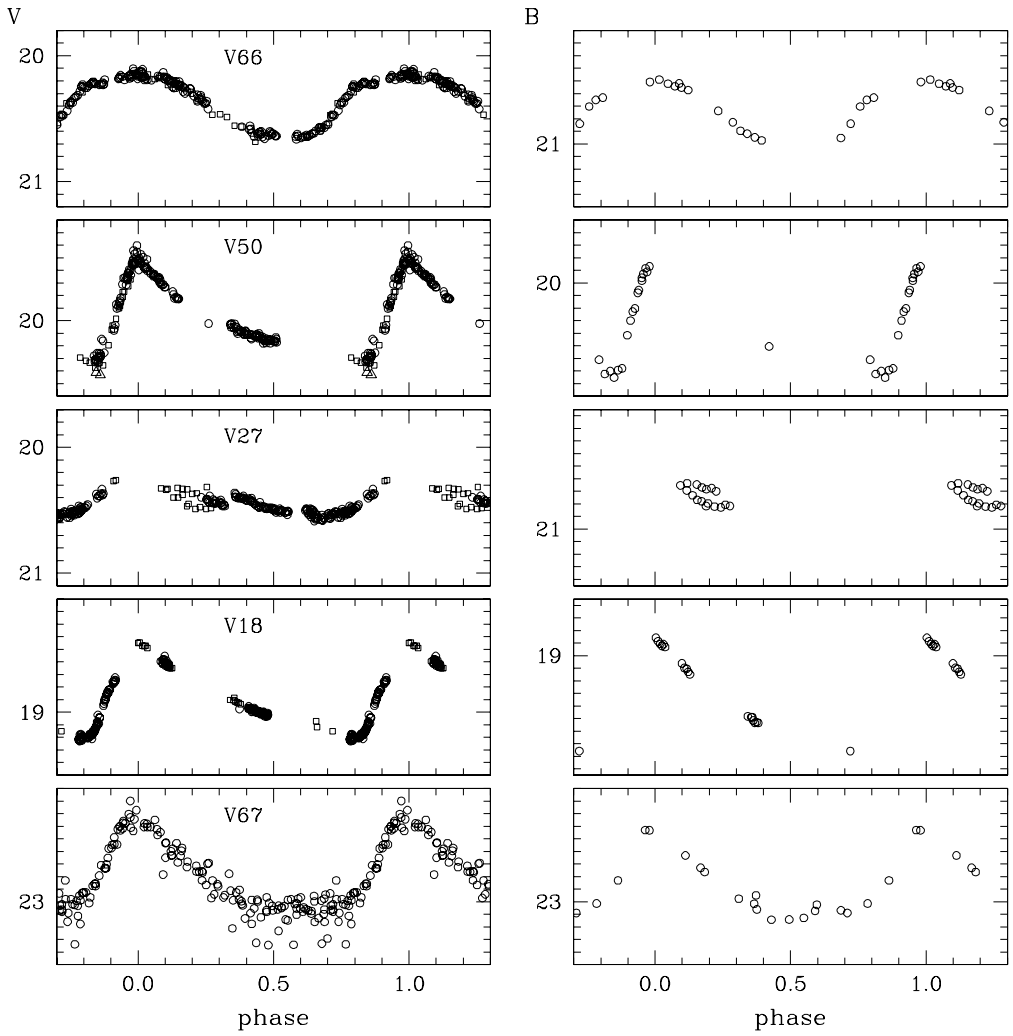

Figure 7.5 Examples of V, B light curves for different types of variable stars in NGC 2419. From top to bottom: *c-type* RR Lyrae, *ab-type* RR Lyrae, a *double mode* RR Lyrae, Cepheid, and SX Phoenicis star. Open squares are Subaru data, open circles are TNG data, and open triangles are HST data.

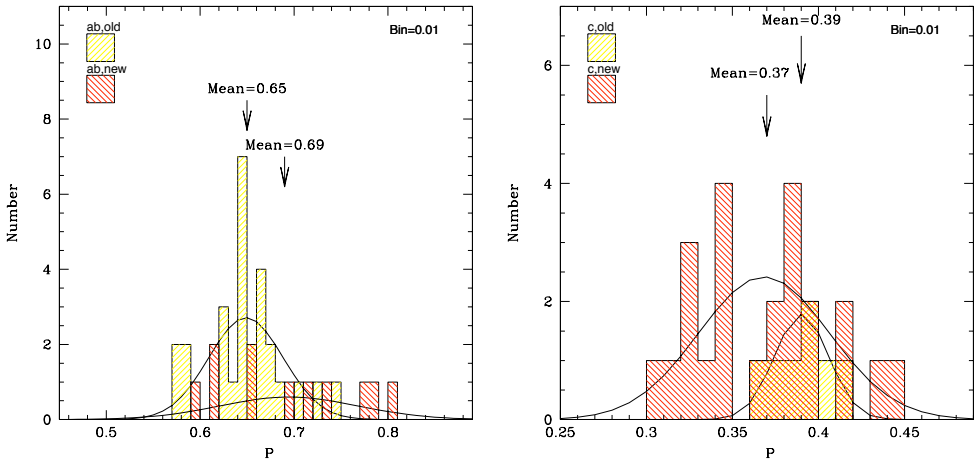

Figure 7.6 Left panel: period distribution of the RRab stars from Pinto & Rosino (1978) (old) and newly discovered ones (new). Right panel: same plot for RRc stars.

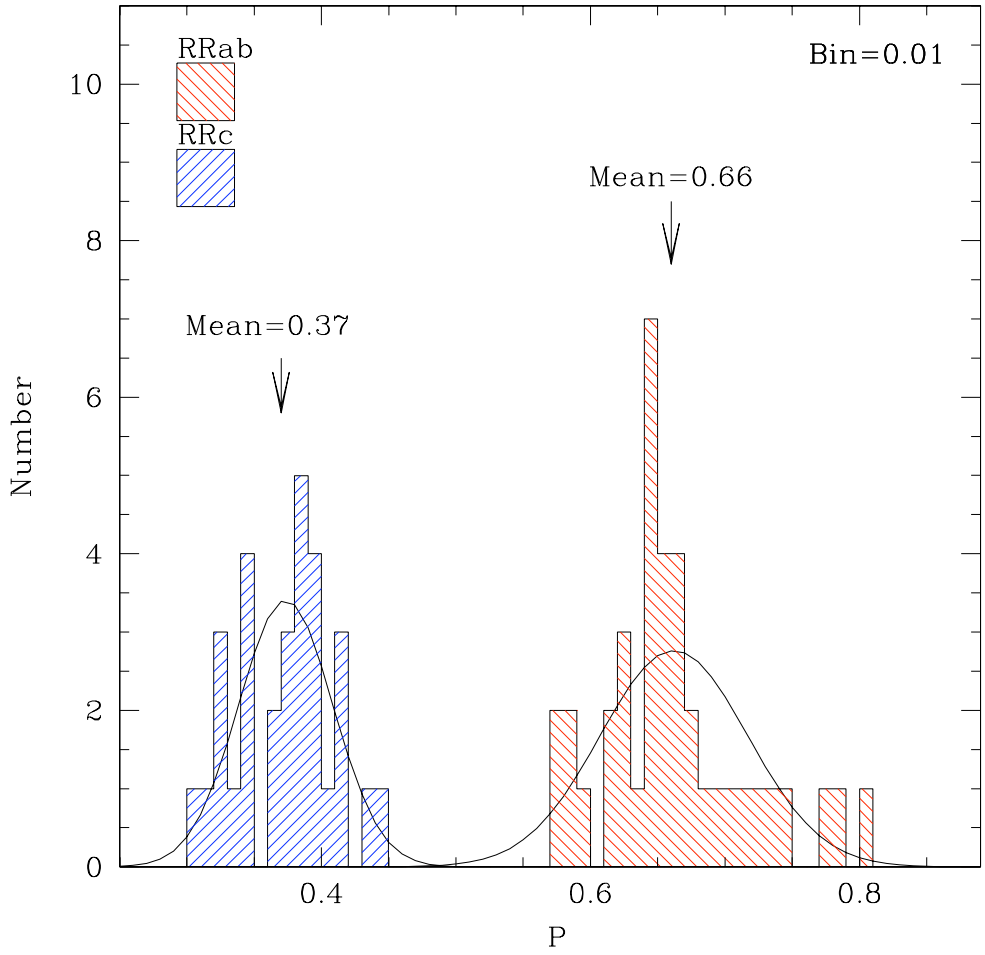

Figure 7.7 Period distribution of the total sample of RR Lyrae stars in NGC 2419.

7.4 Properties and Oosterhoff type of the RR Lyrae Stars

The average period of the NGC 2419 c-type RR Lyrae stars is: $\langle Pc \rangle$ =0.37 d (σ=0.04 d, average on 30 stars). The *ab*-type RR Lyrae stars have $\langle Pab \rangle$=0.66 d (σ=0.05 d, average on 38 stars). All *ab*- and c- RR Lyraehave been considered. The shortest period RRab is star V40 with $P_{ab,min}$=0.5756 d, the longest period RRc is star V62 with $P_{c,max} = 0.4411d$.

The very good sampling of the V band light curves allowed us to obtain very precise fits of the data and very reliable average V magnitudes for the NGC 2419 variables. Given the smaller number of B and I phase points and the uneven distribution of the I data, in particular, average B and I magnitudes are available only for a few objects and are, anyway, much more uncertain. When data sampling was too sparse, to recover the star average magnitudes in B and I, we have used the star's V band fits as templates and properly scale them in the amplitude and fit the observations in the other bands. This procedure was quite straightforward for the B data because the 20 epochs available for this filter are evenly distributed and allowed us fitting the B light curves with a very low errors (< 0.01 mag) for the last majority of the variable stars[‖]. On the other hand, the I band light curves are rather poorly sampled. We used then literature data for RR Lyrae stars in globular clusters to constrain the scaling value, which we estimated to be $A(V)/A(I) = 1.58 \pm 0.03$ base on the average over 130 RR Lyrae stars with good light curve parameters including both *ab*- and c-type variables. A simple simulation with real data demonstrates that, varying the $A(V)/A(I)$ ration by 10%, translates in an error of about 3% on the $< I >$. Being our formal error of $A(V)/A(I) \sim 2\%$, we are confident that our procedure provides very accurate $< I >$, in spite to the small number of epochs available in this band.

The period-amplitude distribution in the V band of the NGC 2419 RR Lyrae stars is shown in Figure 7.8. Figure 7.83 shows clearly the Oosterhoff II true nature of NGC 2419. A few (7/38) of the RRab variables have periods in the intermediate range between Oo I and Oo II types. These stars do not show any special spatial distribution and are likely to represent the short-period tail of the Oosterhoff II period distribution.

Based on our more complete census of the RR Lyrae population, NGC 2419 seems to confirm its nature of a *pure* Oosterhoff II globular cluster with a $Pab = 0.66$ d. This result doesn't exclude, however, the hypothesis of an extragalactic origin for this cluster: also two Local Group dSph galaxies: Ursa Minor and Bootes dSph are pure Oosterhoff type II systems (Cseresnjes, 2001; Dall'Ora et al., 2006) .

7.5 Cluster Distance

The V band average luminosity of the NGC 2419 RR Lyrae stars from the present study is: $\langle V(RR) \rangle$=20.30±0.01 mag (σ=0.09 mag, average on 69 stars). We have discarded two variables (namely, V2 and V77) which are about 0.8-1.0 mag overluminous since heavily contaminated by companion stars. In order to derive the

[‖]On average the resulting $A(B)/A(V)$ ratio ranges from about 1.25 to 1.30 in very good agreement with the value 1.29±0.02 found using literature data for RR Lyrae stars in globular clusters

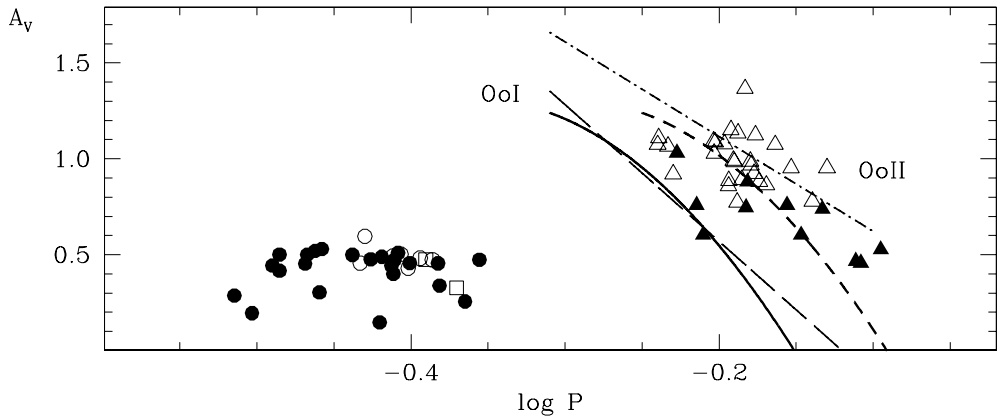

Figure 7.8 V period-amplitude diagrams of NGC 2419 RR Lyrae stars. Triangles are *ab*-type RR Lyrae, circles *c*-type RR Lyrae and squares are double mode RR Lyrae. Filled symbols are the newly discovered variable stars; open ones are previously known and confirmed variable star. The straight lines are the positions of the OoI and OoII Galactic GCs according to Clement & Rowe (2000). Period-amplitude distributions of the *bona fide* regular (solid curves) and well-evolved (dashed curves) *a*b RR Lyrae stars in M3 from Cacciari et al. (2005) are also shown for comparison.

distance to NGC 2419 from the average luminosity of its RR Lyrae stars we need an estimate of the cluster reddening and metallicity, as well as values for the slope and zero point of the RR Lyrae luminosity-metallicity relation. We have assumed an absolute magnitude of M_V = 0.59±0.03 for RR Lyrae stars of [Fe/H] =−1.5 (Cacciari & Clementini, 2003), and $\Delta M_V/[\mathrm{Fe/H}]$=0.214±0.047 (Clementini et al., 2003; Gratton et al., 2004) for the slope of the luminosity-metallicity relation. We then adopt a standard extinction law (A_V=3.1×$E(B-V)$) and a reddening value of $E(B-V)$=0.11 ± 0.02 from Harris (1996). For the cluster metal abundance we adopt [Fe/H]=−2.12, following Harris (1996). This value is in very good agreement with the estimate of [Fe/H]=−2.27 we obtain from the mean period of the cluster fundamental mode RR Lyrae stars ($\langle Pab\rangle$=0.66 d) using relations from Sandage (1993).

The distance to NGC 2419 estimated from the average luminosity of the cluster RR Lyrae stars is then: μ_0=19.50±0.07 (D=79.4±5.1 kpc)** in excellent agreement with Harris (1996). Results from this study are presented in Ripepi et al. (2007).

**Errors are the sum in quadrature of uncertainties of 0.01 mag in $\langle V(RR)\rangle$ (dispersion of the average), 0.02 mag in the zero point of the photometry, 0.02 mag in $E(B-V)$ (corresponding to 0.06 mag in A_V), and of 0.03 mag and 0.047 mag/dex, respectively, in the zero point and in the slope of the RR Lyrae luminosity-metallicity relation.

Table 7.1: Identification and properties of the NGC 2419 variable stars.

Name (a)	Id	α (2000)	δ (2000)	Type	P (days)	Epoch (-2400000)	$\langle V \rangle$	A_V	N_V	$\langle B \rangle$	A_B	N_B	$\langle I \rangle$	A_I	N_I
V1	V17997	7:38:07.78	38:53:17.29	RIV	198.000	52617.000	17.44	0.49	118	18.92	0.822	21	16.12	0.35	9
V2	V23327	7:38:07.96	38:52:33.67	RRab	0.67017	53030.559	19.33	0.88	184	19.84	1.089	20	18.48	0.29	20
V3	V22280	7:38:12.70	38:52:27.36	RRab	0.62599	52617.098	20.34	1.09	189	20.75	1.349	20	19.78	0.79	38
V4	V23625	7:38:15.13	38:52:35.12	RRc	0.39210	52609.125	20.32	0.50	183	20.70	0.645	20	19.84	0.32	14
V5	V33749	7:38:11.14	38:53:38.78	RRab	0.65587	52608.668	20.18	1.36	186	20.59	1.755	20	19.65	0.88	16
V6	V10150	7:38:12.89	38:50:43.78	RRc	0.37161	52617.117	20.37	0.60	181	20.75	0.766	19	19.87	0.40	16
V7	V39159	7:38:16.18	38:54:18.79	RRab	0.62733	52611.094	20.36	1.09	184	20.82	1.076	20	19.79	0.70	17
V8	V33054	7:38:10.97	38:53:23.47	RIV	13.0000	52581.469	17.36	0.12	114	18.72	0.141	21	15.83	0.08	20
V9	V21821	7:38:05.63	38:54:21.16	RRab	0.64473	52608.363	20.22	0.99	183	20.67	1.304	20	19.58	0.51	17
V10	V18271	7:38:08.47	38:53:46.63	RIV	19.000	53053.398	17.12	0.34	116	18.54	0.439	21	15.48	0.22	4
V11	V24835	7:38:16.42	38:52:42.26	RRab	0.58918	52609.016	20.34	0.92	183	20.75	1.183	20	19.81	0.52	16
V12	V41437	7:38:19.79	38:54:40.96	RRab	0.66188	52608.691	20.27	0.97	172	20.72	1.185	20	19.69	0.62	16
V13	V24488	7:38:16.93	38:52:40.20	RRab	0.64027	52609.004	20.30	0.88	183	20.81	1.138	19	19.68	0.47	19
V14	V24717	7:37:58.39	38:52:42.30	RRab	0.74133	52610.098	20.24	0.96	178	20.67	1.179	20	19.61	0.65	15
V15	V32575	7:38:13.66	38:53:30.62	RRab	0.64001	52608.039	20.28	0.86	184	20.79	1.027	20	19.67	0.53	16
V16	V37246	7:38:12.38	38:54:03.39	RRab	0.66608	53032.477	20.30	1.12	184	20.67	1.316	20	19.71	0.72	17
V17	V41439	7:38:17.74	38:54:40.95	RRab	0.64904	52609.059	20.32	1.13	184	20.76	1.413	20	19.79	0.73	16
V18	V41939	7:38:07.16	38:54:46.81	Cef	1.57867	53032.477	18.87	0.75	184	19.41	1.009	20	18.23	0.50	16
V19	V20251	7:37:59.02	38:52:15.01	RRab	0.70260	52611.121	20.28	0.95	185	20.76	1.223	20	19.74	0.66	19
V20	V33657	7:38:13.14	38:52:08.23	RIV	52.9500	52650.000	17.39	0.42	186	18.69	0.535	20	15.93	0.27	16
V21	V31470	7:38:03.58	38:53:23.70	RRab	0.68609	53032.527	20.20	1.07	186	20.68	1.327	20	19.64	0.69	16
V22	V25180	7:38:17.65	38:52:44.35	RRab	0.57664	53032.488	20.36	1.11	185	20.76	1.381	20	19.85	0.74	17
V23	V38186	7:38:10.70	38:54:10.73	RRab	0.62650	52610.121	20.37	1.03	183	20.79	1.322	20	19.76	0.66	17
V24	V25237	7:37:55.61	38:52:45.71	RRab	0.65270	52617.148	20.36	0.89	149	20.80	1.154	20	19.75	0.57	12
V25	V32709	7:38:03.28	38:53:31.71	RRab	0.63627	52608.449	20.33	1.08	185	20.86	1.383	20	19.75	0.69	16
V26	V7326	7:38:02.20	38:52:03.20	RRab	0.66492	52610.078	20.18	0.92	184	20.63	1.085	20	19.57	0.59	16
V27	V12101	7:38:09.78	38:51:09.04	RRd	0.42614	53033.570	20.41	0.34	183	20.78	0.444	18	19.93	0.22	16
V28	V36163	7:37:51.81	38:53:56.14	RRab	0.64560	52609.621	20.34	0.99	186	...	...	...	19.73	0.63	8
V29	V25528	7:38:03.26	38:52:46.94	RRab	0.72556	53032.477	20.28	0.78	184	20.66	0.891	20	19.63	0.50	16
V30	V30275	7:38:06.09	38:53:16.18	RRab	0.58462	53032.590	20.32	1.06	185	20.51	1.389	20	19.75	0.69	20
V31	V5001910	7:38:21.24	38:50:22.92	RRc	0.38753	52608.891	20.34	0.49	39	20.70	0.609	...	19.8	0.32	-
V32	V34111	7:38:06.70	38:53:40.79	RRab	0.64224	52608.328	20.15	1.15	182	20.61	1.434	20	19.57	0.60	16
V33	V23396	7:38:12.27	38:52:33.92	RRc	0.41117	52608.762	20.32	0.47	184	20.68	0.535	19	19.82	0.31	17
V34	V44725	7:38:10.34	38:55:29.06	RRc	0.40355	53053.539	20.36	0.48	183	20.75	0.595	20	19.84	0.31	16
V35	V27712	7:38:12.01	38:52:59.86	RRab	0.67721	53053.578	20.26	0.86	184	20.69	1.097	20	19.61	0.56	16
V36	V33246	7:38:10.30	38:53:35.31	RRab	0.64822	52991.625	20.30	0.77	184	20.64	1.076	18	19.68	0.48	17
V37	V29181	7:38:11.20	38:53:09.06	RRab	0.66103	52991.637	20.28	1.06	186	20.58	1.18	20	19.71	0.68	34
V38	V18676	7:38:08.13	38:52:03.94	RRc	0.36898	52911.637	20.25	0.46	181	20.58	0.569	20	19.79	0.32	16
V39	V10671	7:38:10.72	38:50:51.10	RRd	0.40703	52609.070	20.34	0.61	181	20.57	0.796	20	19.91	0.40	216
V40	V25629	7:38:13.09	38:52:47.21	RRab	0.57565	50770.105	20.22	1.07	188	20.6	1.359	20	19.63	0.76	33
V41	V31405	7:38:07.20	38:53:23.10	RRc	0.39646	53032.512	20.33	0.43	180	20.75	0.553	17	19.73	0.42	35
V42	V25357	7:38:03.54	38:52:16.88	RRab	0.61008	52806.762	20.29	0.76	196	20.04	0.974	21	19.69	0.74	21
V43	V23674	7:38:26.11	38:58:10.17	RRc	0.37996	52610.156	20.22	0.15	83	...	...	...	19.87	0.11	31
V44	V24629	7:38:09.89	38:52:01.07	TIP	0.87583	52906.746	17.39	0.17	113	18.68	0.243	21	15.90	0.17	4
V45	V26853	7:38:10.53	38:52:50.64	RRc	0.31394	52610.121	20.39	0.19	159	20.19	0.484	17	19.96	0.13	42
V46	V26160	7:38:12.11	38:51:59.23	RRab	0.77405	50771.352	20.22	0.45	171	20.45	0.495	12	19.68	0.17	16
V47	V24628	7:38:05.99	38:52:59.62	RRc	0.37490	50771.270	20.21	0.48	185	20.37	0.546	20	19.76	0.31	31
V48	V30239	7:38:08.13	38:53:15.87	RRc	0.32709	50771.234	20.36	0.51	174	20.16	0.485	19	19.96	0.33	33
V49	V27292	7:38:10.29	38:52:16.34	RRc	0.34845	49493.477	20.19	0.53	190	...	...	...	19.78	0.34	26
V50	V30464	7:38:13.85	38:53:37.34	RRab	0.65847	50770.719	20.01	0.80	185	20.35	1.034	20	...	...	40
V51	V27613	7:38:07.56	38:52:35.13	RRc	0.38768	53032.500	20.31	0.40	188	20.6	0.446	19	19.83	0.32	42
V52	V24846	7:38:09.67	38:52:41.32	RRab	0.73638	51622.094	19.95	0.74	200	20.51	0.813	20	19.32	0.48	37
V53	V27780	7:38:01.81	38:53:16.64	RRc	0.38824	52617.059	20.34	0.47	183	20.56	0.544	20	19.69	0.30	34
V54	V29251	7:38:07.99	38:52:24.65	RRab	0.80349	53033.516	20.23	0.53	180	20.56	0.593	20	19.56	0.43	39
V55	V30716	7:38:10.64	38:53:00.33	RRc	0.39050	52991.641	20.30	0.51	181	20.58	0.522	20	19.76	0.31	31
V56	V17882	7:38:06.00	38:52:42.72	RRab	0.59250	52609.273	20.33	1.02	50	20.40	1.478	18	19.99	0.73	22
V57	V30364	7:38:10.98	38:53:16.44	RRc	0.34492	52991.617	20.31	0.52	181	20.59	0.595	21	19.87	0.27	21
V58	V29417	7:38:08.32	38:53:31.44	RRc	0.38675	52611.145	20.34	0.44	181	20.52	0.57	19	19.86	0.29	18
V59	V31497	7:37:52.82	38:54:14.42	RRc	0.33989	52905.738	20.36	0.45	179	20.67	0.569	19	19.92	0.29	14
V60	V25927	7:38:06.66	38:53:18.83	RRc	0.36468	50768.555	20.33	0.50	182	20.74	0.661	...	19.87	0.32	20
V61	V33596	7:38:10.64	38:53:37.73	RRc	0.34093	53053.605	20.43	0.50	180	20.93	0.643	17	19.95	0.28	15
V62	V18026	7:38:11.60	38:53:10.46	RRc	0.44105	52608.652	20.30	0.47	163	20.54	0.531	20	19.80	0.28	39
V63	V19518	7:38:23.14	38:54:11.64	RRc	0.41550	52991.621	20.14	0.34	168	20.77	0.339	19	19.33	0.21	16
V64	V19747	7:38:09.92	38:53:49.52	RRc	0.41463	52991.637	20.38	0.45	185	20.77	0.567	20	19.83	0.24	17
V65	V20512	7:38:06.53	38:52:54.84	RRab	0.78001	49494.543	20.31	0.46	199	20.53	0.635	20	19.63	0.29	24
V66	V19320	7:38:08.60	38:53:14.68	RRc	0.38113	53032.492	20.38	0.49	182	20.75	0.561	19	19.89	0.31	16
V67	V18137	7:38:13.19	38:52:00.02	SX Ph	0.04944	52610.059	22.80	0.77	162	22.85	0.739	20	22.44	0.47	17
V68	V15945	7:38:06.45	38:52:50.76	RRab	0.65684	52617.039	20.31	0.62	187	20.54	0.745	19	19.75	0.32	33
V69	V16192	7:38:11.61	38:51:58.95	RRab	0.61610	53053.594	20.65	0.60	16	21.34	1.019	17	..	10.00	...
V70	V36489	7:38:12.10	38:53:57.42	SX Ph	0.06288	53053.578	22.65	0.42	178	22.97	0.591	20	22.11	0.30	17
V71	V33557	7:38:10.43	38:53:09.50	RRc	0.34728	53053.578	20.32	0.30	182	20.66	0.376	20	19.91	0.25	17
V72	V29591	7:38:10.03	38:52:41.15	RRc	0.32710	52609.055	20.32	0.42	168	20.72	0.534	7	19.92	0.27	14
V73	V21790	7:38:06.19	38:52:57.50	RRc	0.30580	49495.320	20.29	0.29	186	...	...	...	19.86	0.19	47
V74	V16182	7:38:01.46	38:53:11.99	RRab	0.69839	50770.680	20.19	0.79	188	20.25	0.867	19	19.52	0.60	31
V75	V20587	7:38:12.15	38:52:48.97	RRc	0.32360	52991.625	20.35	0.44	182	20.67	0.57	20	19.94	0.27	16
V76	V38108	7:38:01.85	38:54:10.44	SX Ph	0.04999	52608.973	22.91	0.41	180	23.31	0.596	20	22.59	0.33	16
V77	V13009	7:38:19.62	38:53:15.74	RRc	0.43164	52609.113	19.41	0.26	181	20.56	0.518	20	19.73	0.31	15
V78	V30259	7:38:05.96	38:53:38.19	RIV	49.6000	53053.590	17.47	0.29	115	18.82	0.389	21	15.92	0.19	7
V79	V13811	7:38:18.40	38:51:26.32	bin	0.23396	52617.145	23.16	1.20	187	23.54	1.2	21	22.73	1.20	17
V80	V5009772	7:38:07.98	38:53:16.22	RRc	0.39742	52608.719	20.39	0.46	158	20.76	0.51	20	19.89	0.29	14
V81	V38530	7:38:08.72	38:52:45.74	RRd	0.38680	52609.977	20.36	0.47	117	...	s...	...	19.84	0.34	10
V82	V5015266	7:38:06.84	38:53:34.14	RRab	0.71332	52610.051	20.33	0.58	136	...	...	19	19.66	0.37	13

Chapter 8

On the Origin of Oosterhoff Intermediate Globular Clusters

The so-called *Oosterhoff dichotomy* (Oosterhoff, 1939) is one of the clearest, while at the same time most intriguing, properties of the Galactic globular cluster system. It basically consists in the separation of Galactic globular clusters into two groups according to the mean periods of their ab-type (fundamental-mode) RR Lyrae stars: Oosterhoff type I for $\langle P_{\rm ab} \rangle \simeq 0.56$ d, and Oosterhoff type II for $\langle P_{\rm ab} \rangle \simeq 0.66$ d (Clement et al., 2001). The period range $0.58 \leq \langle P_{\rm ab} \rangle ({\rm d}) \leq 0.62$—the so-called *Oosterhoff gap*—is basically not occupied by Galactic globular clusters, based on the globular cluster with 5 or more RRab stars. Since the same behavior is not seen in the old globular cluster systems of nearby dwarf spheroidal galaxies, which have traditionally been viewed as candidate "building blocks" of the Galaxy, the Oosterhoff dichotomy can pose important constraints on the way the Milky Way was formed (Catelan, 2004, 2005).

8.1 About the Oosterhoff Dichotomy

Along with the mean periods of the ab-type RR Lyrae stars, other properties of the RR Lyrae stars are thought to vary when going from Oosterhoff type I (hereinafter Oo I) to Oosterhoff type II (hereinafter Oo II) clusters. Most emphasized in the literature is the number ratio of c-type (or first-overtone) RR Lyrae stars (e.g., Smith, 1995): as early noticed by Oosterhoff (1939), the RR Lyrae populations in Oo I clusters are largely dominated by ab-type pulsators, whereas Oo II clusters such as M15 and ω Centauri are thought to generally contain a more balanced proportion between *c*- and *ab*-type RR Lyrae stars.

What is the physical origin of the Oosterhoff dichotomy? Explanations have tended to emphasize mainly two aspects of the problem: i) The behavior of *individual* cluster stars (e.g., Sandage, Katem & Sandage, 1981; Sandage, 1990; Clement & Shelton, 1999; Clement & Rowe, 2000, 2001), ii) The *global behavior* of the stars in a cluster as a whole (e.g., Coutts, Dickens, Epps & Read, 1975; Cacciari & Renzini, 1976; Castellani & Quarta, 1987; Caputo, Tornambe & Castellani, 1989;

Caputo, 1990). Within the scope of the second aspect one finds the key conjecture of a *hysteresis mechanism* (Van Albada & Baker, 1973) affecting the pulsation mode in the so-called "either-or" zone of the instability strip (a region close to the center of the strip in which both the fundamental and the first overtone modes can in principle be excited): stars falling in this region retain the variability mode in which it pulsated *before* it entered this specific sector of the instability strip. In this context, even a star's evolution *before* the horizontal branch (HB) phase proper may be of relevance in defining the Oosterhoff status of a globular cluster (Caputo, Tornambé & Castellani, 1978).

8.2 Oosterhoff Intermediate Globular Clusters as a Gap or as a Group ?

Many efforts have been devoted to find connections between Oosterhoff types and cluster properties, since the Oosterhoff dichotomy was discovered among the Milky Way clusters. In Chapter 1, we have briefly discussed the few Galactic globulars found to occupy the so called "Oosterhoff gap". They are few in number (8) and actually seem also to avoid the true gap, lying at the edges of the region occupied by the two canonical Oosterhoff groups.

Thanks to improved observing facilities and to development of software optimized to detect variable stars in crowded fields, it is now possible to explore the Oosterhoff behaviour of globular clusters outside the Milky Way. At the same time, the identification of the disrupting Sgr and CMa dSph's in the Milky Way, and of globular clusters once them associated, has shown that a half of the Galactic globulars in the gap, should not be genuine in-Galaxy-born clusters, but were accreted in some merging event. On the other hand, globular clusters that have been observed in Milky Way companion galaxies do fully occupy the "Oosterhoff gap", thus indicating more a lack of Oosterhoff intermediate clusters in the Milky Way rather than an intrinsic dichotomy for the globular clusters. Globular cluster showing Oosterhoff intermediate behaviour have been found in the LMC (Soszynski et al., 2003) and in the Sgr (Cacciari et al., 2002; Salinas et al., 2006) and CMa (Catelan et al., 2006) systems. Mackey & Gilmore (2003b) suggested that also the Fornax dSph globular clusters are Oosterhoff intermediate, and our study does indeed confirm the Oosterhoff intermediate nature of the 4 clusters we have surveyed in Fornax. Nowadays, the sample of globular clusters in the gap deserves to be treated more as a class of object: the Oo-Intermediate (Oo-Int.) type, rather than a non-Oo I/Oo II group, since these clusters do indeed extend the parameter space covered by the Galactic clusters. Globular clusters in the LMC and in the Sgr and CMa dSph's seem to span all three Oosterhoff groups (Oo I, Oo II and Oo-Int), while the Fornax clusters are mainly confined within the gap. Thus, even in smaller system it is not easy to find simple connections among globular cluster properties.

8.3 A Database of "Pulsation Properties" of Galactic and Extragalactic Clusters

To study the properties of the Oosterhoff intermediate globular clusters we are building a complete and homogeneous databases by collecting from the literature data on the pulsation properties of the RR Lyrae stars in Galactic and extragalactic globular clusters fully spanning the three Oosterhoff types. This work is still in progress (see Catelan et al. 2007). It should be pointed out that building such a database is not an easy task since literature data on variable stars in globular clusters are by far inhomogeneous and incomplete.

Indeed, several Galactic globular clusters are still poorly studied in terms of variability, and many, if not all globulars whose variable star population was thought to be exhaustively known since the early 90's are now discovered to be affected by severe incompleteness even in the census of bright variables such as the RR Lyrae stars (Catelan et al., 2006). This is mainly because the before-90's studies were primarily based on photographic photometry, which did not allow to reach deep inside the cluster's cores and in many cases was not precise enough to tell small-amplitude variables from noise. Advent of the CCD photometry, combined with newly developed detection techniques based on the Image Subtraction (see e.g. Alard & Lupton, 1998; Alard, 2000) are now revealing the dramatic incompleteness of the before-90's surveys (see e.g. the case of NGC 2419).

The vast majority of information for our database have been extracted from the Catalogue of Variable Stars in Globular Clusters (Clement et al., 2001, and successive updates), available at http://www.astro.utoronto.ca/∼cclement/read.html. We concentrate on a number of specific pulsational parameters, namely: the mean period of the *ab*-type RR Lyrae ($\langle P_{ab} \rangle$), the mean period of the *c*-type RR Lyrae ($\langle P_c \rangle$), the number of RRab (N_{ab}), the number of RRc (N_c), the ratio between the number of RRc and number of RRab+RRc ($f_c = N_{ab}/N_c$), the minimum period of the RRab stars($P_{ab,min}$) and the maximum period of the RRc stars ($P_{c,max}$). We have looked for correlations between $P_{\rm ab,min}$ and several of the globular cluster parameters, including central surface brightness μ_V, central luminosity density ρ_0, central concentration parameter c, integrated absolute magnitude M_V, and metallicity [Fe/H], using values for the latter quantities as tabulated by Harris (1996). We find that the correlation coefficient r for all these quantities is less than 0.45, indicating poor or non-existent correlations.

Figures presented in the following Section of this Chapter are based on the same references that were used to produce Tables 2 and 3 in Catelan (2005), with updates from the literature when available. Results for many dwarf spheroidal galaxies are from Pritzl et al. (2002). Values for For 2, For 3, For 4 and For 5 and the field stars in Fornax, for NGC 2419 and for the Bootes dwarf are from the studies presented in this thesis. Note that, as clearly indicated in the inset, and following Catelan, globular clusters in our plots are divided into dSph globular clusters, globular clusters associated with different components of the Galaxy ("young" and "old" halo), and LMC globulars. Again as in Catelan, clusters with smaller numbers of RRab's ($5 \leq N_{\rm ab} \leq 10$) are shown with smaller symbols.

8.4 $P_{\rm ab,min}$: the Key Quantity Defining Oosterhoff Status

Figure 8.1 shows the correlation between average period of the ab-type RR Lyrae variables in globular clusters, $\langle P_{\rm ab}\rangle$, and the corresponding *minimum* period of these ab-type stars, $P_{\rm ab,min}$. As can clearly be seen, there is not only a strong *global* correlation between these two quantities, but also strong correlations *within each Oosterhoff group*.* Oosterhoff-intermediate globular clusters are clearly seen, for the first time, to provide a smooth transition between OoI and OoII clusters in this plane.

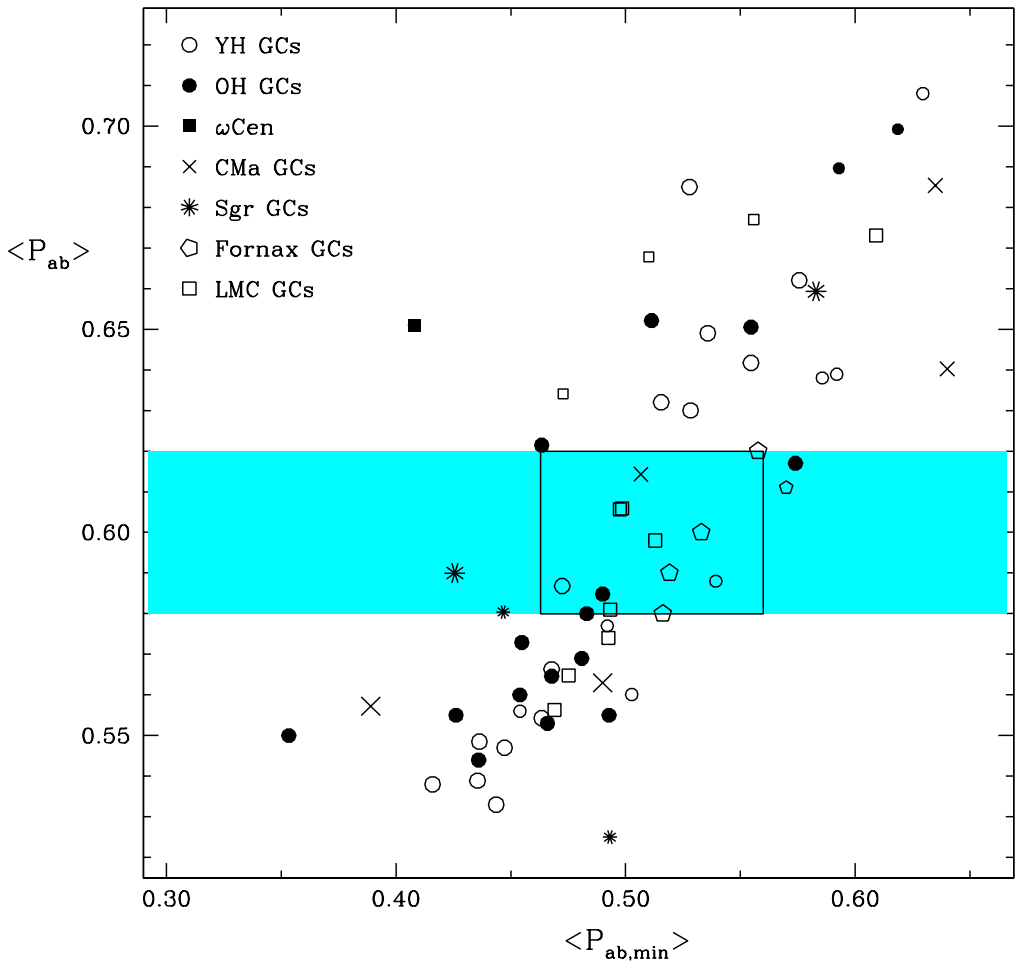

Figure 8.1 The average period of ab-type stars $\langle P_{\rm ab}\rangle$ is shown as a function of the *minimum* period of the ab-type stars $P_{\rm ab,min}$ in well-populated globular clusters. There is a not only a clear and smooth trend between $\langle P_{\rm ab}\rangle$ and $P_{\rm ab,min}$, but it is also clear, for the first time, that Oosterhoff-intermediate clusters tend to occupy an intermediate position in this plane as well.

*Note that some of the "stragglers" towards short values of $P_{\rm ab,min}$ in this plane, ω Cen (NGC 5139) in particular, can be explained in terms of the presence of heterogeneous populations of stars, with the shortest-period ab-type stars probably being representative of any more metal-rich Oo I component that may be present therein.

In Figure 8.1 we have indicated, as a hatched box, the position where most Oosterhoff-intermediate clusters appear to lie. This box, whose edges in $P_{\rm ab,min}$ are defined by

$$0.47 \leq P_{\rm ab,min}({\rm d}) \leq 0.552, \quad ({\rm Oo-Int}) \tag{8.1}$$

is seen to contain as many as 82.3% of all Oosterhoff-intermediate clusters, compared to 52% of all OoI and 43% of all OoII clusters in our sample. Conversely, of all clusters falling in this $P_{\rm ab,min}$ range, 50% are Oosterhoff-intermediate.

In Figure 8.2 the $\langle P_{\rm ab} \rangle$ value is shown as a function of the fraction of c-type RR Lyrae variables, $f_{\rm c} \equiv N_{\rm c}/(N_{\rm c}+N_{\rm ab})$. Note that, since the pioneering work by Oosterhoff (1939), this number fraction has been considered an important indicator of Oosterhoff status. However, this plot suggests that, while there is a *tendency* for Oo I clusters to have smaller values of $f_{\rm c}$ than Oo II clusters, practically any value of $f_{\rm c}$ is allowed for both Oo I and Oo II clusters—thus suggesting that, in fact, $f_{\rm c}$ is *not* a good diagnostic of Oosterhoff status.

For completeness, we also show, in Figure 8.3, the run of average $\langle P_{\rm ab} \rangle$ with the *maximum* period $P_{\rm c,max}$ of the c-type variables, for the same globular cluster sample as analyzed in the previous plots. Likewise, Figure 8.4 shows the run of $\langle P_{\rm ab} \rangle$ with the average c-type period $\langle P_{\rm c} \rangle$. As can be clearly seen from these plots, neither $P_{\rm c,max}$ nor $\langle P_{\rm c} \rangle$ appear to be good indicators of Oosterhoff behavior. We conclude, therefore, that $P_{\rm ab,min}$ (along, of course, with $\langle P_{\rm ab} \rangle$) is the single most important quantity defining Oosterhoff behavior.

8.5 What is the Origin of the Spread in $P_{\rm ab,min}$ within a Given Oosterhoff Group?

As can be seen from Figure 8.1, globular clusters pertaining to each Oosterhoff type present a range in $P_{\rm ab,min}$ values, which can be very substantial. For instance, among Oo II clusters, the bulk of the globular clusters fall in the range $0.51 \lesssim P_{\rm ab,min}({\rm d}) \lesssim 0.63$. What is the origin of this large spread in minimum ab-type periods? In other words, how does an Oo II globular cluster "decide" whether to have a fairly long $P_{\rm ab,min} \simeq 0.6$ d, as opposed to a short $P_{\rm ab,min} \simeq 0.5$ d?

This is not a trivial question to answer, since in the hysteresis scenario, which has been claimed to account well for the existence of Oo II clusters (e.g., Bono et al., 1994), all stars should perform their transition between c-type and ab-type at the blue edge for first overtone pulsation (see, e.g., Fig. 3e in Caputo et al., 1978)—i.e., at the first harmonic blue edge (FHBE). Therefore, in the hysteresis scenario, the observed scatter among Oo II clusters should be a consequence of variations in the masses and luminosities of the RR Lyrae stars among the different Oo II clusters, and the corresponding impact upon the periods of the stars at the FHBE (e.g., Caputo, 1990).

Using a formalism similar to that described by Caputo (1990), with a linear approximation to the complex behavior presented by the FHBE as a function of mass, luminosity and helium abundance, but using updated theoretical predictions for the FHBE based on more recent work on pulsating models by Bono, Caputo

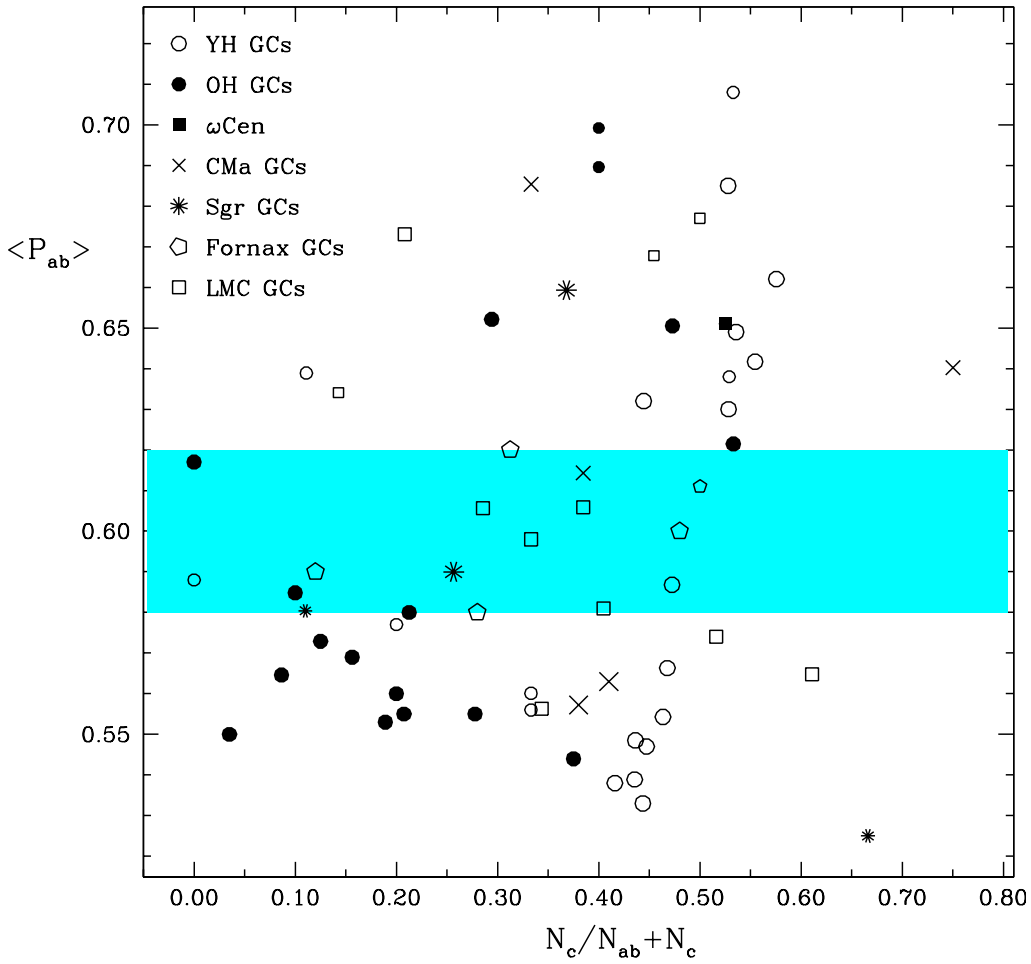

Figure 8.2 Fraction of c-type pulsators with respect to the total in globular clusters. Note that the separation between OoI and OoII clusters in this plane is much less clear-cut than in the $\langle P_{\rm ab} \rangle - P_{\rm ab,min}$ plane shown in Figure 8.1.

& Marconi (1995); Bono, Caputo, Castellani & Marconi (1997) and M. Marconi (1996, priv. comm.), along with the revised period-mean density relation by Caputo, Santolamazza & Marconi (1998), one finds that the aforementioned range of 0.12 d in $P_{\rm ab,min}$ can be accounted for if there is a range in luminosities at the FHBE of $\Delta M_{\rm bol} \simeq 0.30$ mag (at constant mass and chemical composition), or if there is a range in masses at the FHBE of $\Delta M \simeq 0.14\,M_{\odot}$ (at constant luminosity and chemical composition)—in the sense that masses should be smaller and luminosities higher for the longer $P_{\rm ab,min}$ values to obtain. While these ranges in masses and luminosities appear too large compared with that expected from double-mode pulsators (Kovács & Walker, 1999a) and from observational and theoretical constraints on the evolutionary status of RR Lyrae stars in Oo II globular clusters (e.g., Lee & Carney, 1999; Demarque et al., 2000b), a suitable combination of mass and luminosity variations could be successful at explaining the observations. (We also note, for completeness, that a large range in helium abundances, by

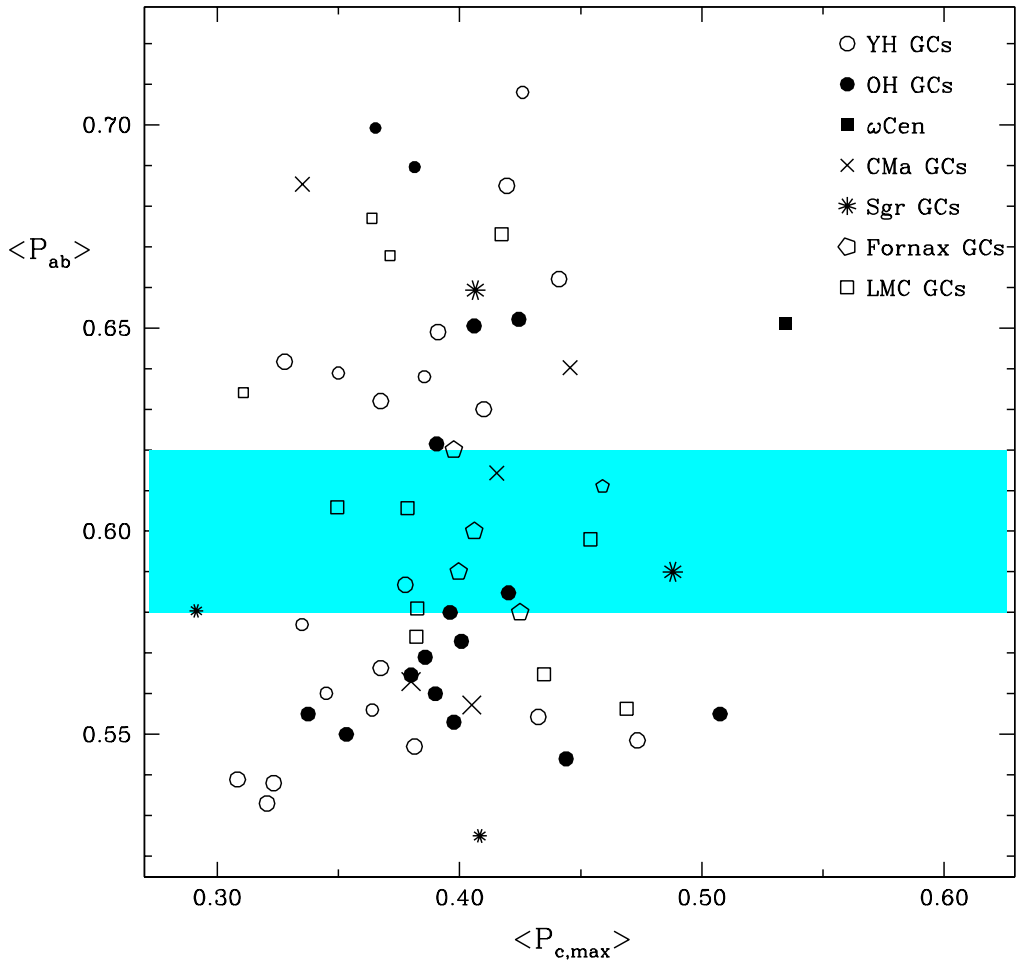

Figure 8.3 Same as Figure 8.1, but showing $P_{\rm c,max}$ as the abscissa.

$\Delta Y \simeq 0.37$, could also account for the observed period range.)

On the other hand, one should note that the expected trend should be for the Oo II clusters with longer $P_{\rm ab,min}$ to be the ones with bluer HB types. However, there is clearly *no* correlation between $P_{\rm ab,min}$ and HB type for Oo II globular clusters, thus casting doubt on the above conclusions. One possible way out of this conundrum could be a statistical effect, in that the clusters with smaller absolute numbers of ab-type variables $N_{\rm ab}$ would tend to have fewer RRab stars close to the FHBE, thereby presenting a longer $P_{\rm ab,min}$ than would have been the case if the cluster had a well-populated instability strip. However, this is not seen in practice: while there is considerable scatter in $P_{\rm ab,min}$ for the globular clusters with the smallest $N_{\rm ab}$, there is no systematic trend between $P_{\rm ab,min}$ and $N_{\rm ab}$ for the Oo II globulars.

That the situation may resist simplistic explanations is shown by a detailed analysis of three RR Lyrae-rich Oo II globular clusters in the LMC, namely NGC 1786, NGC 1841, and NGC 2210. The three clusters have but a small range in metallicity (Δ[Fe/H] $= 0.24 \pm 0.22$ dex) and HB type ($\Delta\mathcal{L} = 0.32 \pm 0.09$), and in spite of having $13 \leq N_{\rm ab} \leq 18$, their corresponding $P_{\rm ab,min}$ values range from

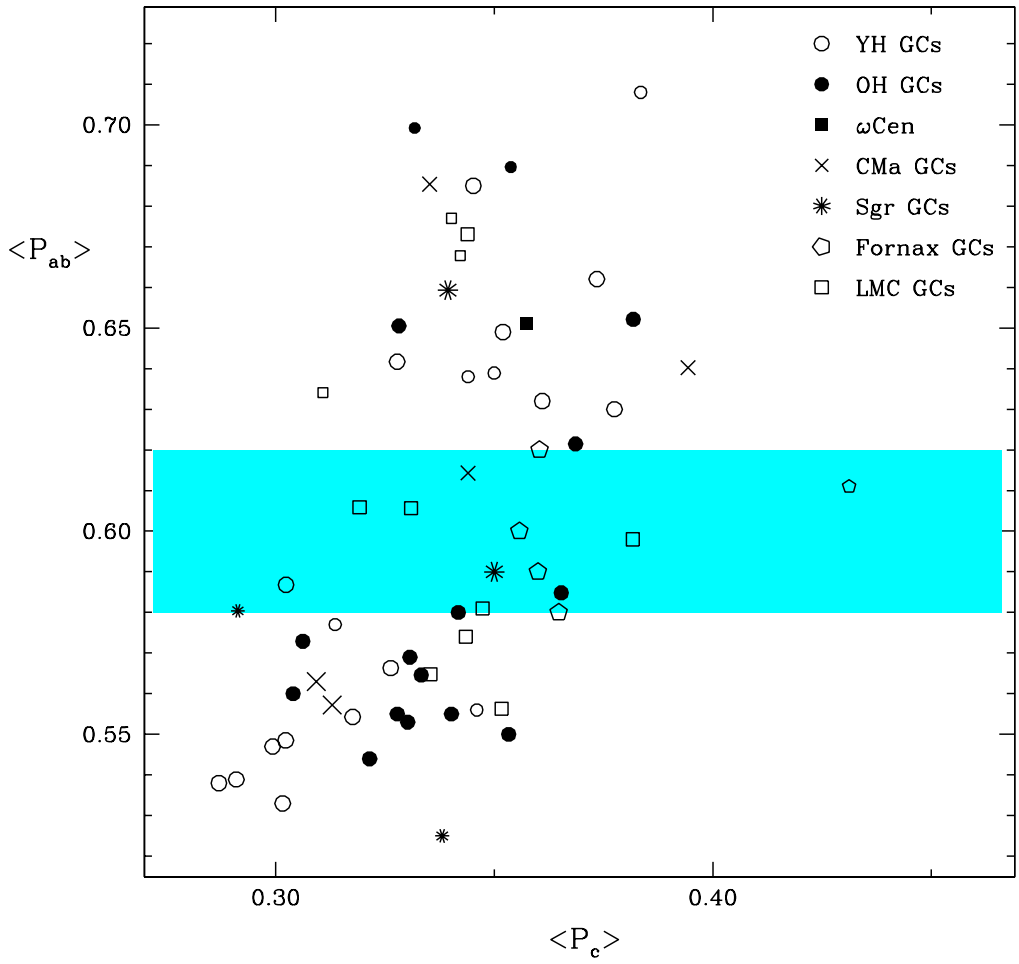

Figure 8.4 Same as Figure 8.3, but for $\langle P_{\rm c} \rangle$.

0.513 d for NGC 2210 up to 0.62 d for NGC 1841. Note that NGC 1841 has an HB that is bluer by only $\Delta\mathcal{L} = +0.06$ compared to NGC 2210, while the latter is the cluster with the *fewer* RRab, contrary to what would be expected according to the statistical effect mentioned above. Unless some of the variables have been misidentified as cluster members in at least some of these clusters, and/or have had their periods incorrectly measured, we are currently at a loss to explain these puzzling pieces of information.

8.6 About the Fornax Globular Cluster System

Properties of the RR Lyrae stars in the globular clusters of the Fornax dSph are summarized in Table 8.1. The various quantities were computed from stars whose membership to the clusters is more likely and contamination from field stars is minimized (see Section 4.4). Results for clusters For 2, 3, 4 and 5 are from the present work, data for For 1 are from Mackey & Gilmore (2003b). The globular clusters of the Fornax dSph are all of Oosterhoff intermediate type, based on the

mean period of their *ab*-type RR Lyrae stars ($\langle P_{ab} \rangle$). Indeed, they are *confined within* the 'gap' and entirely span it from its short period edge (with For 2) to its upper period edge (with For 3). These 5 globulars form a a fairly homogeneous sample of Oosterhoff intermediate clusters and may contribute unveiling the true nature of the Oosterhoff intermediate type, namely whether it is just a transition class or whether it is a distinct group with physical properties common to all Oo-Int clusters. However, results for the Fornax clusters are not straightforward. We note that the mean periods of the c-type RR Lyrae stars in these clusters are more similar to those of Oo II Galactic clusters, and are generally higher than those of of the Oosterhoff intermediate globular clusters in the LMC. On the other hand, the full range of f_c values is spanned by these clusters thus suggesting a weak reliability of this parameter to discriminate among Oosterhoff types, as shown by Figure 8.2. The period-amplitude diagrams of the Fornax dSph clusters (see Figure 8.5) do not provide clearcut indications either, since in this plane the Fornax clusters show a variety of positions ranging from Oo I (e.g. For 2, and For 4) to Oo-Int/Oo II types, thus suggesting that the Oosterhoff intermediate status is not necessarily accompanied by a clearcut intermediate (e.g., between Oo I and Oo II types) position of the RR Lyrae stars in the Bailey diagram. Rather, the Fornax clusters seem to support that the position of the blue edge for first overtone pulsation ($P_{\rm ab,min}$) plays a dominant role in defining the Oosterhoff intermediate status.

Table 8.1 Properties of the RR Lyrae stars in the globular clusters of the Fornax dSph

Name	$< P_{ab} >$	$< P_c >$	$P_{ab,min}$	$P_{c,max}$	N_{ab}	N_c	N_d	f_c^a	Oo Type
For 2	0.58	0.36	0.52	0.42	18	7	-	0.28	Oo-Int
For 3	0.62	0.36	0.56	0.40	11	5	7	0.31	Oo-Int
For 4	0.59	0.36	0.52	0.40	16	3	1	0.16	Oo-Int
For 5	0.60	0.36	0.53	0.41	13	12	1	0.48	Oo-Int
For 1	0.61	0.43	0.57	0.46	5	5	-	0.50	Oo-Int

[a] $f_c = Nc/(N_c + N_{ab})$

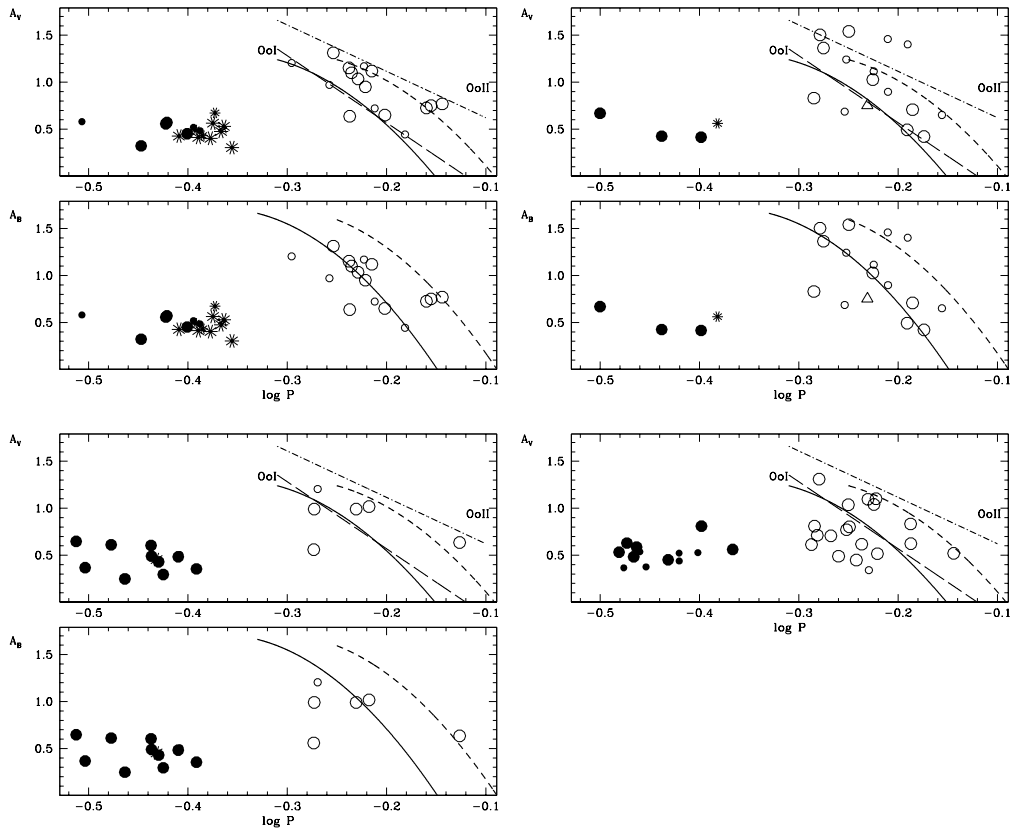

Figure 8.5 V, B period-amplitude diagrams of the Fornax globular cluster RR Lyrae stars. Top left: For 3; bottom left: For 5; top right: For 4; bottom right: For 2. Filled circles are RRab's; open circles are RRc's, and asterisks are double-mode RR Lyrae stars. Larger symbols are used for variable stars more likely belonging to the clusters. The straight lines are the positions of the Oo I and Oo II Galactic globular clusters according to Clement & Rowe (2000). Period-amplitude distributions of the *bona fide* regular (solid curves) and well-evolved (dashed curves) *ab* RR Lyrae stars in M3 from (Cacciari et al., 2005) are also shown for comparison.

Chapter 9

Conclusions

In this thesis we have tried to identify possible "building blocks" of the Galactic halo, by investigating the pulsation properties and Oosterhoff type of variables stars in a number of different stellar systems, starting from a relatively undisturbed dwarf galaxy: the Fornax dSph, through a distorted and tidally disrupting one: the Bootes dSph, to a possible final relic of the disruption process: the Galactic globular cluster NGC 2419. We have mapped the RR Lyrae star population in these systems and firmly placed them on the Oosterhoff plane (see Figure 9.1). We have addressed the question of whether the pulsation properties of the RR Lyrae stars in these systems conform to the Oosterhoff dichotomy characterizing the Milky Way variables. If they do not, the Galaxy's halo cannot have been assembled by protogalactic fragments resembling these present-day companions of the MW. The Oosterhoff behaviour of different stellar systems, including our targets, was also investigated to look for the key quantity defining Oosterhoff status. We have used the RR Lyrae stars to derive hints on the metal abundance and to measure the distance to these systems. Other types of variables were also detected besides the RR Lyrae stars. In the Fornax dSph we have identified the largest sample of Dwarf Cepheids ever detected in an extragalactic system, and have defined their $P - L$ relationship.

Results from the RR Lyrae star population in the systems targeted by this thesis have been summarized in Table 9.1 and Figure 9.1, where these systems are shown by large double symbols.

Main results from the present study are:

- The field RR Lyrae stars in the Fornax dSph (double star in Figure 9.1) posses properties intermediate between Oo I and II types

- Similarly, globular clusters of the Fornax dSph have characteristics intermediate between the canonical Oosterhoff groups, and are "all" *confined* within the "Oosterhoff gap" of the MW globulars (double pentagons in Figure 9.1)

- RR Lyrae stars have been identified in the newly discovered Bootes dSph galaxy, and the system show to posses *pure* Oosterhoff type II characteristics

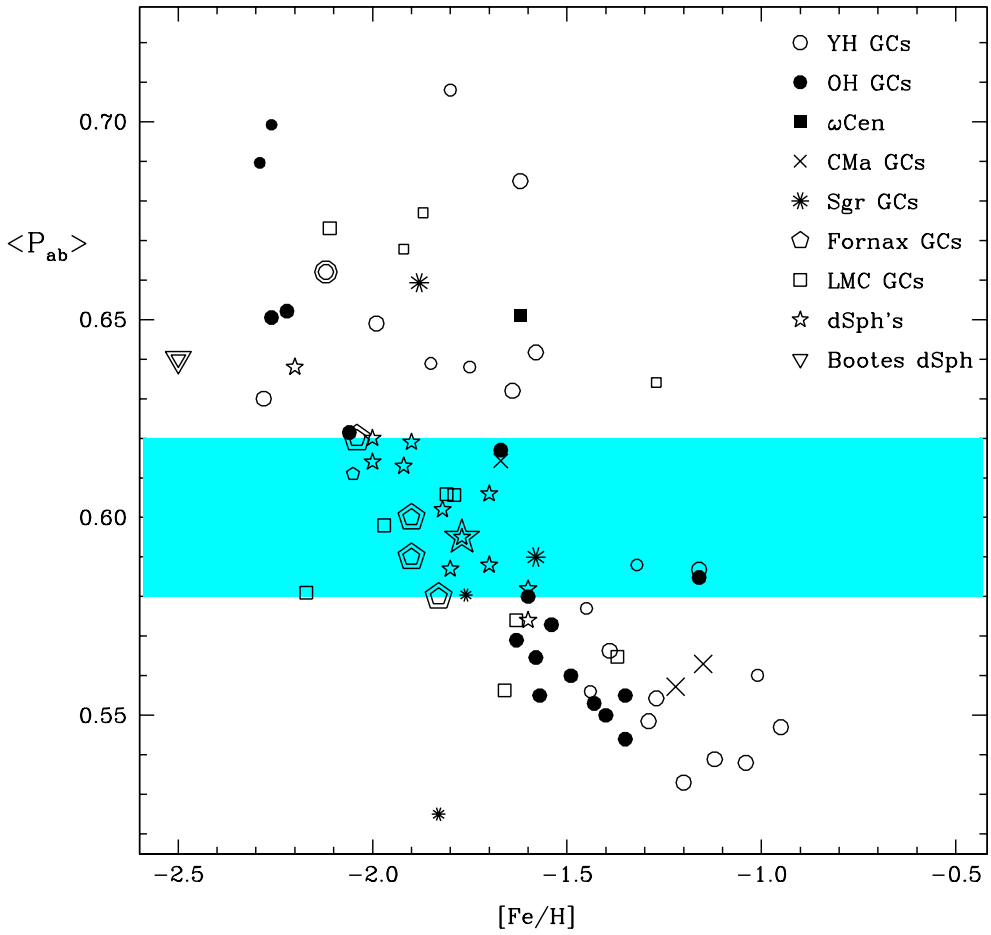

Figure 9.1 Position on the Oosterhoff plane of: globular clusters in the Milky Way, the LMC, the Sgr, CMa and Fornax dSph's, and of field variables in the Milky Way dSph satellites. Field and cluster variables in dSph galaxies and in the LMC preferentially *occupy* the "Oosterhoff gap" (shaded region), in stark contrast with the Galactic globular clusters. Large double symbols mark the stellar systems targeted by this thesis. Double pentagons: clusters For 2, 3, 4 and 5 in the Fornax dSph; double star: field variables of the Fornax dSph; double circle: NGC 2419; inverted double triangle: Bootes dSph.

(inverted double triangle in Figure 9.1)

- Based on our more complete census of the RR Lyrae star population, NGC 2419 confirms to be a *pure* Oosterhoff type II system (double circle in Figure 9.1). This result does not exclude, however, an extragalactic origin of this most intriguing Galactic cluster

- The minimum period of the *ab*-type RR Lyrae stars appears to be the key quantity defining Oosterhoff status.

To conclude, is any of the systems we have investigated more likely to represent a "building block" of the MW halo?

The new Milky Way satellites being discovered by the SDSS, and *pure* Oosterhoff-type systems like the UMi dSph among the previously known dwarf spheroidals, perhaps held best promise for telling us the galactic halo in its early days. We have already gathered time-series data of the UMi dSph to check on its *pure* Oosterhoff type II status in same manner as we have done for NGC 2419. We have also been granted time to observe "all" the newly discovered dwarf spheroidals. Observations are just starting, since these are all "spring" objects, but this is another ...."PhD thesis!"

Table 9.1 Results for RR Lyrae stars in the stellar systems we have analyzed in this work

Name	$< P_{ab} >$	$< P_c >$	$P_{ab,min}$	$P_{c,max}$	N_{ab}	N_c	N_d	f_c^a	Oo Type
For 2	0.58	0.36	0.52	0.42	18	7	-	0.28	Oo-Int
For 3	0.62	0.36	0.56	0.40	11	5	7	0.31	Oo-Int
For 4	0.59	0.36	0.52	0.40	16	3	1	0.16	Oo-Int
For 5	0.60	0.36	0.53	0.41	13	12	1	0.48	Oo-Int
NGC 2419	0.66	0.37	0.58	0.44	38	30	3	0.44	Oo II
Bootes	0.64	0.37	0.58	0.42	5	5	1	0.50	Oo II

[a] $f_c = Nc/(N_c + N_{ab})$

Appendix A

Atlas of light curves: Fornax 2

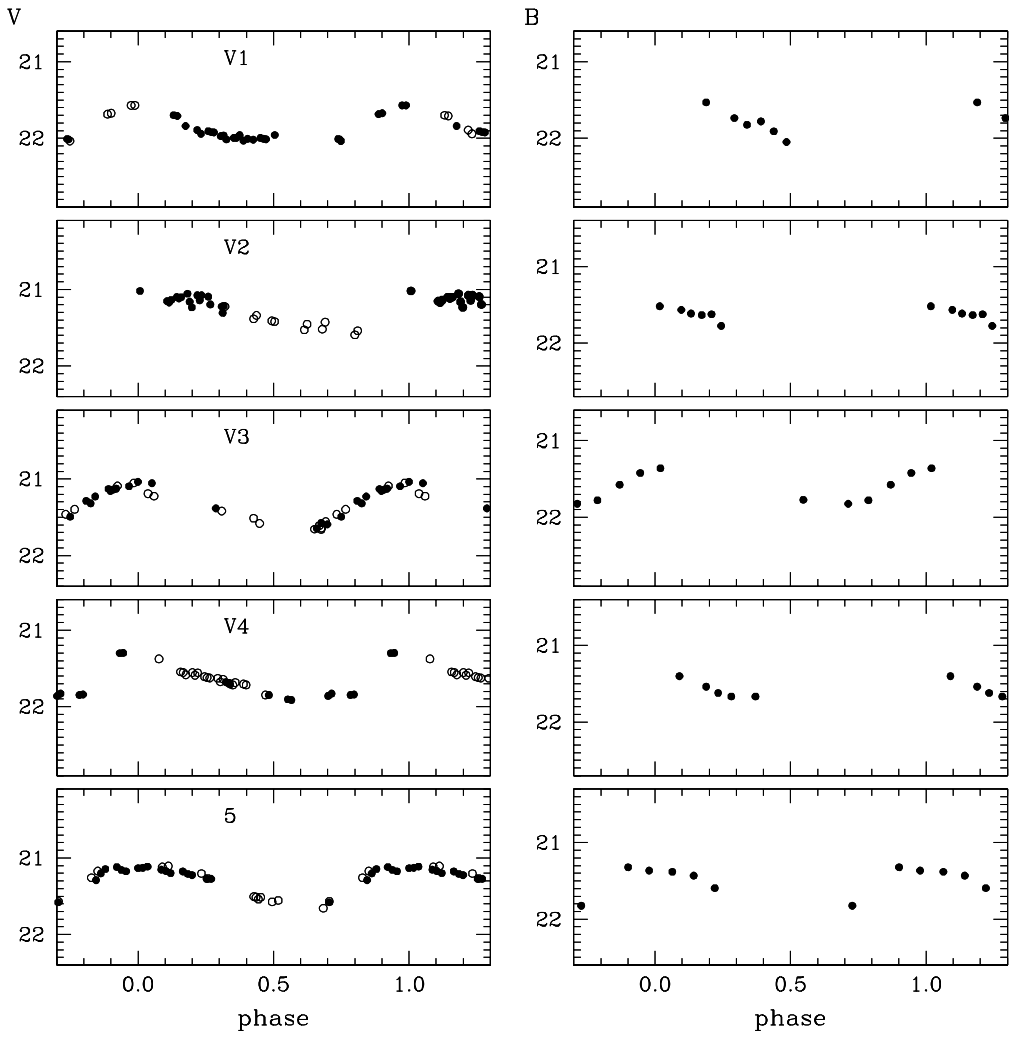

Figure A.1 Magnitude calibrated light curves of For 2 variable stars, as summarized in Table 4.5. Filled circles are Magellan data, open circles HST data.

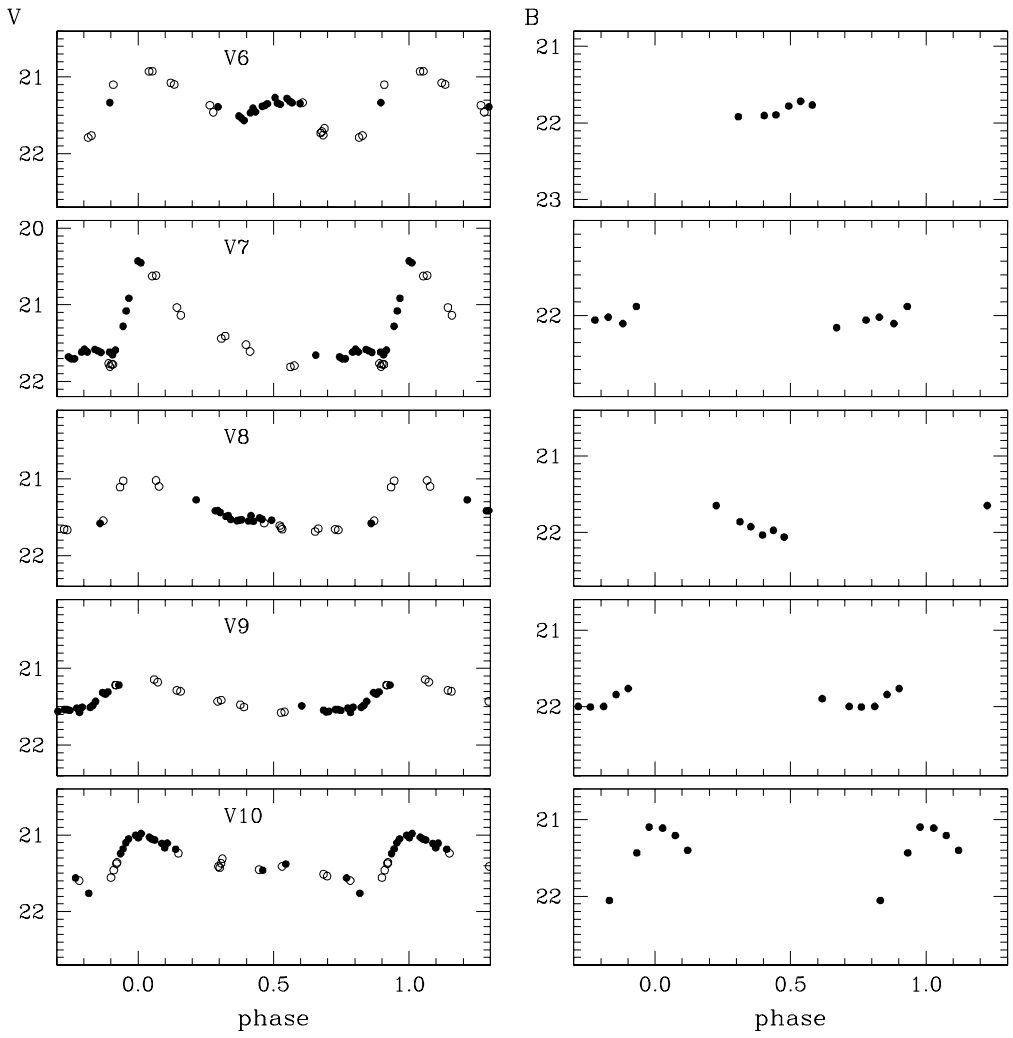

Figure A.2 Magnitude calibrated light curves of For 2 variable stars, as summarized in Table 4.5. Filled circles are Magellan data, open circles HST data.

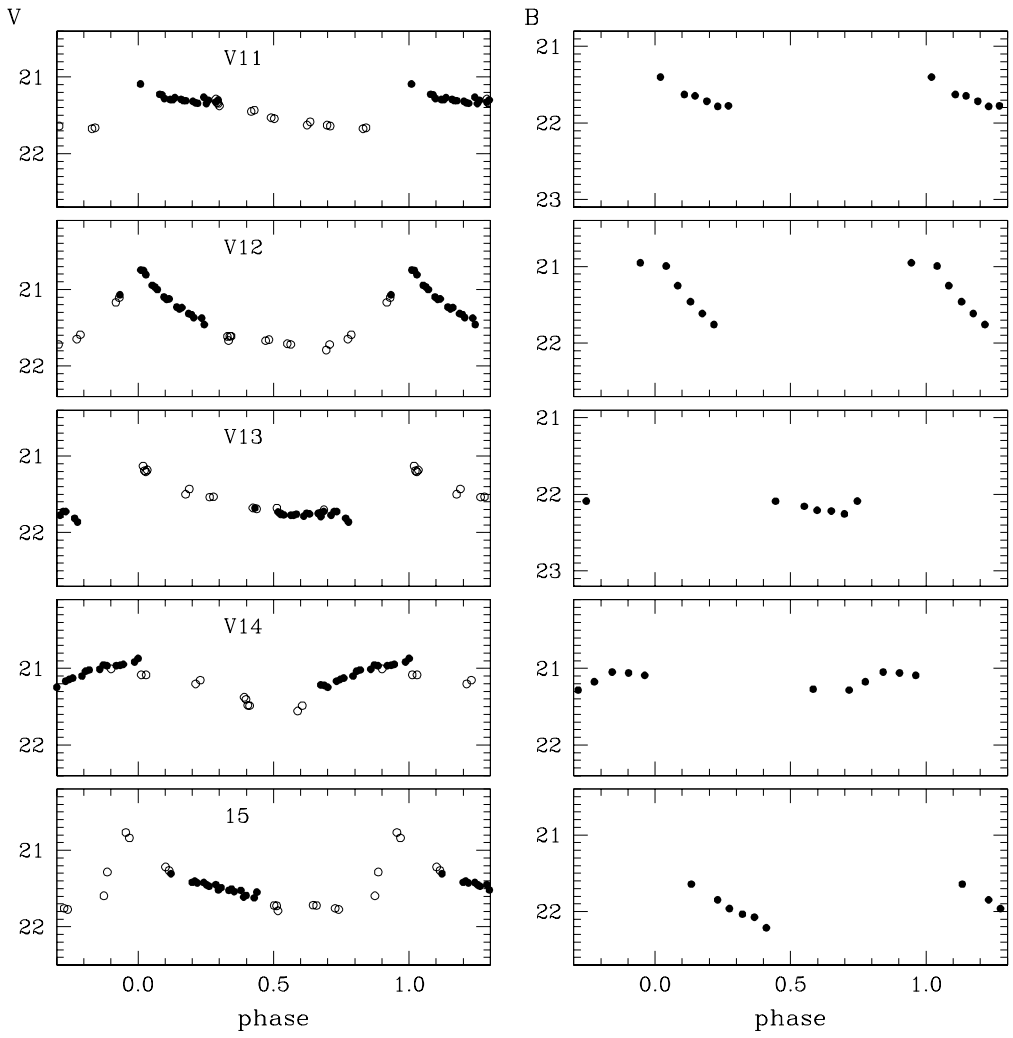

Figure A.3 Magnitude calibrated light curves of For 2 variable stars, as summarized in Table 4.5. Filled circles are Magellan data, open circles HST data.

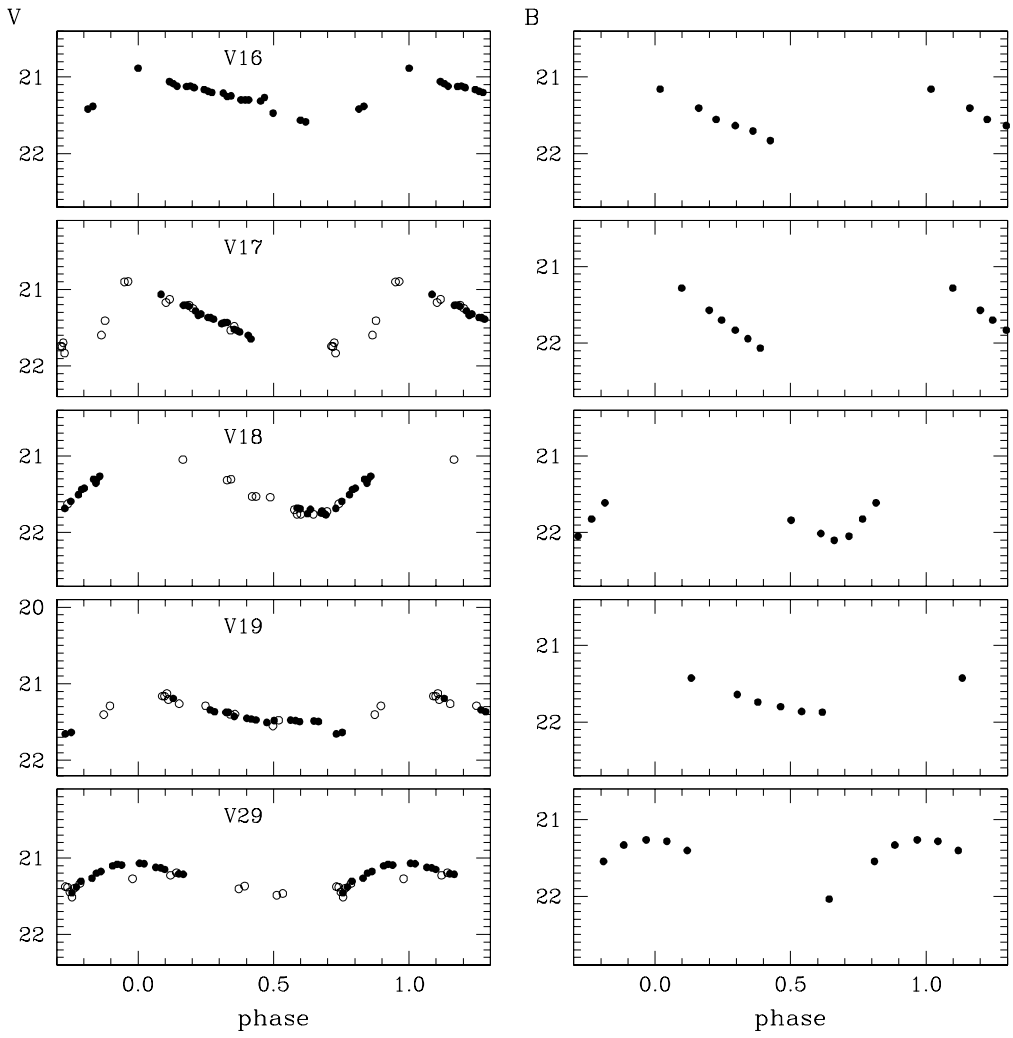

Figure A.4 Magnitude calibrated light curves of For 2 variable stars, as summarized in Table 4.5. Filled circles are Magellan data, open circles HST data.

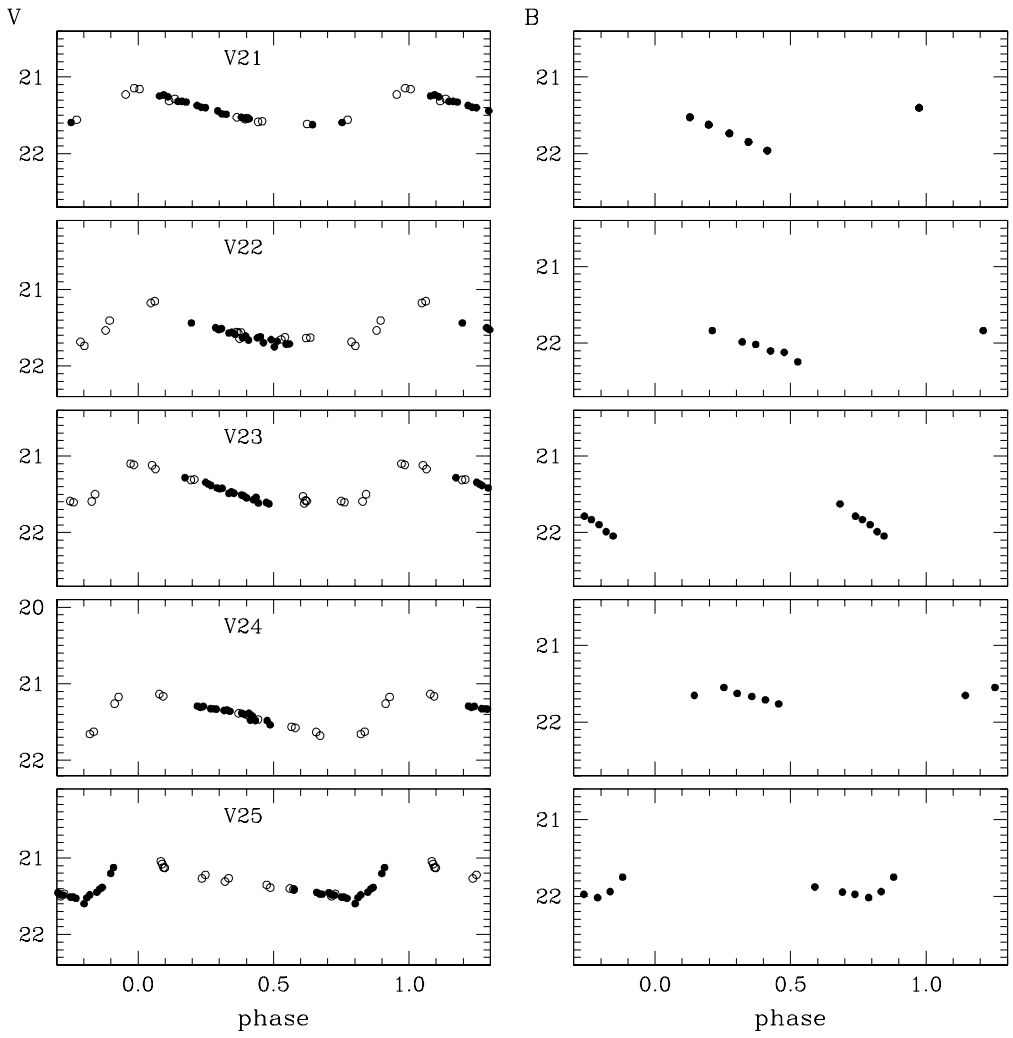

Figure A.5 Magnitude calibrated light curves of For 2 variable stars, as summarized in Table 4.5. Filled circles are Magellan data, open circles HST data.

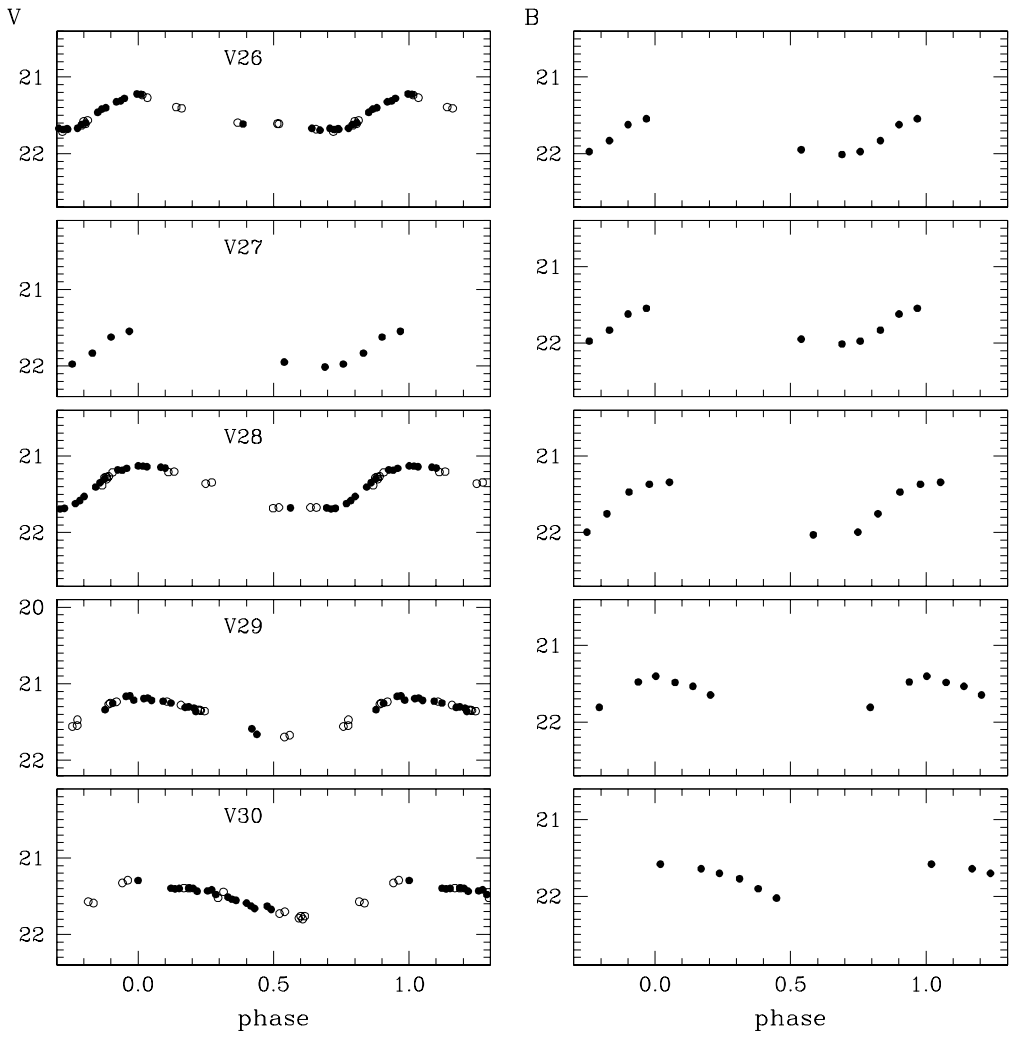

Figure A.6 Magnitude calibrated light curves of For 2 variable stars, as summarized in Table 4.5. Filled circles are Magellan data, open circles HST data.

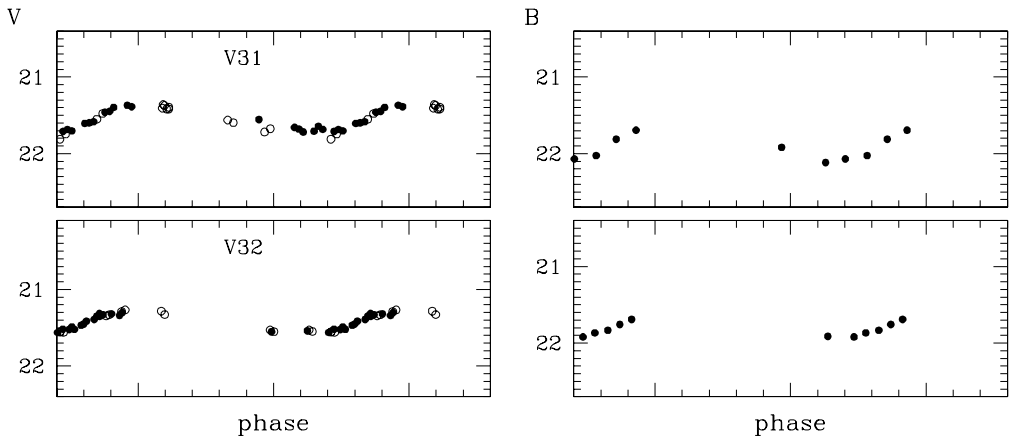

Figure A.7 Magnitude calibrated light curves of For 2 variable stars, as summarized in Table 4.5. Filled circles are Magellan data, open circles HST data.

Appendix B

Atlas of light curves: Fornax 3

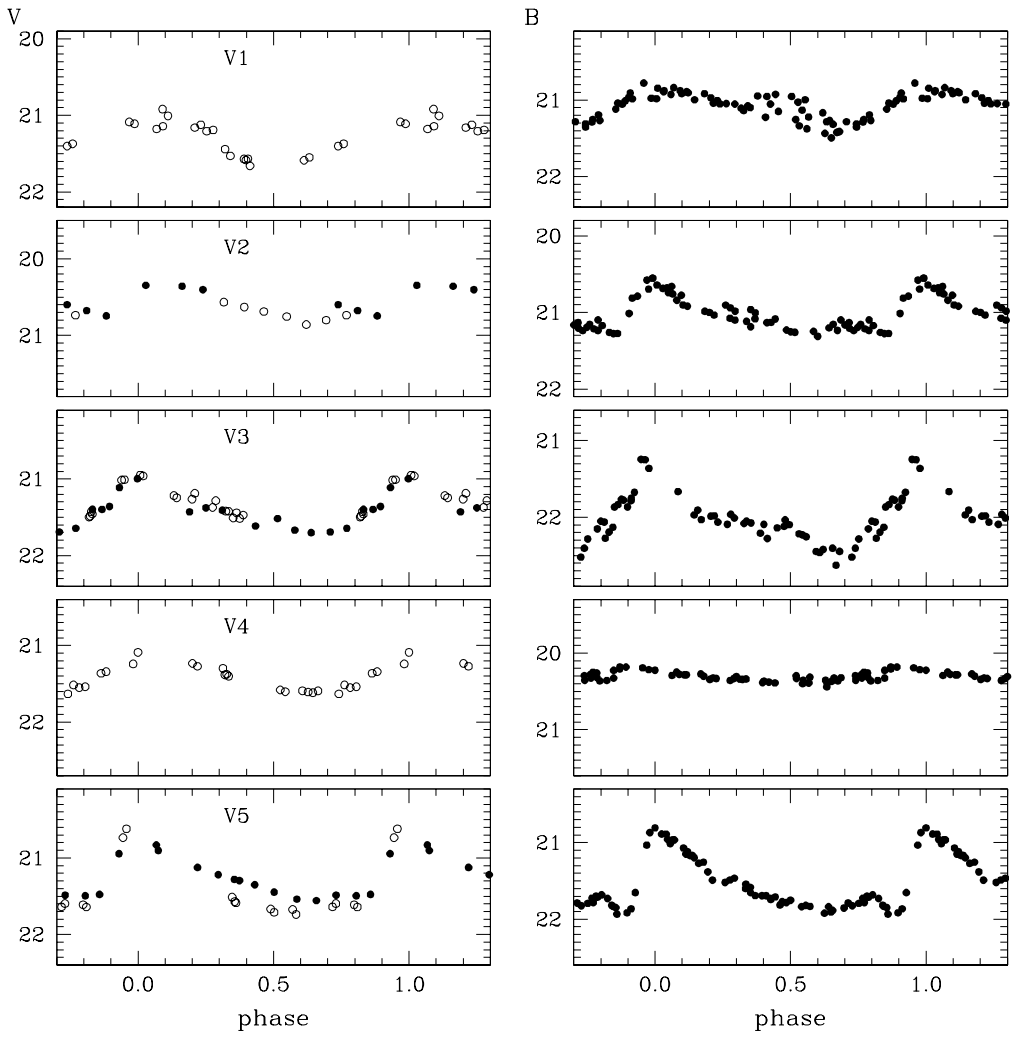

Figure B.1 Magnitude calibrated light curves of For 3 variable stars, as summarized in Table 4.6. Filled circles are ESO-2.2m/WFI data, open circles HST data.

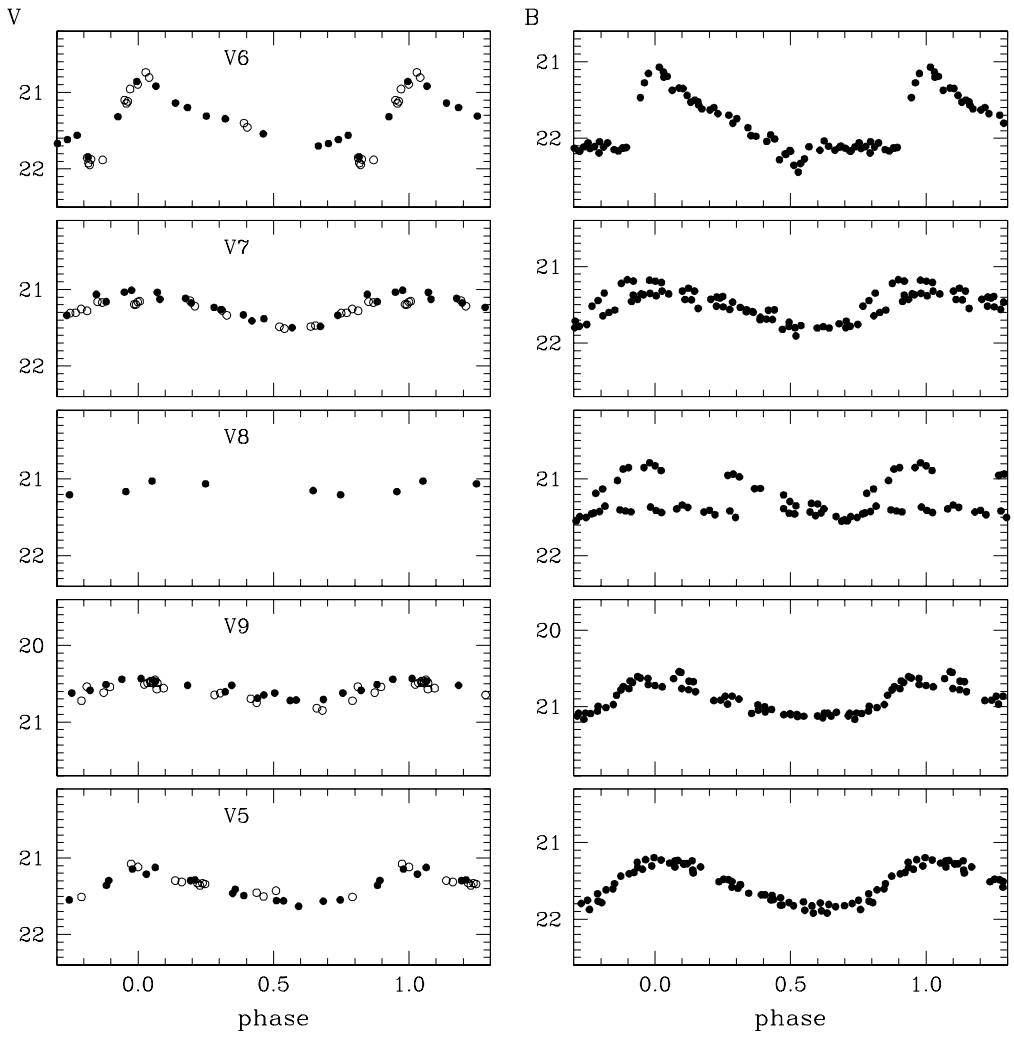

Figure B.2 Magnitude calibrated light curves of For 3 variable stars, as summarized in Table 4.6. Filled circles are ESO-2.2m/WFI data, open circles HST data.

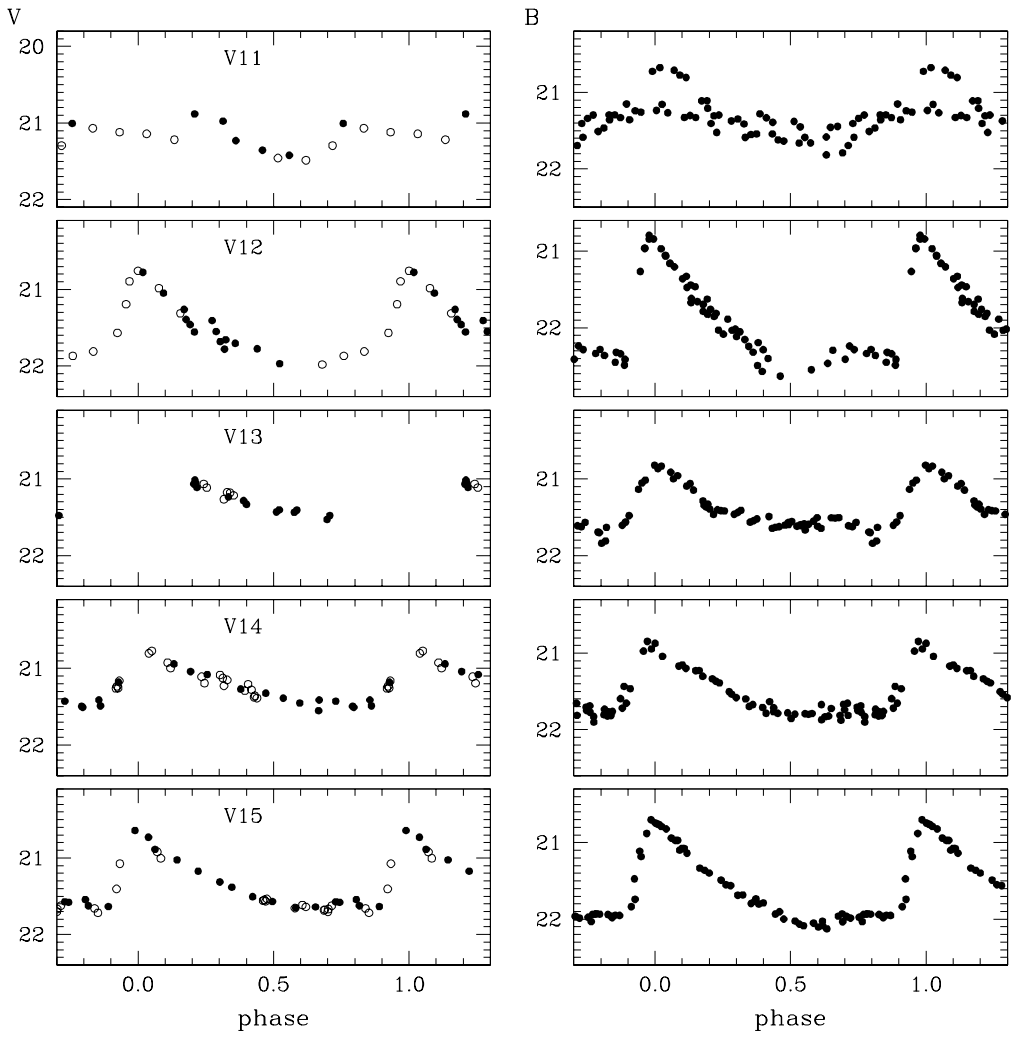

Figure B.3 Magnitude calibrated light curves of For 3 variable stars, as summarized in Table 4.6. Filled circles are ESO-2.2m/WFI data, open circles HST data.

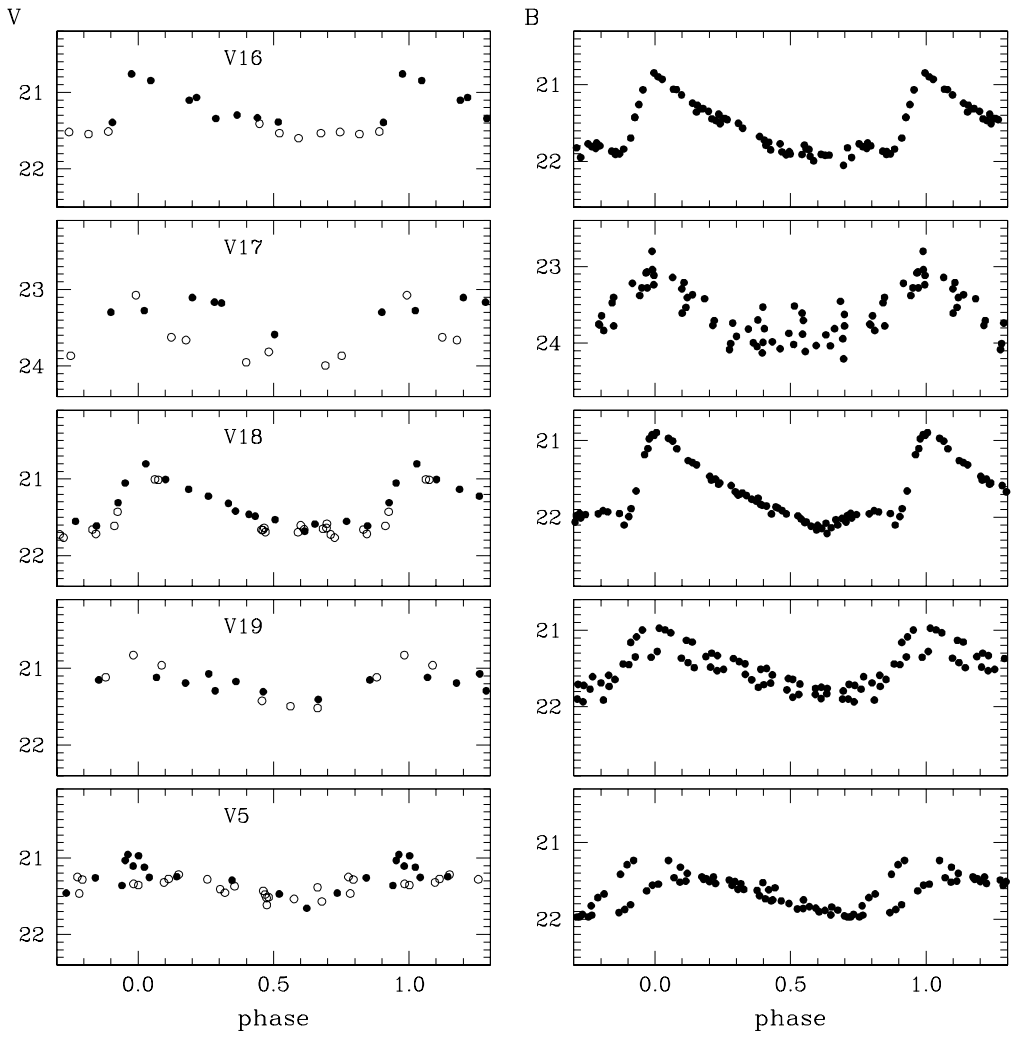

Figure B.4 Magnitude calibrated light curves of For 3 variable stars, as summarized in Table 4.6. Filled circles are ESO-2.2m/WFI data, open circles HST data.

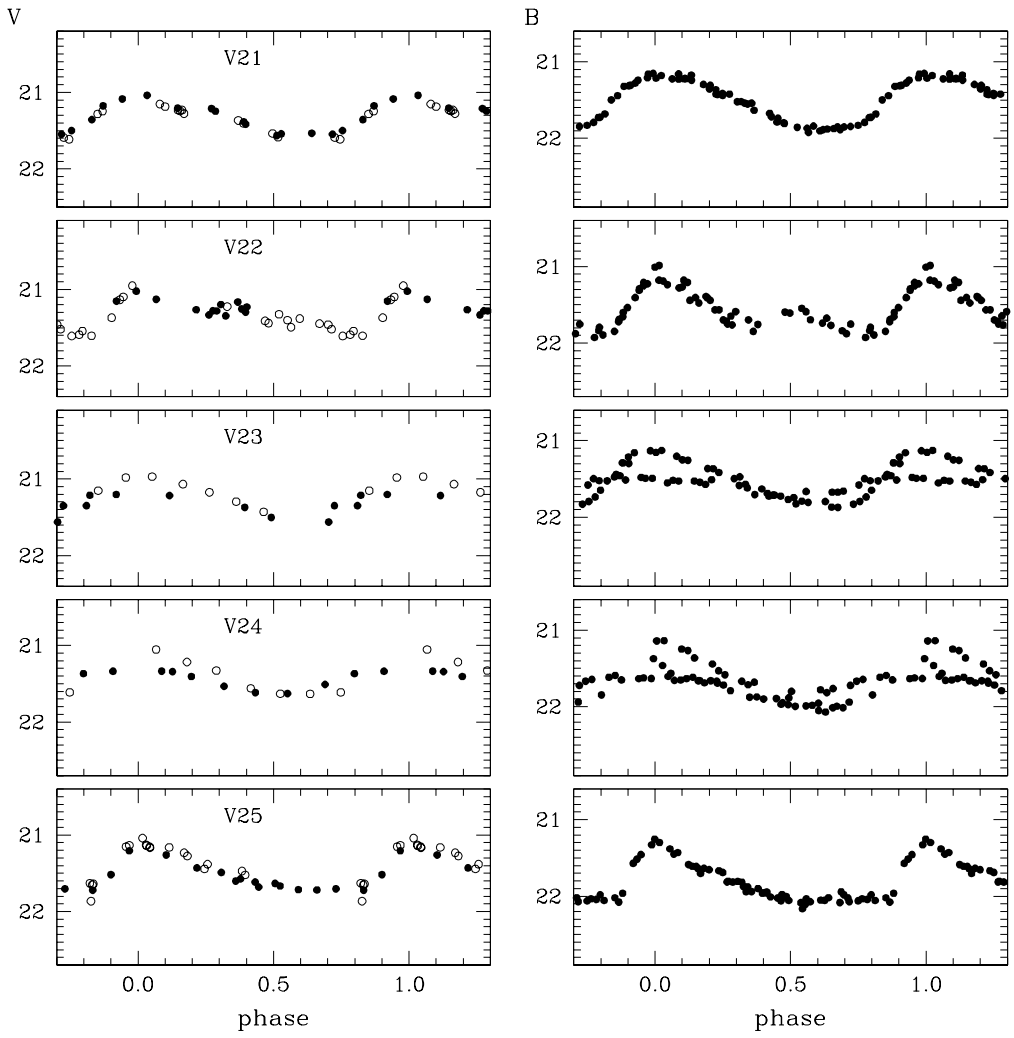

Figure B.5 Magnitude calibrated light curves of For 3 variable stars, as summarized in Table 4.6. Filled circles are ESO-2.2m/WFI data, open circles HST data.

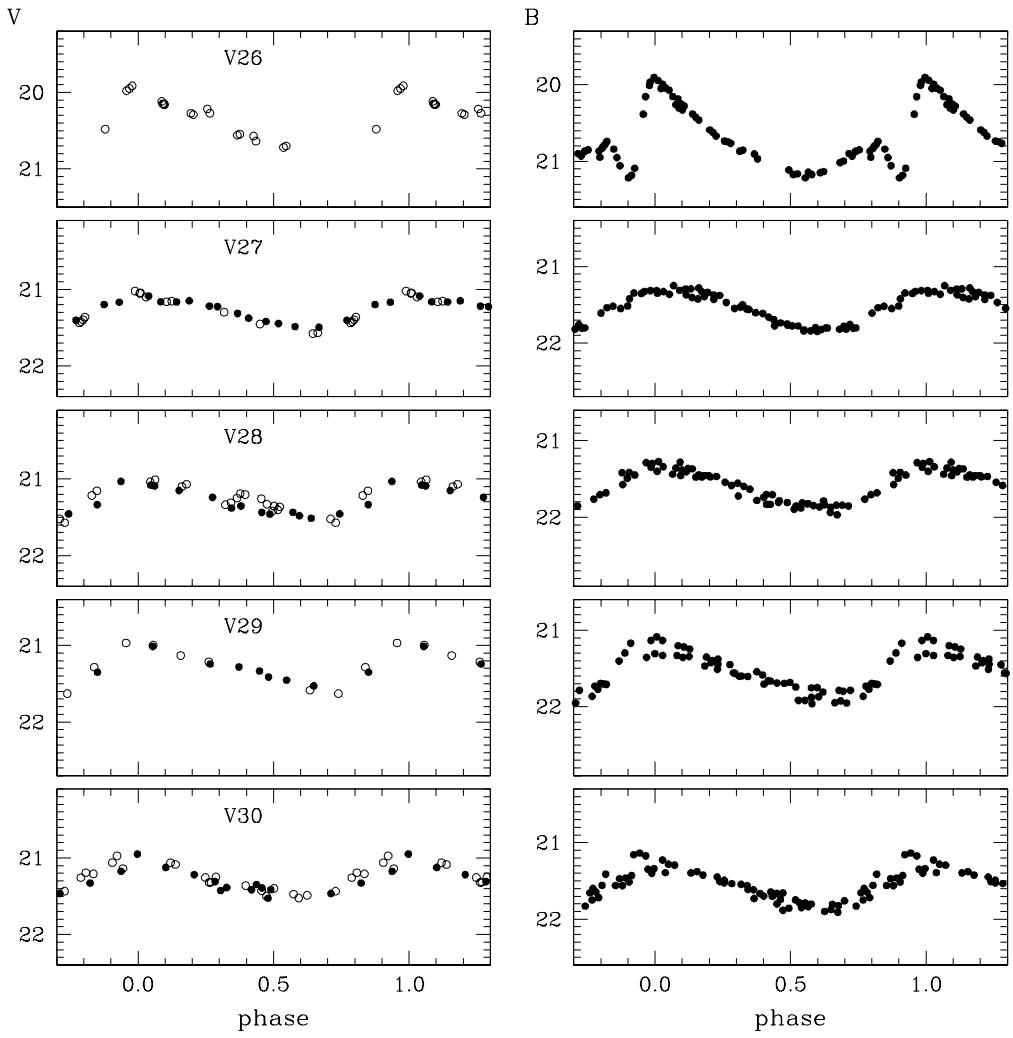

Figure B.6 Magnitude calibrated light curves of For 3 variable stars, as summarized in Table 4.6. Filled circles are ESO-2.2m/WFI data, open circles HST data.

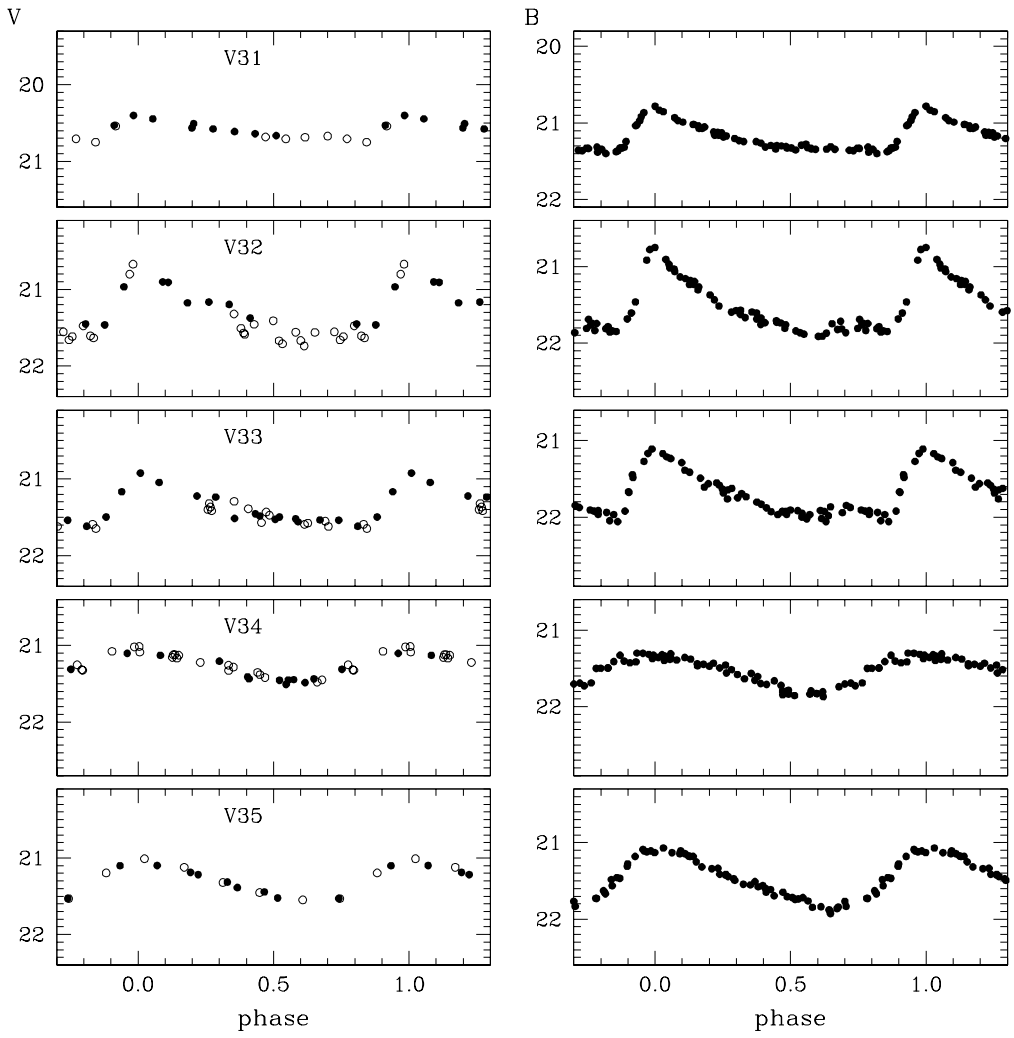

Figure B.7 Magnitude calibrated light curves of For 3 variable stars, as summarized in Table 4.6. Filled circles are ESO-2.2m/WFI data, open circles HST data.

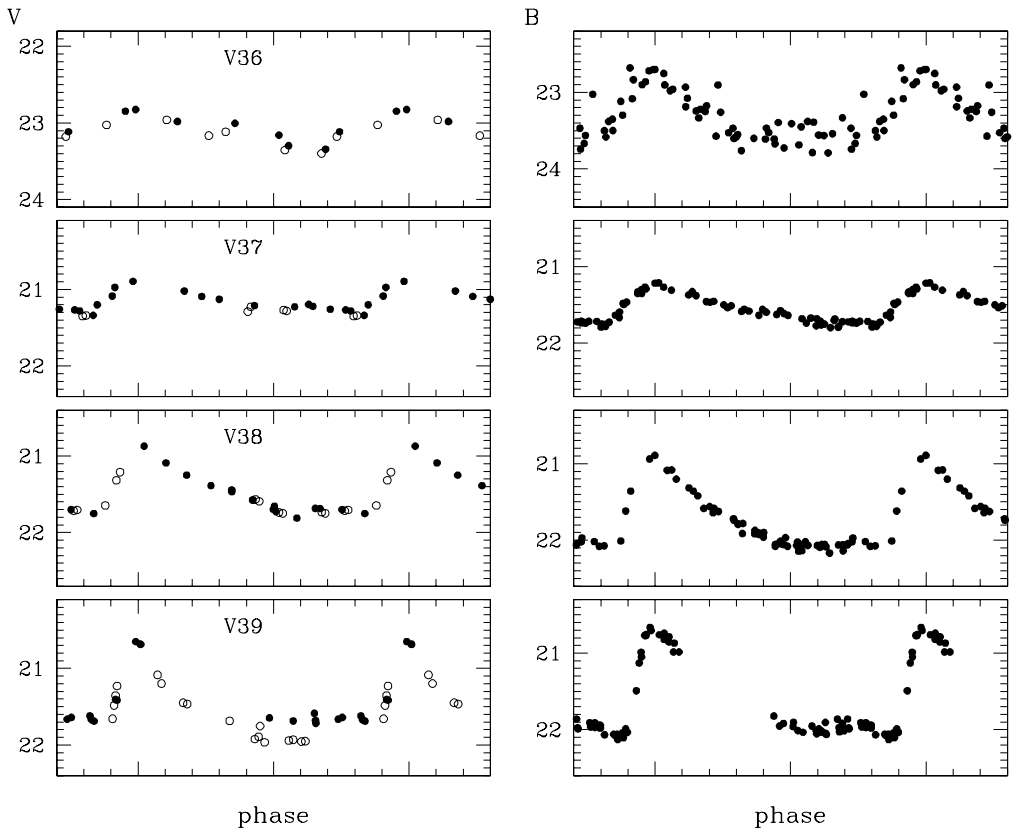

Figure B.8 Magnitude calibrated light curves of For 3 variable stars, as summarized in Table 4.6. Filled circles are ESO-2.2m/WFI data, open circles HST data.

Appendix C

Atlas of light curves: Fornax 4

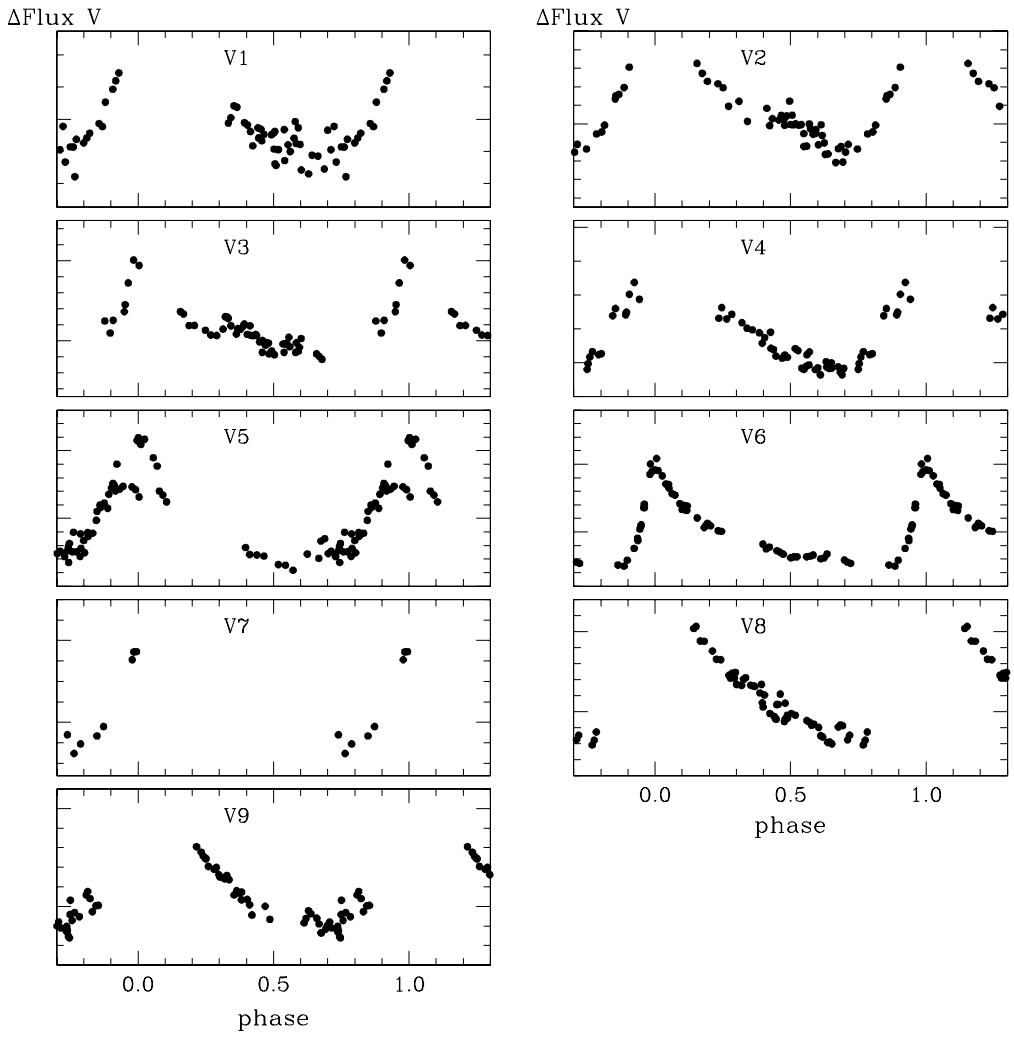

Figure C.1 Differential flux light curves of For 4 variable stars, as summarized in Table 5.3. Filled circles are Magellan data, open circles CTIO-4m/WFI data.

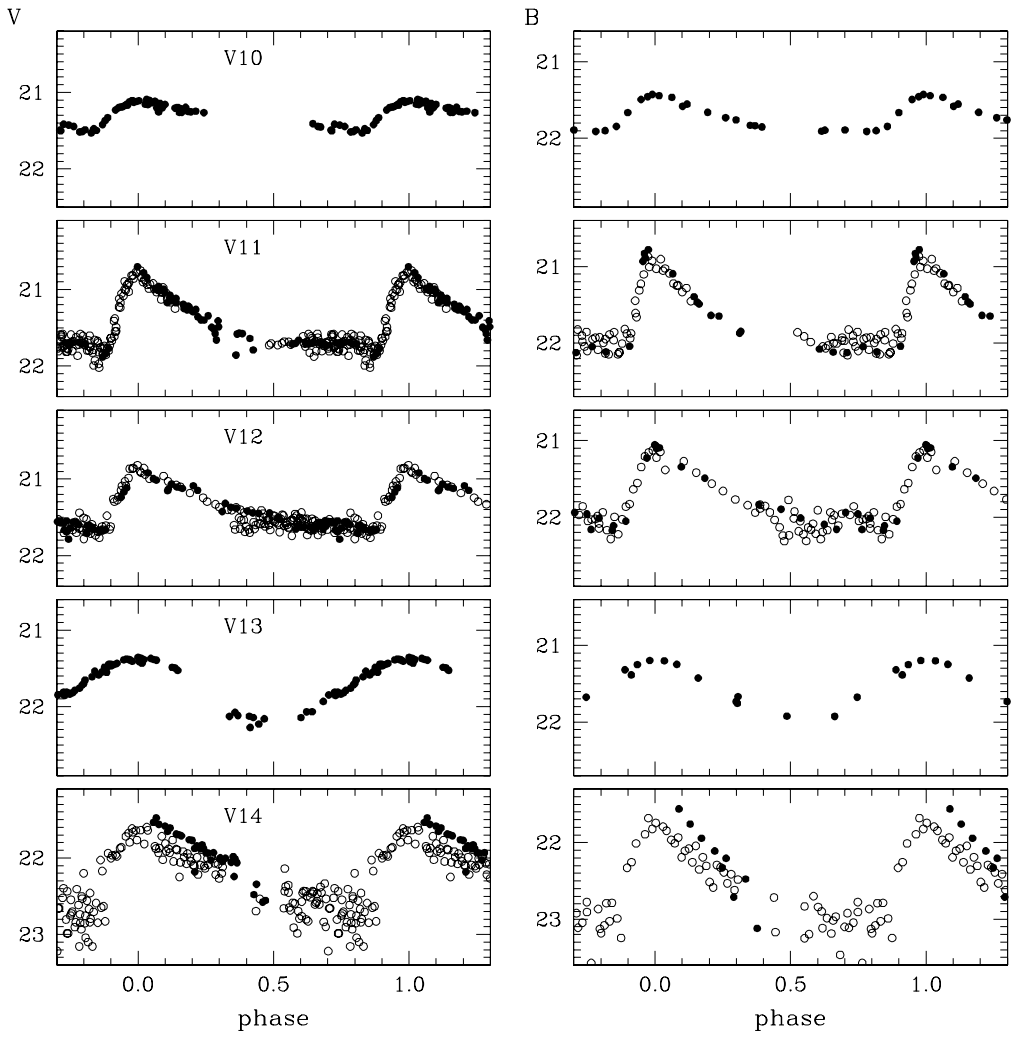

Figure C.2 Magnitude calibrated light curves of For 4 variable stars, as summarized in Table 5.3. Filled circles are Magellan data, open circles CTIO-4m/WFI data.

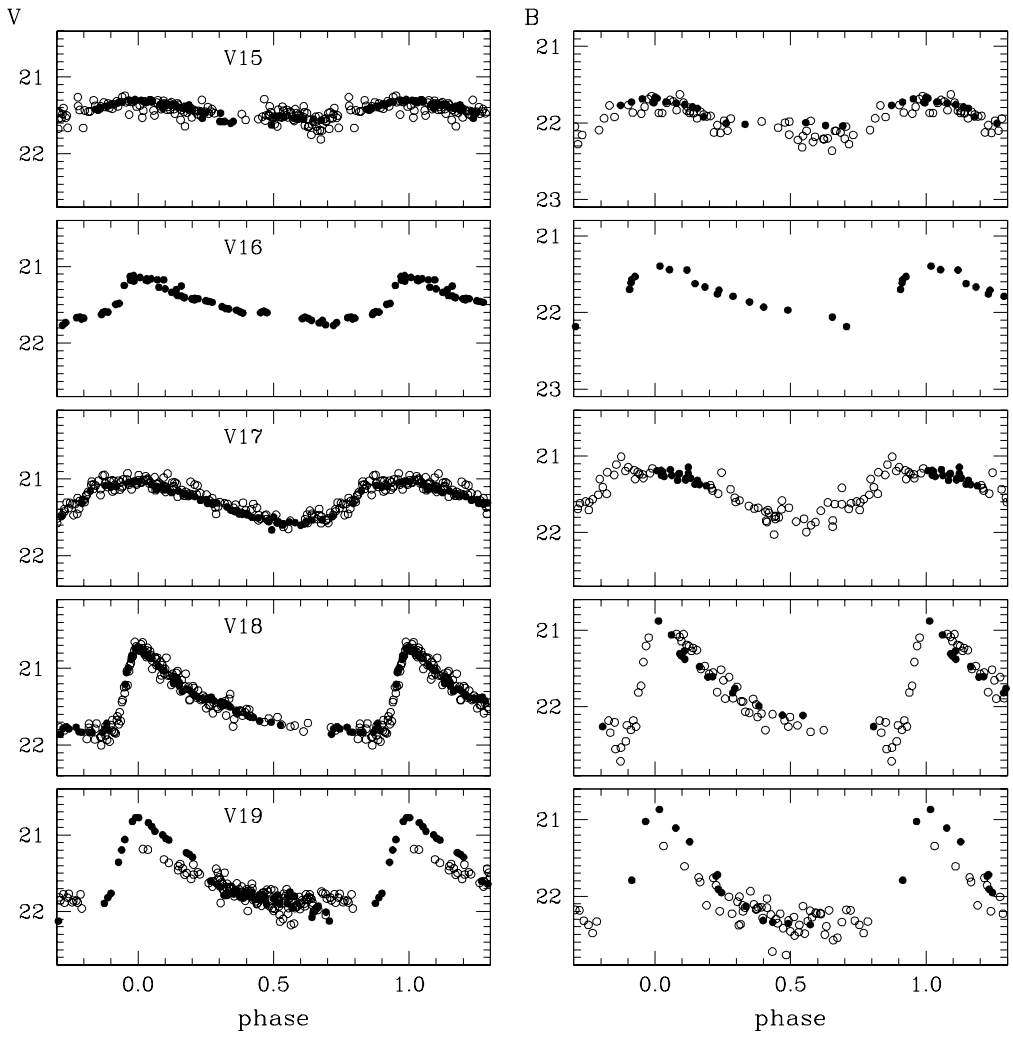

Figure C.3 Magnitude calibrated light curves of For 4 variable stars, as summarized in Table 5.3. Filled circles are Magellan data, open circles CTIO-4m/WFI data.

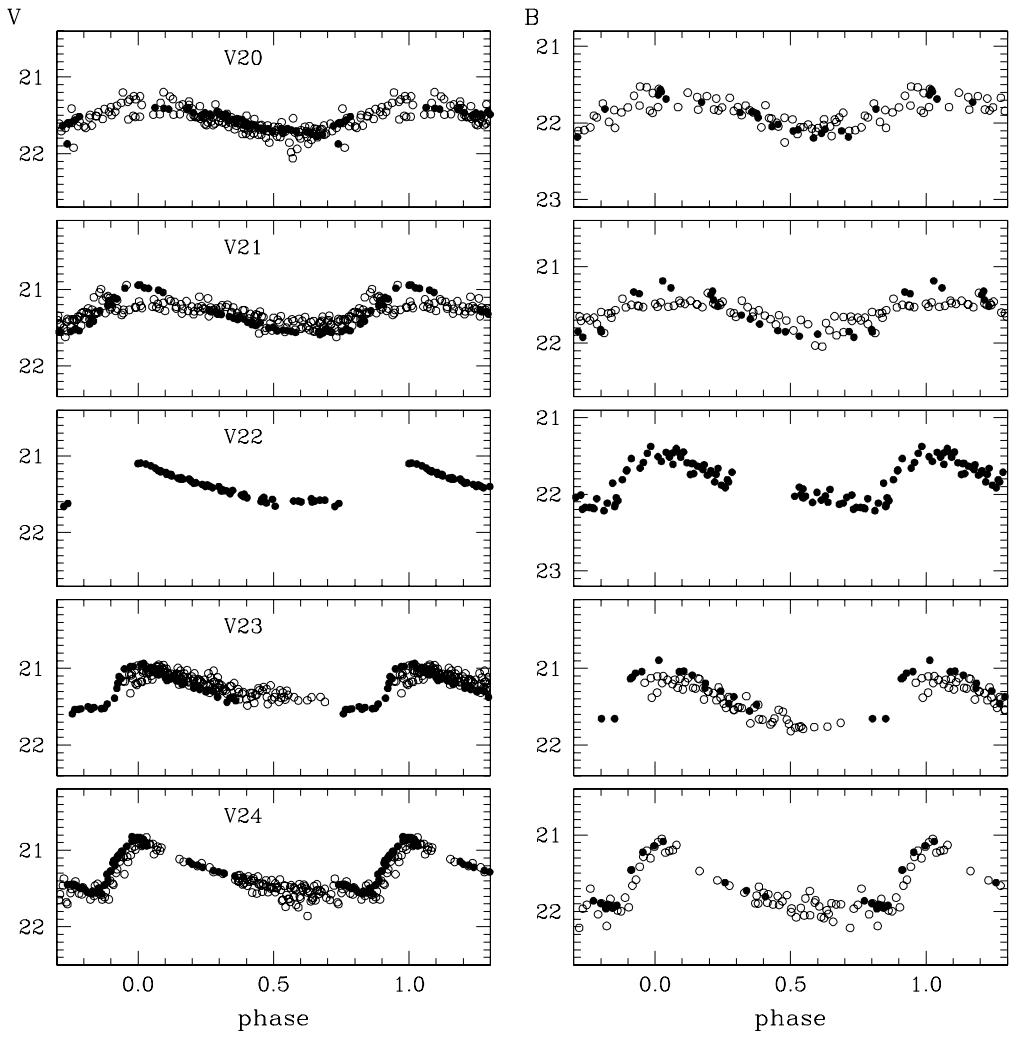

Figure C.4 Magnitude calibrated light curves of For 4 variable stars, as summarized in Table 5.3. Filled circles are Magellan data, open circles CTIO-4m/WFI data.

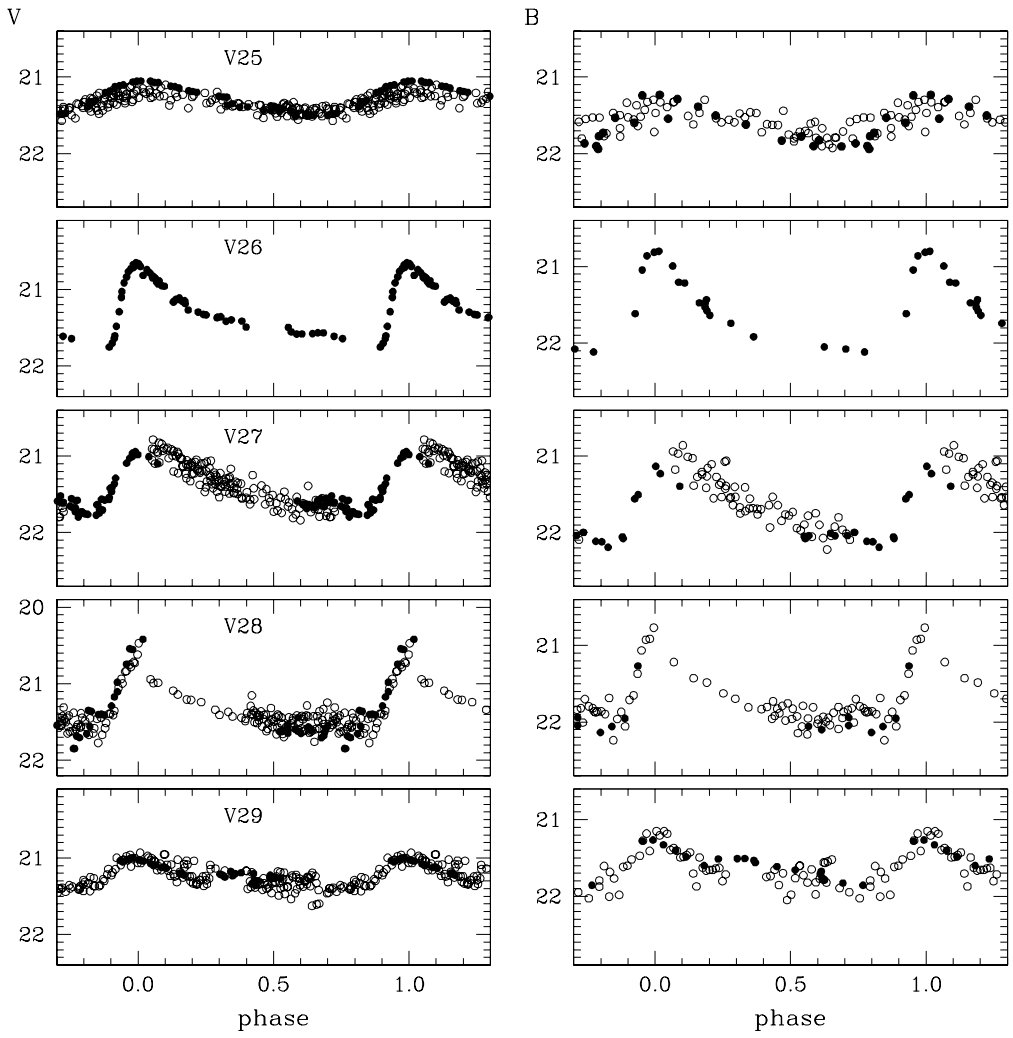

Figure C.5 Magnitude calibrated light curves of For 4 variable stars, as summarized in Table 5.3. Filled circles are Magellan data, open circles CTIO-4m/WFI data.

Appendix D

Atlas of light curves: Fornax 5

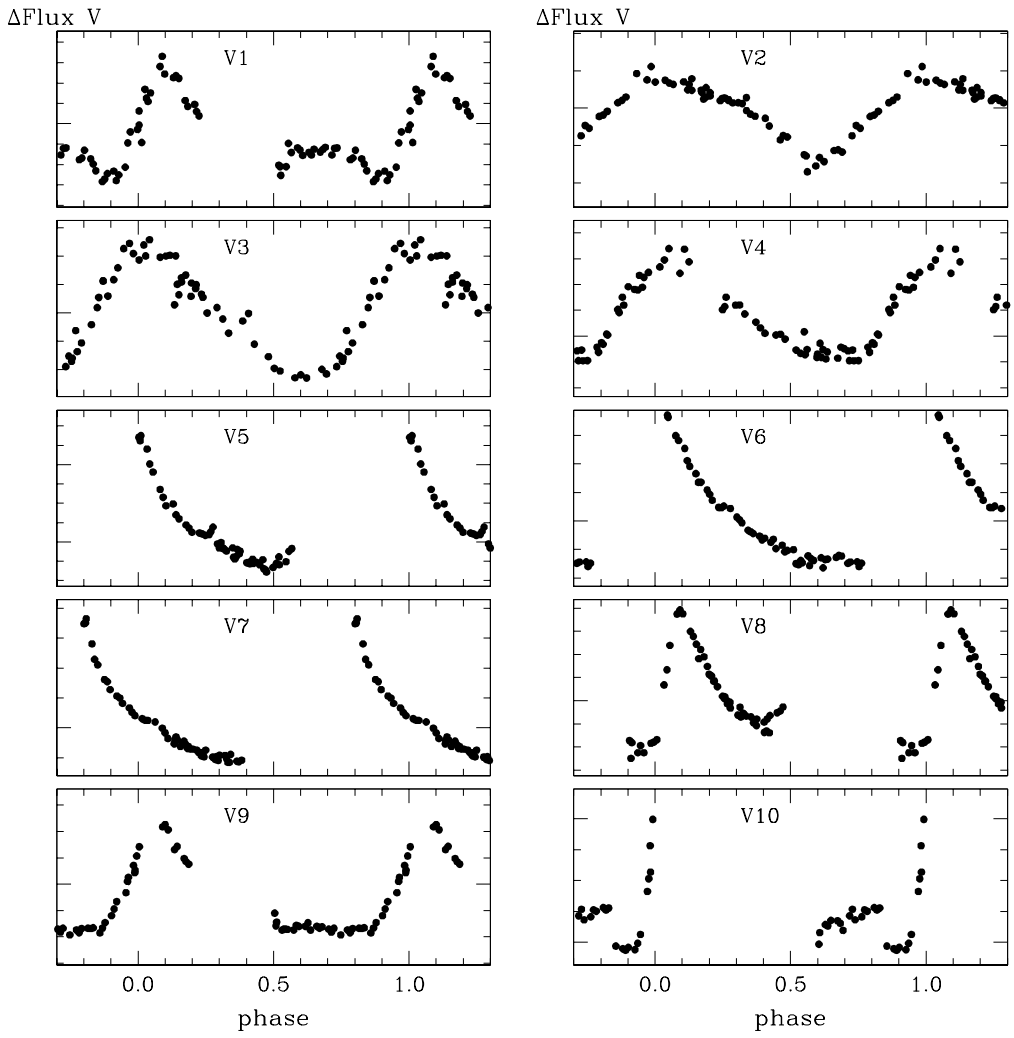

Figure D.1 Differential flux light curves of For 5 variable stars, as summarized in Table 4.7. Filled circles are Magellan data, open circles HST data.

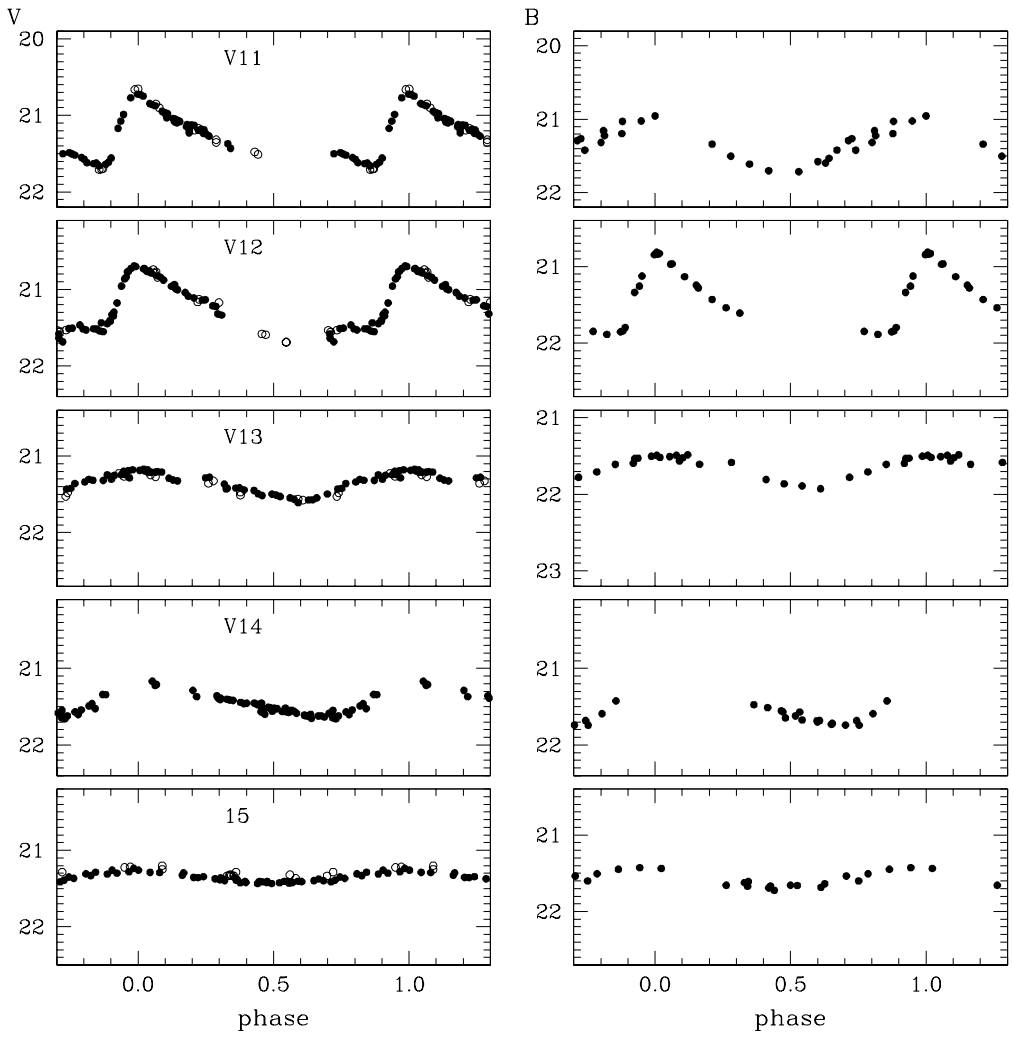

Figure D.2 Magnitude calibrated light curves of For 5 variable stars, as summarized in Table 4.7. Filled circles are Magellan data, open circles HST data.

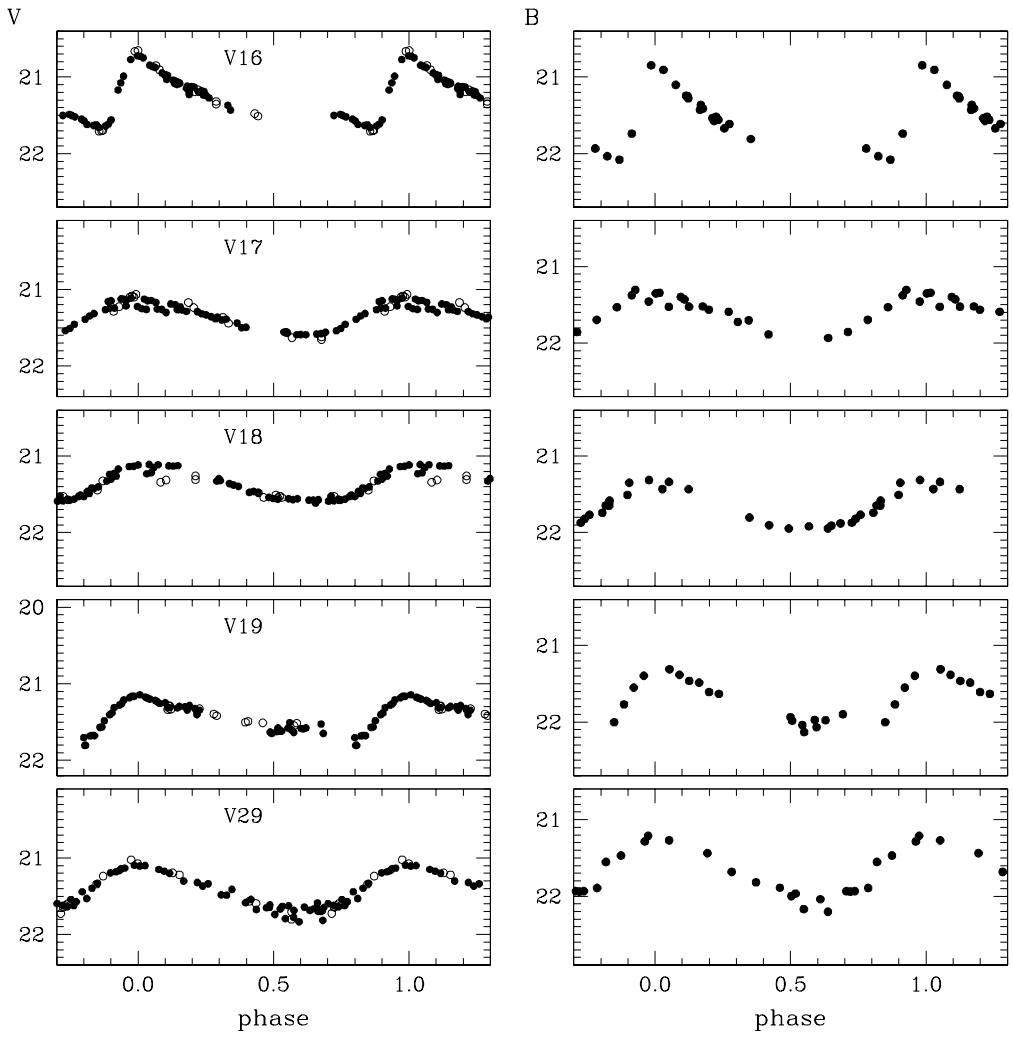

Figure D.3 Magnitude calibrated light curves of For 5 variable stars, as summarized in Table 4.7. Filled circles are Magellan data, open circles HST data.

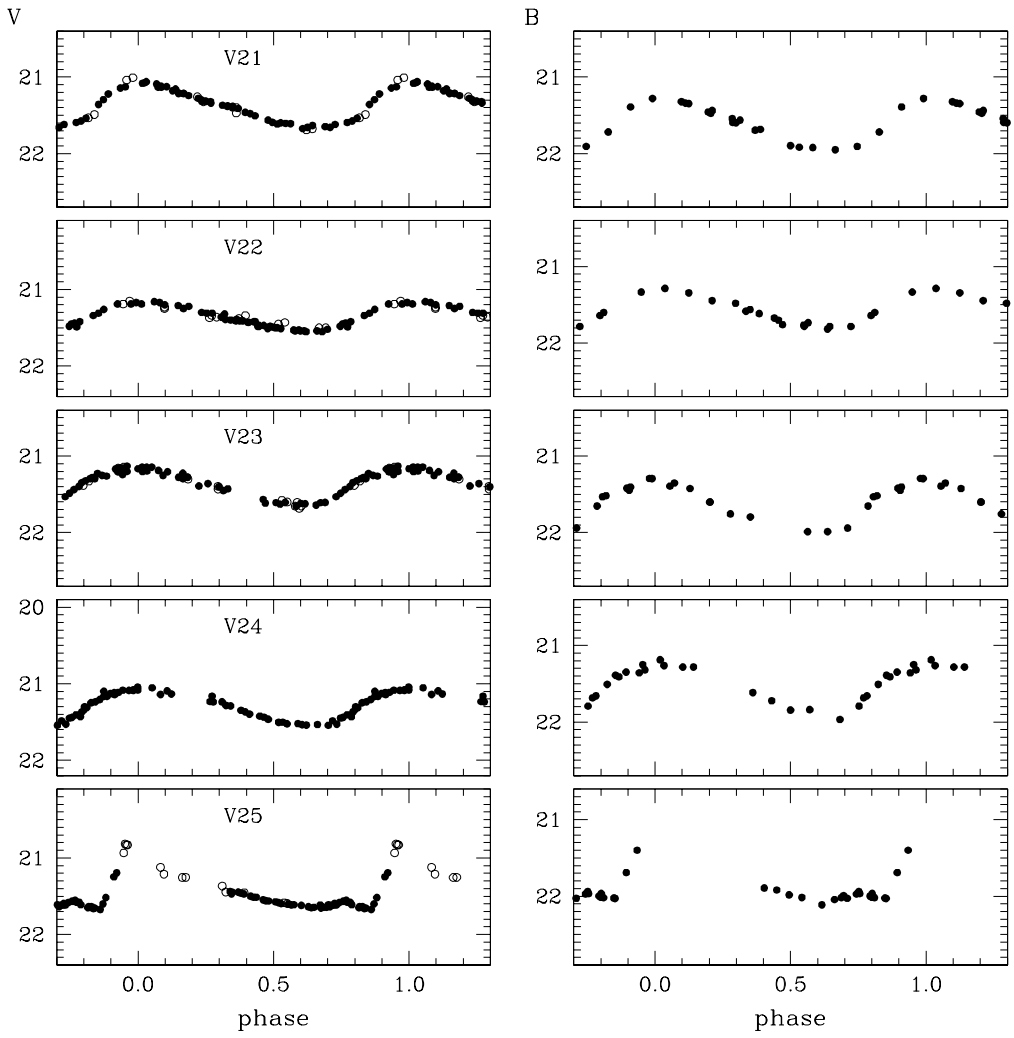

Figure D.4 Magnitude calibrated light curves of For 5 variable stars, as summarized in Table 4.7. Filled circles are Magellan data, open circles HST data.

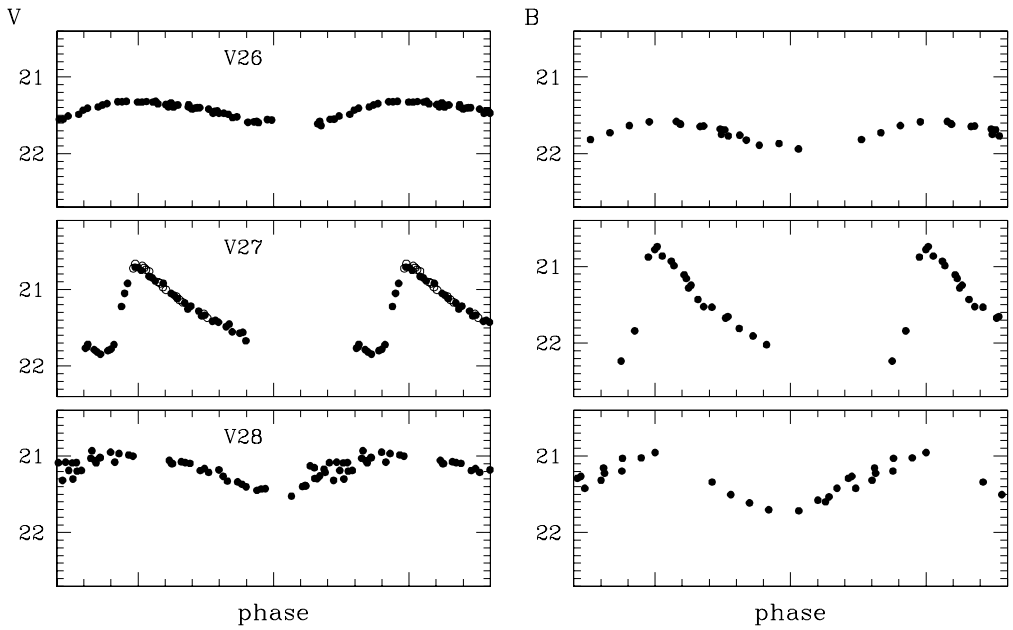

Figure D.5 Magnitude calibrated light curves of For 5 variable stars, as summarized in Table 4.7. Filled circles are Magellan data, open circles HST data.

Bibliography

Aarseth S. J., Heggie D. C., 1998, MNRAS, 297, 794

Alard C., 1999, A&A, 343, 10

Alard C., 2000, A&AS, 144, 363

Alard C., Lupton R. H., 1998, ApJ, 503, 325

Alcock C., et al., 2000, AJ, 119, 2194

Armandroff T. E., 1989, AJ, 97, 375

Ashman K. M., Bird C. M., Zepf S. E., 1994a, AJ, 108, 2348

Ashman K. M., Bird C. M., Zepf S. E., 1994b, AJ, 108, 2348

Baade W., Hubble E., 1939, PASP, 51, 40

Baade W., Swope H. H., 1961, AJ, 66, 300

Bailey S. I., 1899, Annals of Harvard College Observatory, 78

Bailey S. I., 1900, Annals of Harvard College Observatory, 38

Baldacci L., Rizzi L., Clementini G., Held E. V., 2005, A&A, 431, 1189

Barmby P., Perrett K. M., Bridges T. J., 2002, MNRAS, 329, 461

Barning F. J. M., 1963, Bull. Astron. Inst. Netherlands, 17, 22

Battaglia G., Tolstoy E., Helmi A., Irwin M. J., Letarte B., Jablonka P., Hill V., Venn K. A., Shetrone M. D., Arimoto N., Primas F., Kaufer A., Francois P., Szeifert T., Abel T., Sadakane K., 2006, A&A, 459, 423

Battistini P., Bonoli F., Braccesi A., Federici L., Fusi Pecci F., Marano B., Borngen F., 1987, A&AS, 67, 447

Becker A. C., Wittman D. M., Boeshaar P. C., Clocchiatti A., Dell'Antonio I. P., Frail D. A., Halpern J., Margoniner V. E., Norman D., Tyson J. A., Schommer R. A., 2004, ApJ, 611, 418

Beers T. C., Christlieb N., Norris J. E., et al., 2005, in Hill V., Francois P., Primas F., eds, IAU Symposium The Metallicity Distribution Function of the Halo of the Milky Way. pp 175–183

Bekki K., Freeman K. C., 2003, MNRAS, 346, L11

Bellazzini M., 2004a, MNRAS, 347, 119

Bellazzini M., 2004b, MNRAS, 347, 119

Bellazzini M., Ferraro F. R., Ibata R., 2003a, AJ, 125, 188

Bellazzini M., Ferraro F. R., Ibata R. A., 2003b, in Piotto G., Meylan G., Djorgovski S. G., Riello M., eds, ASP Conf. Ser. 296: New Horizons in Globular Cluster Astronomy Globular Clusters in the Sgr dSph Stream. pp 491–+

Bellazzini M., Ferraro F. R., Origlia L., Pancino E., Monaco L., Oliva E., 2002, AJ, 124, 3222

Bellazzini M., Ibata R., Monaco L., Martin N., Irwin M. J., Lewis G. F., 2004, MNRAS, 354, 1263

Belokurov V., et al., 2006a, ApJ, 647, L111

Belokurov V., et al., 2006b, ApJ, 647, L111

Belokurov V., et al., 2007, ApJ, 654, 897

Bersier D., Wood P. R., 2002, AJ, 123, 840

Bertin E., Mellier Y., Radovich M., Missonnier G., Didelon P., Morin B., 2002, in Bohlender D. A., Durand D., Handley T. H., eds, ASP Conf. Ser. 281: Astronomical Data Analysis Software and Systems XI The TERAPIX Pipeline. pp 228–+

Blazhko S., 1907, Astron, Nachr, 175, 325

Bono G., Caputo F., Castellani V., Marconi M., 1996, ApJ, 471, L33+

Bono G., Caputo F., Castellani V., Marconi M., 1997, A&AS, 121, 327

Bono G., Caputo F., Marconi M., 1995, AJ, 110, 2365

Bono G., Caputo F., Stellingwerf R. F., 1994, ApJ, 423, 294

Borissova J., Catelan M., Valchev T., 2001, MNRAS, 324, 77

Bragaglia A., Gratton R. G., Carretta E., Clementini G., Di Fabrizio L., Marconi M., 2001, AJ, 122, 207

Breger M., 2000, in Breger M., Montgomery M., eds, ASP Conf. Ser. 210: Delta Scuti and Related Stars δ Scuti stars (Review). pp 3–+

Brown J. A., Wallerstein G., Zucker D., 1997a, AJ, 114, 180

Brown J. A., Wallerstein G., Zucker D., 1997b, AJ, 114, 180

Brown T. M., Ferguson H. C., Smith E., Kimble R. A., Sweigart A. V., Renzini A., Rich R. M., 2004a, AJ, 127, 2738

Brown T. M., Ferguson H. C., Smith E., Kimble R. A., Sweigart A. V., Renzini A., Rich R. M., 2004b, AJ, 127, 2738

Bullock J. S., Johnston K. V., 2004, in Prada F., Martinez Delgado D., Mahoney T. J., eds, ASP Conf. Ser. 327: Satellites and Tidal Streams Cosmology and the Stellar Halo. pp 80–+

Bullock J. S., Kravtsov A. V., Weinberg D. H., 2000, ApJ, 539, 517

Buonanno R., Corsi C. E., Castellani M., Marconi G., Fusi Pecci F., Zinn R., 1999, AJ, 118, 1671

Buonanno R., Corsi C. E., Fusi Pecci F., Hardy E., Zinn R., 1985, A&A, 152, 65

Buonanno R., Corsi C. E., Zinn R., Fusi Pecci F., Hardy E., Suntzeff N. B., 1998, ApJ, 501, L33+

Cacciari C., Bellazzini M., Colucci S., 2002, in Geisler D., Grebel E. K., Minniti D., eds, IAU Symposium The RR Lyrae Variables in M54 and the Sgr Dwarf Galaxy. pp 168–+

Cacciari C., Clementini G., 2003, in Alloin D., Gieren W., eds, LNP Vol. 635: Stellar Candles for the Extragalactic Distance Scale Globular Cluster Distances from RR Lyrae Stars. pp 105–122

Cacciari C., Corwin T. M., Carney B. W., 2005, AJ, 129, 267

Cacciari C., Renzini A., 1976, A&AS, 25, 303

Caloi V., D'Antona F., Mazzitelli I., 1997, A&A, 320, 823

Caputo F., 1990, A&A, 239, 137

Caputo F., 1997, MNRAS, 284, 994

Caputo F., Castellani V., Marconi M., Ripepi V., 1999, MNRAS, 306, 815

Caputo F., Castellani V., Marconi M., Ripepi V., 2000, MNRAS, 316, 819

Caputo F., Santolamazza P., Marconi M., 1998, MNRAS, 293, 364

Caputo F., Tornambé A., Castellani V., 1978, A&A, 67, 107

Caputo F., Tornambe A., Castellani V., 1989, A&A, 222, 121

Cardelli J. A., Clayton G. C., Mathis J. S., 1989, ApJ, 345, 245

Carraro G., Zinn R., Moni Bidin C., 2007, (astro-ph/0702253)

Cassisi S., Castellani V., degl'Innocenti S., Salaris M., Weiss A., 1999, A&AS, 134, 103

Castellani V., Quarta M. L., 1987, A&AS, 71, 1

Castelli F., Gratton R. G., Kurucz R. L., 1997, A&A, 324, 432

Catelan M., 2004, in Kurtz D. W., Pollard K. R., eds, ASP Conf. Ser. 310: IAU Colloq. 193: Variable Stars in the Local Group RR Lyrae variables in globular clusters and nearby galaxies. pp 113–+

Catelan M., 2005, (astro-ph/0507464)

Catelan M., 2006, in Revista Mexicana de Astronomia y Astrofisica Conference Series, Near-Field Cosmology with Horizontal Branch and RR Lyrae Stars. pp 93–96

Catelan M., et al., 2006, Mem. Soc. Astron. Italiana, 77, 202

Catelan M., Greco C., et al., 2007, *in preparation*

Cescutti G., 2007, (astro-ph/0702573)

Chaboyer B., 1999, in Heck A., Caputo F., eds, ASSL Vol. 237: Post-Hipparcos cosmic candles Globular Cluster Distance Determinations. pp 111–+

Chiosi C., Carraro G., 2002, MNRAS, 335, 335

Christlieb N., Reimers D., Wisotzki L., 2004, The Messenger, 117, 40

Clement C., 1990, JRASC, 84, 434

Clement C. M., Muzzin A., Dufton Q., Ponnampalam T., Wang J., Burford J., Richardson A., Rosebery T., Rowe J., Hogg H. S., 2001, AJ, 122, 2587

Clement C. M., Rowe J., 2000, AJ, 120, 2579

Clement C. M., Rowe J. F., 2001, AJ, 122, 1464

Clement C. M., Shelton I., 1999, ApJ, 515, L85

Clementini G., Corwin T. M., Carney B. W., Sumerel A. N., 2004, AJ, 127, 938

Clementini G., Di Tomaso S., Di Fabrizio L., Bragaglia A., Merighi R., Tosi M., Carretta E., Gratton R. G., Ivans I. I., Kinard A., Marconi M., Smith H. A., Wilhelm R., Woodruff T., Sneden C., 2000, AJ, 120, 2054

Clementini G., Federici L., Corsi C., Cacciari C., Bellazzini M., Smith H. A., 2001, ApJ, 559, L109

Clementini G., Gratton R., Bragaglia A., Carretta E., Di Fabrizio L., Maio M., 2003, AJ, 125, 1309

Clementini G., Greco C., Held E. V., Poretti E., Catelan M., Dell'Arciprete L., Gullieuszik M., Maio M., Rizzi L., Smith H. A., Pritzl B. J., Rest A., De Lee N., 2006, Mem. Soc. Astron. Italiana, 77, 249

Coleman M., Da Costa G. S., Bland-Hawthorn J., Mart'inez-Delgado D., Freeman K. C., Malin D., 2004, AJ, 127, 832

Coleman M. G., Da Costa G. S., Bland-Hawthorn J., Freeman K. C., 2005, AJ, 129, 1443

Coutts C., Dickens R. J., Epps E., Read M., 1975, ApJ, 197, L45+

Cox J. P., 1974, Reports of Progress in Physics, 37, 563

Cseresnjes P., 2001, A&A, 375, 909

Da Costa G. S., Armandroff T. E., 1995, AJ, 109, 2533

Dall'Ora M., Clementini G., Kinemuchi K., Ripepi V., Marconi M., Di Fabrizio L., Greco C., Rodgers C. T., Kuehn C., Smith H. A., 2006, ApJ, 653, L109

De Angeli F., Piotto G., Cassisi S., Busso G., Recio-Blanco A., Salaris M., Aparicio A., Rosenberg A., 2005, AJ, 130, 116

de Grijs R., Wilkinson M. I., Tadhunter C. N., 2005, MNRAS, 361, 311

De Propris R., Phillipps S., Drinkwater M. J., Gregg M. D., Jones J. B., Evstigneeva E., Bekki K., 2005a, ApJ, 623, L105

De Propris R., Phillipps S., Drinkwater M. J., Gregg M. D., Jones J. B., Evstigneeva E., Bekki K., 2005b, ApJ, 623, L105

Dell'Arciprete L., 2006, *Laurea Thesis*, Universitá degli studi di Milano

Demarque P., Zinn R., Lee Y.-W., Yi S., 2000a, AJ, 119, 1398

Demarque P., Zinn R., Lee Y.-W., Yi S., 2000b, AJ, 119, 1398

Demers S., Grondin L., Kunkel W. E., 1990, PASP, 102, 632

Di Criscienzo M., Marconi M., Caputo F., 2004, ApJ, 612, 1092

Di Fabrizio L., 1999, *Laurea Thesis*, Universitá degli studi di Bologna

Di Fabrizio L., Clementini G., Maio M., Bragaglia A., Carretta E., Gratton R., Montegriffo P., Zoccali M., 2005, A&A, 430, 603

Dinescu D. I., Girard T. M., van Altena W. F., 1999, AJ, 117, 1792

Dinescu D. I., Girard T. M., van Altena W. F., López C. E., 2003, AJ, 125, 1373

Dinescu D. I., Keeney B. A., Majewski S. R., Girard T. M., 2004, AJ, 128, 687

Dinescu D. I., Majewski S. R., Girard T. M., Cudworth K. M., 2000, AJ, 120, 1892

Djorgovski S. G., Gal R. R., McCarthy J. K., Cohen J. G., de Carvalho R. R., Meylan G., Bendinelli O., Parmeggiani G., 1997, ApJ, 474, L19+

Dorman B., 1992, ApJS, 81, 221

Drinkwater M. J., Gregg M. D., Hilker M., Bekki K., Couch W. J., Ferguson H. C., Jones J. B., Phillipps S., 2003, nat, 423, 519

Dubath P., Grillmair C. J., 1997, A&A, 321, 379

Durrell P. R., Harris W. E., Pritchet C. J., 2001, AJ, 121, 2557

Efstathiou G., 1992, MNRAS, 256, 43P

Eggen O. J., Lynden-Bell D., Sandage A. R., 1962, ApJ, 136, 748

Faber S. M., Jackson R. E., 1976, ApJ, 204, 668

Fellhauer M., Belokurov V., Evans N. W., Wilkinson M. I., Zucker D. B., Gilmore G., Irwin M. J., Bramich D. M., Vidrih S., Wyse R. F. G., Beers T. C., Brinkmann J., 2006, ApJ, 651, 167

Fellhauer M., Lin D. N. C., 2007, MNRAS, pp 1454–+

Ferguson A. M. N., 2006, (astro-ph/0611412)

Ferguson A. M. N., Irwin M. J., Ibata R. A., Lewis G. F., Tanvir N. R., 2002, AJ, 124, 1452

Fernley J., Skillen I., Carney B. W., Cacciari C., Janes K., 1998, MNRAS, 293, L61

Ferrara A., Tolstoy E., 2000, MNRAS, 313, 291

Ferraro F. R., Messineo M., Fusi Pecci F., de Palo M. A., Straniero O., Chieffi A., Limongi M., 1999, AJ, 118, 1738

Forbes D. A., Masters K. L., Minniti D., Barmby P., 2000, A&A, 358, 471

Freeman K., Bland-Hawthorn J., 2002, ARA&A, 40, 487

Frinchaboy P. M., Majewski S. R., Crane J. D., Reid I. N., Rocha-Pinto H. J., Phelps R. L., Patterson R. J., Muñoz R. R., 2004, ApJ, 602, L21

Gallagher III J. S., Wyse R. F. G., 1994, PASP, 106, 1225

Gautschy A., Saio H., 1995, ARA&A, 33, 75

Gay P. L., 1998, in Bulletin of the American Astronomical Society Variable Stars in the Ursa Minor Dwarf Spheroidal Galaxy: A Story of Star Formation as told by the Horizontal Branch. pp 1353–+

Glatt K., et al., 2007, *in preparation*

Gnedin O. Y., Zhao H., Pringle J. E., Fall S. M., Livio M., Meylan G., 2002, ApJ, 568, L23

Gómez M., Geisler D., Harris W. E., Richtler T., Harris G. L. H., Woodley K. A., 2006, A&A, 447, 877

Graham J. A., 1975, PASP, 87, 641

Gratton R., Sneden C., Carretta E., 2004, ARA&A, 42, 385

Gratton R. G., Bragaglia A., Clementini G., Carretta E., Di Fabrizio L., Maio M., Taribello E., 2004, A&A, 421, 937

Grebel E. K., Gallagher III J. S., Harbeck D., 2003, AJ, 125, 1926

Greco C., 2003, *Laurea Thesis*, Universitá degli studi di Bologna

Greco C., Clementini G., Held E. V., Poretti E., Catelan M., Dell'Arciprete L., Gullieuszik M., Maio M., Rizzi L., Smith H. A., Pritzl B. J., Rest A., De Lee N., 2005, (astro-ph/0507244)

Greco C., et al., 2007a, *in preparation*

Greco C., et al., 2007b, *in preparation*

Greco C., et al., 2007c, *in press*

Hardy E., 2002, in Geisler D., Grebel E. K., Minniti D., eds, IAU Symposium he Globular Clusters of the Fornax Dwarf Spheroidal Galaxy: Properties Environment. pp 62–+

Harris E. O., Neill J. D. M. K. J., Rich R. M., 1996, AJ, 111, 1596

Harris W. E., 1996, AJ, 112, 1487

Harris W. E., 2001, in Labhardt L., Binggeli B., eds, Saas-Fee Advanced Course 28: Star Clusters Globular cluster systems. pp 223–+

Harris W. E., Bell R. A., Vandenberg D. A., Bolte M., Stetson P. B., Hesser J. E., van den Bergh S., Bond H. E., Fahlman G. G., Richer H. B., 1997, AJ, 114, 1030

Harris W. E., Harris G. L. H., Holland S. T., McLaughlin D. E., 2002, AJ, 124, 1435

Hasegan M., 2005, in Bulletin of the American Astronomical Society Faint Stellar Systems: Ultra-Luminous Globular Clusters and Ultra-Compact Dwarf Galaxies. pp 1317–+

Hayashi E., Navarro J. F., Taylor J. E., Stadel J., Quinn T., 2003, ApJ, 584, 541

Held E. V., 2005, in Jerjen H., Binggeli B., eds, IAU Colloq. 198: Near-fields cosmology with dwarf elliptical galaxies The stellar populations of local dwarfs. pp 11–16

Held E. V., Clementini G., Rizzi L., Momany Y., Saviane I., Di Fabrizio L., 2001, ApJ, 562, L39

Hodge P. W., 1961, AJ, 66, 83

Hodge P. W., 1965, ApJ, 141, 308

Hodge P. W., 1969, PASP, 81, 875

Holland S., Fahlman G. G., Richer H. B., 1996, AJ, 112, 1035

Huchra J. P., Brodie J. P., Kent S. M., 1991, ApJ, 370, 495

Huxor A. P., Tanvir N. R., Irwin M. J., Ibata R., Collett J. L., Ferguson A. M. N., Bridges T., Lewis G. F., 2005, MNRAS, 360, 1007

Ibata R., Irwin M., Lewis G., Ferguson A. M. N., Tanvir N., 2001, Nature, 412, 49

Ibata R., Irwin M., Lewis G. F., Stolte A., 2001, ApJ, 547, L133

Ibata R. A., Gilmore G., Irwin M. J., 1994a, Nature, 370, 194

Ibata R. A., Gilmore G., Irwin M. J., 1994b, nat, 370, 194

Ibata R. A., Gilmore G., Irwin M. J., 1995, MNRAS, 277, 781

Ibata R. A., Lewis G. F., Irwin M. J., Cambrésy L., 2002, MNRAS, 332, 921

Ibata R. A., Wyse R. F. G., Gilmore G., Irwin M. J., Suntzeff N. B., 1997, AJ, 113, 634

Ideta M., Makino J., 2004, ApJ, 616, L107

Irwin M., Hatzidimitriou D., 1995a, MNRAS, 277, 1354

Irwin M., Hatzidimitriou D., 1995b, MNRAS, 277, 1354

Jurcsik J., 1995, Acta Astron., 45, 653

Jurcsik J., Kovacs G., 1996, A&A, 312, 111

Kaluzny J., Kubiak M., Szymanski M., Udalski A., Krzeminski W., Mateo M., 1997, A&AS, 125, 343

Kaluzny J., Mochnacki S., Rucinski S. M., 2006, AJ, 131, 407

Kaluzny J., Rucinski S. M., 2003, AJ, 126, 237

Kauffmann G., White S. D. M., Guiderdoni B., 1993, MNRAS, 264, 201

Kinemuchi K., Smith H. A., Lacluyz'e A. P., Clark C. L., Harris H. C., Silbermann N., Snyder L. A., 2002, in Aerts C., Bedding T. R., Christensen-Dalsgaard J., eds, ASP Conf. Ser. 259: IAU Colloq. 185: Radial and Nonradial Pulsationsn as Probes of Stellar Physics RR Lyrae Stars and Anomalous Cepheids in the Draco Dwarf Spheroidal Galaxy. pp 130–+

King I., 1962, AJ, 67, 471

Klessen R. S., Grebel E. K., Harbeck D., 2003, ApJ, 589, 798

Kleyna J. T., Wilkinson M. I., Evans N. W., Gilmore G., 2001, ApJ, 563, L115

Kleyna J. T., Wilkinson M. I., Evans N. W., Gilmore G., 2005, ApJ, 630, L141

Kleyna J. T., Wilkinson M. I., Gilmore G., Evans N. W., 2003, ApJ, 588, L21

Klypin A., Kravtsov A. V., Valenzuela O., Prada F., 1999, ApJ, 522, 82

Knierman K. A., Gallagher S. C., Charlton J. C., Hunsberger S. D., Whitmore B., Kundu A., Hibbard J. E., Zaritsky D., 2003, AJ, 126, 1227

Koch A., Grebel E. K., 2006, AJ, 131, 1405

Koch A., Grebel E. K., Kleyna J. T., Wilkinson M. I., Harbeck D. R., Gilmore G. F., Wyse R. F. G., Evans N. W., 2007, AJ, 133, 270

Kovács G., Kanbur S. M., 1998, MNRAS, 295, 834

Kovács G., Walker A. R., 1999a, ApJ, 512, 271

Kovács G., Walker A. R., 1999b, ApJ, 512, 271

Kovács G., Walker A. R., 2001, A&A, 371, 579

Kravtsov A. V., Gnedin O. Y., Klypin A. A., 2004, ApJ, 609, 482

Kroupa P., 1997, New Astronomy, 2, 139

Kroupa P., Theis C., Boily C. M., 2005, A&A, 431, 517

Kunkel W. E., 1979, ApJ, 228, 718

Kunkel W. E., Demers S., 1976, in The Galaxy and the Local Group The Magellanic Plane. pp 241–+

Landolt A. U., 1992, AJ, 104, 340

Layden A. C., 1998, AJ, 115, 193

Layden A. C., Ritter L. A., Welch D. L., Webb T. M. A., 1999, AJ, 117, 1313

Layden A. C., Sarajedini A., 2000a, AJ, 119, 1760

Layden A. C., Sarajedini A., 2000b, AJ, 119, 1760

Lee J.-W., Carney B. W., 1999, AJ, 118, 1373

Lee Y.-W., Demarque P., Zinn R., 1990, ApJ, 350, 155

Lee Y.-W., Demarque P., Zinn R., 1994, ApJ, 423, 248

Letarte B., Hill V., Jablonka P., Tolstoy E., François P., Meylan G., 2006, A&A, 453, 547

Lomb N. R., 1976, Ap&SS, 39, 447

Lotz J. M., Miller B. W., Ferguson H. C., 2004, ApJ, 613, 262

Lub J., 1977, The RR Lyrae population of the solar neighbourhood. Leiden: Rijksuniversiteit, 1977

Lynden-Bell D., 1976, MNRAS, 174, 695

Lynden-Bell D., 1982, The Observatory, 102, 202

Ma J., de Grijs R., Chen D., van den Bergh S., Fan Z., Wu Z., Wu H., Zhou X., Wu J., 2007, (astro-ph/0702012)

Ma J., van den Bergh S., Wu H., Yang Y., Zhou X., Chen J., Wu Z., Jiang Z., Wu J., 2006a, ApJ, 636, L93

Ma J., van den Bergh S., Wu H., Yang Y., Zhou X., Chen J., Wu Z., Jiang Z., Wu J., 2006b, ApJ, 636, L93

Mackey A. D., Gilmore G. F., 2003a, MNRAS, 340, 175

Mackey A. D., Gilmore G. F., 2003b, MNRAS, 345, 747

Mackey A. D., Gilmore G. F., 2004, MNRAS, 355, 504

Mackey A. D., van den Bergh S., 2005, MNRAS, 360, 631

Majewski S. R., 1994, ApJ, 431, L17

Majewski S. R., Skrutskie M. F., Weinberg M. D., Ostheimer J. C., 2003, ApJ, 599, 1082

Martin N. F., Ibata R. A., Conn B. C., Lewis G. F., Bellazzini M., Irwin M. J., McConnachie A. W., 2004, MNRAS, 355, L33

Martin N. F., Ibata R. A., Irwin M. J., Chapman S., Lewis G. F., Ferguson A. M. N., Tanvir N., McConnachie A. W., 2006a, MNRAS, 371, 1983

Martin N. F., Ibata R. A., Irwin M. J., Chapman S., Lewis G. F., Ferguson A. M. N., Tanvir N., McConnachie A. W., 2006b, MNRAS, 371, 1983

Martínez-Delgado D., Alonso-García J., Aparicio A., Gómez-Flechoso M. A., 2001, apjl, 549, L63

Martínez Delgado D., et al., 2004, in Prada F., Martinez Delgado D., Mahoney T. J., eds, ASP Conf. Ser. 327: Satellites and Tidal Streams Mapping Tidal Streams around Galactic Globular Clusters. pp 255–+

Martínez-Delgado D., Zinn R., Carrera R., Gallart C., 2002a, ApJ, 573, L19

Martínez-Delgado D., Zinn R., Carrera R., Gallart C., 2002b, ApJ, 573, L19

Mateo M., Hurley-Keller D., Nemec J., 1998, AJ, 115, 1856

Mateo M., Olszewski E. W., Vogt S. S., Keane M. J., 1998, AJ, 116, 2315

Mazur B., Krzemi'nski W., Thompson I. B., 2003, MNRAS, 340, 1205

McConnachie A. W., Irwin M. J., 2006, MNRAS, 365, 1263

McConnachie A. W., Irwin M. J., Ibata R. A., Ferguson A. M. N., Lewis G. F., Tanvir N., 2003, MNRAS, 343, 1335

McLaughlin D. E., 2000, in Favata F., Kaas A., Wilson A., eds, ESA SP-445: Star Formation from the Small to the Large Scale The Formation History of Globular Clusters. pp 77–+

McLaughlin D. E., van der Marel R. P., 2005, ApJS, 161, 304

McNamara D., 1997, PASP, 109, 1221

McNamara D. H., 2000, PASP, 112, 1096

McNamara D. H., Clementini G., Marconi M., 2007, (astro-ph/0702107)

McNamara D. H., Rose M. B., Brown P. J., Ketcheson D. I., Maxwell J. E., Smith K. M., Wooley R. C., 2004, in Kurtz D. W., Pollard K. R., eds, ASP Conf. Ser. 310: IAU Colloq. 193: Variable Stars in the Local Group The luminosities of horizontal branches and RR Lyrae stars in globular clusters. pp 525–+

Meylan G., Heggie D. C., 1997, A&A Rev., 8, 1

Meylan G., Sarajedini A., Jablonka P., Djorgovski S. G., Bridges T., Rich R. M., 2001, AJ, 122, 830

Mieske S., Hilker M., Infante L., 2002, A&A, 383, 823

Molaro P., Bonifacio P., Castelli F., Pasquini L., 1997, A&A, 319, 593

Monaco L., Pancino E., Ferraro F. R., Bellazzini M., 2004a, MNRAS, 349, 1278

Monaco L., Pancino E., Ferraro F. R., Bellazzini M., 2004b, MNRAS, 349, 1278

Moore B., Ghigna S., Governato F., Lake G., Quinn T., Stadel J., Tozzi P., 1999, ApJ, 524, L19

Moore B., Quinn T., Governato F., Stadel J., Lake G., 1999, MNRAS, 310, 1147

Morris P. W., Reid I. N., Griffiths W. K., Penny A. J., 1994, MNRAS, 271, 852

Munoz R. R., Carlin J. L., Frinchaboy P. M., Nidever D. L., Majewski S. R., Patterson R. J., 2006, ApJ, 650, L51

Nemec J. M., Nemec A. F. L., Lutz T. E., 1994, AJ, 108, 222

Newberg H. J., Yanny B., Grebel E. K., Hennessy G., Ivezić Ž., Martinez-Delgado D., Odenkirchen M., Rix H.-W., Brinkmann J., Lamb D. Q., Schneider D. P., York D. G., 2003, ApJ, 596, L191

Newberg H. J., Yanny B., Rockosi C., Grebel E. K., Rix H.-W., Brinkmann J., Csabai I., Hennessy G., Hindsley R. B., Ibata R., Ivezić Z., Lamb D., Nash E. T., Odenkirchen M., Rave H. A., Schneider D. P., Smith J. A., Stolte A., York D. G., 2002, ApJ, 569, 245

Norris J., Zinn R., 1975, ApJ, 202, 335

Norris J. E., 2004, ApJ, 612, L25

Odenkirchen M., et al., 2001, AJ, 122, 2538

Odenkirchen M., Grebel E. K., Dehnen W., Rix H.-W., Yanny B., Newberg H. J., Rockosi C. M., Martínez-Delgado D., Brinkmann J., Pier J. R., 2003, AJ, 126, 2385

Oh K. S., Lin D. N. C., Richer H. B., 2000, ApJ, 531, 727

Olech A., Dziembowski W. A., Pamyatnykh A. A., Kaluzny J., Pych W., Schwarzenberg-Czerny A., Thompson I. B., 2005, MNRAS, 363, 40

Olszewski E. W., 1993, in Smith G. H., Brodie J. P., eds, ASP Conf. Ser. 48: The Globular Cluster-Galaxy Connection The Age and Metallicity Distributions Among the Magellanic Cloud Clusters. pp 351–+

Olszewski E. W., Mateo M., Harris J., Walker M. G., Coleman M. G., Da Costa G. S., 2006, AJ, 131, 912

Oosterhoff P. T., 1939, Bull. Astron. Inst. Netherlands, 9, 11

Oosterhoff P. T., 1944, Bull. Astron. Inst. Netherlands, 10, 55

Palma C., Majewski S. R., Johnston K. V., 2002, ApJ, 564, 736

Palma C., Majewski S. R., Siegel M. H., Patterson R. J., Ostheimer J. C., Link R., 2003, AJ, 125, 1352

Pancino E., Seleznev A., Ferraro F. R., Bellazzini M., Piotto G., 2003, MNRAS, 345, 683

Petersen J. O., 1972, A&A, 19, 197

Phillipps S., Parker Q. A., Schwartzenberg J. M., Jones J. B., 1998, apjl, 493, L59+

Phillips A. C., Davis L. E., 1995, in Shaw R. A., Payne H. E., Hayes J. J. E., eds, ASP Conf. Ser. 77: Astronomical Data Analysis Software and Systems IV . pp 297–+

Piatek S., Pryor C., Olszewski E. W., Harris H. C., Mateo M., Minniti D., Monet D. G., Morrison H., Tinney C. G., 2002, AJ, 124, 3198

Pietrinferni A., Cassisi S., Salaris M., Castelli F., 2004, ApJ, 612, 168

Pigulski A., Kolaczkowski Z., Kopacki G., 2003, Acta Astronomica, 53, 27

Pinto G., Rosino L., 1978, å, 28, 427

Pont F., Zinn R., Gallart C., Hardy E., Winnick R., 2004, AJ, 127, 840

Poretti E., 1999, A&A, 343, 385

Poretti E., 2001, A&A, 371, 986

Poretti E., 2003, A&A, 409, 1031

Poretti E., Greco C., et al., 2007, *in preparation*

Pritzl B. J., Smith H. A., Catelan M., Sweigart A. V., 2002, AJ, 124, 949

Pritzl B. J., Smith H. A., Catelan M., Sweigart A. V., 2003, AJ, 125, 2752

Pritzl B. J., Smith H. A., Stetson P. B., Catelan M., Sweigart A. V., Layden A. C., Rich R. M., 2003, AJ, 126, 1381

Pritzl B. J., Venn K. A., Irwin M., 2005a, AJ, 130, 2140

Pritzl B. J., Venn K. A., Irwin M., 2005b, AJ, 130, 2140

Pryor C., Meylan G., 1993, in Djorgovski S. G., Meylan G., eds, ASP Conf. Ser. 50: Structure and Dynamics of Globular Clusters Velocity Dispersions for Galactic Globular Clusters. pp 357–+

Pych W., Kaluzny J., Krzeminski W., Schwarzenberg-Czerny A., Thompson I. B., 2001, A&A, 367, 148

Reitzel D. B., Guhathakurta P., 2002, AJ, 124, 234

Reitzel D. B., Guhathakurta P., Gould A., 1998, AJ, 116, 707

Rest A., et al., 2005, ApJ, 634, 1103

Rey S.-C., Lee Y.-W., Ree C. H., Joo J.-M., Sohn Y.-J., Walker A. R., 2004, AJ, 127, 958

Rich R. M., Corsi C. E., Cacciari C., Federici L., Fusi Pecci F., Djorgovski S. G., Freedman W. L., 2005, AJ, 129, 2670

Rich R. M., Mighell K. J., Freedman W. L., Neill J. D., 1996, AJ, 111, 768

Ripepi V., et al., 2007, *in preparation*

Rodríguez E., López-González M. J., 2000, A&A, 359, 597

Rodríguez E., López-González M. J., López de Coca P., 2000, A&AS, 144, 469

Rood R. T., Dorman B., Ferraro F. R., Paltrinieri B., Fusi Pecci F., 1998, in Wamsteker W., Gonzalez Riestra R., Harris B., eds, ESA SP-413: Ultraviolet Astrophysics Beyond the IUE Final Archive UV Bright Stars in Globular Clusters. pp 515–+

Salinas R., Catelan M., Smith H. A., Pritzl B. J., Borissova J., 2005, Informational Bulletin on Variable Stars, 5640, 1

Salinas R., Catelan M., Smith H. A., Pritzl B. J., Borissova J., 2006, in Revista Mexicana de Astronomia y Astrofisica Conference Series The Sagittarius dSph globular cluster system: variable stars. pp 184–+

Sandage A., 1981a, ApJ, 244, L23+

Sandage A., 1981b, ApJ, 248, 161

Sandage A., 1982a, ApJ, 252, 574

Sandage A., 1982b, ApJ, 252, 553

Sandage A., 1990, ApJ, 350, 631

Sandage A., 1993, AJ, 106, 687

Sandage A., 2006, AJ, 131, 1750

Sandage A., Katem B., Sandage M., 1981, ApJS, 46, 41

Sarajedini A., Layden A. C., 1995, AJ, 109, 1086

Saviane I., Held E. V., Bertelli G., 2000, A&A, 355, 56

Scargle J. D., 1982, ApJ, 263, 835

Schechter P. L., Mateo M., Saha A., 1993, PASP, 105, 1342

Schwarzenberg-Czerny A., 1996, ApJ, 460, L107

Searle L., Zinn R., 1978, ApJ, 225, 357

Seth A., Olsen K., Miller B., Lotz J., Telford R., 2004, AJ, 127, 798

Shapley H., 1938, Nature, 142, 715

Shapley H., 1939, Proceedings of the National Academy of Science, 25, 565

Shetrone M., Venn K. A., Tolstoy E., Primas F., Hill V., Kaufer A., 2003, AJ, 125, 684

Shetrone M. D., Côté P., Stetson P. B., 2001, PASP, 113, 1122

Siegel M. H., 2006, (astro-ph/0607091)

Skrutskie et al., 2006, AJ, 131, 1163

Smith H., 1995, RR Lyrae stars. Cambridge Astrophysics Series, 27

Smith H. A., Silbermann N. A., Baird S. R., Graham J. A., 1992, AJ, 104, 1430

Sollima A., Pancino E., Ferraro F. R., Bellazzini M., Straniero O., Pasquini L., 2005, ApJ, 634, 332

Soszynski I., et al., 2003, Acta Astron., 53, 93

Spergel D. N., et al., 2006, (astro-ph/0603449)

Stetson P. B., 1987, PASP, 99, 191

Stetson P. B., 1992, in Worrall D. M., Biemesderfer C., Barnes J., eds, ASP Conf. Ser. 25: Astronomical Data Analysis Software and Systems I More Experiments with DAOPHOT II and WF/PC Images. pp 297–+

Stetson P. B., 1994, PASP, 106, 250

Stetson P. B., 1996, User's Manual for DAOPHOT II, 99, 191

Stetson P. B., Hesser J. E., Smecker-Hane T. A., 1998, PASP, 110, 533

Strader J., Brodie J. P., Forbes D. A., Beasley M. A., Huchra J. P., 2003, AJ, 125, 1291

Surdin V. G., 1994, Astronomy Letters, 20, 15

Tolstoy E., Irwin M. J., Helmi A., Battaglia G., Jablonka P., Hill V., Venn K. A., Shetrone M. D., Letarte B., Cole A. A., Primas F., Francois P., Arimoto N., Sadakane K., Kaufer A., Szeifert T., Abel T., 2004, ApJ, 617, L119

Tolstoy E., Venn K. A., Shetrone M., Primas F., Hill V., Kaufer A., Szeifert T., 2003, AJ, 125, 707

Unavane M., Wyse R. F. G., Gilmore G., 1996, MNRAS, 278, 727

Valdes F., 1997, in Hunt G., Payne H., eds, ASP Conf. Ser. 125: Astronomical Data Analysis Software and Systems VI IRAF Data Reduction Software for the NOAO Mosaic. pp 455–+

Van Albada T. S., Baker N., 1973, in Fernie J. D., ed., ASSL Vol. 36: IAU Colloq. 21: Variable Stars in Globular Clusters and in Related Systems On the Two Oosterhoff Groups of Globular Clusters. pp 196–+

van den Bergh S., 1968, The Observatory, 88, 168

van den Bergh S., 1993a, MNRAS, 262, 588

van den Bergh S., 1993b, ApJ, 411, 178

van den Bergh S., 1999, AJ, 117, 2211

van den Bergh S., 2005, (astro-ph/0511701)

van den Bergh S., Mackey A. D., 2004, MNRAS, 354, 713

VandenBerg D. A., Swenson F. J., Rogers F. J., Iglesias C. A., Alexander D. R., 2000, ApJ, 532, 430

Vanicek P., 1971, Ap&SS, 12, 10

Venn K. A., Irwin M., Shetrone M. D., Tout C. A., Hill V., Tolstoy E., 2004, AJ, 128, 1177

Villanova S., Piotto G., King I. R., Anderson J., Bedin L. R., Gratton R. G., Cassisi S., Momany Y., Bellini A., Cool A. M., Recio-Blanco A., Renzini A., 2007, (astro-ph/0703208)

Walker M. G., Mateo M., Olszewski E. W., Bernstein R., Wang X., Woodroofe M., 2006, AJ, 131, 2114

Wilkinson M. I., Kleyna J. T., Evans N. W., Gilmore G. F., Irwin M. J., Grebel E. K., 2004, ApJ, 611, L21

Wilkinson M. I., Kleyna J. T., Gilmore G. F., Evans N. W., Koch A., Grebel E. K., Wyse R. F. G., Harbeck D. R., 2006, The Messenger, 124, 25

Willman B., et al., 2005a, ApJ, 626, L85

Willman B., et al., 2005b, ApJ, 626, L85

Willman B., Masjedi M., Hogg D. W., Dalcanton J. J., Martinez-Delgado D., Blanton M., West A. A., Dotter A., Chaboyer B., 2006, (astro-ph/0603486)

Yanny B., Newberg H. J., Grebel E. K., Kent S., Odenkirchen M., Rockosi C. M., Schlegel D., Subbarao M., Brinkmann J., Fukugita M., Ivezic Ž., Lamb D. Q., Schneider D. P., York D. G., 2003, ApJ, 588, 824

Yoon S.-J., Lee Y.-W., 2002, Science, 297, 578

York D. G., et al., 2000, AJ, 120, 1579

Young L. M., 1999, AJ, 117, 1758

Zentner A. R., Bullock J. S., 2003, ApJ, 598, 49

Zhao H., 2005, (astro-ph/0508635)

Zinn R., 1993a, in Smith G. H., Brodie J. P., eds, ASP Conf. Ser. 48: The Globular Cluster-Galaxy Connection The Galactic Halo Cluster Systems: Evidence for Accretion. pp 38–+

Zinn R., 1993b, in Smith G. H., Brodie J. P., eds, ASP Conf. Ser. 48: The Globular Cluster-Galaxy Connection The Galactic Halo Cluster Systems: Evidence for Accretion. pp 38–+

Zinn R., 1996, in Morrison H. L., Sarajedini A., eds, ASP Conf. Ser. 92: Formation of the Galactic Halo...Inside and Out The Galaxy's Globular Clusters. pp 211–+

Zinn R., Dahn C. C., 1976, AJ, 81, 527

Zinn R., Searle L., 1976, ApJ, 209, 734

Zinn R., West M. J., 1984, ApJS, 55, 45

Zucker D. B., et al., 2004, ApJ, 612, L121

Zucker D. B., et al., 2006a, ApJ, 650, L41

Zucker D. B., et al., 2006b, ApJ, 643, L103

Zucker D. B., et al., 2006c, (astro-ph/0601599)